RATIONAL DESIGN AND SYNTHESIS OF BODIPY DYES FOR MOLECULAR SENSING, LIGHT HARVESTING AND PHOTODYNAMIC APPLICATIONS

A DISSERTATION SUBMITTED TO
MATERIALS SCIENCE AND NANOTECHNOLOGY PROGRAM
OF THE GRADUATE SCHOOL OF ENGINEERING AND SCIENCE
OF BILKENT UNIVERSITY
IN PARTIAL FULFILLMENT OF THE REQUIREMENTS
FOR THE DEGREE OF
DOCTOR OF PHILOSOPHY

By
TUĞBA ÖZDEMİR KÜTÜK
September, 2014

I certify that I have read this thesis and that in my opinion it is fully adequate, in scope and in quality, as a thesis of the degree of Doctor of Philosophy.

…….

Prof. Dr. Engin U. Akkaya (Advisor)

I certify that I have read this thesis and that in my opinion it is fully adequate, in scope and in quality, as a thesis of the degree of Doctor of Philosophy.

…….

Assoc. Prof. Dr. Dönüş Tuncel

I certify that I have read this thesis and that in my opinion it is fully adequate, in scope and in quality, as a thesis of the degree of Doctor of Philosophy.

…….

Assist. Prof. Dr. Salih Özçubukçu

I certify that I have read this thesis and that in my opinion it is fully adequate, in scope and in quality, as a thesis of the degree of Doctor of Philosophy.

…….

Assist. Prof. Dr. Serdar Atılgan

I certify that I have read this thesis and that in my opinion it is fully adequate, in scope and in quality, as a thesis of the degree of Doctor of Philosophy.

…….

Assist. Prof. Dr. H. Tarık Baytekin

Approved for the Graduate School of Engineering and Science:

…….

Prof. Dr. Levent Onural

Director of the Graduate School of Engineering and Science

ABSTRACT

RATIONAL DESIGN AND SYNTHESIS OF BODIPY DYES FOR MOLECULAR SENSING, LIGHT HARVESTING AND PHOTODYNAMIC APPLICATIONS

Tuğba Özdemir Kütük

PhD in Materials Science and Nanotechnology

Supervisor: Prof. Dr. Engin Umut Akkaya

September, 2014

BODIPY dyes have been addressed in many applications due to highly important features. These unique properties can be summarized as high photostability, high extinction coefficient, easy functionality, etc. Thus, tremendous studies have been published and, ion sensing, photodynamic therapy, dye-sensitized solar cells and light harvesting are some of the areas that BODIPY dyes have been utilized. In this thesis, BODIPY dyes were functionalized to be used for different concepts. In the first study, the main purpose was to seek for ion signaling differences of two isomeric tetra-styryl BODIPY dyes with charge donor ligand located at 1,7 *versus* 3,5 positions. Second work focuses on the light harvesting concept with the use of tetra-styryl BODIPY derivatives. Third study describes the coupling of energy transfer with internal charge transfer to monitor the alterations in intensity ratios, so, dynamic range of the fluorescent probe is improved. Design and synthesis of BODIPY dyes for detection of biological thiols in aqueous solution both chromogenically and fluorogenically was given in fourth study. Another biologically important molecule, hydrogen sulfide is selectively detected via BODIPY-based probe and depicted in the fifth study. In the sixth work, persistent luminescent nanoparticles are attached to BODIPY-based photosensitizer to activate the photodynamic action.

Keywords: ion sensing, excitation energy transfer, light harvesting, biological thiols, hydrogen sulfide, photodynamic therapy, BODIPY.

ÖZET

BODIPY BOYASININ MOLEKÜLER SENSÖRLER, IŞIK HASAT EDEBİLEN SİSTEMLER VE FOTODİNAMİK TERAPİ UYGULAMALARI İÇİN RASYONEL TASARIMI VE SENTEZİ

Tuğba Özdemir Kütük
Malzeme Bilimi ve Nanoteknoloji, Doktora
Tez Yöneticisi: Prof. Dr. Engin Umut Akkaya
Eylül, 2014

BODIPY sahip olduğu çok önemli özelliklerinden dolayı, birçok uygulamada kullanılmaktadır. Bu önemli özellikler, ışık altında bozulmaması, yüksek ektinksiyon katsayısına sahip olması, kolaylıkla fonksiyonlandırılabilmesi olarak özetlenebilir. Bu sebeple, yüksek sayıda yayınlar yapılmaktadır ve iyon sensörleri, fotodinamik terapi, boya duyarlı güneş pilleri, ışık hasat edebilen sistemler, BODIPY boyasının kullanıldığı alanlardan bazılarıdır. Bu tezde, BODIPY boyası farklı konseptler için fonksiyonlandırılmıştır. İlk çalışmada, başlıca amaç, iki adet tetra-stiril isomerik BODIPY boyalarının, yük verici ligandın 1 ve 7 veya 3 ve 5 pozisyonlarına bağlanmasına göre vereceği sinyalin farklılığının incelenmesidir. İkinci çalışma tetra-stiril BODIPY türevleri kullanılarak, ışık hasat edebilen sistemler konseptini içermektedir. Üçüncü çalışma, enerji transferi konsepti ile molekül içi yük transferi konsepti, sinyal şiddeti oranlarındaki farklılıkları gözlemlemek üzere birleştirilmiştir ve böylece fluoresans probun dinamik aralığı geliştirilmiştir. BODIPY boyalarının biyolojik tiyollerin suda kromojenik ve florojenik algılanmasının tasarımı ve sentezi dördüncü çalışmada verilmiştir. Biyolojik açıdan büyük öneme sahip olan hidrojen sülfür molekülünün, BODIPY-tabanlı boya kullanılarak seçici olarak algılanması beşinci çalışmanın konusunu oluşturmaktadır. Altıncı çalışmada, kalıcı lüminesans özelliği gösteren nanopartiküllerin, BODIPY tabanlı fotosensitizere kovalent olarak bağlanması ve fotodinamik terapinin aktifleşmesi hedeflenmektedir.

Anahtar kelimeler: iyon sensörü, ekzitasyon enerji transferi, ışık hasat edebilen sistemler, biyolojik tiyoller, hidrojen sülfür, fotodinamik terapi, BODIPY.

Dedicated to my family

ACKNOWLEDGEMENT

First and foremost, I would like to thank my supervisor, Prof. Dr. Engin Umut Akkaya, for his deep insight, intense knowledge and support throughout my graduate studies. No words can express my feelings deeply but I feel very lucky to be a member of Prof. Akkaya's Supramolecular Laboratory and work with him. Beyond his academic supervision in my projects, Akkaya's enthusiasm, cheerfulness and his positive attitudes towards us inspire me. Shortly, he has been a great advisor and none of the accomplishments in this thesis would be possible without his mentorship. I consider choosing the Akkaya's group for my graduate studies to be the one of the best decisions that I made in my life.

I would like to gratefully acknowledge my Thesis Committee Members, Assoc. Prof. Dr. Dönüş Tuncel and Assist. Prof. Dr. Salih Özçubukçu for their encouraging and fruitful discussions and advices for four years. Also, I would like to express my deep appreciation to Assist. Prof. Dr. H. Tarık Baytekin for participating the dissertation committee.

Also special thanks to Assist. Prof. Dr. Serdar Atılgan and Assoc. Prof. Dr. Özgür Altan Bozdemir, for their advices and invaluable friendships from the very beginning. Thank you very much for your endless support starting from the day I started lab studies to today. You will be in my life in perPeTuity.

I would like to thank Dr. Ruslan Guliyev, Dr. Fazlı Sözmen, Dr.Onur Büyükçakır, Dr. Esra Tanrıverdi Eçik, Dr. Murat Işık and Ziya Köstereli for their patience, great friendship and all their valuable contributions to the projects that we worked on together.

Big thanks must be given to my comrade, Safacan Kölemen for his friendship and for all of the fun times we had in and out of lab. I will truly miss working with him. We had great memories and we will have great memories. It is because of him that I kept my sanity during very hard times at the beginning of my PhD.

I would also like to thank our collaborators: Assist. Prof. Dr. Yavuz Dede and Soydan Yalçın for conducting theoretical studies and invaluable discussions. I also want to thank Assist. Prof. Dr. Turgay Tekinay and Dr. Sevcan Mamur for the cell culture studies.

I would like to thank former and present group members of the Akkaya group Dr. Yusuf Çakmak, Dr. Sündüs Erbaş Çakmak, Tuğçe Durgut, Yiğit Altay, Tuba Yaşar, Tuğrul Nalbantoğlu, Bilal Uyar, Ahmet Atılgan, Nisa Yeşilgül, Hale Atılgan, Tuğçe Karataş, Jose Bila, Ceren Çamur, Darika Okayev, Cansu Kaya, Melek Baydar, Dr. Özlem Seven, Dr. Dilek Taşgın, Seylan Ayan, Özge Yılmaz, Veli Polat, Işın Sakallıoğlu and Deniz Yıldız for creating a great environment in which to work and for their valuable input to my projects. I had wonderful people around me.

In particular, and in no particular order, thank you my dear friends, Oya&Bora Bilgiç, Dr. Asuman& Dr. Görkem Günbaş, Birsu Teoman, Nurhan& Reşat Çiftçi and their beautiful daughter Cemre for ever-lasting support, great friendship and for all of the fun times we had. We are a great family. Besides being close friends, I would like to thank Bora Bilgiç for design of the graphical abstracts and Dr. Görkem Günbaş for the assistance in End Note and invaluable discussions.

I would like to thank my mother, Sevim Özdemir and father, Ergün Özdemir. No words can describe how lucky I am to have you as my parents. Your constant love, support and guidance made me who I am today. My amazing sister, Sakine Özdemir, I can only say that the world would be meaningless without you. Also, I would like to thank Lals for their endless support and great love. Furthermore, I would like to thank to my mother- and father-in-law, Şükran and Nihat Kütük who have always loved me as their own daughter. Furthermore, thank you to second sister and brother, Suna-Bülent Kavan and their beautiful daughter Beren for support and kindness.

Most importantly, I would like to thank my husband, İlker Kütük for his endless love, kindness, patience and understanding. Thank you for being there for me every time I needed you. He has stood by me throughout this journey and continually inspires me.

LIST OF ABBREVIATIONS

AcOH	**:**	Acetic Acid
BODIPY	**:**	Boradiazaindacene
$CHCl_3$	**:**	Chloroform
DDQ	**:**	Dichlorodicyanoquinone
DMF	**:**	Dimethylformamide
ET	**:**	Energy Transfer
Et_3N	**:**	Triethylamine
FRET	**:**	Förster Resonance Energy Transfer
HOMO	**:**	Highest Occupied Molecular Orbital
ICT	**:**	Internal Charge Transfer
IFE	**:**	Inner Filter Effect
LUMO	**:**	Lowest Unoccupied Molecular Orbital
MALDI	**:**	Matrix-Assisted Laser Desorption/Ionization
MS	**:**	Mass Spectroscopy
NMR	**:**	Nuclear Magnetic Resonance
PeT	**:**	Photoinduced Electron Transfer
TFA	**:**	Trifluoroacetic Acid
THF	**:**	Tetrahydrofuran
TLC	**:**	Thin Layer Chromotography
TOF	**:**	Time of Flight

TABLE OF CONTENTS

1. INTRODUCTION 1

2. BACKGROUND 6

2.1. Photophysical Processes in Fluorescent Probes 6

2.1.1. Photoinduced Electron Transfer (PeT) 7

2.1.2. Internal Charge Transfer (ICT) 9

2.1.3. Energy Transfer Mechanism 11

2.1.3.1. Dexter Type Energy Transfer 12

2.1.3.2. Förster Type Energy Transfer 13

2.1.3.3. FRET-based Fluorescent Probes 16

2.1.3.4. Determination of FRET Efficiency 19

2.1.4. Excimer Formation 20

2.2. Near-infrared fluorescent probes 21

2.2.1. BODIPY 22

2.3. Significance of Mercury (II) 26

2.3.1. Hg (II) Fluorescent Probes 27

2.4. Importance of Biological Thiols 29

2.4.1. Detection of Thiols Based on Michael addition 30

2.4.2. Detection of Thiols Based on Cleavage of Sulfonamide and sulfonate 32

2.4.3. Detection of Thiols Based on Cyclization with Aldehydes 33

2.4.4. Detection of Thiols Based on Disulfide Bond Cleavage 34

2.4.5. Detection of Thiols Based on Metal Ions 34

2.5. Significance of Hydrogen Sulfide (H_2S) 35

2.5.1. H_2S Probes Based on Reduction reactions 36

2.5.2. H_2S Probes Based on Nucleophilic Attack 38

2.5.3. H_2S Probes Based on Copper ion 41
2.6. Photodynamic Therapy 41
2.6.1. Fundamentals of Photophysics behind PDT 42
2.6.2. Fundamentals of Photochemistry behind PDT 43
2.6.3. Importance of Light 44
2.6.4. Photosensitizers 45
2.6.4.1. BODIPY Dyes as Photosensitizers 46
2.6.5. Modes of Cell Death 49
2.6.6. Activatable Probe Design 50
2.6.7. Disulfide Bridge as a Clevable Linker-activation by Glutathione 53
2.6.8. Persistent Luminescence 55
2.6.8.1. Persistent Luminescent Nanoparticles 58
3. Rational Design of Ion Responsive, Isomeric Near-IR BODIPY Dyes 61
3.1. Objective 62
3.2. Introduction 62
3.3. Results and Discussions 63
3.4. Conclusion 72
3.5. Experimental Details 73
4. Dendritic Energy Transfer and Determination of Energy Transfer Based on Tetra-Styryl BODIPY Derivatives 82
4.1. Objective 83
4.2. Introduction 83
4.3. Result and Discussion 84
4.4. Conclusion 89
4.5. Experimental Details 90

5. Coupling ICT Process to Excitation Energy Transfer: Improved Stokes Shift for Selective Hg (II) Sensing 97

5.1. Objective 98

5.2. Introduction 98

5.3. Result and Discussion 99

5.4. Conclusion 104

5.5. Experimental Details 105

6. Chromogenic and Fluorogenic Sensing of Biological Thiols in Aqueous Solutions Using BODIPY-Based Reagent 112

6.1. Objective 113

6.2. Introduction 113

6.3. Results and Discussion 114

6.4. Conclusion 121

6.5. Experimental Details 121

7. Fast Responding and Selective Near- IR BODIPY Dyes for Hydrogen Sulfide Sensing 129

7.1. Objective 130

7.2. Introduction 130

7.3. Results and Discussion 131

7.4. Conclusion 136

7.5. Experimental Details 137

8. Persistent Luminescent Nanoparticles (PLNP) Mediated Activation of Photosensitizers for Photodynamic Therapy 141

8.1. Objective 142

8.2. Introduction 142

8.3. Results and Discussion 144
8.4. Conclusion 156
8.5. Experimental Details 157
9. CONCLUSION 169
10. BIBLIOGRAPHY 172
11. APPENDIX 193

LIST OF FIGURES

Figure 1. Molecular orbital diagrams for reductive PET. 7
Figure 2. PeT-based probe for Zn (II). 8
Figure 3. Some examples of fluorescent PET sensors for biomacromolecules. 8
Figure 4. Band gap changes on interactions with cations of ICT type sensors. 10
Figure 5. Example for ICT type sensor for Hg (II). 10
Figure 6. Schematic illustration of Förster and Dexter types of energy transfer. 11
Figure 7. Schematic representation of Dexter electron exchange mechanism. 12
Figure 8. Literature example for through bond energy transfer. 13
Figure 9. Schematic representation of FRET 14
Figure 10. Schematic representation of Förster energy transfer mechanism. 14
Figure 11. Literature example of Förster mechanism. 15
Figure 12. Design principles of FRET-based fluorescent probes (Copyright © 2013, American Chemical Society, Reprinted with permission from ref (26)).[26] 16
Figure 13. Fluorescent probes 1–3 based on a FRET mechanism. 17
Figure 14. Fluorescent probes 1–3 based on a FRET mechanism. 18
Figure 15. Fluorescent probes 1–3 based on a FRET mechanism (Copyright © 2009, American Society for Biochemistry and Molecular Biology, Reprinted with permission from ref (29)).[29] 18
Figure 16. Schematic representation of excimer formation (Copyright © 2013, American Chemical Society, Reprinted with permission from ref (26)).[26] 20
Figure 17. Literature example of fluorescent probes functioning *via* excimer formation. 20
Figure 18. Some of the common dyes used in fluorescent probes. 21
Figure 19. The numbering in BODIPY core 22
Figure 20. Available positions for electrophilic sustitution on BODIPY core 23
Figure 21. Knoevenagel condensation of 3,5-methyl substituents with aromatic aldehydes 24
Figure 22. Structures of the tetra-styryl BODIPY derivatives 24
Figure 23. Schematic view of 1,3,5,7-tetrastyryl BODIPY derivatives 25

Figure 24. Illustration of tetra-styryl derivatives including formyl groups at 7-, and 1,7-positions. 25
Figure 25. The visual representation of tetra styryl BODIPY dye in PBS buffer pH 7.4 in the absence and presence of L-cysteine 26
Figure 26. FRET-based fluorescent probe for detection of Hg (II). 27
Figure 27. BODIPY-based fluorescent probe for detection of Hg (II). 28
Figure 28. BODIPY-based fluorescent probe utilizing PET and ICT processes for detection of Hg (II)..... 28
Figure 29. Chemical structures of cysteine, homocysteine and glutathione. 29
Figure 30. Some examples for thiol probe based on Michael addition..... 30
Figure 31. Example for thiol probe based on open chain Michael addition 31
Figure 32. Thiol probe based on nitro-olefin moiety 31
Figure 33. Thiol probe based on ring opening Michael addition..... 32
Figure 34. PeT-based thiol probe based on Michael addition..... 32
Figure 35. Thiol probe based on cyclization of aldehydes..... 33
Figure 36. Thiol probe based on disulfide bond cleavage 34
Figure 37. Thiol probe based on metal ions..... 34
Figure 38. Endogenous synthesis of H_2S in mammalian cells (Copyright © 2013, American Chemical Society, Reprinted with permission from ref (69)).[69] 35
Figure 39. Examples for fluorescent H_2S probe based on azide reduction. 37
Figure 40. Another example for fluorescent H_2S probe based on azide reduction. ... 37
Figure 41. Reduction-based H_2S fluorescent probes in the literature. 38
Figure 42. H_2S detection based on nucleophilic attack to an aldehyde followed by intramolecular attack on an olefin..... 39
Figure 43. H_2S detection based on nucleophilic attack on an activated electrophile followed by attack on an ester-bound fluorophore. 40
Figure 44. The reaction mechanism for Michael addition-cyclization for H_2S and other thiols..... 40
Figure 45. H_2S detection based on nucleophilic attack on an electrophilic center to break fluorophore conjugation. 40
Figure 46. H_2S detection based on copper ion affinity of sulfides..... 41
Figure 47. Photophysical processes in PDT.[90] 42

Figure 48. Molecular structures of non-halogenated and halogenated BODIPY dyes 47
Figure 49. Halogenated BODIPY derivatives for photodynamic therapy application.[37] 47
Figure 50. BODIPY- C_{60} derivative for photodynamic therapy application. 48
Figure 51. Orthogonal BODIPY dimers for photodynamic therapy application. 49
Figure 52. Self-quenching based activable probe. 52
Figure 53. Gold nanorod based activable probe. (Copyright © 2013, John Wiley and Sons, Reprinted with permission from ref (117)) 52
Figure 54. Disulfide reduction based FRET probe. 54
Figure 55. Disulfide reduction based FRET probe. (Copyright © 2014, American Chemical Society, Reprinted with permission from ref (122)) 55
Figure 56. Schematic representation of energy diagram for fluorescence, phosphorescence and afterglow. 56
Figure 57. PLNPs in in vivo imaging.[131] 58
Figure 58. Modification of PLNP with biotin and Rak-2. 59
Figure 59. Schematic demonstration of the FRET based inhibition assay for AFP using PLNPs. 60
Figure 60. Structures of target compounds 1, 2, 3, 4. (Copyright © 2014, Royal Society of Chemistry, Reprinted with permission from ref (142)).[142] 63
Figure 61. Synthesis of target compounds (Copyright © 2014, Royal Society of Chemistry, Reprinted with permission from ref (142)). 64
Figure 62. Electronic absorption and emission spectra of 1 (0.5 μM) in THF in absence and presence of various metal ions. Added metal ion concentrations were 5 μM. Excitation wavelength was 710 nm. (Copyright © 2014, Royal Society of Chemistry, Reprinted with permission from ref (142)) 65
Figure 63. Electronic absorption and emission spectra of 2 (1.0 μM) in THF in absence and presence of various metal ions. Added metal ion concentrations were 10 μM. Excitation wavelength is 725 nm. (Copyright © 2014, Royal Society of Chemistry, Reprinted with permission from ref (142)) 65

Figure 64. Emission intensityresponse of 1 (0.5 μM) , with 5 μM of a comPeTing metal ion followed by addition of 5 μM Hg^{2+} in THF.Excitation wavelength was 710 nm with a slit width of 5-5 nm. (Copyright © 2014, Royal Society of Chemistry, Reprinted with permission from ref (142)) 66
Figure 65. Emission intensityresponse of 2 (1.0 μM) with 10 μM of a comPeTing metal ion followed by addition of 10 μM Hg^{2+} in THF. Excitation wavelength was 725 nm with a slit width of 5-5 nm. (Copyright © 2014, Royal Society of Chemistry, Reprinted with permission from ref (142)) 66
Figure 66. The electronic absorption and emission spectra of 3 (1.9 μM) in presence of excess Hg(II) in 10 mM HEPES:CH_3CN (50:50, v/v, pH=7.20, 25 °C). (excitation wavelength =730 nm) (Copyright © 2014, Royal Society of Chemistry, Reprinted with permission from ref (142)) 67
Figure 67. The electronic absorption and emission spectra of 4 (2.8 μM) in presence of excess Hg(II) in 10 mM HEPES:CH_3CN(50:50, v/v, pH=7.20,25°C). (Copyright © 2014, Royal Society of Chemistry, Reprinted with permission from ref (142)) ... 67
Figure 68. Calorimetric binding isotherm for the compound 3 (right, 0.4 mM 3 titrated with 5 mM $Hg(ClO_4)_2$) and 4 (left, 0.14 mM 4 titrated with 2 mM $Hg(ClO_4)_2$) in acetonitrile. (Copyright © 2014, Royal Society of Chemistry, Reprinted with permission from ref (142)) 68
Figure 69. Computational models. (Copyright © 2014, Royal Society of Chemistry, Reprinted with permission from ref (142)) 69
Figure 70. Computed absorption spectra. (Experimental values in parentheses) (Copyright © 2014, Royal Society of Chemistry, Reprinted with permission from ref (142)) 69
Figure 71. MO plots and energies (eV) for transitions with high oscillator strength. (Copyright © 2014, Royal Society of Chemistry, Reprinted with permission from ref (142)) 71
Figure 72. Reaction pathway of target compounds. (Copyright © 2012, American Chemical Society, Reprinted with permission from ref (158))[158] 85
Figure 73. Absorbance spectra of compounds 4, 6, 7, 8 and 9 at equal absorbances in $CHCl_3$, at 525 nm for 4 and 8, at 655 nm for 6 and 9, at 730 nm for 7, 8 and 9.

(Copyright © 2012, American Chemical Society, Reprinted with permission from ref (158)) 86
Figure 74. The emission spectra of 4, 7, and 8 at equal absorbances at 525 nm in $CHCl_3$. Inset: Energy transfer from peripheral BODIPY units 4 to tetrastyryl-BODIPY core 7 in light harvesting dendrimer 8. (Copyright © 2012, American Chemical Society, Reprinted with permission from ref (158)) 86
Figure 75. The emission spectra of 6, 7, and 9 at equal absorbances at 655 nm in $CHCl_3$. Inset: Energy transfer from di-styryl BODIPY units 4 to tetrastyryl-BODIPY core 7 in light harvesting dendrimer 9. (Copyright © 2012, American Chemical Society, Reprinted with permission from ref (158)) 87
Figure 76 . Percent energy transfer efficiency of 8 (black solid). Excitation spectrum of 8 (dot line) and absorption spectrum of 8 (dashed) (normalized at 735 nm). (Copyright © 2012, American Chemical Society, Reprinted with permission from ref (158)) 87
Figure 77. Percent energy transfer efficiency of 9 (black solid). Excitation spectrum of 9 (dot line) and absorption spectrum of 9 (dashed) (normalized at 735 nm). (Copyright © 2012, American Chemical Society, Reprinted with permission from ref (158)) 87
Figure 78. Synthesis of the target compound. (Copyright © 2010, American Chemical Society, Reprinted with permission from ref (165))[165] 100
Figure 79. Absorbance spectra of the chemosensor compound 12 (1.5 μM) in THF in the absence and presence of various metal ions. Added metal ion concentrations were 10 μM. (Copyright © 2010, American Chemical Society, Reprinted with permission from ref (165)) 101
Figure 80. Emission spectra of compound 12 in THF (1.5 μM) in THF in the absence and presence of various metal ions. Added metal ion concentrations were 10.0×10^{-6} M. Excitation wavelength is 480 nm. (Copyright © 2010, American Chemical Society, Reprinted with permission from ref (165)) 101
Figure 81. Excitation spectra of a model compound (4) and compound 12 with and without 10 μM Hg(II). For compound 4, the emission data was collected at 518 nm, and for the longer wavelength peak the data was collected at the isoemissive point

710 nm. (Copyright © 2010, American Chemical Society, Reprinted with permission from ref (165))..... 102
Figure 82. Hg(II) titration of the chemosensor compound 12. Hg (II) concentration is varied between 0 to 15 μM in THF. The concentration of 12 was 1.5 μM. (Copyright © 2010, American Chemical Society, Reprinted with permission from ref (165)). 102
Figure 83. Hg (II) titration of the chemosensor 12 in THF. Ion concentration was varied between 0 to 15 μM. The chemosensor concentration was held at 1.5 μM. (Copyright © 2010, American Chemical Society, Reprinted with permission from ref (165))..... 103
Figure 84. The free dye 12 (chemosensor) concentration was set at 1.5 μM, the concentration of the comPeTing cation 100 mM and concentration of Hg^{2+} was 10 mM. Excitation was at 500 nm with a slit width 5.0 nm. (Copyright © 2010, American Chemical Society, Reprinted with permission from ref (165))..... 104
Figure 85. Design elements of the nitroethenyl-BODIPY conjugate thiol probe 1. (Copyright © 2010, American Chemical Society, Reprinted with permission from ref (196))[196]..... 114
Figure 86. Stacked partial ^{1}H-NMR spectra of thiol probe 2 (A) and conjugate addition product 3 (B) in $CDCl_3$ at 25 °C. (Copyright © 2010, American Chemical Society, Reprinted with permission from ref (196))..... 115
Figure 87. Synthetic route for the target Thiol Probe 1. (Copyright © 2010, American Chemical Society, Reprinted with permission from ref (196))..... 116
Figure 88. UV-vis absorption spectra (A) and fluorescence spectra (B) of the thiol probe 1 (4 μM) upon increased Cys concentrations (0-400 equiv.) in 50 mM HEPES:CH_3CN (80:20, v/v, pH=7.20, λ_{ex} 500 nm at 25 °C). (Copyright © 2010, American Chemical Society, Reprinted with permission from ref (196))..... 116
Figure 89. Absorption and fluorescence spectra of Thiol Probe 1 (4 μM) upon addition of 200 eqv. of Cys, Hcy and GSH in 50 mM HEPES:CH_3CN (80:20, v/v, pH=7.2, λex 500 nm at 25 °C). (Copyright © 2010, American Chemical Society, Reprinted with permission from ref (196))..... 117
Figure 90. Kinetic measurements of Thiol Probe 1 upon addition of 200 eqv. of Cys, Hcy and GSH in 50 mM HEPES:CH_3CN (80:20, v/v, pH=7.2, λex 518 nm at 25 °C,

time interval: 30s). (Copyright © 2010, American Chemical Society, Reprinted with permission from ref (196)) 118
Figure 91. UV-vis absorption and fluorescence spectra of the Thiol Probe 1 (4 μM) upon increased Cys concentrations (0-400 equiv.) in 50 mM HEPES (pH=7.2, λex 500 nm at 25 °C). (Copyright © 2010, American Chemical Society, Reprinted with permission from ref (196)) 118
Figure 92. Fluorescence response of the thiol probe 1 (4 μM) towards biothiols (Cys, Hcy and GSH; 200 equiv. each)) and other natural amino acids (400 equiv.) in 50 mM HEPES:CH_3CN (80:20, v/v, pH=7.20, λ_{ex} 500 nm at 25 °C). (Copyright © 2010, American Chemical Society, Reprinted with permission from ref (196)) 119
Figure 93. Red-emitting nitroolefin-BODIPY conjugate thiol probe 7. (Copyright © 2010, American Chemical Society, Reprinted with permission from ref (196)) 119
Figure 94. Synthetic route for the target Thiol Probe 7. (Copyright © 2010, American Chemical Society, Reprinted with permission from ref (196)) 120
Figure 95. UV-vis absorption and fluorescence spectra of the Thiol Probe 7 (4 μM) upon increased Cys concentrations (0-1000 equiv.) in 50 mM HEPES:CH_3CN (80:20, v/v, pH=7.2, λex 600 nm at 25 °C). (Copyright © 2010, American Chemical Society, Reprinted with permission from ref (196)) 121
Figure 96. Synthesis of target probe 1. (Copyright © 2014, Royal Society of Chemistry, Reprinted with permission from ref (220))[220] 132
Figure 97. Absorption and emission spectra of 1 (2.0 μM) in 20 mM HEPES:CH_3CN (40:60, v/v, pH=7.20, 25 °C) in increasing Na_2S concentrations. Excitation wavelength is 650 nm. Experiments were done in triplicate. (Copyright © 2014, Royal Society of Chemistry, Reprinted with permission from ref (220)) 133
Figure 98. Absorption and emission spectra of probe 1 (2.0 μM) in 20 mM HEPES:CH_3CN (40:60, v/v, pH=7.20, 25 °C) in absence and presence of various anions. Added Na_2S concentration is 50 μM and anion concentrations were 100 μM. Excitation wavelength is 650 nm. Experiments were done in triplicate. (Copyright © 2014, Royal Society of Chemistry, Reprinted with permission from ref (220)) 134
Figure 99. Emission intensity response of probe 1 (2.0 μM) with 50 equiv. of a comPeTing anions followed by addition of 50 equiv. Na_2S in 20 mM

HEPES:CH_3CN (40:60, v/v, pH=7.20, 25 °C). Excitation wavelength was 650 nm with a slit width of 5-5 nm. (Copyright © 2014, Royal Society of Chemistry, Reprinted with permission from ref (220)) 134
Figure 100. Stacked partial ^{1}H-NMR spectra probe 1 (A) and the same spectrum after the addition of Na_2S (B) in acetonitrile-D_3 at 25 ^oC. (Copyright © 2014, Royal Society of Chemistry, Reprinted with permission from ref (220)) 135
Figure 101. Mass spectrum of Compound 1 after addition the addition of Na_2S (Calcd: 1094.568 [M+Na]+ , Found:1094.563 [M+Na]+, Δ=4.52 ppm.) (Copyright © 2014, Royal Society of Chemistry, Reprinted with permission from ref (220)) . 135
Figure 102. Confocal microscopy images of showing the H_2S response of probe 1 in MCF-7 cells. (Left) MCF-7 cells incubated with probe 1 (4 μM) for 30 min. at 37 ^oC (Right) MCF-7 cells incubated with probe 1 (4 μM) for 2 h, after which 100 eqv. Na_2S was added. The cells were imaged after additional incubation for 30 min. at 37 ^oC. (Copyright © 2014, Royal Society of Chemistry, Reprinted with permission from ref (220)) 136
Figure 103. The chemical structure and the functions of the groups attached..... 143
Figure 104. The working principle of the target. 144
Figure 105. The synthetic route of the PLNP. 145
Figure 106. Size of the different nanoparticles determined by DLS (top) and Zeta potential measurements (bottom) of synthesized PLNP. 146
Figure 107. Transmission electron microscopy image (scale bar = 200 nm) (A), XRD pattern (B) and excitation spectrum (C) of synthesized PLNP. 147
Figure 108. Previous reaction pathway of target compounds 148
Figure 109. (a) Excitation (blue curve, at the emission of 695 nm) and emission (red curve, excitation at 254 nm) spectra of the LPLNPs powder. The inset shows the digital photos of LPLNPs powder under 254 nm UV excitation (left), and 5 s after stopping UV irradiation (right). (b) Excitation spectra of undoped ZGGO powder (red curve) and LPLNPs powder (blue curve) at the emission of 695 nm, and emission spectra of undoped ZGGO powder (black curve) under the excitation of 254 nm. The inset shows the digital photo of undoped ZGGO powder under 254 nm UV excitation. (c) Excitation (blue curve, emission at 700 nm) and emission (red

curve, excitation at 254 nm) spectra of the aqueous dispersion of LPLNPs (1 mg ml−1). The inset shows the digital photo of the aqueous dispersion of LPLNPs under 254 nm UV excitation. (Copyright © 2013, American Chemical Society, Reprinted with permission from ref (234)) 151
Figure 110. The proposed mechanism for persistent energy transfer between ZGGO and Cr^{3+}. (Copyright © 2013, American Chemical Society, Reprinted with permission from ref (234)) 152
Figure 111. Current reaction pathway of target compounds. 153
Figure 112. The synthetic pathway of compound 16 and PLNP-Compound 16 conjugate. 154
Figure 113. The (a) digital photograph and (b) absorbance spectra of only PLNP and PLNP-Compound 16 conjugate. 155
Figure 114. Reaction of singlet oxygen with 2,2'-(Anthracene-9,10-diylbis(methylene))dimalonic acid..... 155
Figure 115. Relative singlet oxygen efficiency of only trap, only PLNP and PLNP-Compound 16 conjugate in aqueous solution detected by the absorbance decrease of 2'-(Anthracene-9,10 diylbis (methylene))dimalonic acid (ADMDA) at 376 nm with time. During 20 minutes, the samples were kept under dark and the following 60 min; the samples were irradiated with 254 nm light using UV lamp..... 156

LIST OF TABLES

Table 1. Binding Constants Determined by Isothermal Titration Calorimetry (ITC) for compound 3 and 4. (Copyright © 2014, Royal Society of Chemistry, Reprinted with permission from ref (142)) 68
Table 2. Summary of TDDFT Results [a] (Copyright © 2014, Royal Society of Chemistry, Reprinted with permission from ref (142)) 70
Table 3. MO Plots and Energies (eV) of BODIPY and Styryl-Substituted Derivatives at UB3LYP/cc-pVTZ//6-31G(d) Level of Theory. (Copyright © 2014, Royal Society of Chemistry, Reprinted with permission from ref (142)) 72
Table 4. Spectral data for BODIPY, distyryl-BODIPY and tetrastyryl-BODIPY dyes and light harvesting dendrimers. (Copyright © 2012, American Chemical Society, Reprinted with permission from ref (158)) 88
Table 5. Energy Transfer rate and efficiencies of Light harvesting dendrimers 8 and 9. (Copyright © 2012, American Chemical Society, Reprinted with permission from ref (158)) 89
Table 6. Lifetimes, FRET rate constants and efficiencies of Compound 4, 12, 12+ Hg(II). (Copyright © 2010, American Chemical Society, Reprinted with permission from ref (165)) 103
Table 7. Optical properties of the probes 1 and 7. (Copyright © 2010, American Chemical Society, Reprinted with permission from ref (196)) 120

CHAPTER 1

INTRODUCTION

During the last three decades, BODIPY has been used widely as a fluorescent probe and it still maintains its popularity. This popularity arises due the superior characteristics of BODIPY. To begin with, its derivatives can have strong absorption and/or fluorescence in the visible and near-IR region. Derivatization on the BODIPY core, which has seven positions suitable for functionalization, provides versatile characteristics. In addition, BODIPY dyes can be functionalized to be soluble in both organic and water. Moreover, they have high quantum yields and large extinction coefficients and they are stable under continuous illumination. Besides, they are almost insensitive to solvent polarity and pH of the medium and have narrow absorption and emission bandwidths, and so they give sharp peaks on emission spectra compared to other fluorophores such as fluorescein. In all chapters, BODIPY dyes were utilized for different applications.

In Chapter 3, the design and syntheses of two isomeric tetra-styryl BODIPY dyes and investigation of the signaling differences in terms of Hg (II) binding were described. The fluorescent detection and biological imaging of the specific molecules which are crucial in living systems have aroused attention due to its highly sensitive nature, cheapness and ease of processability compared to handling radioactive tracers for most biochemical measurements. Therefore, fluorescent chemosensors have a significant value for their simplicity and high sensitivity. According to the presence (or concentration) of the analyte which binds to the sensor, there can be changes in the fluorescence intensity, lifetime or a shift in fluorescence wavelength can occur. Nowadays, in the design of the chemosensors, near-IR dyes are widely used. Near-IR dyes having the spectral range between 650-900 nm are very advantageous. Firstly, background signal is reduced and light scattering turns out to be low. Therefore, deep penetration becomes feasible and it allows fluorescence imaging *in*

vivo and open the way for applications in photodynamic therapy. In this project, our aim was to investigate that according to attached positions, photophysical response of the BODIPY dyes upon ion binding are different. To explore this idea, we synthesized two isomeric tetrastryrl BODIPY dyes with Hg (II) responsive crown moiety. In the first design, crown moieties are placed on 1 and 7 positions of BODIPY core by Knoevenagel condensation. In the second one, these crown moieties are attached to 3 and 5 positions. When we performed the spectral measurements, we investigated some differences in terms of ion responses. Since the improvements in water soluble fluorescent probes are highly demanding for biological applications, to make these dyes biologically applicable, we synthesized the water soluble versions of the BODIPY dyes. Introduction of polyethylene glycol methyl ether and triethylene glycol groups enhances the water solubility; this is why we incorporated the PEG_{2000} and TEG groups to BODIPY unit. Theoretical calculations were conducted and principles underlying different spectroscopic properties and fluorescence turn on responses were explained *via* orbital analysis.

Chapter 4 describes the use of tetra-styryl BODIPY derivatives as light harvesters and the determination of energy transfer efficiency is discussed. The crucial role of excitation energy transfer arises as a result of involving in the biological processes such as photosynthesis which is a light harvesting system. In photosynthesis, the sun light is collected and the energy transferred to the reaction center to induce the initiation of reaction in chlorophyll. Excitation energy involves donor and acceptor parts and these parts are not conjugated, so this energy transfer is named as “through space” energy transfer. Since there is no conjugation between the units, the spectral overlap, the distance between them and relative orientation of the transition dipoles are required to be optimal in order to achieve efficient “through space” energy transfer. Efficacious harvesting of solar radiation needs careful design of chromophores. Multichromophoric systems which involve more than one donor chromophore to get absorbance in entire visible spectrum and near-IR is needed. The efficiency of energy transfer can be determined by using quantum yields or lifetime. However, it is estimated that the efficiency of multichromophoric assembles involving flexible linkers are originally bimolecular model showing upper limit for

calculated energy transfer. With this study, we tried to clarify the calculation of energy transfer efficiency which holds some permanent mistakes. Thus, in our design, we synthesized two tetra-styryl BODIPY harvesters and investigate the energy transfer efficiencies.

In Chapter 5, we coupled excitation energy transfer with internal charge transfer which is a standard signal transduction process. The importance of energy transfer and Hg (II) sensing is discussed above. In this design, since the energy transfer is efficient, an important amount of pseudo-Stokes shifts are obtained successfully. Another important achievement is that modulation of the excitation energy transfer via ion binding allows monitoring the changes in intensity ratios at a wider range, consequently, increasing the dynamic range of the molecular sensor. With this sense, we attached donor and acceptor BODIPY moieties with Click chemistry. Binding of Hg (II) to crown part causes a blue shift in emission, which correspondingly increases the spectral overlap between the donor and the acceptor. Additionally, ratiometric response is a bonus that is achieved with this design.

In Chapter 6, BODIPY was designed to give response for biological thiols both chromogenically and fluorogenically in aqueous solution. Both extracellular and intracellular concentrations of cysteine, homocysteine and glutathione are important biological parameters. Cysteine (Cys) deficiency may lead to childhood developmental problems, hair depigmentation, edema, lethargy, liver damage, and skin lesions. Homocysteine (Hcy) is a risk factor for Alzheimer's disease and may also indicate deficiencies in folate and cobalamine (Vit. B12). In addition, Hcy deficiency has been linked to cardiovascular disease as well. Glutathione (GSH) is a primary defense agent against oxidative damage with its high concentration that can go up to 5 mM inside the cells. In healthy cells and tissues, 90 % of it is present in the reduced GSH form, whereas 10 % is found in the oxidized disulfide form (GSSG). Due to above reasons, imaging of biological thiols with fluorescent probes that respond to these thiols by color change, emission wavelength change, or both is of prime importance. In our study, we designed two BODIPY dyes carrying nitroethenyl substituents in conjugation with the BODIPY core which yields probes that responds to biological thiols upon change in both absorbance and emission

wavelength. Both probes showed very fast and sensitive responses with color changes and “turn-on” fluorescence. As expected, this fluorescence enhancement is because of the reduction in the efficiency of the PeT process upon the reaction between Cys and nitroethenyl substituent on the probe yielding an increment in the energy level of the BODIPY centered LUMO. Under identical conditions, other biological thiols, such as homocysteine (Hcy) and glutathione (GSH), are resulted similar turn on fluorescence responses. Yet, controlling reaction time leads to faster response of Cys than that to Hcy and GSH.

Chapter 7 describes the design and synthesis of a BODIPY based, highly selective probe for hydrogen sulfide. This probe is then studied in living cells. Hydrogen sulfide (H_2S) is known as characteristic repulsive odor of rotten eggs, and attracts attention due to the roles on biological processes. As in the case of the other two gaseous signaling molecules, carbon monoxide (CO) and nitric oxide (NO), hydrogen sulfide is a biosynthetic gasotransmitter. Their production and function of these small gaseous molecules are different from the other messenger molecules. Also, having small size and charge neutrality, they can easily pass through the cellular membranes without affecting any cell signaling response. H_2S plays important role on many metabolic processes, such as cardiovascular protection, neuroprotective effect, arrangement of cell growth, calcium homeostasis and regulation of neurotransmission. Thus, the detection and real-time monitoring of H_2S is very crucial. In our design, two arylazido groups were used because H_2S is able to reduce this group. The reduction causes change in the charge transfer characteristics of the 3,5-distyryl substituents on the BODIPY core, producing a 20 nm bathochromic spectral shift in the absorption band, and quenching of the emission by 85% compared to the original intensity, through photoinduced electron transfer. The selectivity and fast responding properties offer the potential utility of the probe. In addition, hydrophilic moieties in its structure make the probe water soluble and thus appropriate for biological applications. Furthermore, added H_2S was successfully imaged inside the cells, suggesting that imaging of endogenously produced H_2S in real-time and in the near IR region of the spectrum can be realized.

Chapter 8 is related to the activation of photodynamic action with use of persistent luminescent nanoparticles. Photodynamic therapy has been considered to be a promising alternative to traditional cancer therapy methodologies such as surgery, chemotherapy and radiation therapy. However, its broader acceptance by the medical community is hampered since an external light energy is required to active the therapy. Light, even at the most tissue penetrating wavelengths (red to near IR) can go through mammalian tissues only a few millimeters. This limits the application of PDT to surface tumors, or those to which light can be delivered by fiber-optics. In our research group, we are trying to offer alternative methodologies to sensitize the dye (photosensitizers) component, so that external photonic excitation would not be needed. Once the photosensitizer is excited (by any means) it is expected to transfer its excitation energy to the dissolved oxygen in tumor tissues and thus generate singlet oxygen, which is the primary cytotoxic agent in photodynamic therapy. In this project, we are planning to use persistent luminescent nanoparticles (PLNP), which once excited, keep on emitting light for 24-48 hours. The photosensitizers that we synthesized were attached to the PLNP covalently. However, continuous excitation is not desired, as that would be harmful to the tissues starting from the injection site. To control the activity, we will incorporate a quencher unit, which will stop singlet oxygen generation unless it is cleaved from the PLNP by high glutathione concentrations found in cancer cells. So, the nanoconstruct, will not generate singlet oxygen in most tissues, but it will be activated in cancer cells, resulting in a selective agent which will destroy tumors the way PDT does, but without any need for external excitation. We studied the activity of our system by following singlet oxygen generation using chemical traps. The project is likely to offer a solution to remove one of the bottlenecks for the widespread application of photodynamic therapy.

CHAPTER 2

BACKGROUND

2.1. Photophysical Processes in Fluorescent Probes

Fluorescence sensing and imaging are highly demanding and strong techniques for detection of different chemical and biological analytes. After the report of Roger Y. Tsien's fluorescent probe for Ca^{2+} in 1980,[1] this technique drew remarkable attention in the past two decades. Important requirements must be satisfied for the sensor to be applicable in biological applications and these requirements can vary according to application. Selectivity for a specific analyte in presence of other analytes is one of the most important parameter.[2] Also, water-solubility is another key parameter for biological applications. For certain probes, cell-permeability, excitation at near-IR wavelength to reduce background fluorescence and low-toxicity can become the major considerations. Beside, ratiometric analysis allows more reliable quantitative analysis by minimizing extraneous factors such as photobleaching.[3] Although there are several parameters to consider, in general, fluorescent probes are superior compared to other techniques in terms of higher selectivity, sensitivity, fast response and higher resolution. Fluorescent sensors are mainly composed of two main moieties: receptor (recognition part) and fluorophore (reporter). The receptor part should have specific affinity towards the analyte and so it should not be affected by the light, pH, temperature, etc. The fluorophore part reports differences in signal when receptor binds to analyte. These differences can be in fluorescence intensity, shift in fluorescence wavelength or lifetime.[4]

In the design of the fluorescent probes, non-covalent interactions (hydrogen bonding, electrostatic, hydrophobic, hydrophilic, π-π, anion-π and coordination-based interactions) as well as many different types of reactions can be utilized.[5]

2.1.1. Photoinduced Electron Transfer (PeT)

In PeT process, there are three units: fluorophore (signaling unit), receptor for recognition of analyte and spacer between these two parts.

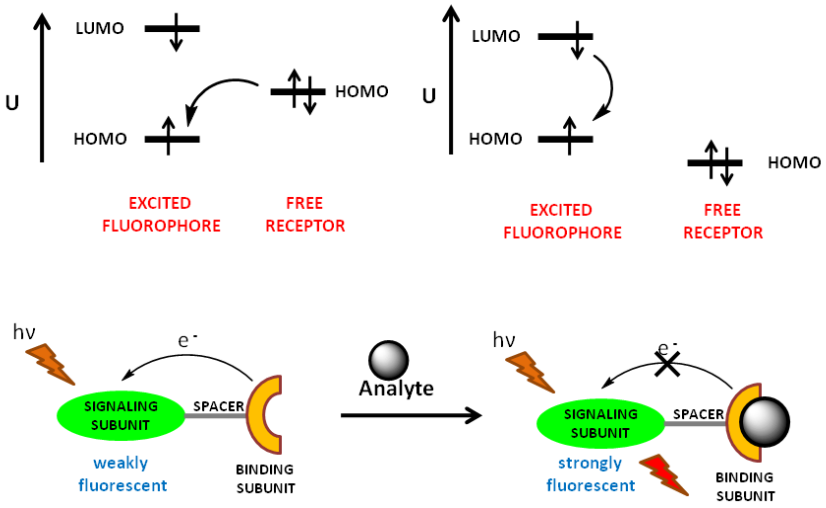


Figure 1. Molecular orbital diagrams for reductive PeT.

In the design of the PeT based probes, fluorophore is attached to high energy non-bonding electron pair containing (like nitrogen atom) receptor part via spacer unit. In the "off" state, the electron transfer from unbound receptor part to excited fluorophore causes fluorescence quenching. Yet, "on" state occurs when the receptor binds to analyte and so electron transfer is blocked and fluorescence intensity increases. With the irradiation of fluorophore, an electron in the highest occupied molecular orbital (HOMO) is raised to the lowest unoccupied molecular orbital (LUMO). If the non-bonding electron pair in the HOMO of the receptor has more energy than HOMO of the fluorophore, intramolecular PeT process becomes active and so fluorescence quenching occurs. With the binding of receptor to analyte, energy of the HOMO of the bound receptor decreases since oxidation potential of the donor increases. As a result, fluorescence enhancement takes place. (Figure 1) The principle of PeT process is the comPeTition between electron transfer and fluorescence.[6]

PeT based mechanism of sensing has been widely utilized in literature. For example, as shown in Figure 2, ZnAB was designed to detect Zn (II) cation by functionalization of BODIPY core at *meso* position with *N,N*-Bis (2-pyridyl-methyl)ethylenediamine.[7] *N,N*-Bis(2-pyridyl-methyl)ethylenediamine was used for acceptor moiety for Zn (II) and attached to BODIPY part via benzene ring. PeT

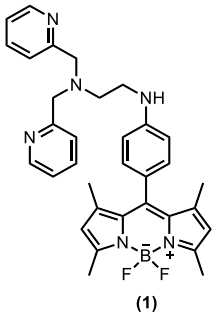


Figure 2. PeT-based probe for Zn (II).

mechanism is controlled by benzene ring at *meso* position because the dihedral angle between the benzene ring and BODIPY core is almost 90^{o}. Before addition of Zn (II), PeT process quenches the fluorescence so the emission intensity is low. On the other hand, with coordination of Zn (II), the reduction potential of the *meso*-substituent will be more negative and PeT process is blocked so fluorescence intensity increases.

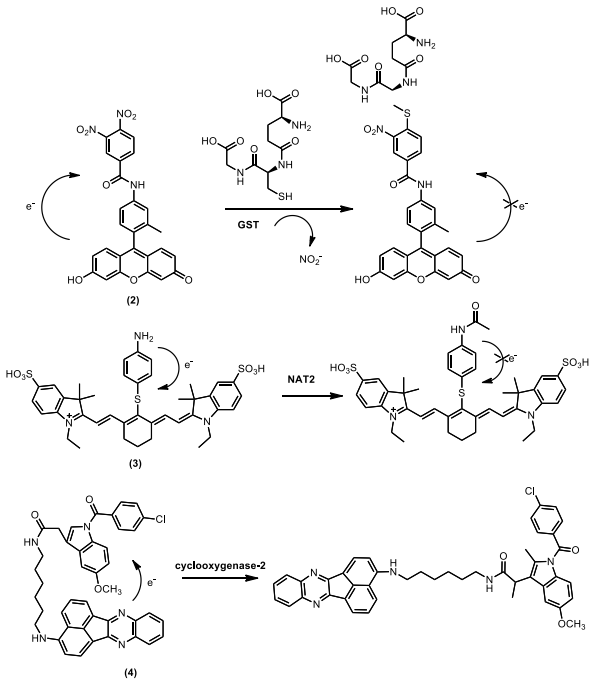


Figure 3. Some examples of fluorescent PET sensors for biomacromolecules**.**

PeT process is one of the most widely used sensing mechanisms in design of the small molecule fluorescent probes for bioimaging. Tremendous amount of examples are available in the literature and some of them are given in Figure 3. In the first example, "off-on" fluorescent probe for GST (Glutathione *S*-transferase, important for biological processes such as drug metabolism, protecting our body against endogenous reactive oxygen species (ROS)) is designed on the basis of PeT mechanism.[8] Second example decribes the PeT-based NAT (Arylamine *N*-acetyltransferases, having role on various significant pharmacological and toxicological reactions such as bioactivation reactions of arylamine carcinogens) fluorescent probe.[9] Fluorescent probe for COX-2 (Cyclooxygenase-2, biomarker for almost all cancer cell lines and used to differentiate cancer cells from normal ones) is well established based on PeT pathway as described in the third example.[10]

2.1.2. Internal Charge Transfer (ICT)

In the ICT type probes, receptor is directly attached to the fluorophore without spacer between the fluorophore and receptor parts, in other words, there is a conjugation between receptor and the π-electron system fluorophore moiety. In this design, fluorophore must include an electron-donating group such as $–NH_2$ and an electron-pulling group. With the excitation, ICT occurs from donor to acceptor.[11] Upon interaction of a receptor (electron- pushing moiety) with a cation, electron- pushing character of receptor decreases. Therefore, the conjugation is affected and blue shift is observed in the absorption spectrum. Charge-dipole interactions can be used to clarify this mechanism. With excitation, amino group will be positively charged and due to the interaction between this positively charged amino group and the cation, the excited state will be destabilized. Energy gap between S_0 and S_1 will increase and as a consequence of this process, blue shift is observed. Moreover, if the acceptor group like carbonyl group interacts with the cation, electron-pulling character of the receptor increases. According to charge-dipole interactions, the acceptor group is affected by the electron receptor and so the excited state is stabilized. Finally, red shift occurs upon decrease in energy gap between S_0 and S_1.[12] (Figure 4)

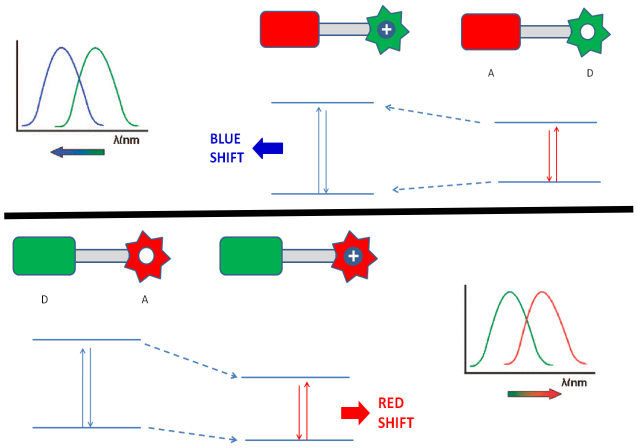


Figure 4. Band gap changes on interactions with cations of ICT type sensors.

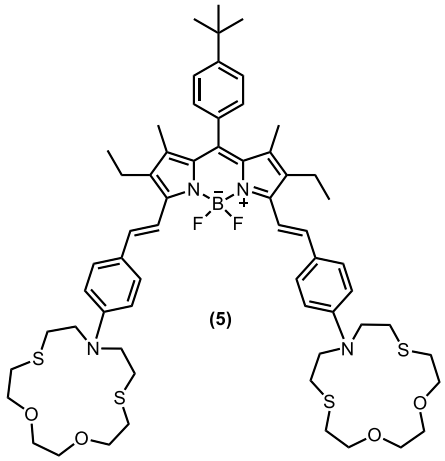


Figure 5. Example for ICT type sensor for Hg (II).

Figure 5 shows an example of ICT-based probe for Hg (II) ions.[13] Two chelating moieties were attached to BODIPY core via Knoevenagel condensation. In this design, dithia-dioxa-aza macrocycle is used as receptor part and known as Hg (II) selective ligand. In the absorbance spectrum, blue shift is observed due to the blocking of ICT process upon coordination of Hg (II) ions to the nitrogen donor atoms. Moreover, in absence of Hg (II), fluorescence is highly quenched due to the ICT process from crown moiety to BODIPY core. However, in presence of Hg (II), decrease in electron donation ability of two amino groups leads to strong fluorescence intensity with a large blue shift.

2.1.3. Energy Transfer Mechanism

In nature, photosynthesis involves light harvesting antenna system and light harvesting chromophores can seize photons from sunlight and channels its energy to the single reaction center. In this process, charge-separated states result in transformation of solar energy to chemical potential energy.[14] With this manner, design and synthesis of supramolecular systems that serve as artificial light harvesting systems have aroused great deal of interest in the past decade.[15] In energy transfer process, there are two main parts: donor (D) and acceptor (A). Energy is transferred from a chromophore in excited state (D) to the other chromophore in ground state (A).[16] Energy transfer can be observed via comparison of lifetimes, quantum yields, quenching of the donor emission or increase in acceptor emission.

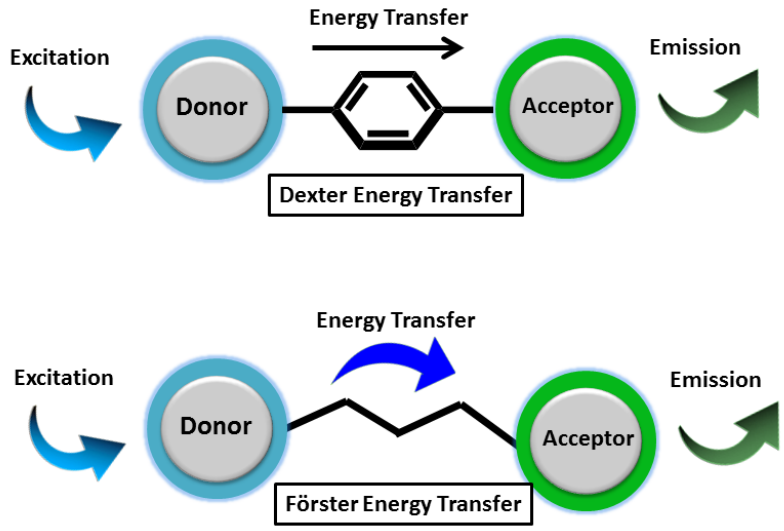


Figure 6. Schematic illustration of Förster and Dexter types of energy transfer.

Various deactivation pathways of the excited system can affect the energy transfer so appropriate chromophores should be used to overcome such distractions.[17]

There are two different types energy transfer mechanism which are Förster and Dexter mechanisms. (Figure 6)

2.1.3.1. Dexter Type Energy Transfer

Dexter type energy transfer is also known as electron transfer by "electron exchange". In this type, orbital overlap is required to enable the exchange of electrons from the highest occupied level of the donor to the lowest unoccupied level of the acceptor.[18] (Figure 7)

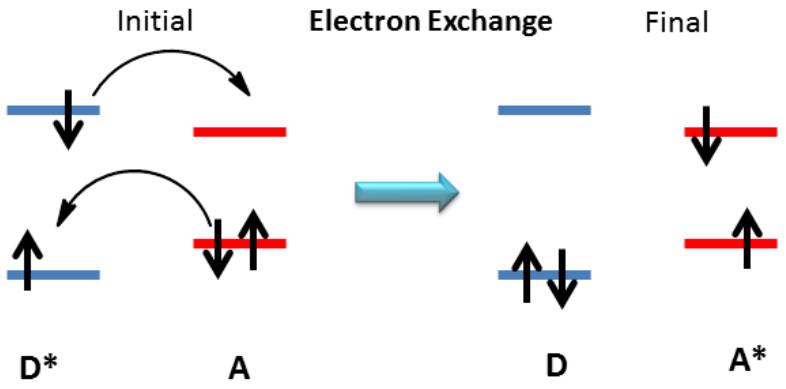


Figure 7. Schematic representation of Dexter electron exchange mechanism.

Rate constant equation for this type of energy transfer is given below.

$$K_{dexter} = K\ J\ \exp(-2R_{DA} / L)$$

where K is orbital interaction, J is the normalized spectral overlap integral, R_{DA} is the distance between donor and acceptor and finally L is the sum of van der Waals radii.[17]

Since orbital interaction decreases exponentially with distance from nuclei, the transfer probability changes almost exponentially with the donor-acceptor distance. Therefore, to get efficient Dexter type of energy transfer, very short distances between D-A is required so that overlap of electronic orbitals is fulfilled.[19] Dexter type of energy transfer is also called as short range energy transfer.

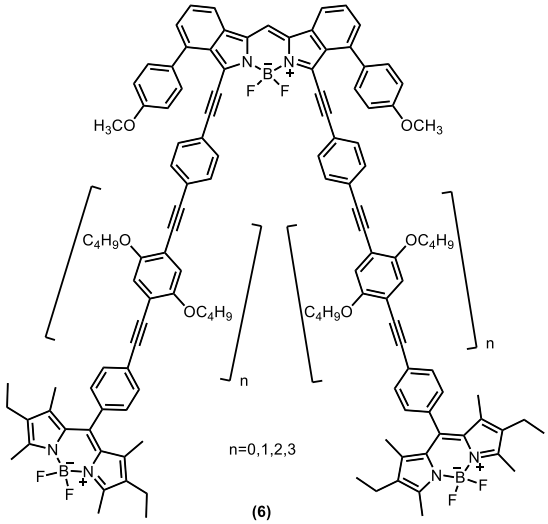


Figure 8. Literature example for through bond energy transfer.

In the example shown in Figure 8, two BODIPY units have been linked to a terminal acceptor BODIPY unit via aromatic linkers having various lengths.[20] Because of polyaromatic spacer units, absorption of these compounds shifts to the longer wavelengths with the increasing length of the spacer units. The absorbed energy was transferred quantitatively to the terminal BODIPY. The distance between the acceptor and donor units are 18, 24, 31, and 38 Å for n = 0, 1, 2 and 3, respectively. It is shown that as the distance between acceptor and donor substituents increases, energy transfer rate decreases.

2.1.3.2. Förster Type Energy Transfer

Fluorescence (Förster) Resonance Energy Transfer (FRET) refers to the energy transfer from excited donor chromophore to the acceptor chromophore through a non-radiative pathway. Theory of electronic excitation transfer was given first by Förster in 1948 and this phenomenon was used by several biologists to investigate certain distances in proteins.[14] The energy transfer efficiency is dependent on several parameters. One of them is that the donor chromophore must be fluorescent and since efficiency of this process is highly dependent on the distance between donor-acceptor pair, the distance between donor and acceptor is highly important. The efficiency is inversely proportional with the sixth power of the radius, where radius is the distance between the centers of the donor and acceptor dipoles. Another

important requirement is the spectral overlap between emission of the donor molecule and absorption of the acceptor chromophore. FRET is a valuable technique to investigate protein-protein interactions, protein -DNA interactions, protein - membrane interactions and the three dimensional structure of molecules in living cells,[14] in molecular imaging,[21] biosensors,[22] DNA mechanical movements.[23]

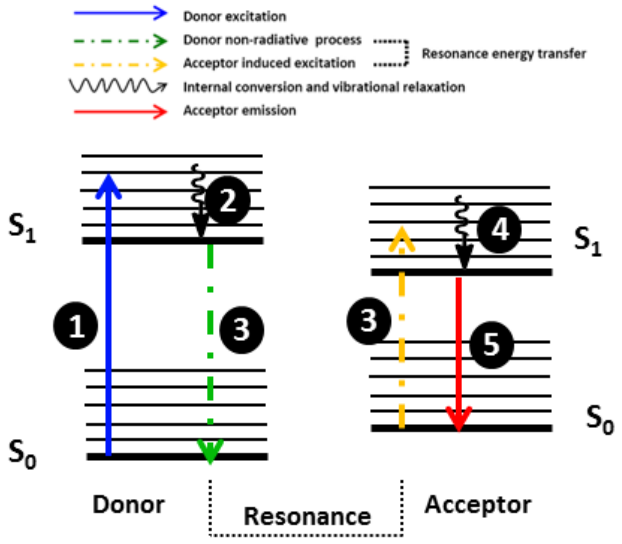


Figure 9. Schematic representation of FRET.

As depicted in Figure 9, the donor chromophore is excited to the lowest excited singlet state, S_1. If the acceptor is close enough, the energy released while electron goes back to the ground state (S_0) can excite the donor chromophore at the same time. This radiationless pathway is called as "resonance". Upon excitation, a photon is emitted by the acceptor moiety and returns to the ground state, when other deactivation processes does not occur.

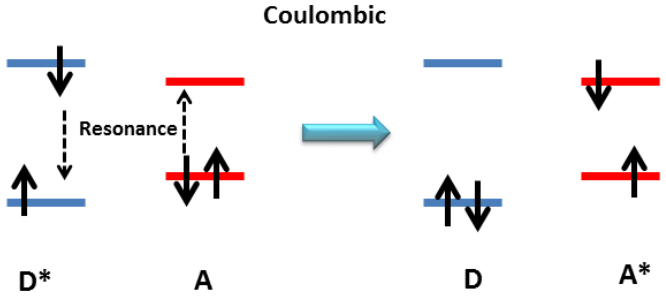


Figure 10. Schematic representation of Förster energy transfer mechanism.

Förster mechanism involves a dipole-dipole interaction between the electronic states of the donor and the acceptor. Long range Coulombic forces are responsible for through space interaction and the interaction between dipole of excited donor (excited electron in LUMO) and dipole of ground state acceptor (electron in the HOMO) is the basis of the mechanism. (Figure 10) The rate of Förster energy transfer is calculated as shown below:

$$k_{ET} = \frac{1}{\tau_D}\left(\frac{R_c}{d}\right)^6$$

where τ_D is the excited state lifetime of donor in the absence acceptor, and d is the distance of donor–acceptor pair. Rc is critical radius (the distance at which the energy transfer rate k_{ET} is equal to the intrinsic decay rate of the donor) and equation of Rc is given below:

$$R_c^6 = \frac{9000(\ln 10)K^2\Phi_D}{128\pi^5 N n^4}J$$

where K^2 is the orientation factor (related to the relative orientation of the donor and acceptor dipoles), Φ_D is the emission quantum yield of donor in the absence of acceptor, n is the refractive index of the solvent, N is the Avogadro's number and J is the spectral overlap integral.[24]

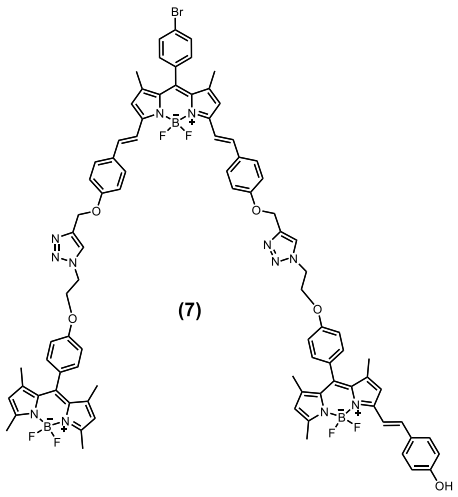


Figure 11. Literature example of Förster mechanism.

To attach three different emitting BODIPY units to get through space energy transfer array, click chemistry has been utilized (Figure 11).[25] The styryl groups were

attached to BODIPY core to acquire absorption and emission at longer wavelength. When the excitation was performed at 501 nm (BODIPY core) and 572 nm (mono-styryl part), emission intensity was seen at 662 nm (di-styryl part). It was stated that the energy transfer efficiency was 99% in both situation.

2.1.3.3. FRET-based Fluorescent Probes

The FRET operation is often employed for the design of the fluorescent probes since large pseudo Stokes shifts and ratiometric probes can be obtained. There are three types of FRET-based metal ion probes as shown in Figure 12.

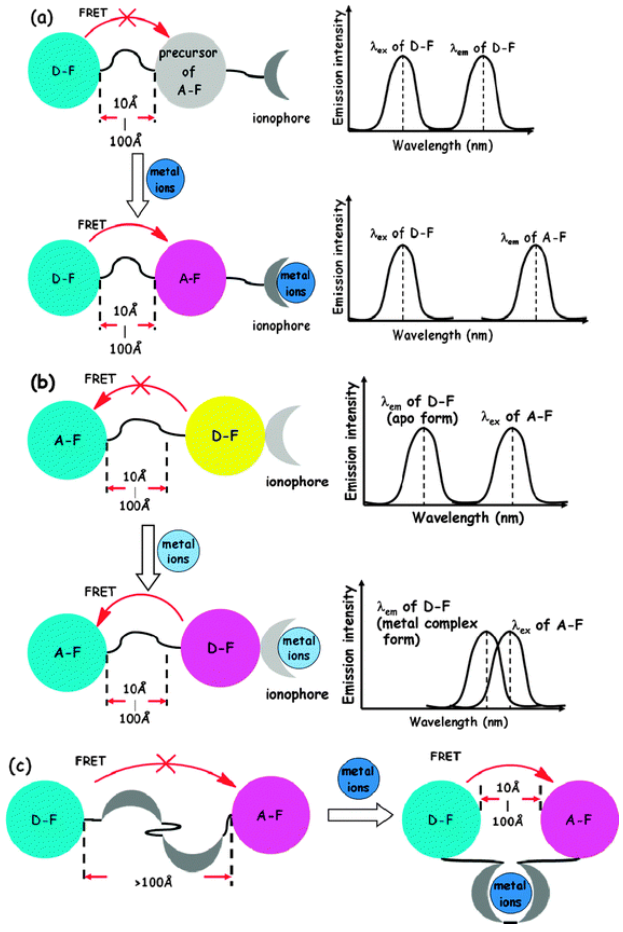


Figure 12. Design principles of FRET-based fluorescent probes (Copyright © 2013, American Chemical Society, Reprinted with permission from ref (26)).[26]

In the first type, ionophore (receptor part) is attached to the non-emissive acceptor fluorophore and upon binding of metal ion, non-emissive acceptor fluorophore

turns into highly emissive fluorophore. For example, probe 9 in Figure 13 is a FRET-based Cu (II) probe consisting of coumarin and rhodamine as the donor – fluorophore (D-F) and acceptor- fluorophore (A-F), respectively. Before addition of Cu (II), since the rhodamine is in the ring-closed form, coumarin does not transfer its energy to the rhodamine unit. Therefore, FRET is not active in this case. However, in presence of Cu (II), ring-closed form of rhodamine is converted to the ring-opened form due to the hydrolysis of rhodamine-B hydrazide to rhodamine-B. In this form, FRET turns on and emission of rhodamine part is observed upon excitation of coumarin unit.[27]

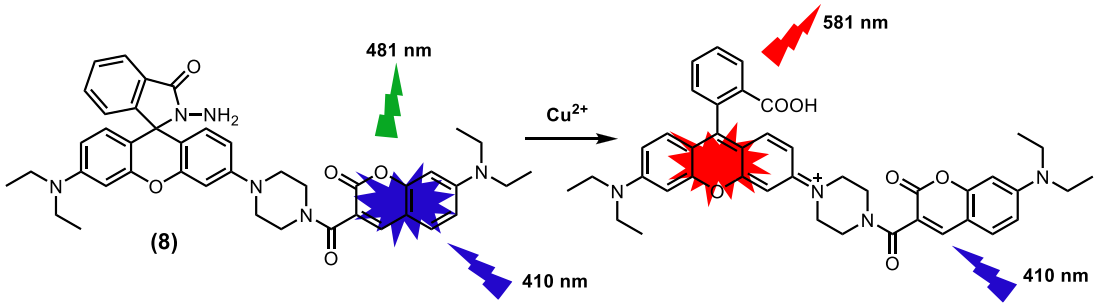


Figure 13. Fluorescent probes 1–3 based on a FRET mechanism.

In the second type, the ionophore (receptor) unit is directly attached to the D-F or A-F and upon metal addition, change in overlap between the emission spectrum of D-F and absorption spectrum of A-F triggers a FRET-based response. Design given in Figure 14 is an example for this kind. In this example, 5-(4-methoxystyryl)-50-methyl- 2,20-bipyridine (bpy) with diamino-substituted naphthalimide (NDI) were chosen as D-F and A-F, respectively. In absence of Zn (II), since the overlap between the emission spectrum of D-F and the absorption spectrum of A-F, FRET does not occur. On the other hand, coordination of bpy with Zn (II) causes a bathochromic shift in emission spectrum of bpy-Zn (II). Thus, spectral overlap between the emission of the bpy/Zn^{2+} complex and the absorption band of NDI increases and FRET is on state.[28]

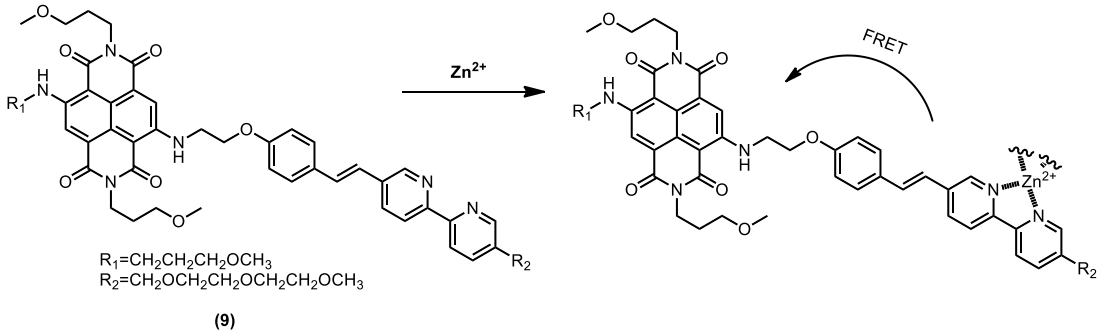


Figure 14. Fluorescent probes 1–3 based on a FRET mechanism.

The last item for FRET-based fluorescent probes can be achieved basically by modulation of the dipole–dipole distance between D-F and A-F upon metal coordination. This design requires ionophore not only as a receptor but also as a spacer unit. Before metal coordination, the distance between D-F and A-F is longer than 100 A and so as expected, FRET is not in action. Yet, metal coordination leads to a change in the spacer form and resulting decrease in distance between D-F and A-F, causes FRET to become active. Protein-based probes are mostly this type. In Figure 15, Zn (II) binding domain was attached between a cyan fluorescent protein (CFP) and a yellow fluorescent protein (YFP).[29] The distance and orientation of the fluorophores with respect to each other affects the dipole-dipole coupling, so Zn (II) binding causes a conformational change in the system and a change in the energy transfer between the two fluorophores.

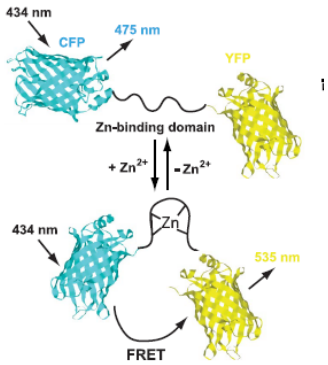


Figure 15. Fluorescent probes 1–3 based on a FRET mechanism (Copyright © 2009, American Society for Biochemistry and Molecular Biology, Reprinted with permission from ref (29)).[29]

2.1.3.4. Determination of FRET Efficiency

The FRET efficiency of a donor-acceptor pair can be determined mainly in two ways experimentally: steady state and time-resolved.[4] Steady state technique depends on the decrease in quantum yield of donor unit. The equation is given below:

$$E = 1 - \Phi_{DA} / \Phi_{D}$$

where Φ_{DA} and Φ_{D} represents quantum yield of donor in the presence and absence of acceptor respectively. Another equation to determine energy transfer efficiency which, uses excitation spectra or enhancement in fluorescence emission of the acceptor, is below:

$$E = A_A(\lambda_D) / A_D(\lambda_D) * [I_{AD}(\lambda_{Aem}) / I_A(\lambda_{Aem}) - 1]$$

where A_A and A_D is absorbance values of acceptor and donor at the maximum absorbance wavelength of donor. The integrated emission area of the acceptor in the presence and absence of the donor at λ_{Aem} is I_{AD} and I_A, respectively.

Energy transfer efficiency determination based on steady state is more prone to errors because of the differences in reference and sample. Extra care should be taken in order to avoid inaccurate measurements while using the concentration or the absorbance of the sample.

Time-resolved technique offers more reliable data because lifetime of donor is not dependent on the concentration. This technique requires the lifetime of donor in presence of acceptor and without acceptor and equation is stated below:

$$E = 1 - \tau_{DA}/\tau_{D}$$

where E is the energy transfer efficiency, τ_D and τ_{DA} indicates the excited state lifetime of donor in the absence and presence of acceptor respectively.

2.1.4. Excimer Formation

A weak interaction between a fluorophore in the excited state and another fluorophore in the ground state, facilitates the formation of an excimer. These interactions can be π–π* stacking. There are many probes based on this approach in the literature. In these type of probes, two same fluorophores are linked with a spacer (ionophore). Upon metal coordination, these two fluorophores approach each other and this results in a weak interactions between them. (Figure 16)

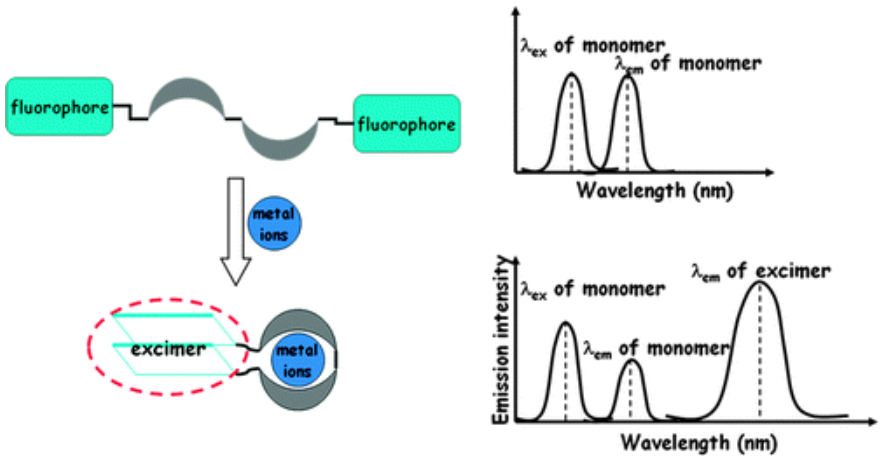


Figure 16. Schematic representation of excimer formation (Copyright © 2013, American Chemical Society, Reprinted with permission from ref (26)).[26]

Emission of an excimer is characteristically red-shifted and broad with respect to the monomer emission. Difficulty in prediction of the distance between fluorophores and poor water solubility limits the utilization of this kind of sensing mechanism.

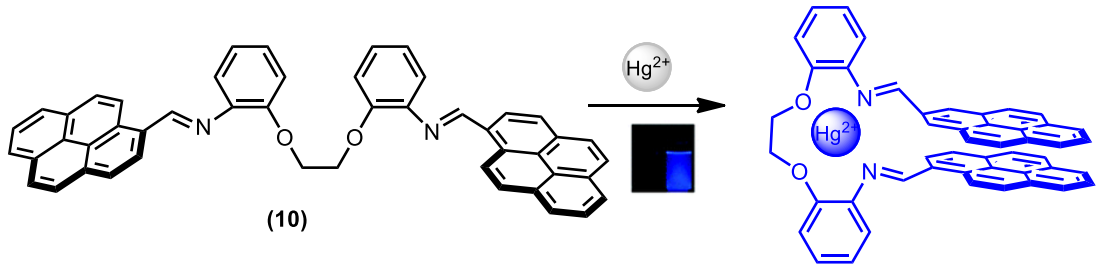


Figure 17. Literature example of fluorescent probes functioning *via* excimer formation.

A pyrene-based Hg (II) probe consisting of an azadiene group was designed by Yao and coworkers (Figure 17).[30] Weak pyrene monomer emissions turns out to strong pyrene excimer emission because Hg (II) addition induces the conformational alteration.

2.2. Near-Infrared Fluorescent Probes

Near-IR dyes in the range of 650-900 have attracted intensive attention owing to their diverse applications in imaging science, biomedical materials, molecular biology, material science, analytical and environmental chemistry, drug discovery and tissue diagnostics.[31] Ongoing interest arises from their unique advantages. Near-IR dyes ensure improved sensitivity by reducing interference of absorption and fluorescence from biological molecules (autofluorescence) and scattering is low at this region. The excitation source (laser diodes) is relatively inexpensive. Another important feature of this region is that tissue penetration depth increases.[32] For practical biological applications, some features should be incorporated to these dyes. They should be water-soluble, chemically stable, functionalizable for further modifications and have high quantum yield.[33] Great efforts have been focused to minimize these problems and to improve photochemical and photophysical features. There are a few categories of near-IR dyes available in the literature. These can be classified as cyanines, rhodamine analogs, 4,4-difluoro-4-bora-3a,4a-diaza-s-indacene (BODIPYs), squaraines, phthalocyanines, and porphyrin derivatives. The chemical structures of these probes are given in Figure 18. Phthalocyanine and squaraine dyes in biological systems are not suitable because of poor water solubility and formation of aggregates. Although cyanine dyes have strong absorption and fluorescence, their fundamentally small Stokes shift causes scattered light interferences.[32] The main focus will be given widely used 4,4-difluoro-4-bora-3a,4a-diaza-s-indacene (BODIPYs) because of their distinct properties.

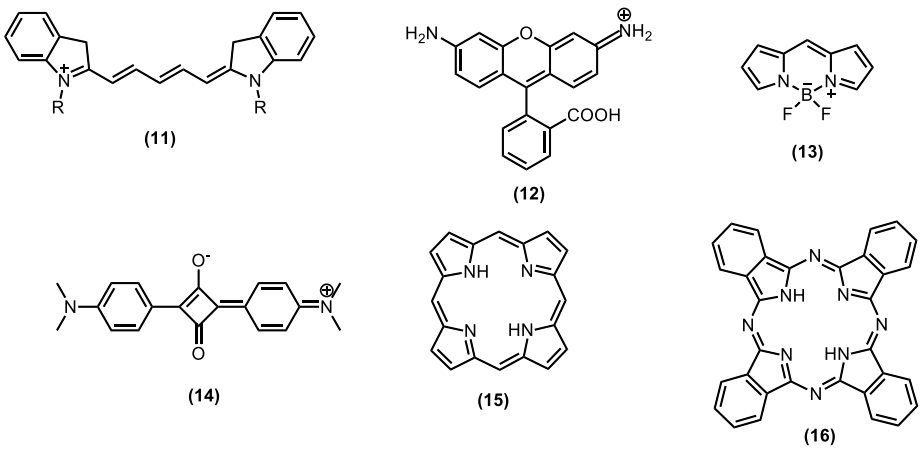


Figure 18. Some of the common dyes used in fluorescent probes.

2.2.1. BODIPY

BODIPY is the abbreviation of 4,4-Difluoro-4-bora-3a,4a-diaza-s-indacene and was firstly described by Treibs and Kreuzer in 1968. BODIPY has a fully delocalized system since the BF_2 bridge enhances the planarity of the dipyrrin, thus, facilitating the fluorescence. Nucleophilic and electrophilic substitutions can be performed on the corresponding reaction sites of the BODIPY core and ease of modification make the BODIPY core applicable for diverse fields.[34]

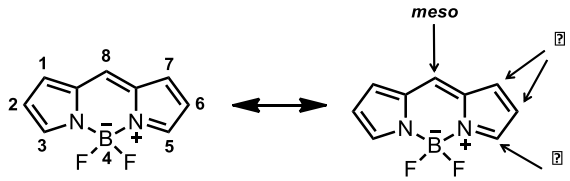


Figure 19. The numbering in BODIPY core.

There are numerous superior properties of BODIPY compared to other fluorophores. For example, BODIPY dyes have strong narrow absorption and emission in the visible, even in near-IR region, high molar absorption coefficients and high quantum yields. Moreover, they generally show thermal and photostability not only in solution but also in solid form. Its solubility in organic solvents is good and it is insensitive to pH and polarity of the medium.

To improve water solubility, shift the absorption and emission wavelength to the longer wavelength, functionalize for bioconjugation, and make BODIPY application for various applications (photodynamic therapy, dye-sensitized solar cells, chemosensors, etc.), in short, to tune the photophysical properties of BODIPY core, synthetic modifications can be performed by using different methodologies.

Modification on the C-8 (*meso*) position is carried out with acid-catalyzed condensation of pyrrole with suitable aryl aldehydes or acyl chlorides. With this functionalization, donor-acceptor moieties, water-solubilizing units and ligands can be incorporated to BODIPY core towards different application areas. Meanwhile, owing to orthogonal geometry of the *meso* substituent and the BODIPY fluorophore, the influence of electron-donating and electron-withdrawing groups on the photophysical properties of BODIPY dyes is not drastic.

To functionalize 2 and/or 6-positions of BODIPY, electrophilic substitution reactions are needed because these positions hold less positive charge. These electron rich positions allow sulfonation,[35] nitration,[36] halogenation,[37] and formylation[38] on the BODIPY core.

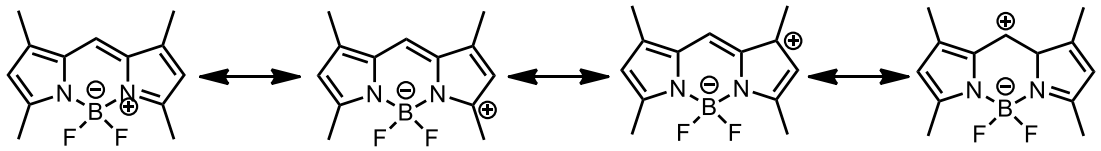


Figure 20. Available positions for electrophilic substitution on BODIPY core.

Introduction of heavy atoms like iodine and bromine to 2 and/or 6-positions of BODIPY triggers the intersystem crossing, thus, fluorescence decreases. For photodynamic therapy application, these atoms are incorporated for generation of singlet oxygen. Moreover, functionalization on these positions with conjugated systems via palladium-mediated coupling can result in extension of π-conjugation.[39]

Modifications on 1, 3, 5, 7 positions can be performed by a number of reactions and different properties of BODIPY dyes could be attained depending on the type of modification. Presence of good leaving groups at these positions lets nucleophilic aromatic substitutions on the electron poor BODIPY core as well as different palladium-catalyzed couplings such as Heck, Sonogashira, Stille and Suzuki. Another widely used reaction to modify 1, 3, 5, 7 positions is Knoevenagel condensation.[40] The acidity of the 3,5-methyl groups on the BODIPY core are comparatively acidic to condense with aromatic aldehydes to give Knoevenagel reaction.[41] This condensation requires basic medium and water should be removed from reaction mixture. To remove water from medium, Dean-Stark apparatus is generally used. This reaction is easy to handle and less time-consuming compared to other approaches. Also, wide range of electron donating and electron withdrawing aldehydes can be introduced to BODIPY core. The generation of styryl substituents with these aldehydes allows tunability of the BODIPY absorption and emission spectra. For example, since *p*-dimethylaminostyryl is used as an aldehyde, electron donating ability pushes BODIPY emission into near-IR region (Figure 21).[42]

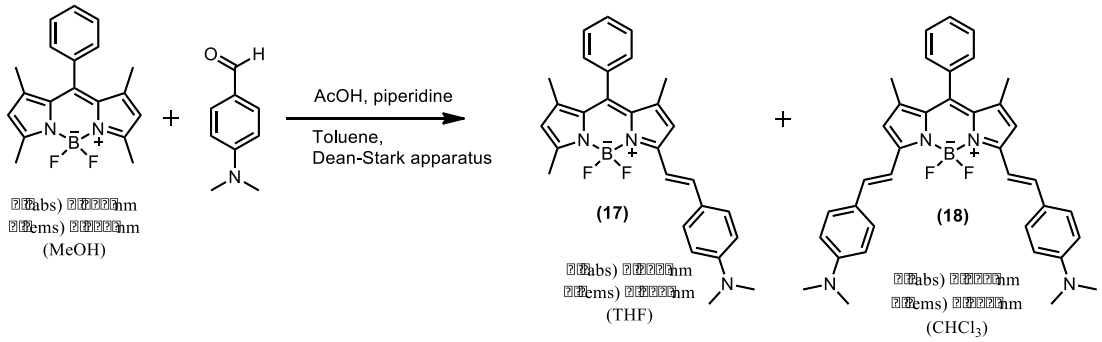


Figure 21. Knoevenagel condensation of 3,5-methyl substituents with aromatic aldehydes.

In 2009, Akkaya group reported that the methyl groups on positions 1 and 7 are as acidic as 3,5-methyls and tetra-styryl BODIPY dyes could be synthesized utilizing this acidity.[43] In this work, bromine atoms and pyridine groups were introduced in order to increase the acidity further (Figure 22).

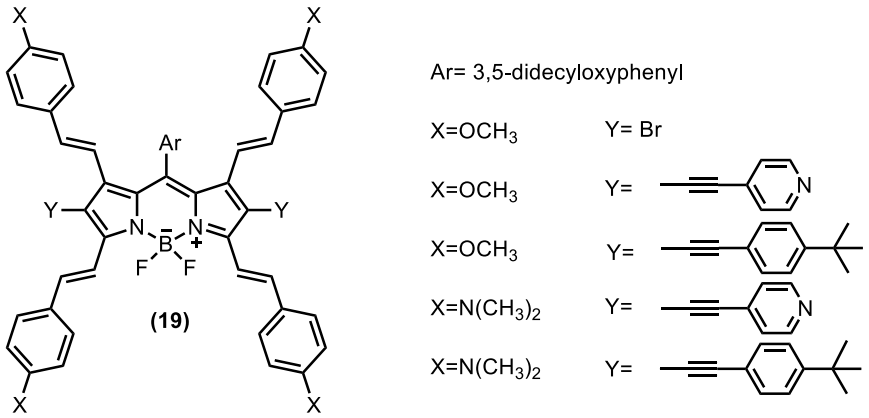


Figure 22. Structures of the tetra-styryl BODIPY derivatives.

After this report, Ziessel and coworkers published tri and tetra substituted derivatives of BODIPY dyes by using different aldehydes.[44] It was stated that these new dyes had absorption peaks near 720 nm and emission wavelengths approximately at 800 nm (Figure 23). Both Akkaya and Ziessel's work demonstrated that methyl groups located in 3,5- positions are relatively more reactive than those located in 1,7-positions to give Knoevenagel condensation. Meanwhile, the introduction of dimethylamino and phenol groups on those positions makes these dyes acid and base sensitive. Thus, these dyes enable the modulation of optical characteristics over a broad wavelength range with change in pH.

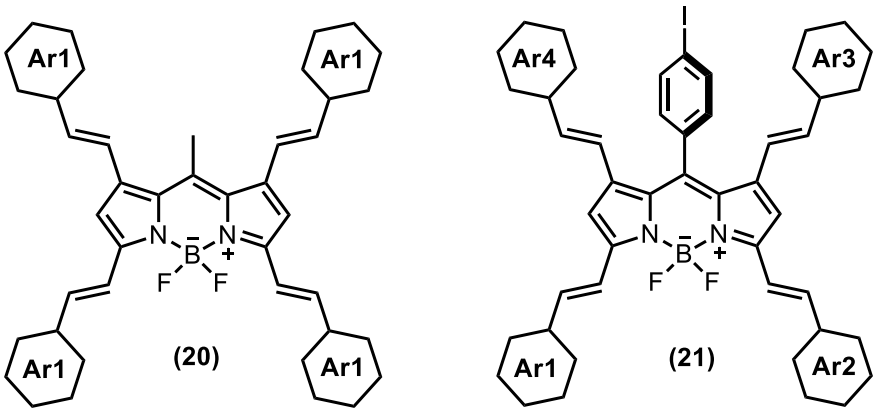


Figure 23. Schematic view of 1,3,5,7-tetrastyryl BODIPY derivatives.

Another tetra styryl derivative was reported by Liu group (Figure 24).[45] In this study, it was shown that if 6- or 2,6- positions involve formyl group, methyl groups at the 7, and 1,7-positions are more prone to undergo Knoevenagel condensations rather than 3,5- positions. The presence of styryl groups at 7-, and 1,7-positions allows another Knoevenagel reactions of the methyl groups at the 3,5- positions. They introduced oligo (ethylene glycol) methyl ether units to improve the water solubility and so, these dyes can operate as building blocks for conjugated oligomers and sensing materials.

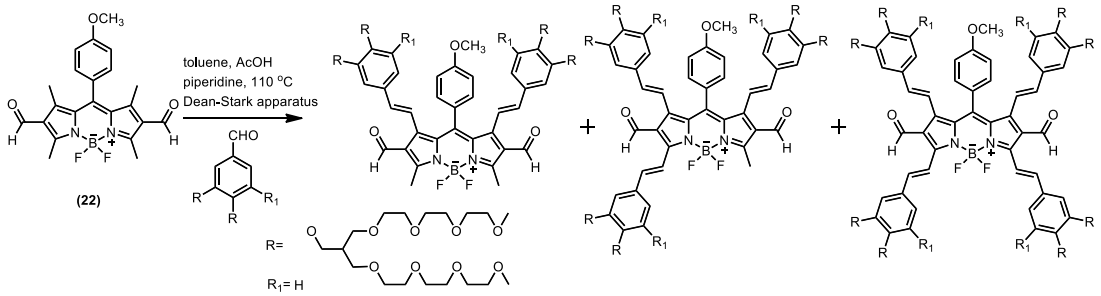


Figure 24. Illustration of tetra-styryl derivatives including formyl groups at 7-, and 1,7-positions.

In addition, in this study, tetra-styryl BODIPY including oligo (ethylene glycol) methyl ether as a water soluble units and formyl moieties as a cysteine reactive group was shown as fluorescent probe for cysteine. When formyl groups on 1- and 7-positions react with cysteine, thiazolidine is formed and π-conjugation is disrupted so absorption spectrum shows blue shift (from green to blue). (Figure 25) In presence of cysteine, emission intensity is enhanced and this dye can be used as a potential water soluble near-IR sensing and labeling probe for N-terminal cysteine residues in peptides or proteins.

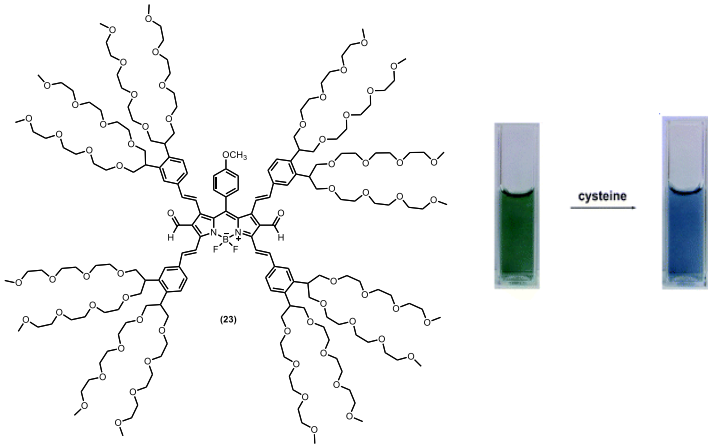


Figure 25. The visual representation of tetra styryl BODIPY dye in PBS buffer pH 7.4 in the absence and presence of L-cysteine.

Proper and straightforward derivatization of BODIPY dyes with four styryl moieties assure that these new chromophores can be used in different fields such as photodynamic therapy, dye sensitized solar cells, dendritic light harvesting and supramolecular building blocks.

2.3. Significance of Mercury (II)

The mercury cycling in the ecosystem is rather complicated and affected by various elements such as human activities, climate variations and natural disasters. Mercury is thought as highly toxic and major source of mercury contamination is pollution in natural waters. There are two main sources of mercury release: Industrial and natural. Coal and gold mining, fossil fuel combustion and wood pulping are industrial sources. The other major cause of mercury pollution is resulted from volcanic and oceanic emissions.[46] If there is no inadvertent use, seafood consumption is the only source for human exposure. Mercury ions can smoothly cross the biological membranes and have severe effects on the central nervous system and endocrine system.[47] Furthermore, they lead to oxidative stress[48] and lipid peroxidation[49] and prevent neuron division and migration at cellular level.

2.3.1. Hg (II) Fluorescent Probes

Considering the importance of the effect of mercury ion (Hg (II)) on environmental and biological aspects, the detection of Hg (II) becomes an important task for scientists. Within the different approaches, fluorescence-based techniques attract more attention due to their superior characteristics such as high sensitivity, selectivity and being inexpensive and user-friendly. Additionally, fluorescence-based methods give the opportunity to study in living systems and environmental samples.[50]

Intrinsic characteristics of Hg (II) allow modulation of affinity and selectivity of receptor unit. Due to its $5d^{10}6s^2$ electronic configuration and absence of ligand field stabilization energy, Hg (II) can have diverse coordination numbers and geometries. Widely known types are two-coordinate linear and four coordinate tetrahedral ones. In the design of the receptor unit for Hg (II), soft donor atoms like sulfur and nitrogen are generally used to improve the affinity because Hg (II) is known to be a soft acid. Another parameter to get the rational design is the signaling unit. Depending on the desired absorption and emission wavelength, fluorophore should be chosen or functionalized properly. Water solubility is a key parameter that must be fulfilled and usually it is difficult to get water-soluble probes. Therefore, the water soluble probes are rare in the literature. Photoinduced electron transfer (PeT) and internal charge transfer (ICT) have both been utilized commonly to tune absorption and emission properties of the fluorophore. In addition, ICT-based probes offer ratiometric sensing which is important to get rid of artifacts and quantify the analyte. FRET-based fluorescent probes also provide ratiometric analysis as well as a large Stokes shift can be obtained and so sensitivity of the probe is improved.

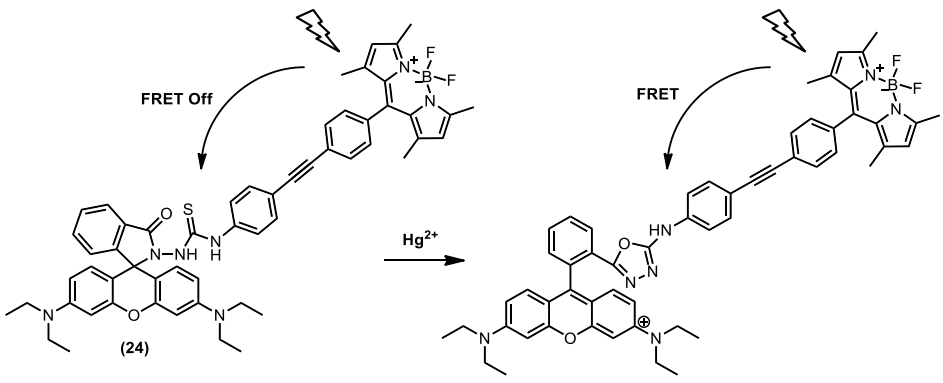


Figure 26. FRET-based fluorescent probe for detection of Hg (II).

A FRET-based fluorescent probe for detection of Hg (II) is demonstrated in Figure 26.[50] Rhodamine and BODIPY dyes were selected as a donor and acceptor moieties, respectively. Also, leuco-rhodamine specie was used as a receptor part because upon reaction with Hg (II), ring opening reaction enhances fluorescence emission of rhodamine. In this design, phenyl-ethynyl-phenyl groups are used to facilitate the through-space energy transfer. In presence of Hg (II), fluorescence of BODIPY unit decreases and rhodamine emission increases. As a result, it can be concluded that FRET process was modulated upon addition of Hg (II) and ratiometric probe was studied in living cells.

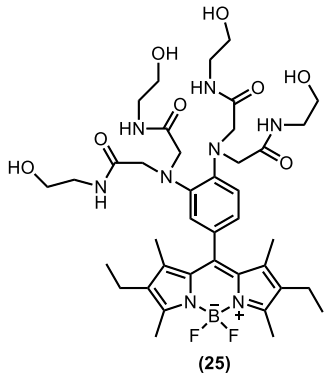


Figure 27. BODIPY-based fluorescent probe for detection of Hg (II).

Qian and Wang reported a BODIPY based probe working with PET mechanism for Hg (II) detection in aqueous solution as depicted in Figure 27.[51] In absence of Hg (II), electron-donating property of receptor part quenches the emission of BODIPY core via PET mechanism. On the other hand, addition of two equivalent of Hg (II) blocks the PET process and fluorescence of BODIPY enhances.

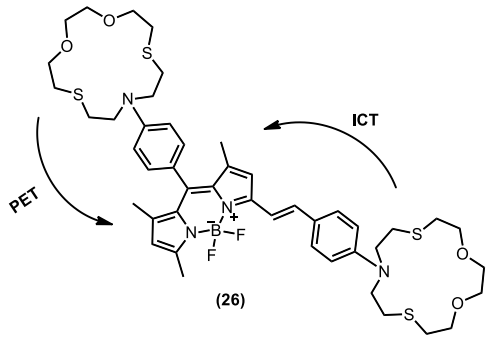


Figure 28. BODIPY-based fluorescent probe utilizing PET and ICT processes for detection of Hg (II).

In another example, both PET and ICT mechanisms were utilized in a single molecule in Figure 28.[52] BODIPY core was functionalized with two crown ether moieties on *meso* and 3- positions. The dithia-dioxa-aza macrocycle on the *meso* position facilitates PET process; however, dithia-dioxa-aza macrocycle on the 3-position causes ICT process due to the conjugation directly to BODIPY fluorophore. With addition of Hg (II), PET process is blocked due to the decrease in electron-donating ability of dithia-dioxa-aza macrocycle and ICT process causes blue shift owing to lack of electron-donation ability of dithia-dioxa-aza macrocycle. The authors proposed that PET process causes 7-fold increase in emission intensity, but, ICT mechanism triggers the big changes in both absorption and fluorescence properties.

2.4. Importance of Biological Thiols

Biological thiols such as cysteine (Cys) (**27**), homocysteine (Hcy) (**28**) and glutathione (GSH) (**29**) are essential physiological components because of the strong nucleophilicity of the sulfhydryl group. Being excellent nucleophiles, they play key roles on enzyme functionality and maintenance of redox states.[53] The variations in the levels of biological thiols is attributed to many diseases such as premature arteriosclerosis, occlusive vascular and neurodegenerative disorders, leukemia, diabetes, and acquired immunodeficiency syndrome.[54]

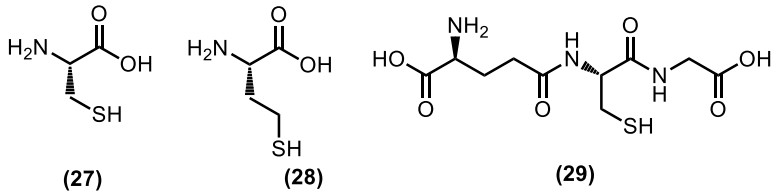


Figure 29. Chemical structures of cysteine, homocysteine and glutathione.

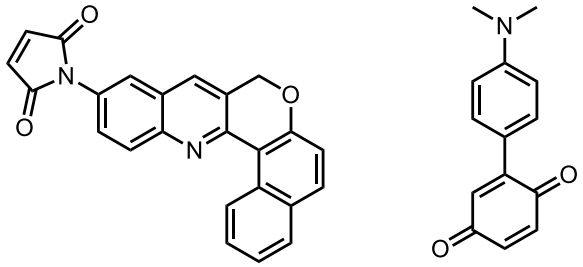
Cysteine (Cys) is produced in the liver and appears in a wide range of biological processes such as synthesis of certain proteins and removal of toxins.[55] The low concentration of Cys can cause slow growth, and liver and skin damage whereas high concentrations leads to the neurotoxicity.[56] Homocysteine (Hcy) is another sulfhydryl-containing amino acid, synthesized in the body. Demethylation of

methionine leads to production of Hcy. Elevated levels of Hcy are linked to cardiovascular disease and Alzheimer's disease. Glutathione (GSH) is a tripeptide of glutamate, glycine and cysteine and γ-glutamylcysteine synthetase and GSH synthetase are used as catalysts sequentially in the synthesis of GSH. GSH is responsible for antioxidant response, regulation of gene expression, cell proliferation, etc. Deficiency in GSH can result in Alzheimer's disease, Parkinson's disease, AIDS, cancer and heart attack.[57]

Thus, detection of these thiol containing molecules is of great importance towards biological applications. Once again, fluorescence-based techniques drew significant attention due to the simplicity and sensitivity. Additionally, allowing the study in intracellular environment brings fluorescence-based approach in the first place. Efficient nucleophilic character and high affinity towards metal ions are two widely used properties of thiols in the design of fluorescence-based probes. For thiol reactive probes, various types of reactions can be employed including nucleophilic substitution, Michael addition, cyclization, cleavage of disulfide bond, metal complexes coordination, and redox reactions. Due to effect of pH on nucleophilicity of the sulfhydryl group (pKa of SH in Cys: 8.15, Hcy: 8.7, GSH: 8.56), pH of the medium becomes an important parameter that should be taken into account for reaction rates.[56]

2.4.1. Detection of Thiols Based on Michael Addition

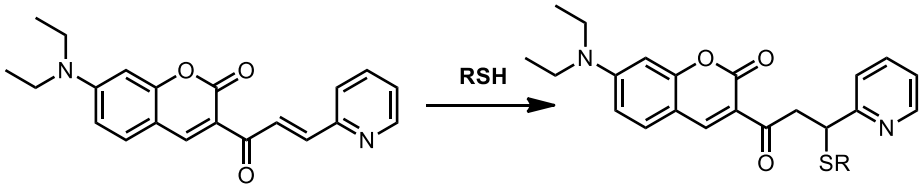
Owing to strong nucleophilicity of the sulfhydryl group, Michael acceptors which are good electrophiles are attached to fluorophore to give Michael addition.[58] PET, ICT and FRET processes can be utilized to get desired optical properties.



(30) (31)

Figure 30. Some examples for thiol probe based on Michael addition.

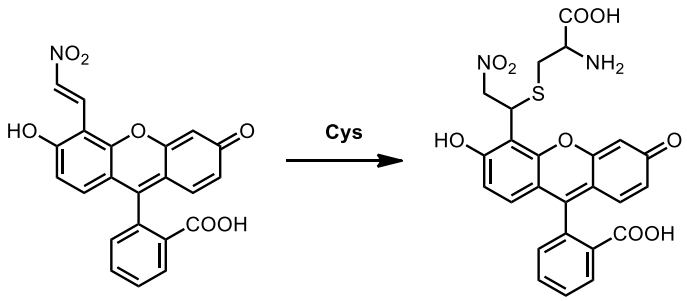
Maleimide groups (**30**) are widely used in the design of the fluorescent probes. The detection limits of nearly 20 nm for Cys was achieved and human metastatic breast cancer cells (MDA-MB 231) were studied for imaging.[59] Although maleimides are frequently used as thiol reactive groups, the quinone groups (**31**) are also highly utilized in fluorescent probes. For instance, compound **31** was designed to detect thiols based on ICT mechanism. Before addition of thiols, the absorption peak was centered at 582 nm owing to ICT process. In presence of thiols, nucleophilic addition of thiols on the quinone unit decreases the absorption peak and emission intensity increases.[59]



(32)

Figure 31. Example for thiol probe based on open chain Michael addition.

For the design of the fluorescence-based probes for thiols, open chain Michael acceptor can also be used. For example, as can be seen in Figure 31, α, β-unsaturated ketone derivative was non-fluorescent, but, presence of thiol groups disturbs the conjugation and emission of coumarin turns "on" state.[60]

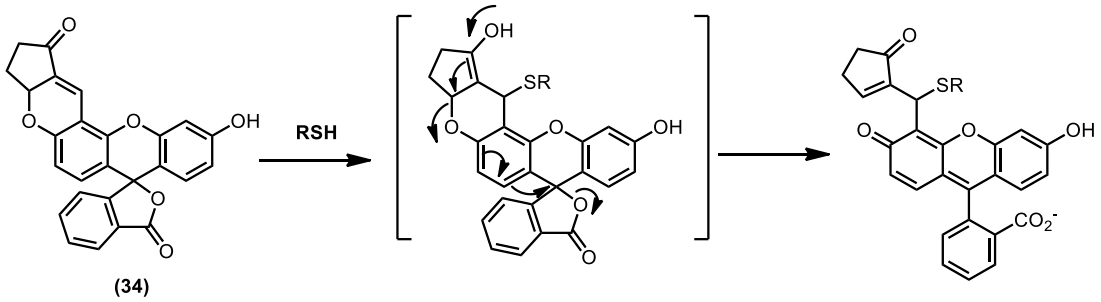


(33)

Figure 32. Thiol probe based on nitro-olefin moiety.

In the sensing of thiols, nitro Michael acceptors are frequently utilized due to the high reactivity of sulfhydryl groups towards these acceptors. Wang and coworkers utilized fluorescein as a fluorophore part and nitro alkene unit which is thiol reactive group to detect the thiols in water (Figure 32).[61] Before the addition of thiols, PeT process is in action due to the electron deficiency on nitro group so fluorescence is low. In presence of thiols, conjugate addition to nitroalkenes takes place and as a result, PeT mechanism is blocked and fluorescence is restored. Meanwhile, ICT

process from the phenyl carboxyl acid group to the electron-poor nitroalkene moiety leads a blue shifted absorption peak upon thiol addition. This probe is further studied in intracellular medium and imaging of thiols in living cells were investigated.



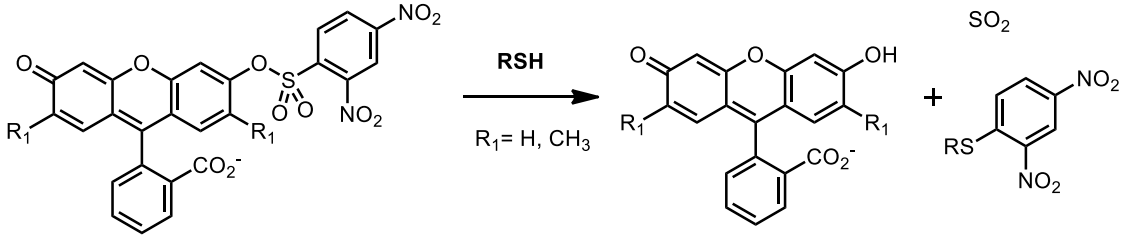
(34)

Figure 33. Thiol probe based on ring opening Michael addition.

Michael addition based ring opening reaction is applied in the design of the biothiol probes. In 2010, a fluorescein-based thiol probe was addressed (Figure 33).[62] 1,4-addition of thiol to α,β-unsaturated ketone in the sensor followed by the spiro ring opening of fluorescein triggers the increment in emission intensity and absorption peak is shifted from 454 nm to 500 nm.

2.4.2. Detection of Thiols Based on Cleavage of Sulfonamide and Sulfonate

Cleavage of sulfonamides and sulfonates is a promising way to detect the biothiols and highly employed in the design of the fluorescence-based probes.



(35)

Figure 34. PeT-based thiol probe based on Michael addition.

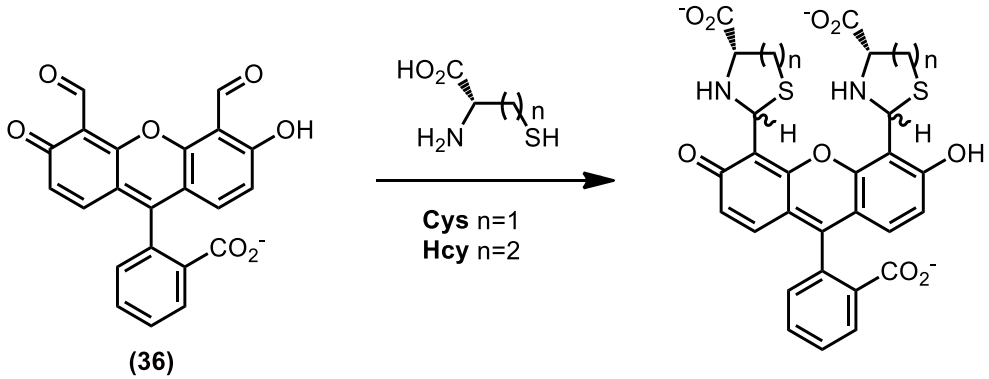
For example, Itoh and coworkers utilized PeT mechanism together with Michael addition reaction for detection of thiols (Figure 34).[63] Electron-deficient of the phenyl unit on the 2,4-dinitrophenyl sulfonyl (DNBS) is incorporated into fluorescein fluorophore. From fluorescein moiety to electron deficient DNBS unit, PeT process occurs. In presence of thiols, DNBS undergoes de-sulfonylation, as a

result, fluorescence of fluorescein is restored. Low detection limits for GSH and Cys were achieved and this probe was studied in cholinesterase assays.

2.4.3. Detection of Thiols Based on Cyclization with Aldehydes

Selectivity among thiols is indispensable when taking into consideration the different biological roles different thiols. Therefore, unique detection makes the quantification of these thiols more useful. Also, the concentration of each thiol differs in biological medium and selectivity becomes more important to investigate the disease that occurs due to the fluctuations in the levels of these individual thiols.

The reaction between aldehydes and N-terminal cysteines to form thiazolidines is a type of reaction that utilized for detection of Hcy and Cys. In this reaction, a rapid 6- or 5-membered ring formation occurs with 1,3- or 1,2-aminothiols. Hence GSH does not give any response because GSH does not form any ring.



(36)

Figure 35. Thiol probe based on cyclization of aldehydes.

Efficient detection of Cys and Hcy was achieved by the compound **36**.[64] Bisaldehyde was used as a thiol reactive group and the reaction between the aldehyde moiety and Cys yields thiazolidine and shifts the absorption peak 25 nm to the longer wavelength and emission intensity decreases. Hcy showed similar optical changes with the formation of six-membered ring. However, monoaldehyde derivative of this compound demonstrated the selectivity to Cys over Hcy. The reason of the selectivity may come from the favored formation of a five-membered ring.[65]

2.4.4. Detection of Thiols Based on Disulfide Bond Cleavage

Thiols are known with their strong reducing character and this property allows the detection of them via the reduction of disulfide bond. Disulfide bond can be inserted into the fluorophores to get fluorescence-based response upon addition of thiols.

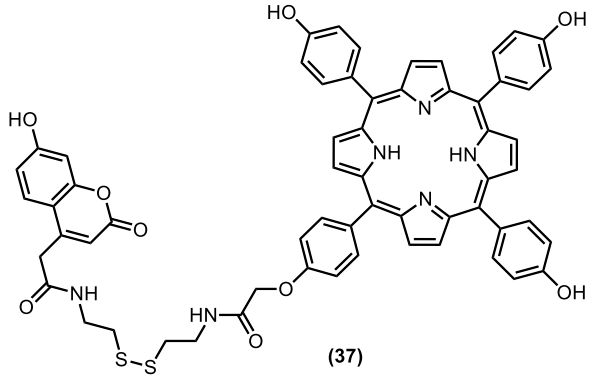


Figure 36. Thiol probe based on disulfide bond cleavage.

The promising example for this type of detection is given in Figure 36.[66] Coumarin and tetrakis(4-hydroxyphenyl)porphyrin fluorophores were selected as donor and acceptor moieties, respectively were attached by a disulfide bond. Before the addition of thiols, emission of the coumarin is quenched because of the FRET process from the coumarin as a donor to porphyrin as an acceptor. With the addition of thiols, disulfide bond is cleaved and FRET process is blocked. Thus, fluorescence of coumarin is enhanced.

2.4.5. Detection of Thiols Based on Metal Ions

Another distinctive property of biothiols is their high affinity towards metal ions and this feature allows the detection of these species by using metal ions. Additionally, this metal ion based system has a distinct advantage in the investigation of biological samples since metal ionic pairs intrinsically assist the water-solubility.

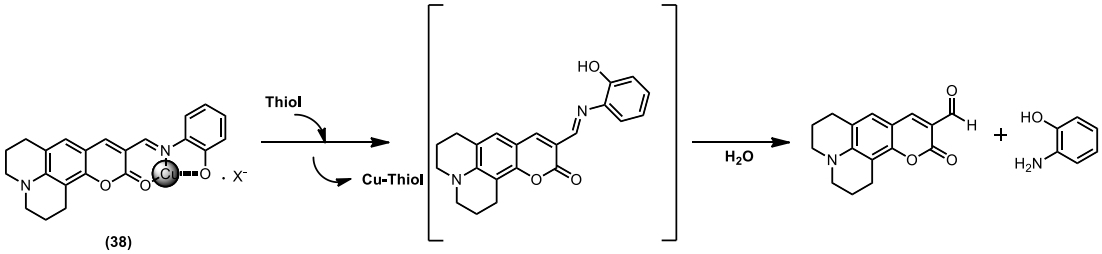


Figure 37. Thiol probe based on metal ions.

Kim *et. al.* were reported iminocoumarin–Cu(II) derivative to detect the biothiols at pH 7.4 under aqueous conditions (10 mM PBS buffer, pH 7.4, 1.0% DMSO). In the presence of thiols, decomplexation of the Cu (II) ion from non-fluorescent **38** takes place followed by hydrolytic cleavage of the resulted Schiff base to yield highly emissive coumarinaldehyde.[67] This turn–on probe was further studied in detection of intracellular thiols.

2.5. Significance of Hydrogen Sulfide (H_2S)

Hydrogen sulfide (H_2S) is a type of reactive sulfur species because it gives redox reactions with proteins to influence their actions. In the past, it was thought as a toxic gas, however, recently, H_2S have known as the third gaseous endogenously-produced signaling molecule after nitric oxide (NO) and carbon monoxide (CO). Other typical feature of this small gasotransmitter is the foul odor (rotten egg smell). It is synthesized endogenously from L-cystathionine, L-homocysteine and L-cysteine with the help of four different enzymes: cystathionine betasynthetase (CBS, EC4.2.1.22), cystathionine g-lyase (CSE, EC4.4.1.1), 3-mercaptopyruvate sulfur transferase (3-MST, EC 2.8.1.2) and cysteine lyase (CL, EC 4.4.1.10) (Figure 38).[68] Non-enzymatic synthesis involves the production by reduction of elemental sulfur.

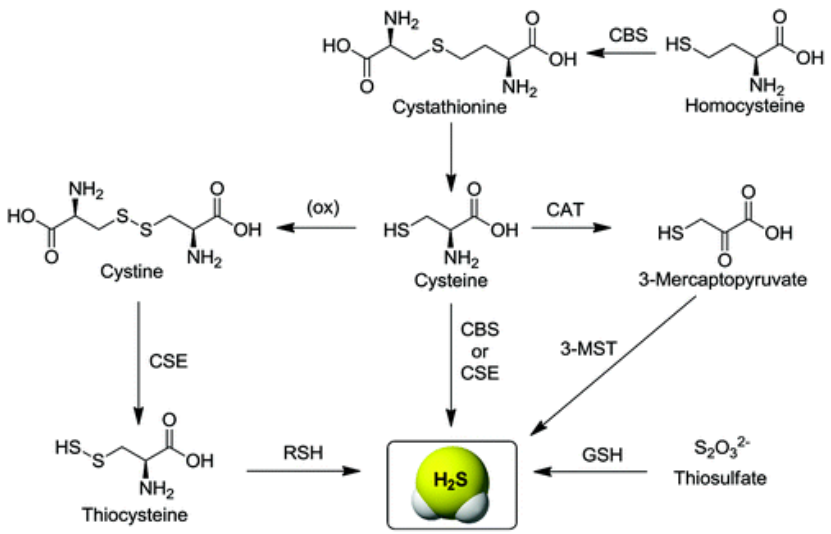


Figure 38. Endogenous synthesis of H_2S in mammalian cells (Copyright © 2013, American Chemical Society, Reprinted with permission from ref (69)).[69]

The ordinary concentration of H_2S in blood is between 10 and 100 μm.[70] Hydrogen sulfide is a weak acid (pKa_1: 6.76, pKa_2: 19.6) so it appears especially as SH^- (82%) rather than H_2S (18%) or S^{2-} (< 0.1%) under physiological conditions. This hydrosulfide anion has more nucleophilic character than Cys or reduced glutathione (GSH) under physiological conditions due to the lower pKa of this small gasotransmitter compared to Cys or GSH.[69] H_2S diffuses easily through the cell membranes and takes part in different type of biological processes such as regulation of cell growth,[71] cardiovascular protection,[72] stimulation of angiogenesis,[73] antioxidative effects[74] and modulation of neurotransmission.[75] Recent studies have proven that altered levels of H_2S can be linked with different types of diseases such as diabetes, arterial and pulmonary hypertension, liver cirrhosis, and Alzheimer's disease.[68]

Of course, there are several obstacles are present in the detection of H_2S. First of all, the reactions should be bioorthogonal to study in native cellular medium. Secondly, probe should give fast response to monitor H_2S due to its transient nature. Another requirement is that probe should selectively respond to H_2S, in other words, it should not interfere with other thiols.[76] Traditional techniques such as electrochemical or gas chromatography are not convenient for detection of H_2S because sample preparation is complex and monitoring of transient species is not trivial. On the other hand, small molecule fluorescence-based techniques tender high sensitivity, real-time monitoring and ease of operation. To design these probes, H_2S-specific reactions are employed in order to get desired optical properties. Thanks to its dual nucleophilicity, high reducing character, high binding affinity towards copper ions and specific addition reaction towards unsaturated double bonds, there are several type of H_2S-reactive reactions.[77] The most utilized reactions in the design of the fluorescence-based probes can be categorized as reduction-based, Michael-addition based and copper ion-based.

2.5.1. H_2S Probes Based on Reduction reactions

H_2S is a strong reducing agent and this feature can be used in the design of the fluorescence-based probes. In this sense, azides and nitro groups can be reduced via

H_2S. Although azides have been reduced by using H_2S over 30 years, the usage of this reaction in the H_2S probes is very recent. Furthermore, even the reduction potential of H_2S is lower than Cys or GSH, it can reduce azides or nitro groups faster than GSH and other biothiols.[69]

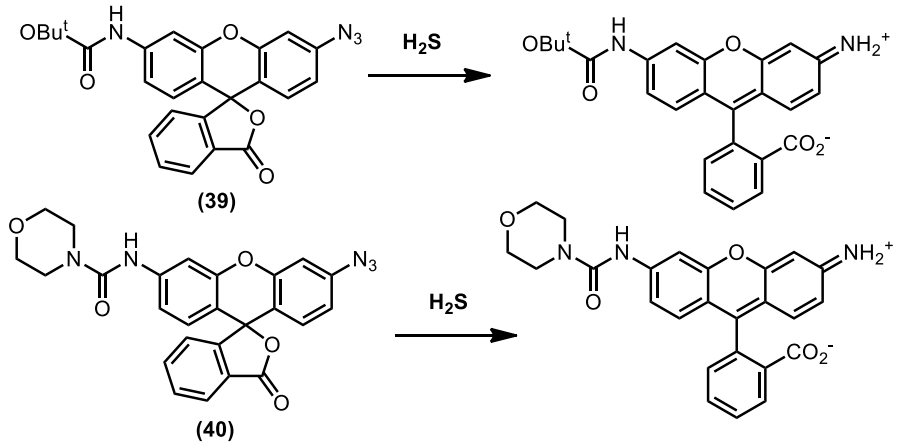


Figure 39. Examples for fluorescent H_2S probe based on azide reduction.

Based on this strategy, Chang *et. al.* utilized two fluorescent probes for detection of H_2S (Figure 39).[78] In these probes, fluorescein dyes are linked directly to azido units. In presence of H_2S, azido groups are reduced to amino groups and fluorescence of the dyes are restored. Another important criterion is fulfilled with these molecules which are the selectivity among other species such as GSH, Cys, Na_2SO_3, NO, H_2O_2 and O^{2-}. These probes were further studied in vivo cell imaging in HEK293T cells.

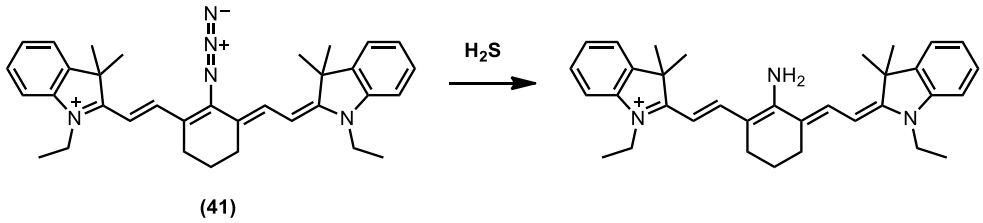


Figure 40. Another example for fluorescent H_2S probe based on azide reduction.

Another azide reduction based fluorescent probe for cellular H_2S was reported by Han group.[79] In their design, ICT process is utilized within NIR heptamethine cyanine dye (**41**) to develop optical changes in absorption and fluorescence spectra with addition of H_2S. When the electron withdrawing azido group is reduced with electron donor amino group, absorption peak is shifted to the longer wavelength and fluorescence signal of the cyanine dye increases, as a result, ratiometric detection of

H_2S is achieved. In this work, compound **41** was investigated to detect various intracellular H_2S in RAW264.7 cells.

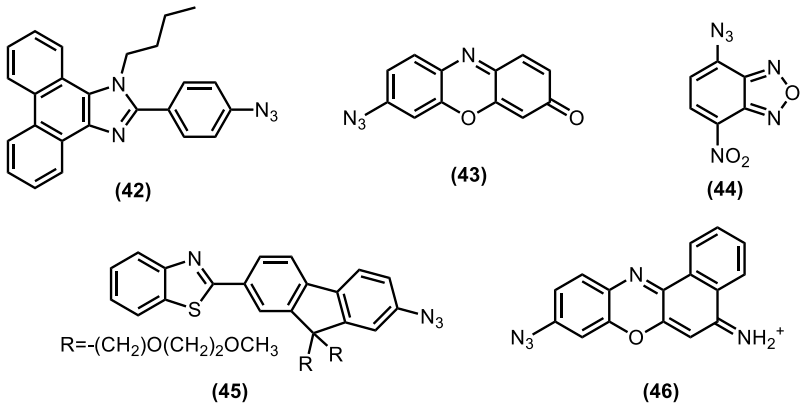


Figure 41. Reduction-based H_2S fluorescent probes in the literature.

Owing to the good selectivity and reactivity, reduction-based type is promising and useful in sensing of H_2S. Therefore, reduction-based detection is rapidly emerging as a H_2S sensing strategy and various fluorophores have been employed such as phenanthroimidazole,[80] resorufamine,[81] nitrobenzofurazan,[82] benzathiazole fluorine[83] and cresyl violet (Figure 41).[84]

2.5.2. H_2S Probes Based on Nucleophilic Attack

Besides its reducing ability, H_2S is a strong nucleophile. At physiological pH, it exists as SH^- while other biothiols are in neutral state. Thus, the different in pK_as makes H_2S more nucleophilic under these conditions. For sensing of H_2S becomes promising considering the diprotic nature and its potential to undergo two sequential nucleophilic attacks.

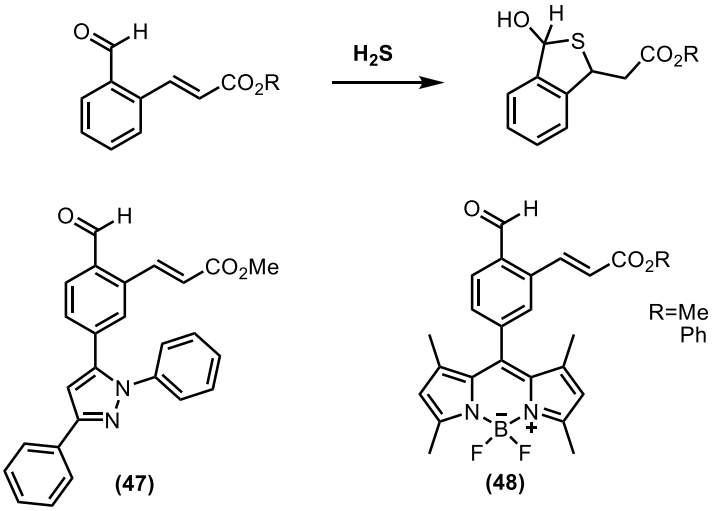


Figure 42. H_2S detection based on nucleophilic attack to an aldehyde followed by intramolecular attack on an olefin.

On the basis of dual nucleophilic character, H_2S initially attacks to the aldehyde and thiol is formed leading to second attack on α-β-unsaturated olefin. This mechanism was utilized in compound **47**. Addition of H_2S results in fluorescence enhancement and selectivity 3-4 fold over Cys and GSH is achieved. Another example is given in compound **48**. BODIPY based fluorophore is well established to detect H_2S. In a recent example, it was shown that reaction completion takes 3-4 hours and so the rate of fluorescence enhancement is slow.[85] This challenge was overcame by using more electrophilic olefin which facilitates faster nucleophilic addition of SH^- to electron poor C=C double bond. Thus, compound **48** reacts with H_2S more rapidly and detects H_2S in 30 minutes. With this modification, compound **48** was studied in blood plasma and brain tissue of mice to detect the H_2S.[76]

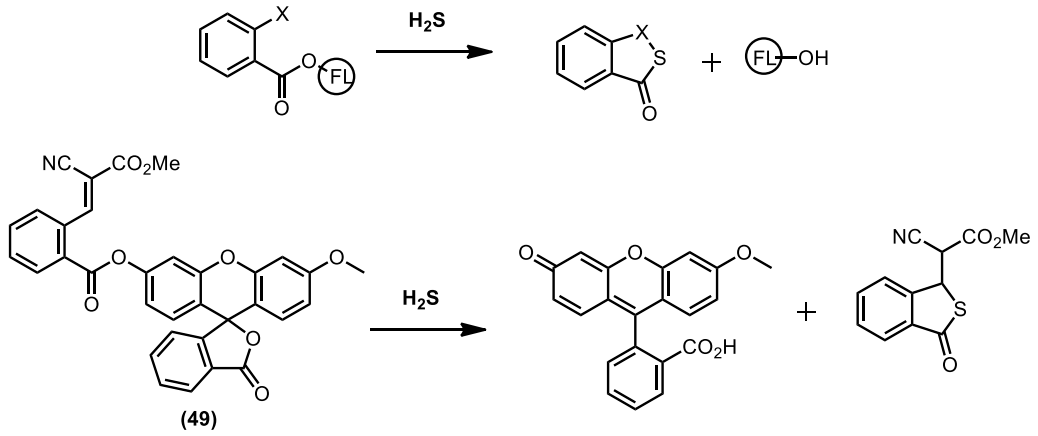


Figure 43. H_2S detection based on nucleophilic attack on an activated electrophile followed by attack on an ester-bound fluorophore.

Another similar approach based on the electrophilic olefins has been employed in H_2S sensing. As shown in Figure 43, compound **49** has both nitrile and ester functionality to improve the electrophilicity. In presence of H_2S, Michael addition-cyclization sequence takes place and fluorescence turn "on" is achieved.

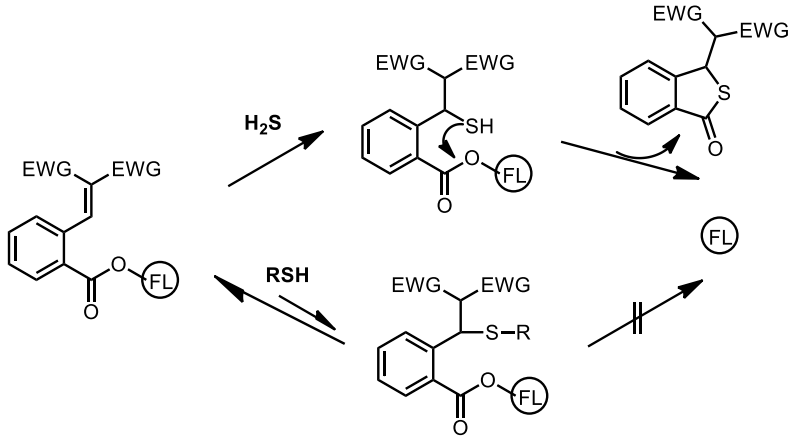


Figure 44. The reaction mechanism for Michael addition-cyclization for H_2S and other thiols.

Moreover, due to the good selectivity over other biothiols, Cys and glutathione did not give response. The reaction between Michael acceptors and biothiols is generally reversible and does not yield intramolecular cyclization.[86]

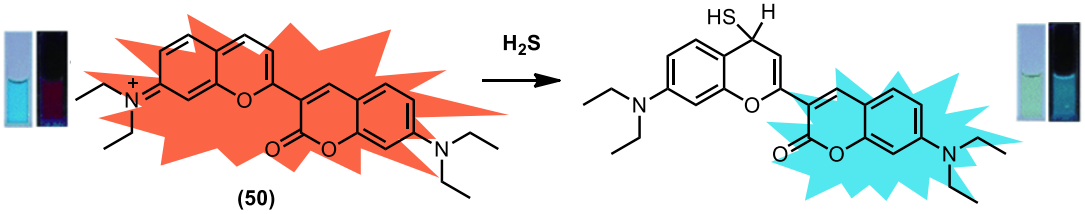


Figure 45. H_2S detection based on nucleophilic attack on an electrophilic center to break fluorophore conjugation.

Dual nucleophilicity of H_2S is employed for the distruption of the conjugation of the fluorophores. Guo and coworkers reported a falvylium dye-based ratiometric probe for H_2S working with nucleophilic attack of H_2S on the electrophilic center of benzopyrylium group (Figure 45). Addition of H_2S resulted in a 240 nm blue shift in absorption spectrum and fluorescence increase at 500 nm is observed.[87]

2.5.3. H_2S Probes Based on Copper ion

The strong interaction between sulfide and copper ion inspires the scientists to develop H_2S probe using fluorescence techniques.

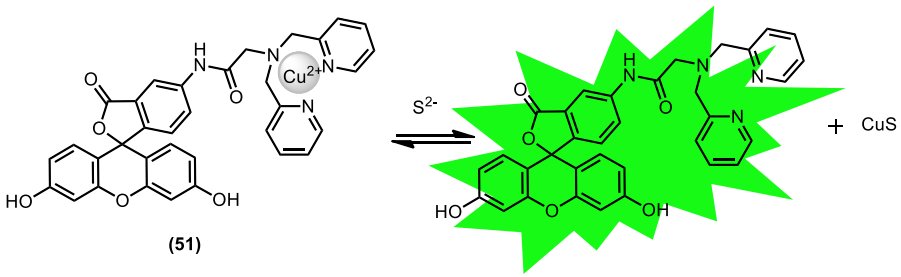


Figure 46. H_2S detection based on copper ion affinity of sulfides.

Chang *et. al.* developed a fluorescein based H_2S probe by using dipicolylamine moiety as a binding unit for Cu (II) (Figure 46).[88] Due to the chelation between Cu (II) and dipicolylamine, fluorescence was quenched. On the other hand, in presence of H_2S in 10 mM HEPES buffer at pH 7.0, Cu (II) was released and CuS was formed. Thus, fluorescence of fluorescein moiety was enhanced.

2.6. Photodynamic Therapy

Photodynamic therapy (PDT) is a very effective and novel methodology for cancer treatment. It is non-invasive compared to chemotherapy or radiotherapy. Photodynamic therapy is based on the activation of a nontoxic photosensitizer by an appropriate light source in the presence of molecular oxygen. In other words, there are three main components of photodynamic therapy: photosensitizer, light, and O_2. There are many advantages of PDT compared to chemotherapy and radiotherapy. To begin with, long-term side effects are minimal due to the local implementation. Additionally, both photosensitizer and light enable dual selectivity. Another significant advantage is that it can be applied before, after or simultaneously with another type of therapies and performed many times at the same location without causing any harmful effects. Modulation of photosensitizers, drug carriers and drug-light time intervals and ability to target diverse cellular components opens the way for different type of applications. The main drawback of this therapy is the lack of penetration of the light through the tissue. This limitation is the reason why PDT is

not as widespread as it is thought to be. Even when longer wavelength light sources are used, the maximum penetration depth reaches 5-10 mm.[89]

2.6.1. Fundamentals of Photophysics behind PDT

The basic theory behind the photodynamic therapy is that drug (photosensitizer) is injected and then light especially in the near-IR region is applied. The photophysical processes that are involved in PDT are shown in Figure 47. Photosensitizers (dyes) possess highly conjugated delocalized π systems. When photosensitizers are in their ground state, they have two electrons with opposite spins in low energy orbital. The proper absorption of light causes excitation of one electron

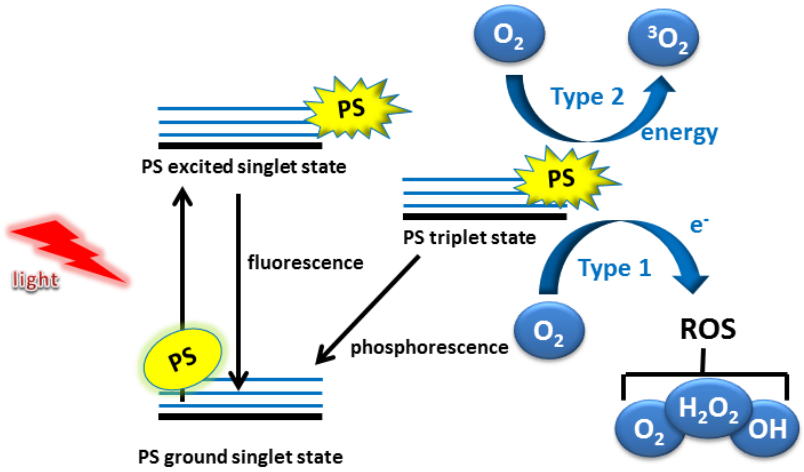


Figure 47. Photophysical processes in PDT.[90]

from highest occupied molecular orbital to the lowest unoccupied molecular orbital with conversion of spin. This first excited singlet state is not stable and short-lived so it releases its energy by different paths such as fluorescence, internal conversion or intersystem crossing. By intersystem crossing, the spin of the excited electron inverts to generate long-lived excited triplet-state having the electron spins parallel. The reason why triplet state of photosensitizer has a long time is that loss of energy via the phosphorescence process is spin-forbidden. Therefore, spin allowed nature of triplet-triplet transition allows the reaction between the triplet of photosensitizer and molecular oxygen which has triplet character in its ground state. The reaction generates highly reactive singlet oxygen species.[91]

2.6.2. Fundamentals of Photochemistry behind PDT

As it is stated above, molecular oxygen has triplet character in ground state meaning that the two outmost orbitals have unpaired and spin-parallel electrons. Photosensitizer in the triplet state can react with triplet oxygen in two different ways. Type I involves the direct reaction with a substrate like cell membrane or a molecule via an electron transfer or occasionally together with proton donation to triplet oxygen to generate superoxide anion which is not reactive to give oxidative damage. However, this superoxide anion reacts with itself to generate other ROS such as the hydroxyl radical and hydrogen peroxide.[92] Hydrogen peroxide is a biologically important species and capable of passing through the cell membranes. It plays fundamental roles on functionality of enzymes and its reaction with ferric iron (Fenton reaction) generates hydroxyl radical.

$$H_2O_2 + Fe^{2+} \rightarrow OH^- + \bullet OH + Fe^{3+}$$

The ferrous iron, Fe^{2+}, catalyzes the homolytic cleavage of oxygen-oxygen bond in hydrogen peroxide and produces a hydroxyl radical (•OH) and a hydroxide ion (OH^-). Reaction between the superoxide and a hydroxyl radical (•OH) forms singlet oxygen and when superoxide reacts with nitric oxide (NO^-) to generate peroxynitrite ($OONO^-$), which is a strong oxidizing agent. Similar to hydrogen peroxide, hydroxyl radical (•OH) is also permeable through cells and it can add to and oxidize the organic substances. This oxidized species become a radical, which induces other reactions. Thus, resulted chain reactions give oxidative damage to lipids or fatty acids.[93]

In Type II mechanism, spin of the outmost triplet oxygen electron inverts and moves into the orbital containing the other electron so one orbital becomes completely unoccupied. This highly reactive singlet oxygen has a short lifetime and reacts directly with biological components. Singlet oxygen reacts with double bonds and sulfur groups with highly complex mechanisms. For example, oxidative cleavage of DNA involves a [4 + 2] cycloaddition to the C-4 and C-8 carbons of the purine ring resulting an unstable endoperoxide. The sequential complex reactions and the product are dependent on the presence of guanine unit on double stranded DNA.[94]

In PDT, Type I and Type II reactions take place at the same time but the percentage differs according to the photosensitizers used and the concentrations of the substrate and molecular oxygen.[95] Because of the high reactivity and short half-life of singlet oxygen, it gives damage locally where the photosensitizer is present. It is estimated that in the half-life, it diffuses approximately 40 nm, thus, the radius of the activity is of the order of 20 nm.[96]

2.6.3. Importance of Light

From sunlight to highly complex light sources, light used in PDT has been subject to a transformation over the years. Advancement in the optical technology offers new light delivery device and novel light sources.[97] The light sources utilized in PDT can be divided into two groups as lasers and non-laser sources. Laser systems offer high quality because they are highly intense, monochromatic, have minimal thermal influence and can be modified for fiber optic delivery. However, conventional laser (potassium-titanyl-phosphate (KTP) dye, metal vapor lasers) sources have some drawbacks. For example, they are highly expensive and have large size. Development of diode lasers offers some advantages compared to conventional laser sources such that they are less expensive, portable and most importantly, they can be modified to have multi-channel unit to accomplish the complicated PDT process (Ceralas PDT 762 nm; CeramOptec GmbH of Biolitec AG).[98] Also, non-laser systems bring some superior features. First of all, they are cheaper, user-friendly and smaller in size. Besides, they can cover a broad range of the spectrum. However, they suffer from the thermal effect and lower intensities. All in all, light emitting diodes are up-to-date non-laser sources exhibiting easy-handling and non-coherent properties.

The developments of laser sources are crucial in PDT because in target tissue, the spatial and temporal distribution of light affects the PDT efficiency. Applied light can be absorbed or scattered in tissue. Depending on the tissue type and wavelength, the amount of these processes can vary. There are some obstacles while dealing with biological tissue. To begin with, presence of macromolecules, organelles, cell layer, etc. causes inhomogeneity and turbidity causes significant scattering and loss of

directionality.[93] Also, the absorption of molecules such as hemoglobin is another issue that must be addressed. The low absorption wavelength of natural components along with minimal light scattering at longer wavelengths and presence of water absorption above 1300 nm results in an "optical window" that PDT can be effective. The average penetration depth is 1-3 mm at 630 nm and this number nearly doubles at 700-850 nm.[99]

To conclude, in PDT, light must pass through the tissue to activate photosensitizer. In this manner, not only the optical characteristics of the tissue but also the wavelength of the light plays crucial role for penetration efficiency (depth where light has to reach). The maximum penetration through tissue can be obtained at the near – IR (700- 1100 nm). In this region, the absorption of the natural tissue chromophores (oxyhemoglobin, deoxyhemoglobin, melanin) is weak. However, most photosensitizers rarely absorb above 800 nm and this limits the application of PDT. To overcome light delivery problem, we proposed a novel PDT system in which persistent luminescent nanoparticles are used (see Chapter 8).

2.6.4. Photosensitizers

Photosensitizers are generally highly conjugated aromatic organic molecules. Modifications allow the change in the delocalization system and so absorption properties can be modulated.[90] Photosensitizers should have high absorption in therapeutic window and high singlet oxygen quantum yield. Also, they must have low dark toxicity, in other words, it should be active only when they are irradiated and photobleaching should be low. Moreover, they should accumulate preferentially accumulate in the target tissue and show high chemical stability. A considerable amount of photosensitizers has been synthesized since 1980. Typically, they can be classified into two groups as natural-porphyrin-based and non-porphyrin-based. First generation natural-porphyrin-based photosensitizer, Photofrin, is approved for clinical applications. However, first generation photosensitizers show weak absorption intensity at 630 nm which prevents the deep penetration of light. Additionally, due to the planar structures, π-π stacking causes aggregation in solutions. Furthermore, synthesis of porphyrin is not straightforward and selectivity

is not achieved. Thus, second generation photosensitizers have been developed to address the drawbacks of the first generation. These photosensitizers involve the synthetic version of natural porphyrins such as chlorins, purpurins, bacteriochlorins, phthalocyanine, squarine and perylene diimide.[100] However, the chemical- and photo-stability upon storage and aggregation in polar medium are major issues that need to be addressed. Additionally, phthalocyanine dyes can chelate to diamagnetic metals such as aluminum, zinc which contributes to phototoxicity. A second generation non-phorphyrin dye, rose bengal, shows low singlet oxygen yield so decreases the PDT efficiency.[101] Third generation photosensitizers are non-naturally-occurring, conjugated pyrrolic ring systems and contain modified photosensitizers and biological components like antibodies or liposomes.

2.6.4.1. BODIPY Dyes as Photosensitizers

BODIPY dyes have attracted great attention as suitable photosensitizers for photodynamic therapy owing to their intrinsic characteristics. They can be modified to have strong absorption in near-IR region and high stability in ambient conditions is another important feature. Besides its stability, the light to dark toxicity ratio is higher than other photosensitizers. To get better photodynamic action, some modifications have been employed on the BODIPY core. The main aim is to increase the triplet sensitization. Halogenation, using fullerene C_{60} derivatives and logically designed BODIPY dimers have been utilized frequently in this sense and are described below.

Halogenation: To begin with, “heavy atom effect” is a way of increasing intersystem crossing and so triplet sensitization offers singlet oxygen generation. Incorporation of heavy atoms like iodine or bromine improves the spin-orbit coupling and this leads to an improvement of intersystem crossing without energy loss from excited states.[102]

Nagano and coworkers reported non-halogenated and halogenated tetramethyl BODIPY dyes as shown in Figure 48.[103] Non-halogenated derivative showed strong fluorescence so low singlet oxygen generation yield. On the other hand, diiodo-

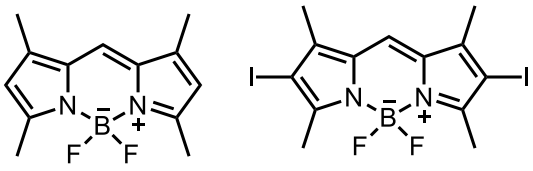


Figure 48. Molecular structures of non-halogenated and halogenated BODIPY dyes

tetramethyl BODIPY derivative demonstrated low fluorescence intensity and high efficiency in generation of singlet oxygen. The decrease in fluorescence quantum yield explains the effect of intersystem crossing due to the presence of iodine atoms.

As it was mentioned before, the strong absorption in near-IR region and water-solubility are important criteria to meet in the design of photosensitizers. Akkaya *et. al.* synthesized novel compounds to achieve the desired properties.[37] The group attached the triethylene glycol moieties to improve the water solubility and bromine atoms to enhance the intersystem crossing (Figure 49). Besides, they used distyryl BODIPYs to get absorption in near-IR region to have deep penetration. These water-soluble, near-IR absorbing BODIPY dyes produced singlet oxygen efficiently and was tested in K562 human erythroleukemia cells.

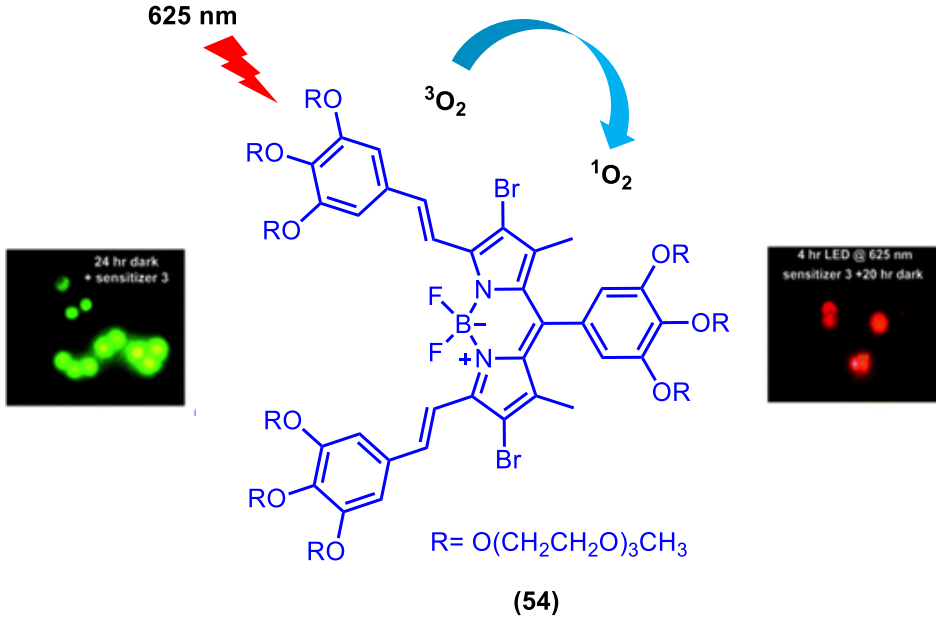


Figure 49. Halogenated BODIPY derivatives for photodynamic therapy application.[37]

Incorporation of C_{60} unit: In addition to heavy atoms, fullerene C_{60} is another way to increase spin-orbit coupling to enhance intersystem crossing. Excitation of C_{60} by light causes transition of singlet excited state to triplet excited state with the help of intersystem crossing with almost quantitative efficiency.[104] Only C_{60} is not suitable for photodynamic therapy because of low absorption in the near-IR region, however, this low absorption is enough to get intramolecular energy transfer in C_{60}-organic dyes conjugates. To accomplish efficient photosensitizers, Zhao group designed and synthesized BODIPY- C_{60} conjugate (**55**).[105] In the design, they used di-styryl BODIPYs to get strong absorption in nearly 660 nm and C_{60} moiety to behave as spin convertor. With this construction, long-lived triplet excited state was achieved. The measurement and evaluation of the data showed that BODIPY-C_{60} conjugate demonstrated great performance in terms of singlet oxygen generation efficiency and stability over commonly used photosensitizers such as methylene blue and tetraphenylporphyrin. The paper also indicated that there was not much difference in photodynamic therapy efficiency when the number of C_{60} was increased.

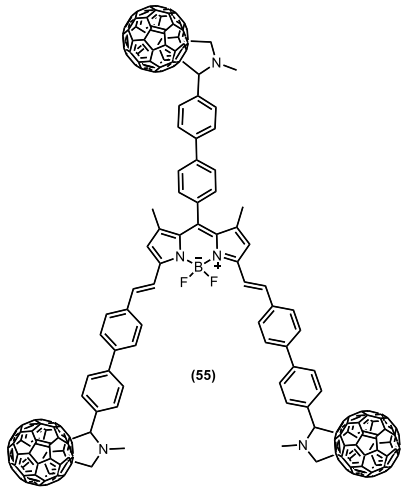


Figure 50. BODIPY- C_{60} derivative for photodynamic therapy application.

BODIPY dimers: Triplet sensitization can be obtained with substituents which have molecular orbitals with suitable multiplicity and energy levels. Lately, Akkaya group published a new category of bis(BF_2)-2,2‘-bidipyrrins (BisBODIPYs) showing interesting properties (compound **57** and **58**). These dimers are able to undergo intersystem crossing efficiently compared to the monomer derivatives. They

consolidated their design with computational studies. Computational studies suggest that BODIPY monomer exhibits low triplet quantum yield and in the excited state, there are two orbitals with single occupancy. On the other hand, orthogonal BODIPY dimers show doubly-substituted excited state configuration which promotes singlet excited state and triplet excited state coupling. In this publication, it was shown that singlet oxygen quantum yield of orthogonal BODIPY dimers is comparably high and photocytotoxicity experiments were conducted well in K562, human erythroleukemia cells.

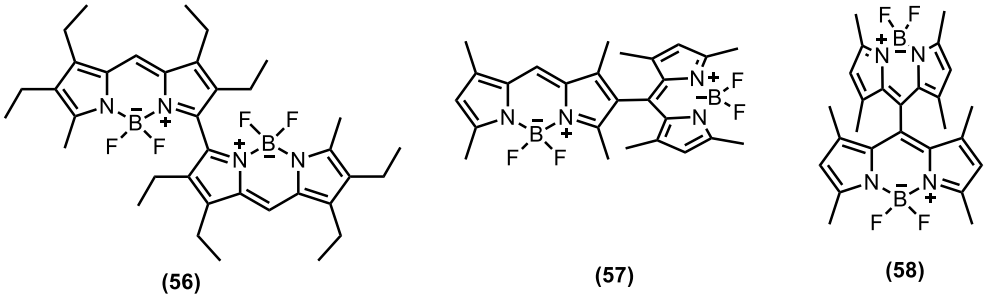


Figure 51. Orthogonal BODIPY dimers for photodynamic therapy application.

2.6.5. Modes of Cell Death

There are two main types of cell death triggered by photodynamic therapy. First type is apoptosis and second one is named as necrosis. Which type of cell death is dominant is dependent on several elements such as type of cell, the subcellular localization of the photosensitizers, the concentration of photosensitizer and the applied light dose to stimulate photosensitizer locally.[106] In addition, it is suggested that lower dose of photodynamic therapy dominates apoptosis, whereas higher doses contributes significantly to necrosis.[107]

Apoptosis is a highly complicated process and includes several steps. This programmed cell-death mode is encoded genetically in all cells in the body.[108] Generally, mitochondrial release of cytochrome c initiates the apoptosis. This event causes the activation of caspase cascades termed as executioner caspases including caspase-3, -6 and -7.[109] These caspases bring about the cleavage of cellular components that causes the changes in biochemistry and morphology processes seen in dying cells.[110] After cleavage of nuclear lamins, chromatin condensation and

nuclear shrinkage take place successively. Then, DNA fragmentation is caused by cleavage of inhibitor of the DNaseCAD (caspase activated deoxyribonuclease). Finally, cleavage of proteins in cytoskelaton cause cell fragmentation and apoptotic bodies.[111] The main characteristics of the apoptosis are cell shrinkage, plasma membrane blebbing and organelles.

Necrosis is the second type of cell-death mode in photodynamic therapy. Unlike apoptosis, this type of mode is known as highly violent and an accidental cell death. Its main features are cytoplasm swelling, damaging of organelles and demolishment of the plasma membrane. With these series of events, intracellular substituents are released and inflammation takes place.[112] In necrosis, dying of the cells happens accidentally and it is termed as unprogrammed cell death. The biochemical and morphological changes can be explained as pyknotic nucleus, cytoplasmic swelling and loss of integrity in cytoplasmic membranes.

Apoptosis and necrosis are the direct tumor cell killing modes as well as they play role on the vascular damage and immune response which are other mechanism in tumor cell destruction.[113] Direct tumor cell killing, vascular damage (shutting down of tumor vascular causes lack of nutrients and oxygen) and immune response (release of cytokinase and stress response proteins) affect each other and it should be highlighted that combination of those contributes the photodynamic therapy efficiency.[92]

2.6.6. Activatable Probe Design

In photodynamic therapy, one of the main superiority is that delivery of light and localization of photosensitizer can lead to dual-specificity. In contrast to other mechanisms, delivery of light in a localized area offers high specificity and healthy cells far from this area are not affected from generation of singlet oxygen. As a third item for specificity, molecular activation attracts attention. In other words, the combination of localization of photosensitizers in tumor tissue, the activation of photosensitizer by tumor tissue and applied light in specific area promote the damage

of targeted tumor cells. Thus, activatable probes hold great potential towards differentiation between healthy and unhealthy tissue.[114]

At first, the activatable probes is non-fluorescent owing to the spatial proximity between dye and quencher moieties and with the interaction between the biological stimuli, fluorescence of the probe is restored upon the cleavage of the linker located between the dye and inhibitor. Activation can be done via proteolytic activity, disulfide bridge and pH-sensitive hydrozone groups.[115]

The activatable probes can be divided into three groups based on photochemistry namely; self-quenching based, inorganic component based and energy transfer based (between donor and acceptor dyes).

Before describing each group in detail, a brief quenching mechanism should be given for clarity. There are two types of quenching: dynamic and static quenching. Dynamic quenching involves Förster resonance energy transfer, Dexter type energy transfer and exciplex formation. In all these processes, donor and acceptor parts are not in contact with each other and the excited state is involved. However, in static quenching, bonding between the donor and acceptor moieties occurs in ground state and ground state complex shows its own properties. For example, owing to the hydrophobic interactions, stacking between dye molecules causes dye aggregation.

Self-quenching based activatable probes rely on the aggregation formation in aqueous medium. To illustrate, Texier and coworkers utilized Cy5.5 dye, disulfide bridge and RAFT-$(cRGD)_4$ (Figure 52).[116] In the first case, dimerization of Cy5.5 was shown by absorption spectrum and decrease in fluorescence quantum yield. However, in presence of mercaptoethanol, with the cleavage of disulfide, absorption peak of Cy5.5 appeared and fluorescence quantum yield increased.

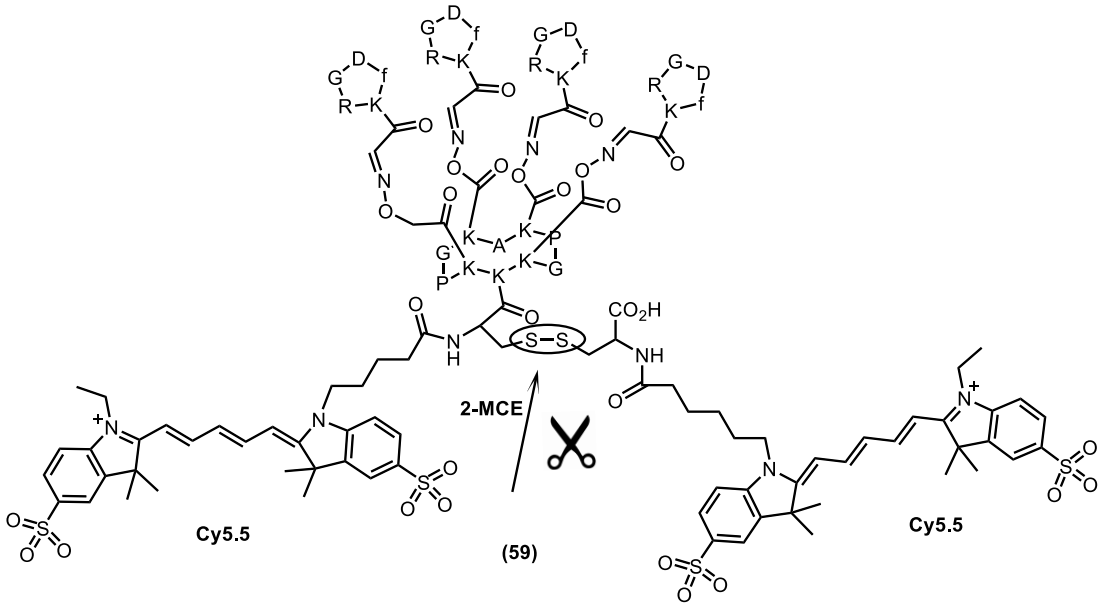


Figure 52. Self-quenching based activable probe.

For inorganic structure based activation, gold nanoparticles and gold nanorods have been employed frequently. Tuang group reported gold nanorod based probe for photodynamic therapy.[117] In their design, they used Aptamer Sgc8 to target leukemia T cells specifically and this aptamer is hybridized with chlorin e6 as a photosensitizer for formation of a DNA double helix as depicted in Figure 53. In the absence of leukemia T cells, due to quenching of chlorin e6, there was no photodynamic action. On the other hand, presence of target cells caused the change in structure of Aptamer Sgc8, so with the applied light, released chlorin e6 generated singlet oxygen efficiently.

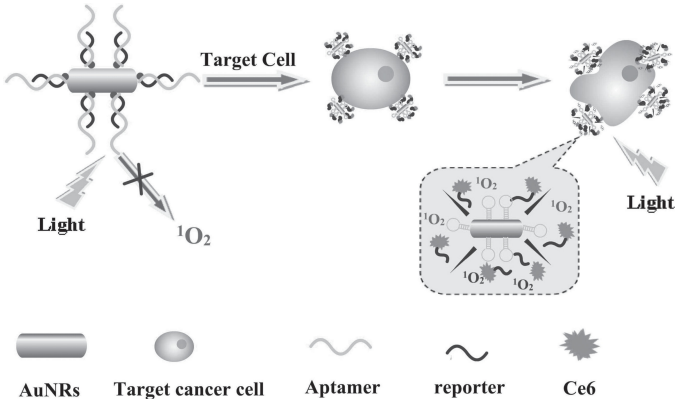


Figure 53. Gold nanorod based activable probe (Copyright © 2013, John Wiley and Sons, Reprinted with permission from ref (117)).

Last group depends on the organic dye and quencher conjugates. These quenchers are utilized with resonance energy transfer. The spectral overlap between the emission of the dye and absorption of quencher facilitates the energy transfer. The most employed near-IR quenchers are BHQ3, Cy7Q, QSY21, FluoQuench 661*, etc.* besides convenient near-IR dyes.

2.6.7. Disulfide Bridge as a Clevable Linker-activation by Glutathione

Glutathione is a thiol containing tripeptide and its concentration in tumor cells is higher up to 1000-fold. In tumor cells, the irregular blood flow causes hypoxic state, decreased oxygen level and so the activity of reductive enzymes increases (high glutathione concentrations).[118] In previous studies, it was well stated that GSH is elevated in breast cancer[119] and colon cancer[120] cells, *etc.* In the presence of high intracellular concentration of glutathione, disulfide bonds are broken. On the other hand, disulfide bonds are thermodynamically stable and provide reasonably good stability in the bloodstream in the absence of sulfhydryl groups. Therefore, synthesis of glutathione-activatable photosensitizers via a disulfide linker is a promising strategy to develop photodynamic therapy reagents. This design is not very common in the literature.

As shown in Figure 54, disulfide reduction is utilized in BODIPY and rhodamine based folate-FRET probe for imaging application.[121] Folic acid is decorated because it shows high affinity toward folate receptor and to improve water solubility, hydrophilic peptide spacer is used. Also, BODIPY and rhodamine derivatives are placed as donor and acceptor moieties, respectively. BODIPY and rhodamine is linked to folate by an amide and disulfide bond, respectively. With the disulfide reduction, FRET is blocked due to the release of rhodamine unit and the fluorescence of BODIPY is enhanced.

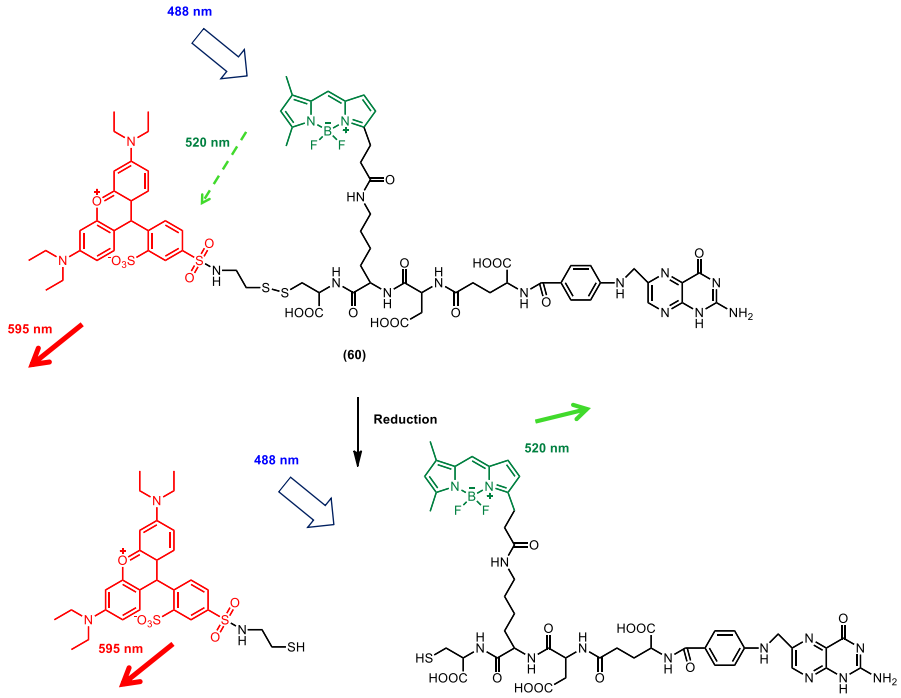
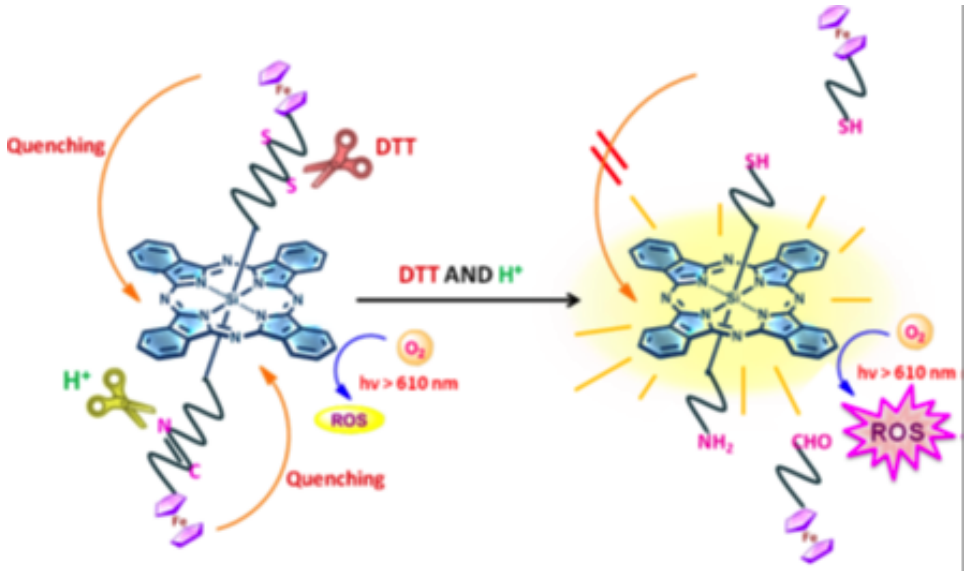


Figure 54. Disulfide reduction based FRET probe.

In another example, disulfide bridge is used as well as a hydrazone linker, which can be activated by acidic environment.[122] In this example, two ferrocenyl units (donor) are attached to silicon (IV) phtalocynanine moeity (acceptor and photosensitizer compartment) via disulfide and hydrazone groups (Figure 55). These groups offer dual-activation and so specifity is enhanced. Since tumor cells environment is slightly acidic (pH = 4.5−6.8), hydrazone unit is activated by acid. Moreover, reducing environment of tumor tissues allows the reduction of disulfide bridge. Presence of both acid and dithiothreitol causes cleavage of hydrazone and disulfide linker, thus releasing of two-ferrocenyl units and blocking of FRET. As a result, singlet oxygen generation is achieved with the application of light.



(61)

Figure 55. Disulfide reduction based FRET probe (Copyright © 2014, American Chemical Society, Reprinted with permission from ref (122)).

Nanoparticles offer several advantages compared to bulk materials in application of photodynamic therapy. Due to their small size and light weighing, they can be modified easily to enhance water solubility. In addition to increase water solubility and to minimize surface energy, stabilizers are used. Stabilizers can vary according to types of nanoparticles. Moreover, high surface to volume ratio, presence of dangling bonds makes them electrically charged. Thus, nanoparticles can adsorb charged ions and Coulombic forces make the nanoparticles repel each other so they can be dispersed in water. Another important advantage is that they can easily pass through the cells due to their small size. These mentioned properties allow nanoparticles to be applied in biological environment. Persistent luminescent nanoparticles are one of the biologically important nanosystems to be used in imaging and photodynamic action.

2.6.8. Persistent Luminescence

The term “luminescence” is referred to non-thermal emission of light contrary to the incandescence. Sometimes, it is called as “cold” light and results from electron transitions from higher energy states to lower energy states. There are different types of luminescence according to their energy source such as chemiluminescence caused

by chemical reaction or electroluminesence resulting from electric current passing through a material, etc. Photoluminescence is another type of luminescence and its source is excitation of electrons to higher energy states via absorption of electromagnetic radiations. The work described in this thesis is mainly concerned with photoluminescence which covers fluorescence, phosphorescence and persistent luminescence (afterglow) (Figure 56). From the point of duration of the emission after turning off the excitation source, there are three types of luminescence: fluorescence, phosphorescence and afterglow. Since fluorescence is described in the previous parts, phosphorescence and afterglow will be explained here. The lifetime of fluorescence is approximately 10^{-8} s, however, in the phosphorescence; it reaches to milliseconds even seconds. Phosphorescence is known as a spin-forbidden process. When an electron absorbs energy, it goes to higher energy levels in the first singlet excited state. Then, upon spin conversion, this electron goes to triplet state via intersystem crossing and then does phosphorescence while going back to the ground state.

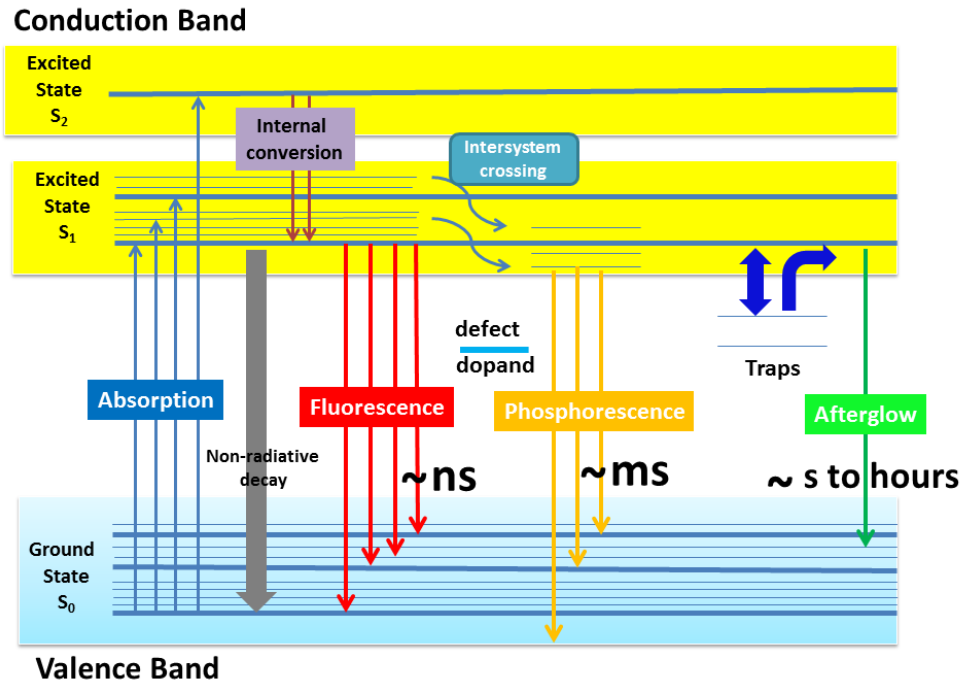


Figure 56. Schematic representation of energy diagram for fluorescence, phosphorescence and afterglow.

In the persistent luminescence, sometimes mixed with phosphorescence, the stored excitation energy by traps is released slowly and thermally to emitting centers and the light emission can last for hours.[123] The excitation sources can be visible or ultraviolet (UV) light or X-rays, *etc*. The "persistent luminescence" event dates back to 17th century.[124] Although the ancient Chinese paintings described the persistent luminescence obtained by combining the colors with a different type of pearl shell, first scientific description was made by Italian shoemaker and alchemist V. Casciarolo in 1602. He discovered the intense luminescence caused by a mineral barite, $BaSO_4$, known as Bologna Stone. At first, it was thought that barium sulfate is the main reason, however, actually the reason why this stone luminesce for hours is the natural impurities like monovalent copper. The interest for persistent luminescence was intensified by the end of 20th century. For example, zinc sulfide doped with copper or cobalt has been used commercially for glow-in-dark products or paintings.[125] To increase the usage of these products for practical goals, the duration of the luminescence as well as the brightness should be improved. In this sense, radioactive elements (promethium, tritium) were incorporated in these materials, however, to achieve reasonable brightness, considerable amount of material should be used. In the persistent luminescence compounds, generally, rare earth ions are introduced as dopants in the host lattice to activate inorganic host matrix.[124] Matsuzawa and coworkers reported green-emitting afterglow $SrAl_2O_4:Eu^{2+}$ codoped with the rare earth dysprosium (Dy^{3+}) showing long-lasting bright emission after cessation of excitation source.[126] This material showed superior properties compared to ZnS:Cu,Co. After their work, lots of publications have reported afterglow materials with different properties. These studies showed that in persistent luminescent materials, there are two centers named as emitters and traps. Emitters are responsible for radiation emitting after excitation, while traps, which can be lattice defects or codopants, are present to store and then release the excitation energy. Thus, it can be stated that the emitters determine the emission wavelength and traps are responsible for the observed intensity and duration of afterglow.[127] As a result, near-IR persistent luminescent materials are generally have a proper emitter being able to emit near-IR light and an appropriate host having capacity for generating traps and boosting the persistence of the afterglow. The brightness and

duration of the afterglow materials are dependent on many factors such as codoping with rare earth, choice of starting material, dopant and codopant concentration, *etc*.[128]

2.6.8.1. Persistent Luminescent Nanoparticles

Optical imaging probes have attracted great attention for biomedical applications. In this type of imaging, light is used to activate the luminescent component in tissues and detection is done with capturing the transmitted or reflected light.[129] Developments in optical techniques have brought optical imaging to a convincing method for biomedical applications. Although optical probes offers significant outputs in early detection that is an essential item for the timely diagnosis and efficacious treatment of all cancer types, conventional optical probes suffer from some limitations for practical use. Cytotoxicity, poor signal-to-noise ratio from tissue autofluorescence under external light, cell death resulting from short-wavelength irradiation are some of the drawbacks.[130] To overcome such problematic issues, persistent luminescent nanoparticles (PLNPs) arise as optical imaging tool. These materials are capable of luminescence several hours after irradiation source has been switched off. The irradiation source can be UV or visible light. Optical excitation before injection is another promising property of these materials. Improved signal-to-noise ratio is achieved because of the removal of background fluorescence caused by in situ excitation and deep penetration is achieved. Thus, real-time monitoring becomes feasible and these materials with their unique properties draw attention for biological applications. However, in the literature, the use of PLNPs in biological applications is limited maybe due to the difficulty in the synthesis of these materials. The synthesis of PLNPs requires high temperature and yields are generally very low.

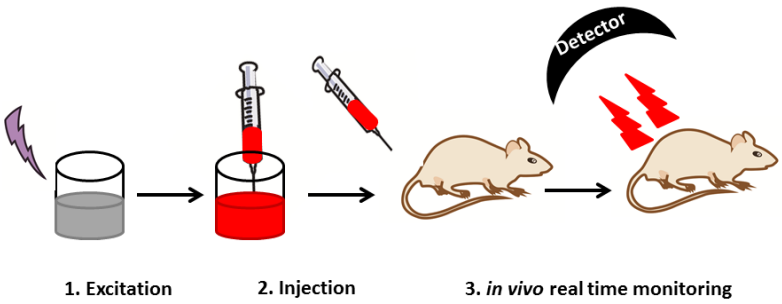


Figure 57. PLNPs in in vivo imaging.[131]

In 2007, Scherman *et. al.* reported red emitting PLNP whose composition is $Ca_{0.2}Zn_{0.9}Mg_{0.9}Si_2O_6$ doped with Eu^{2+}, Dy^{3+} and Mn^{2+}.[131] In this work, nanometric size red emitting long lasting afterglow was first described and in vivo imaging studies were shown successfully. These nanoparticles were used in real-time monitoring of living mice for more than 1 hour after intravenous injection without any external excitation. These nanoparticles showed very narrow size distribution between 50-100 nm and the emission intensity is centered at 690 nm. After synthesis of PLNPs, surface modification was performed to explore the biodistribution properties. For this purpose, hydroxy-functionalized NPs were coated with amino, carboxyl and polyethylene (PEG) groups. The accumulation and circulation time is changed according to the type of modification.

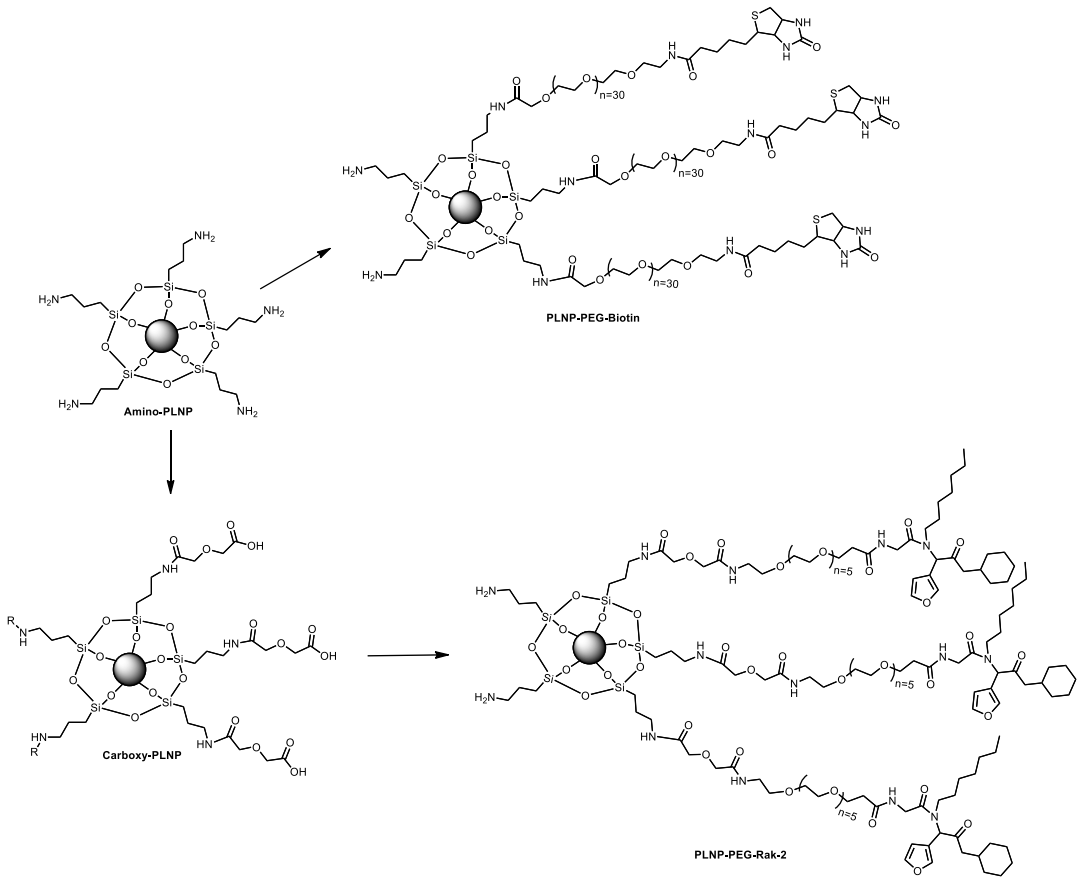


Figure 58. Modification of PLNP with biotin and Rak-2.

In another work, Scherman and coworkers further developed these PEG containing nanoparticles with attaching targeting groups to increase the accumulation in targeted tissue.[132] They used two different small targeting moieties which are biotin and Rak-

2. (Figure 58) Biotin functionalized PEG containing PLNP showed affinity to streptavidin coated plate and Rak-2 demonstrated affinity towards PC-3 cells. After characterization of modified nanoparticles by different methods, in vitro studies were conducted. These studies showed that PLNP-PEG-Biotin conjugate binds to streptavidin plate and PLNP-PEG-Rak-2 conjugate binds to prostate cancer cells.

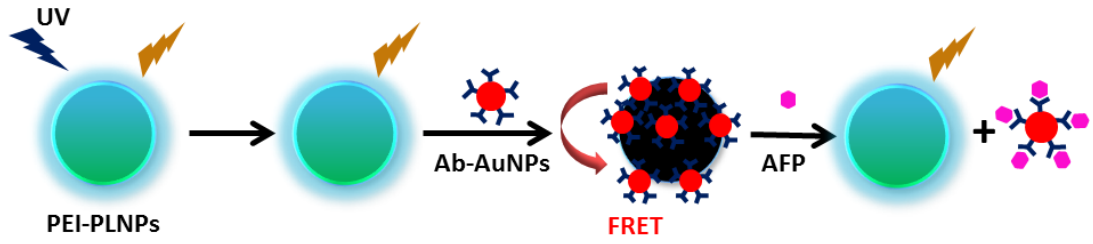


Figure 59. Schematic demonstration of the FRET based inhibition assay for AFP using PLNPs.

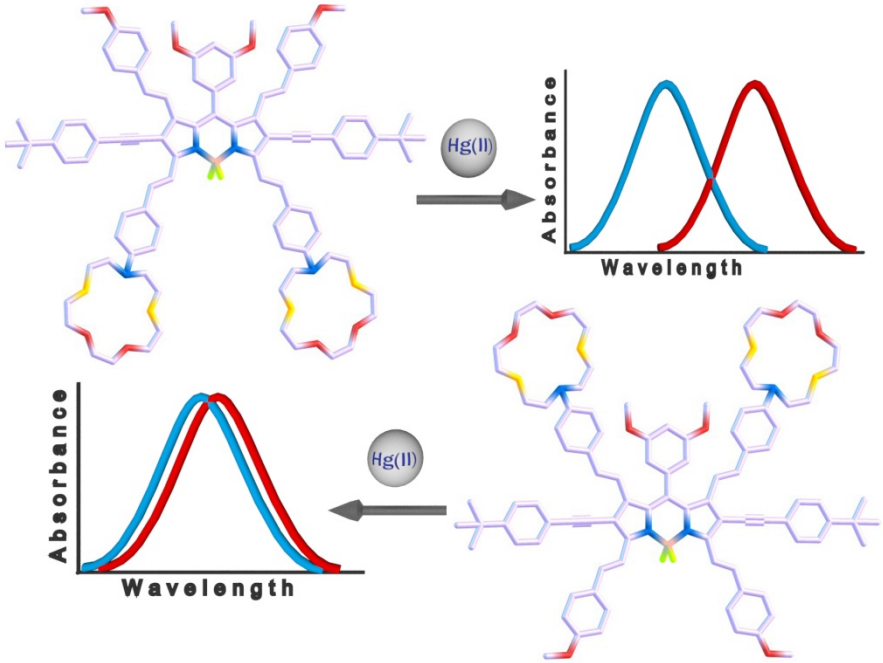
Another important work was described by Yan group shown in Figure 59.[133] In this study, water soluble PLNPs whose composition is $Ca_{1.86}Mg_{0.14}ZnSi_2O_7$ doped with Eu^{2+} and Dy^{3+} were used to get FRET based inhibition assay for α-fetoprotein (AFP) excreted during cancer cell growth. AFP is known as serum biomarker for hepatocellular carcinoma (HCC) in which survival rates are very low due to the difficulty in prognosis. Rapid liver cancer cell growth and cirrhosis increases the level of AFP so detection of the AFP allows the early diagnosis of HCC. Due to the spectral overlap between emissions of polyethylene imine coated PLNPs which is positively charged and absorbance of antibody coated gold nanoparticles which is negatively charged, FRET process occurs. After interaction between AFP, FRET process is blocked, thus, the emission from PLNPs were observed.

CHAPTER 3

Rational Design of Ion Responsive, Isomeric Near-IR BODIPY Dyes

This work is partially described in the following publication:

Ozdemir, T.; Kostereli, Z.; Guliyev, R.; Yalcin, S.; Dede, Y.; Akkaya, E. U. *RSC Adv.*, **2014**,*4,* 14915-14918.



3.1. Objective

Tetrastyryl-substituted BODIPY dyes are likely to evolve into a new class of near IR fluorophores. In this work we demonstrate that 1,7 and 3,5-positions show marked differences in charge transfer characteristics. Using a Hg (II) selective ligand, the signal transduction potentials were explored: One isomer shows a large blue shift in electronic absorption spectrum, while the other just shows an intensity increase in the emission spectrum. Electronic structure calculations were undertaken to elucidate the reasons for different signals on metal ion binding in relation to core BODIPY properties.

3.2. Introduction

Fluorescent dyes exhibiting near-IR absorption and emission are rare,[134-136] and considering their potential utility in many fields such as biological imaging,[137] photodynamic therapy,[138] light harvesters,[139] solar cells,[140] there is a strong motivation for developing such organic compounds. Longer wavelength emitting fluorescent dyes are relatively free from background signals, resulting either from Rayleigh scattering or autofluorescence in biological media.[141] BODIPY dyes are truly unique in their capacity for chemical modifications at all positions of the parent dye.[40] Derivatization at the 1,3,5,7 positions *via* Knoevenagel condensation results in large bathochromic shifts, pushing the $S_0 \rightarrow S_1$ absorption band towards near IR. Recently, tetra-styryl BODIPY derivatives have been successfully synthesized and shown to be stable chromophores with reasonable fluorescence quantum yields. Following our initial report,[43] quadruple Knoevenagel condensation on 1,3,5,7-tetramethyl BODIPY dyes has become a well-established protocol and even controlled sequential reaction of methyl groups at these positions with different aldehydes being demonstrated.[45] Tetrastyryl-BODIPYs are now very well-positioned to become a structurally flexible class of near IR dyes.

In the present work, our aim was to explore the ion signaling potential of the dyes with charge donor ligands placed in conjugation at 1,7 *versus* 3,5 positions of the BODIPYs, i.e., four isomeric tetra-stryryl BODIPY compounds which were functionalized with Hg(II) selective dithiaazacrown ligands (Figure 60).

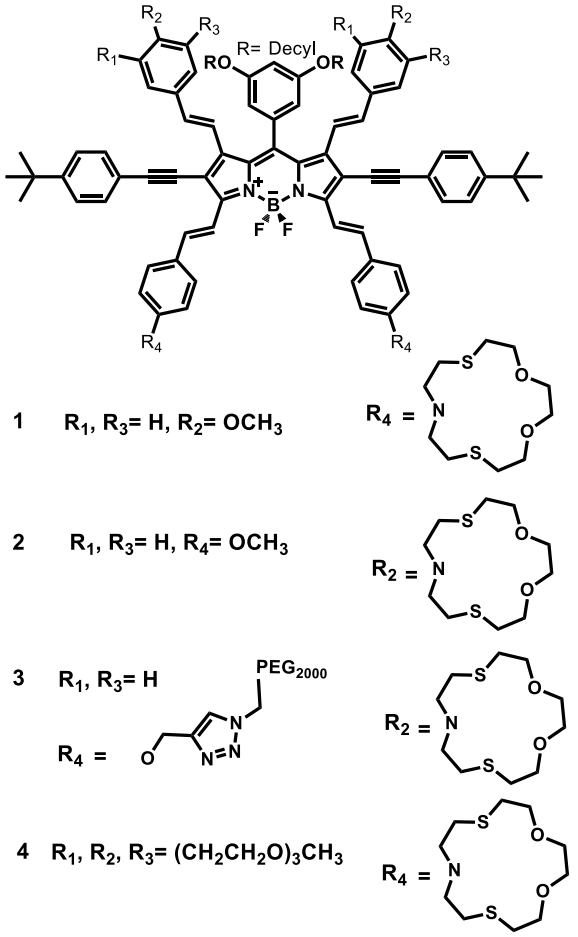


Figure 60. Structures of target compounds **1**, **2**, **3**, **4** (Copyright © 2014, Royal Society of Chemistry, Reprinted with permission from ref (142)).[142]

3.3. Results and Discussions

These derivatives were readily synthesized based on already established protocols (Figure 61). Appropriate aromatic aldehydes undergo Knoevenagel reaction in the presence of acetic acid and piperidine using a Dean-Stark trap. Besides, being a convenient and efficient reaction, Knoevenagel condensation gives reasonable yields.

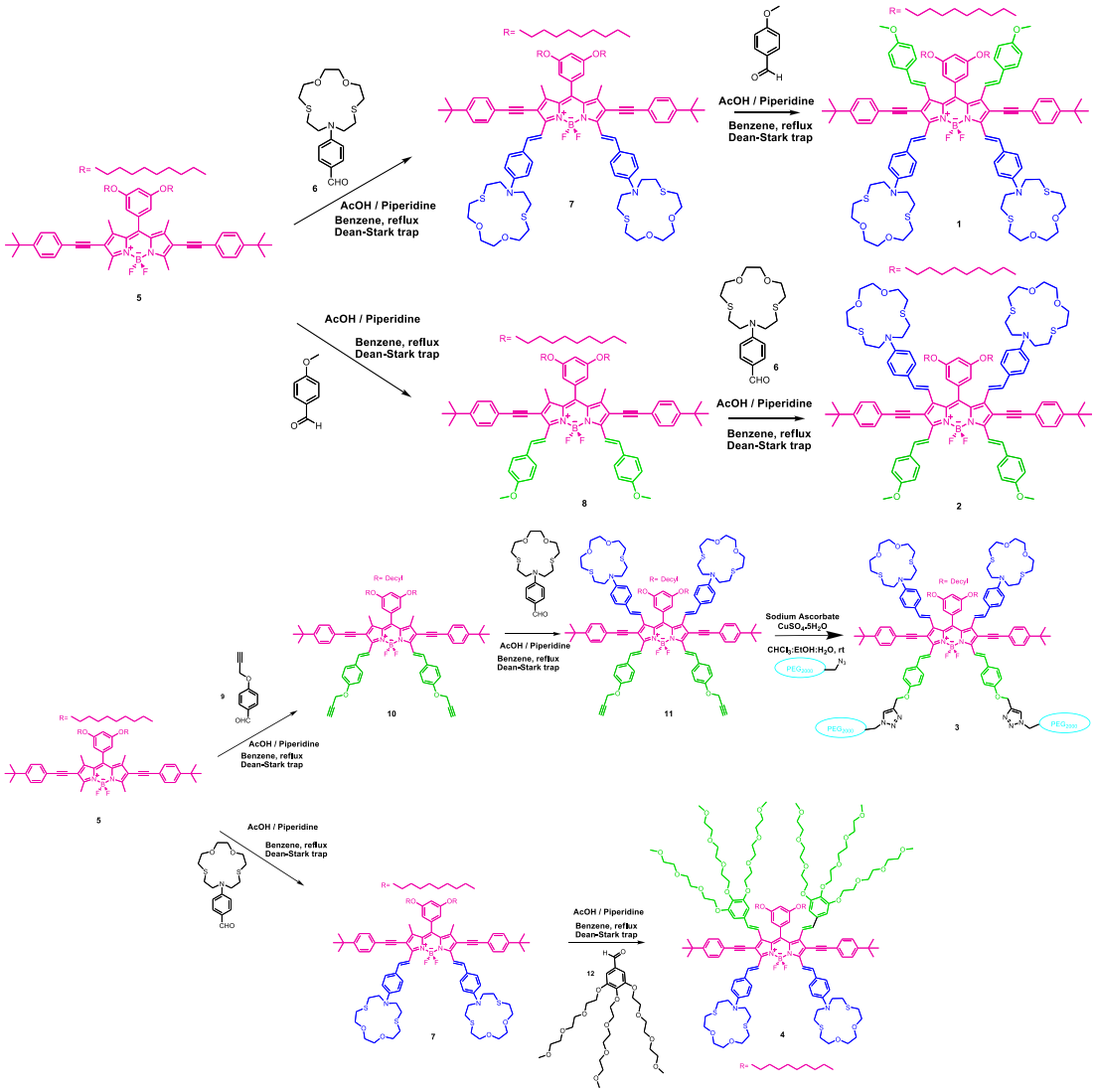


Figure 61. Synthesis of target compounds (Copyright © 2014, Royal Society of Chemistry, Reprinted with permission from ref (142)).

Investigation of the electronic absorption and fluorescence spectra of the isomeric probes reveals a very different spectral response pattern regarding ion response. In electronic absorption spectra, an impressive hypsochromic shift was observed for **1** in response to Hg (II) ions (Figure 62). Initially, the absorbance band has a peak centered at 800 nm in THF and upon the addition of Hg (II) ions, a blue shift is observed and the peak maximum moves to 715 nm. Also, when excited at 710 nm, the emission intensity is essentially switched on, from a non-fluorescent state to a brightly fluorescent metal ion complex. Since the ligand of our choice, the dithiaazacrown, is known to be highly Hg (II) selective,[13] other metal ions do not

interfere and thus, there is no change in either electronic absorption or fluorescence spectra

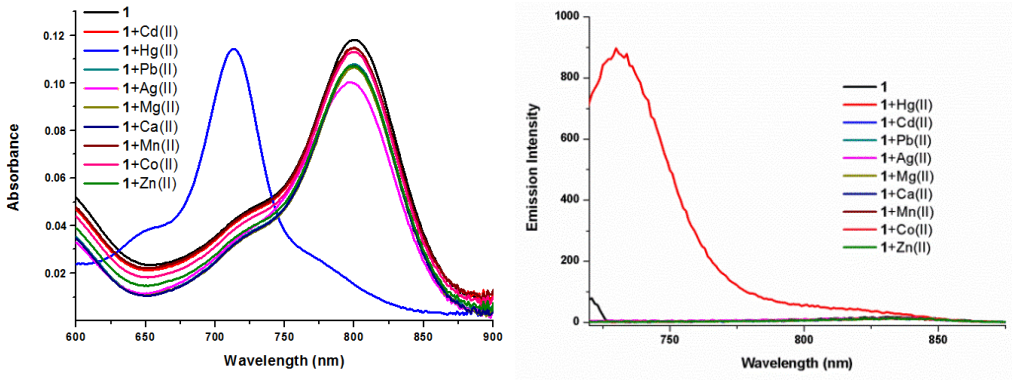


Figure 62. Electronic absorption and emission spectra of **1** (0.5 μM) in THF in absence and presence of various metal ions. Added metal ion concentrations were 5 μM. Excitation wavelength was 710 nm (Copyright © 2014, Royal Society of Chemistry, Reprinted with permission from ref (142)).

under the experimental conditions of the study. Thus, we have a highly selective chemosensor for Hg (II) operating at near IR region of the spectrum.

Surprisingly, electronic absorption spectrum of isomer **2** shows a peak at 745 nm and the addition of Hg (II) ions does not alter the electronic absorption

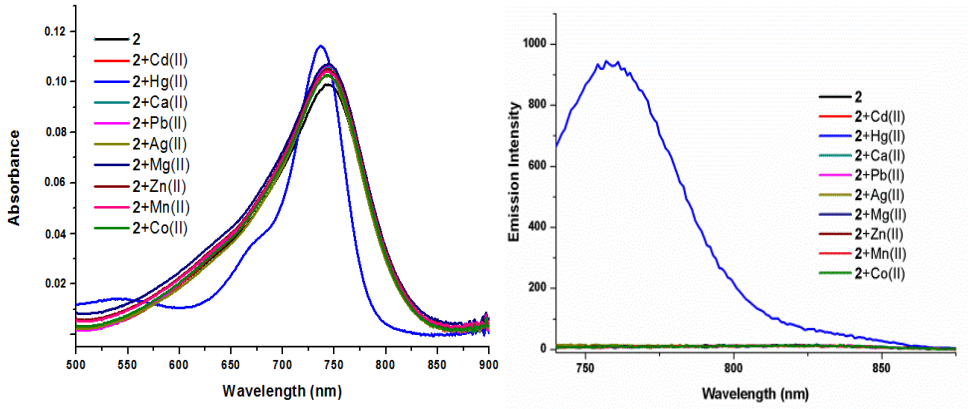


Figure 63. Electronic absorption and emission spectra of **2** (1.0 μM) in THF in absence and presence of various metal ions. Added metal ion concentrations were 10 μM. Excitation wavelength is 725 nm (Copyright © 2014, Royal Society of Chemistry, Reprinted with permission from ref (142)).

characteristics. However, just like the isomer **1**, emission intensity of **2** shows a remarkable increase (excitation wavelength is 725 nm). Similarly, as a well-known Hg (II) specific ligand, dithiaazacrown moeity does not respond to other metal ions

(Figure 63). Data for comPeTition/interference experiments with isomers **1** and **2** (using Hg (II) and selected metal ions) are given in Figure 64 and Figure 65.

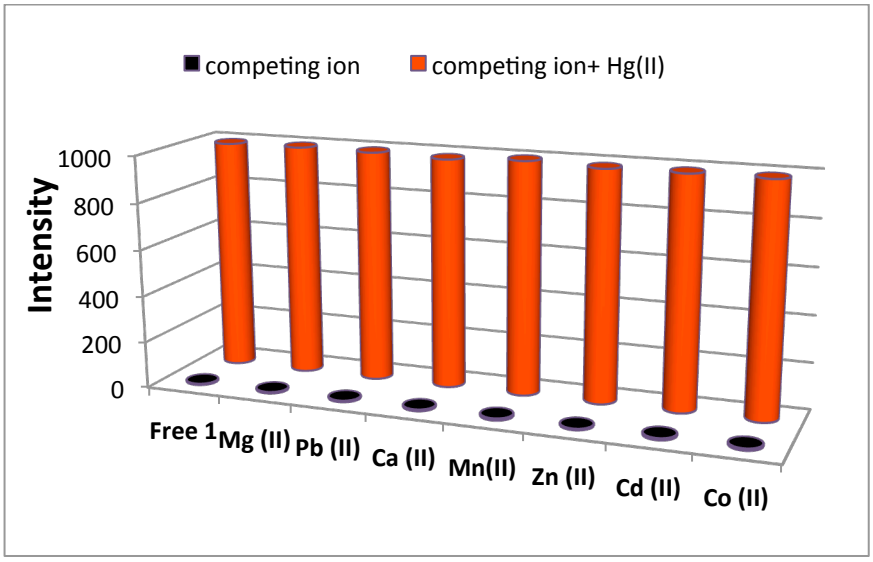


Figure 64. Emission intensity response of **1** (0.5 μM) , with 5 μM of a comPeTing metal ion followed by addition of 5 μM Hg^{2+} in THF.Excitation wavelength was 710 nm with a slit width of 5-5 nm (Copyright © 2014, Royal Society of Chemistry, Reprinted with permission from ref (142)).

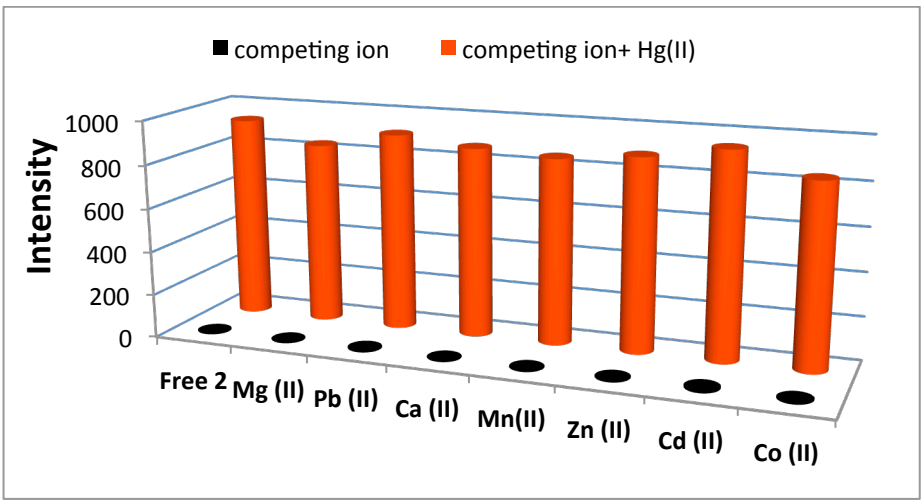


Figure 65. Emission intensity response of **2** (1.0 μM) with 10 μM of a comPeTing metal ion followed by addition of 10 μM Hg^{2+} in THF. Excitation wavelength was 725 nm with a slit width of 5-5 nm (Copyright © 2014, Royal Society of Chemistry, Reprinted with permission from ref (142)).

Water soluble fluorescent probes are especially in high demand for biological applications. To that end, polyethylene glycol (PEG) and triethylene glycol groups were attached to BODIPY unit *via* Knoevenagel condensation reactions, compound **3** and **4** were obtained with adequate yields. Electronic absorption and emission spectra in aqueous solutions (10 mM HEPES: CH_3CN, 50:50, v/v, pH=7.2, 25 °C) of probes showed results in accordance with the organic soluble counterparts (Figure 66 and Figure 67).

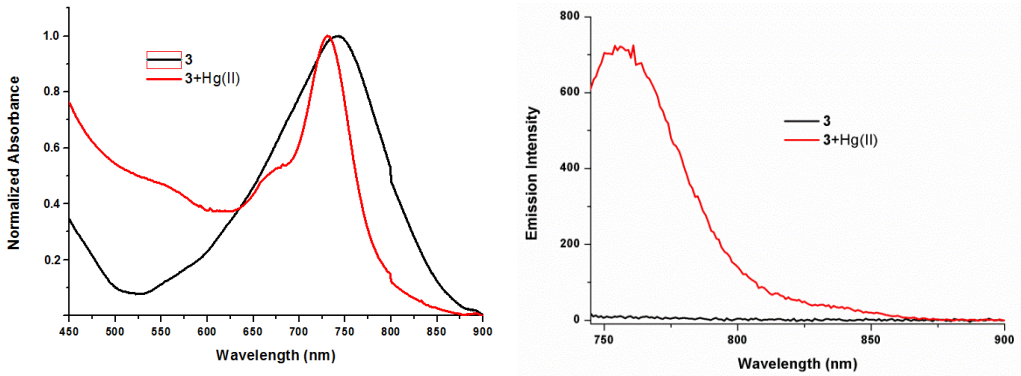


Figure 66. The electronic absorption and emission spectra of **3** (1.9 μM) in presence of excess Hg(II) in 10 mM HEPES:CH_3CN (50:50, v/v, pH=7.20, 25 °C). (excitation wavelength =730 nm) (Copyright © 2014, Royal Society of Chemistry, Reprinted with permission from ref (142)).

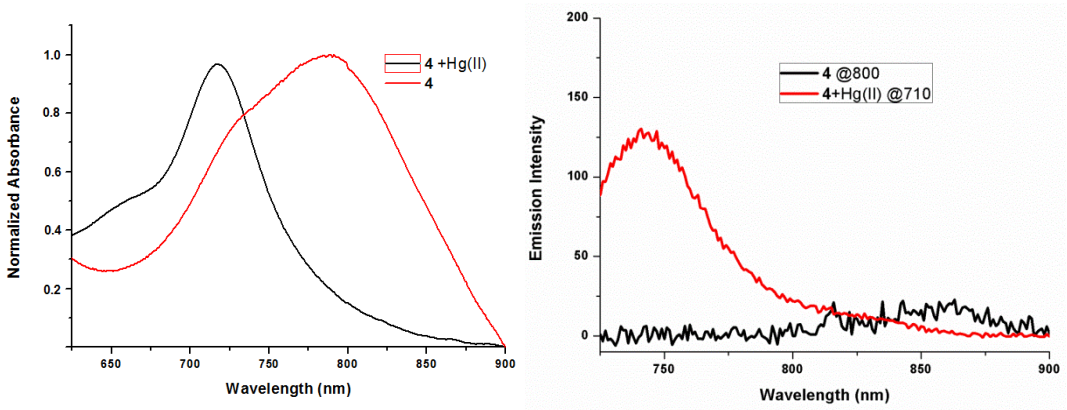


Figure 67. The electronic absorption and emission spectra of **4** (2.8 μM) in presence of excess Hg(II) in 10 mM HEPES:CH_3CN(50:50, v/v, pH=7.20,25°C) (Copyright © 2014, Royal Society of Chemistry, Reprinted with permission from ref (142)).

To determine binding constants, isothermal titration calorimetry (ITC) was performed. Based on the inflection point in the titration curve (heat vs. molar ratio of metal ion to ligand), the stoichiometry of complexation was determined.

Table 1. Binding Constants Determined by Isothermal Titration Calorimetry (ITC) for compound **3** and **4** (Copyright © 2014, Royal Society of Chemistry, Reprinted with permission from ref (142)).

Compound	K (M^{-1})	ΔH (kcal/mol)	ΔS cal/(mol · K)	model
3 (1:1 binding)	$(7.15\pm1.95)\times10^5$	$-1.82\times10^4\pm1.03\times10^3$	-34.2	One set of sites
3 (1:2 binding)	$4.43\times10^4\pm6.90\times10^3$	-8288±514	-6.53	Two sets of sites
4 (1:1 binding)	$(7.23\pm1.41)\times10^6$	$-2.64\times10^4\pm682$	-57.4	One set of sites
4 (1:2 binding)	$2.0\times10^5\pm2.5\times10^4$	$-1.27\times10^4\pm285$	-18.6	Two sets of sites

Table **1** describes the binding characteristics for isomers **3** and **4**. These water soluble isomeric compounds showed 1:2 complex in acetonitrile as expected (Fig. 68).

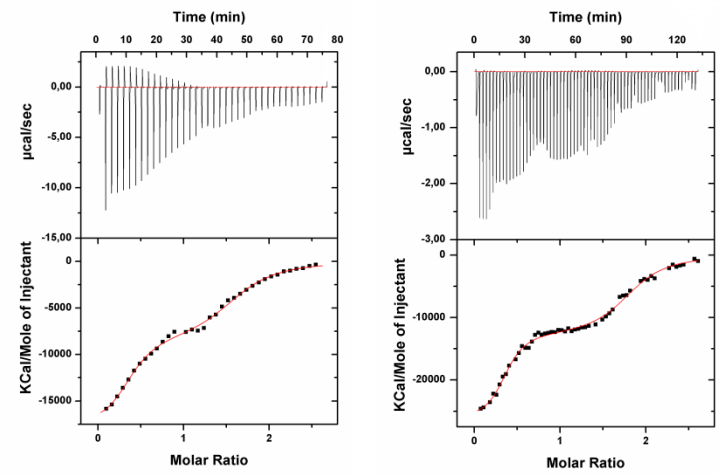


Figure 68. Calorimetric binding isotherm for the compound **3** (right, 0.4 mM 3 titrated with 5 mM $Hg(ClO_4)_2$) and 4 (left, 0.14 mM 4 titrated with 2 mM $Hg(ClO_4)_2$) in acetonitrile (Copyright © 2014, Royal Society of Chemistry, Reprinted with permission from ref (142)).

Significantly different spectral responses of **1** and **2** to Hg (II) binding indicate an electronic structure difference among the two probes. Theoretical studies employing the Time-Dependent (TD) formalism of Density Functional Theory (DFT) were performed to gain insight into the excitation characteristics and fluorescence turn on of **1** and **2**. The presumed impact of structural differences of **1** and **2** on emission

characteristics were studied by constructing the models **1a** and **2a** (Figure 69). Effect of metal binding was

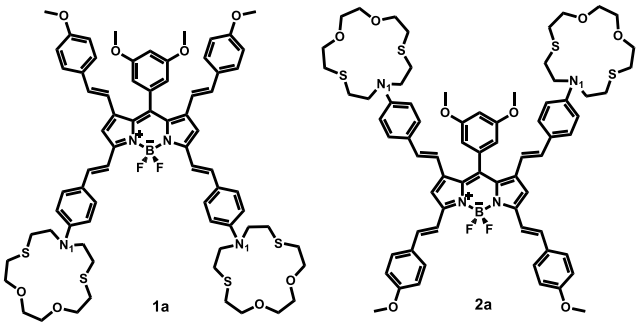


Figure 69. Computational models (Copyright © 2014, Royal Society of Chemistry, Reprinted with permission from ref (142)).

investigated via protonation at N_1 (**1aH** and **2aH**). TD-DFT results (Figures 70, 71 and Table 2) are in good agreement with the spectroscopic measurements and reveal that the fluorescence turn on is due to extinguishing the electron density on N_1 lone pair upon metal binding. Note that the dative N_1:→Hg (II) bonding diminishes the n→π* contribution to the $S_0 \rightarrow S_1$ excitation. Consequently any input

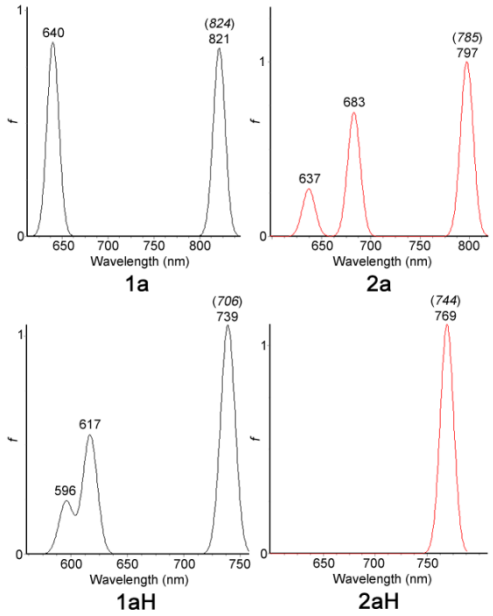


Figure 70. Computed absorption spectra. (Experimental values in parentheses) (Copyright © 2014, Royal Society of Chemistry, Reprinted with permission from ref (142)).

Table 2. Summary of TDDFT Results [a] (Copyright © 2014, Royal Society of Chemistry, Reprinted with permission from ref (142)).

Species	Major transitions & orbital contributions		ΔE (eV)	λ^{COMP} (nm)	λ^{EXP} (nm)	Oscillator strength
1a	237A→238A	0.625	1.51	821	798	1.103
	236A→238A	0.665	1.94	640	584	1.137
	237A→240A	0.675	2.85	436	470	1.325
1aH	237A→238A	0.621	1.68	739	706	1.185
2a	237A→238A	0.629	1.56	797	740	1.141
	236A→238A	0.670	1.82	683	-	0.811
	232A→238A	-0.369				
	237A→239A	0.466	2.90	427	403	0.820
	237A→240A	-0.274				
2aH	237A→238A	0.615	1.61	769	744	1.132
	236A→238A	0.662	2.22	558	-	0.911
	237A→239A	0.579	2.71	458	410	0.709
	234A→238A	0.329				
	237A→241A	0.616	3.24	382	-	0.918

[a] Experimental values belong to **1** and **2**.

(metal or proton) able to utilize the N_1 lone pair in binding is well suitable for fluorescence turn on. Understanding different spectral responses requires a simple, yet fundamental approach. Considering the decisive role of the position of substitution on BODIPY core, we compared the frontier MO energies of di- and tetra-styryl substituted BODIPY derivatives (Table 1). Remarkably, 3,5 substitution was superior to 1,7 in altering the HOMO – LUMO gap of BODIPY, mainly by destabilization of HOMO. Improvement by obtaining the tetra-styryl derivative was minor when compared to 3,5-distyrylBODIPY. Thus, 3 and 5 positions are more important when perturbations to the electronic structure are sought however, this observation can be traced back to fundamental features of BODIPY core.

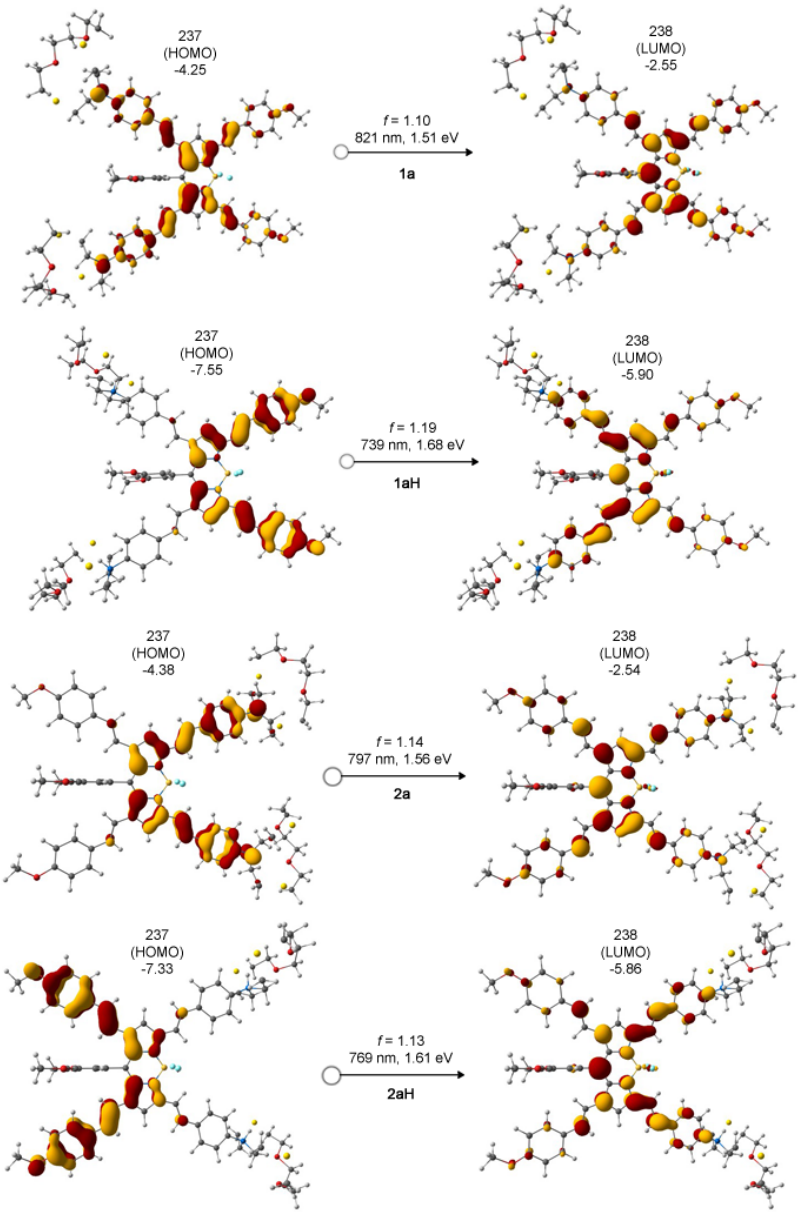
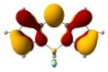
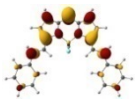
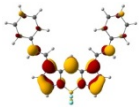
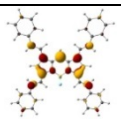
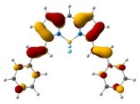
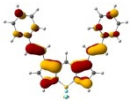
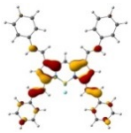


Figure 71. MO plots and energies (eV) for transitions with high oscillator strength (Copyright © 2014, Royal Society of Chemistry, Reprinted with permission from ref (142)).

Comparison of MO plots for di- and tetra-styryl derivatives (Table 3) reveals that extension of the π-system at 3,5-positions preserves the character of HOMO of BODIPY core whereas 1,7-modification yields a HOMO with a different character than BODIPY HOMO. Moreover, BODIPY HOMO hosts more electronic density at 3 and 5 positions than 1 and 7 which gives rise to an increased Coulombic repulsion that destabilizes the HOMO. The aforementioned difference in destabilization of

HOMO (Table 3) is thus justified. Consequently, electronic structure of **1a** upon proton or cation binding experiences larger perturbations than **2a** and this is also the case for **1** when compared to **2**. Therefore the discrepancy in the absorption shifts of **1** and **2** is mainly due to the π-system of BODIPY core treating the charge injections unequally, i.e. as dictated by the spatial distribution of HOMO.

Table 3. MO Plots and Energies (eV) of BODIPY and Styryl-Substituted Derivatives at UB3LYP/cc-pVTZ//6-31G(d) Level of Theory (Copyright © 2014, Royal Society of Chemistry, Reprinted with permission from ref (142)).

MO	BODIPY	3,5-distyryl BODIPY	1,7-distyryl BODIPY	1,3,5,7-tetrastyryl BODIPY
LUMO				
	-3.2	-3.1	-3.3	-3.2
HOMO				
	-6.3	-5.3	-5.7	-5.2
ΔE HOMO-LUMO	3.1	2.2	2.4	2.0

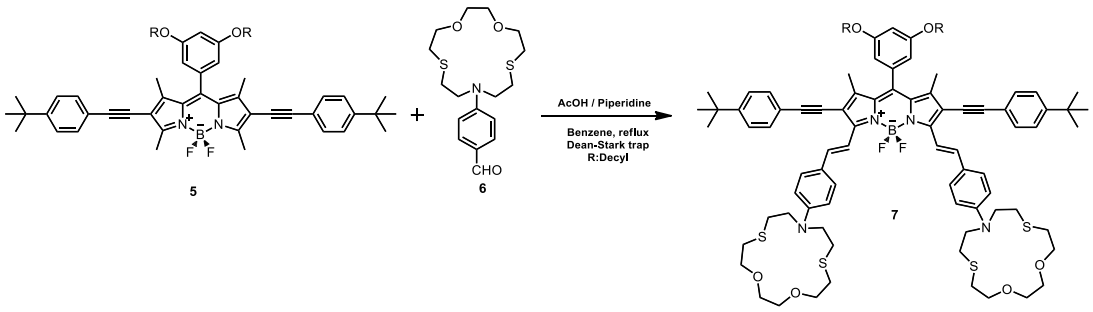
3.4. Conclusion

In conclusion, we demonstrated that tetrastyryl- BODIPY dyes can be derivatized to yield ion responsive compounds functioning in the near IR wavelengths. Also, we provided the first examples of divergent ion response resulting from a difference in the locations of styryl-linked donor groups on the BODIPY core and the impact of their changing charge donation properties on ion binding. Principles underlying different spectroscopic properties and fluorescence turn on response are explained *via* orbital analysis. It is very likely that these stable and near IR emissive probes, or others built upon the ideas developed here will be quickly added to growing arsenal of ion probes successfully interrogating cellular events, or monitoring environmental parameters.

3.5. Experimental Details

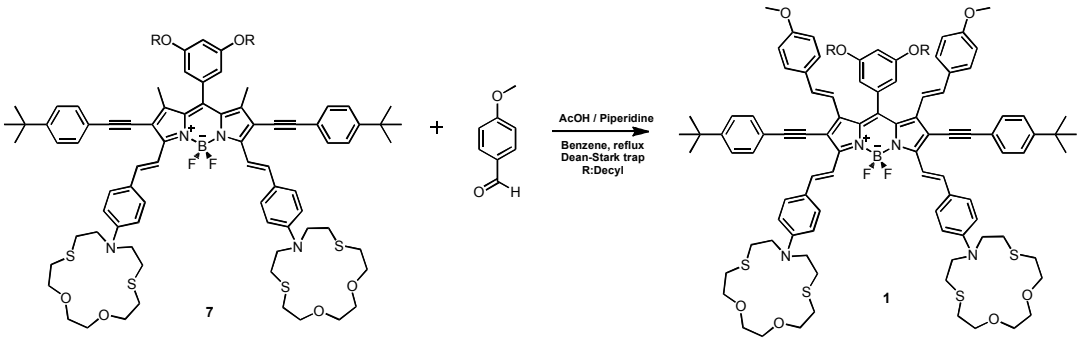
General: ^{1}H NMR and ^{1}3C NMR spectra were recorded on Bruker DPX-400 (operating at 400 MHz for ^{1}H NMR and 100 MHz for ^{13}C NMR) in $CDCl_3$ with tetramethylsilane as internal standard. All spectra were recorded at 25^{0}C and coupling constants (J values) are given in Hz. Chemical shifts are given in parts per million (ppm). Absorption spectra were performed by using a Varian Cary-100 spectrophotometer. Fluorescence measurements were conducted on a Varian Eclipse spectrofluorometer. Mass spectra were recorded on Agilent Technologies 6530 Accurate-Mass Q-TOF LC/MS. Reactions were monitored by thin layer chromatography using Merck TLC Silica gel 60 F254. Silica gel column chromatography was performed over Merck Silica gel 60 (particle size: 0.040-0.063 mm, 230-400 mesh ASTM). Compounds **5**,[13] **6**,[143] **9**[43] and PEG_{2000}-N_3[143] were synthesized according to literature. All other reagents and solvents were purchased from Aldrich and used without further purification. For a typical ITC run, the instrument chamber (200 μL) contained a solution of a ligand (0.125 mM) while a 2.5 mM solution of $Hg(ClO_4)_2$ was taken up in a 40 μL injection syringe. The syringe was assembled into the chamber for equilibration while stirring at 750 rpm. The chamber temperature was set to 25 °C. The injections were programmed at 0.5 μL each, added over 3 sec and spaced 2 min apart.[144] Association enthalpy (ΔH° in cal/mol), "number of sites" (N), and association constant (K in M-1) were obtained by fitting the titration data using the "Two Set of Sites model" algorithm provided in the S3 MicroCal Origin Software package (version 7.0). Association entropy (ΔS in cal/mol/K) is calculated from fitted values of ΔH^{o} and K.

Synthesis of Compound 7:



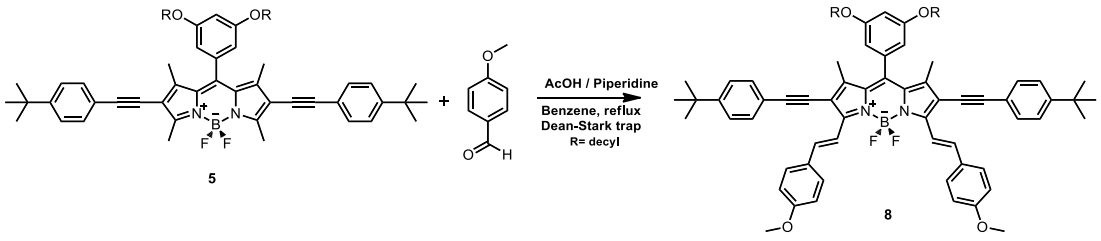
In a 100 ml round-bottomed flask containing 50 ml benzene, Compound **5** (0.137 mmol, 130 mg) and compound **6** (0.342 mmol, 121 mg) piperidine (0.3 ml) and acetic acid (0.3 ml) were added. The mixture was heated under reflux by using a Dean Stark trap and progress of the reaction was monitored by TLC dichloromethane. When all the starting material had been consumed, the mixture was cooled to room temperature and solvent was evaporated. Water (100 ml) added to the residue and the product was extracted into the chloroform (3 x 100 ml). Organic phase dried over Na_2SO_4, evaporated and residue was purified by silica gel column chromatography using dichloromethane as the eluent. (144 mg, 65%).^{1}H NMR (400 MHz, Chloroform-*d*) δ 8.48 (d, *J* = 16.0 Hz, 2H), 7.69 (d, *J* = 16.1 Hz, 2H), 7.61 (d, *J* = 8.7 Hz, 4H), 7.48 (d, *J* = 8.4 Hz, 4H), 7.42 (d, *J* = 8.5 Hz, 4H), 6.73 (d, *J* = 8.5 Hz, 4H), 6.59 (s, 1H), 6.49 (s, 2H), 3.97 (t, *J* = 6.6 Hz, 4H), 3.84 (t, *J* = 8.0 Hz, 8H), 3.74 (m, 8H), 3.68 (s, 8H), 2.97 (m, 8H), 2.84 – 2.78 (m, 8H), 1.78 (m, 10H), 1.51 - 1.31 (m, 48H), 0.9 (t, 6H).

Synthesis of Compound 1:



In a 100 ml round-bottomed flask containing 50 ml benzene, Compound **7** (0.023 mmol, 40 mg) and p-anisaldehyde (0.14 mmol, 18 mg) piperidine (0.3 ml) and acetic acid (0.3 ml) were added. The mixture was heated under reflux by using a Dean Stark trap and progress of the reaction was monitored by TLC chloroform. When all the starting material had been consumed, the mixture was cooled to room temperature and solvent was evaporated. Water (100 ml) added to the residue and the product was extracted into the chloroform (3 x 100 ml). Organic phase dried over Na_2SO_4, evaporated and residue was purified by silica gel column chromatography using chloroform as the eluent. (15 mg, 34%).^{1}H NMR (400 MHz, Chloroform-*d*) δ 8.58 (d, *J* = 16.2 Hz, 2H), 7.74 (d, *J* = 16.2 Hz, 4H), 7.65 (d, *J*= 8.5 Hz, 4H), 7.50 – 7.46 (m, 4H), 7.45 – 7.39 (m, 4H), 7.06 (d, *J* = 8.8 Hz, 4H), 6.81 (d, *J* = 8.8 Hz, 4H), 6.78 – 6.72 (m, 5H), 6.64 (d, *J* = 2.3 Hz, 2H), 6.08 (d, *J* = 16.3 Hz, 2H), 3.89 – 3.83 (m, 18H), 3.81 – 3.72 (m, 8H), 3.71 – 3.64 (m, 8H), 2.99 (m, 8H), 2.81 (m, 8H), 1.60 (s, 8H), 1.37 (s, 16H), 1.30 – 1.19 (m, 32H), 0.88 (t, *J* = 6.8 Hz, 6H). ^{13}C NMR (100 MHz, $CDCl_3$) δ 161.4, 151.4, 149.7, 147.91, 139.4, 137.1, 133.3, 132.7, 130.4, 130.4, 129.7, 128.0, 125.7, 125.6, 120.9, 119.4, 113.8, 111.9, 111.4, 111.1, 108.51, 98.4, 74.2, 70.7, 69.5, 68.6, 55.3, 52.0, 34.8, 31.3, 31.2, 29.7, 29.5, 29.3, 28.9, 25.9, 14.1. Calcd: 1880.962 [M+Na]+ , Found: 1880.969 [M+Na]+, Δ=3.62 ppm.

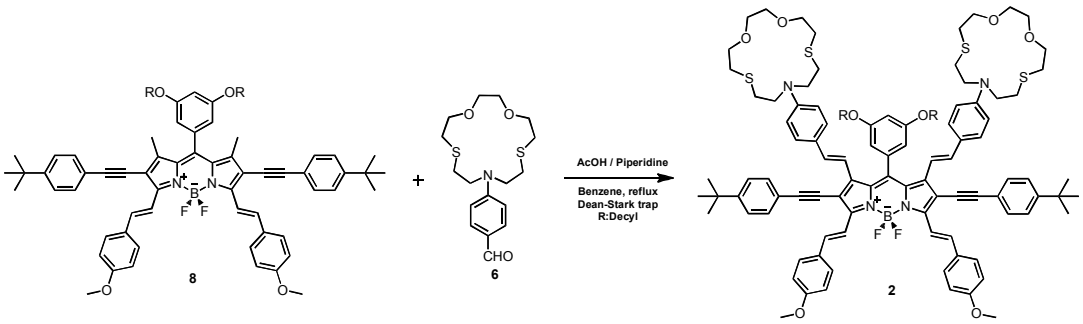
Synthesis of Compound 8:



In a 100 ml round-bottomed flask containing 50 ml benzene, Compound **5** (0.053 mmol, 50 mg) and p-anisaldehyde (0.080 mmol, 10.7 mg) piperidine (0.3 ml) and acetic acid (0.3 ml) were added. The mixture was heated under reflux by using a Dean Stark trap and progress of the reaction was monitored by TLC chloroform. When all the starting material had been consumed, the mixture was cooled to room temperature and solvent was evaporated. Water (100 ml) added to the residue and the

product was extracted into the chloroform (3 x 100 ml). Organic phase dried over Na_2SO_4, evaporated and residue was purified by silica gel column chromatography using chloroform as the eluent. (34 mg, 55%).^{1}H NMR (400 MHz, Chloroform-*d*) δ 8.49 (d, *J* = 16.2 Hz, 2H), 7.77 (d, *J* = 16.3 Hz, 2H), 7.67 (d, *J* = 8.8 Hz, 4H), 7.51 – 7.45 (m, 4H), 7.45 – 7.38 (m, 4H), 7.00 (d, *J* = 8.7 Hz, 4H), 6.62 (t, *J* = 2.3 Hz, 1H), 6.50 (d, *J* = 2.2 Hz, 2H), 3.99 (t, *J* = 6.6 Hz, 4H), 3.90 (s, 6H), 1.81 (m, 10H), 1.54 – 1.28 (m, 46H), 0.91 (m, 6H). ^{13}C NMR (100 MHz, $CDCl_3$) δ 161.4, 161.2, 160.7, 152.4, 151.6, 144.6, 138.7, 138.7, 136.4, 132.5, 130.8, 130.5, 130.0, 129.3, 125.5, 117.0, 114.3, 113.8, 106.7, 102.6, 98.5, 98.3, 83.3, 68.51, 55.4, 34.8, 31.9, 31.2, 29.7, 29.6, 29.6, 29.6, 29.4, 29.4, 29.2, 22.7, 14.1, 13.1.

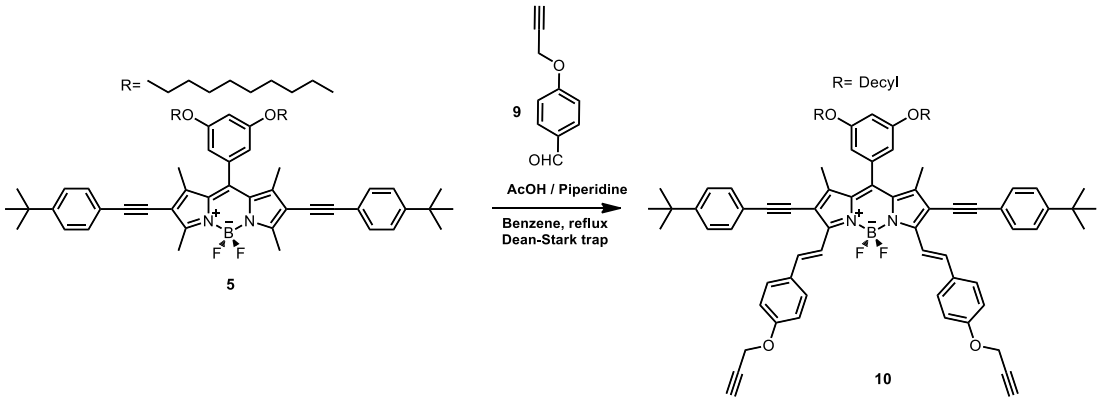
Synthesis of Compound 2:



In a 100 ml round-bottomed flask containing 50 ml benzene, compound **8** (0.021 mmol, 27 mg) and compound **6** (0.124 mmol, 44 mg) piperidine (0.3 ml) and acetic acid (0.3 ml) were added. The mixture was heated under reflux by using a Dean Stark trap and progress of the reaction was monitored by TLC chloroform. When all the starting material had been consumed, the mixture was cooled to room temperature and solvent was evaporated. Water (100 ml) added to the residue and the product was extracted into the chloroform (3 x 100 ml). Organic phase dried over Na_2SO_4, evaporated and residue was purified by silica gel column chromatography using chloroform as the eluent. (11 mg, 29%).^{1}H NMR (400 MHz, Chloroform-*d*) δ 8.55 (d, *J* = 16.3 Hz, 2H), 7.82 (m, *J* = 22.1, 16.4 Hz, 4H), 7.69 (d, *J* = 8.7 Hz, 4H), 7.49 (d, *J* = 8.4 Hz, 4H), 7.43 (d, *J* = 8.4 Hz, 4H), 7.01 (d, *J* = 8.8 Hz, 8H), 6.82 (s, 1H), 6.66 (d, *J* = 2.3 Hz, 2H), 6.57 (s, 4H), 6.05 (d, *J* = 16.1 Hz, 2H), 3.91-3.63 (m, 34H), 2.98 – 2.90 (m, 8H), 2.84 – 2.75 (m, 8H), 1.63-1.58 (m, 6H), 1.58- 1.18 (m,

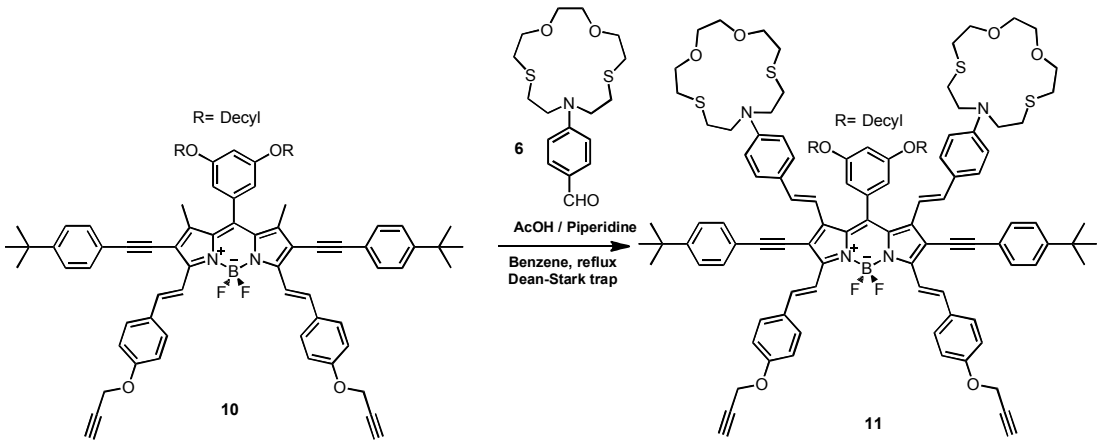
44H), 0.91 – 0.80 (m, 6H). ^{13}C NMR (100 MHz, $CDCl_3$) δ 161.6, 161.4, 160.6, 160.6, 153.2, 151.4, 146.9, 142.6, 138.4, 136.9, 134.6, 132.8, 130.8, 130.4, 130.2, 129.2, 128.6, 127.8, 125.7, 125.6, 117.4, 117.1, 114.3, 114.1, 111.6, 108.3, 103.4, 98.5, 86.3, 74.3, 70.8, 70.5, 69.6, 68.7, 55.4, 51.9, 39.2, 34.9, 31.9, 31.3, 31.2, 31.15, 29.7, 29.7, 29.6, 29.4, 29.4, 29.0, 25.9, 22.7, 14.1, 11.0. Calcd: 951.9757 $[M+2Na]^{+2}$, Found: 951.9921 $[M+2Na]^{+2}$, Δ=17.25 ppm.

Synthesis of Compound 10:



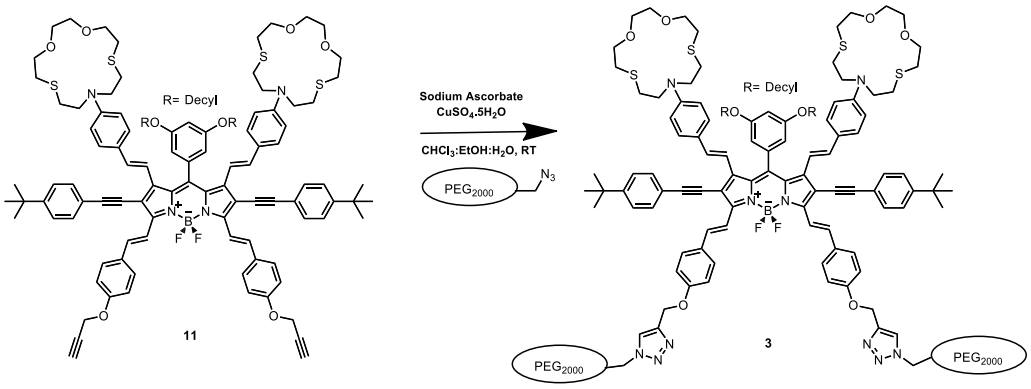
In a 100 ml round-bottomed flask containing 50 ml benzene, Compound **5** (0.12 mmol, 120 mg) and compound **9** (0.25 mmol, 40 mg) piperidine (0.3 ml) and acetic acid (0.3 ml) were added. The mixture was heated under reflux by using a Dean Stark trap and progress of the reaction was monitored by TLC chloroform. When all the starting material had been consumed, the mixture was cooled to room temperature and solvent was evaporated. Water (100 ml) added to the residue and the product was extracted into the chloroform (3 x 100 ml). Organic phase dried over Na_2SO_4, evaporated and residue was used without further purification.

Synthesis of Compound 11:



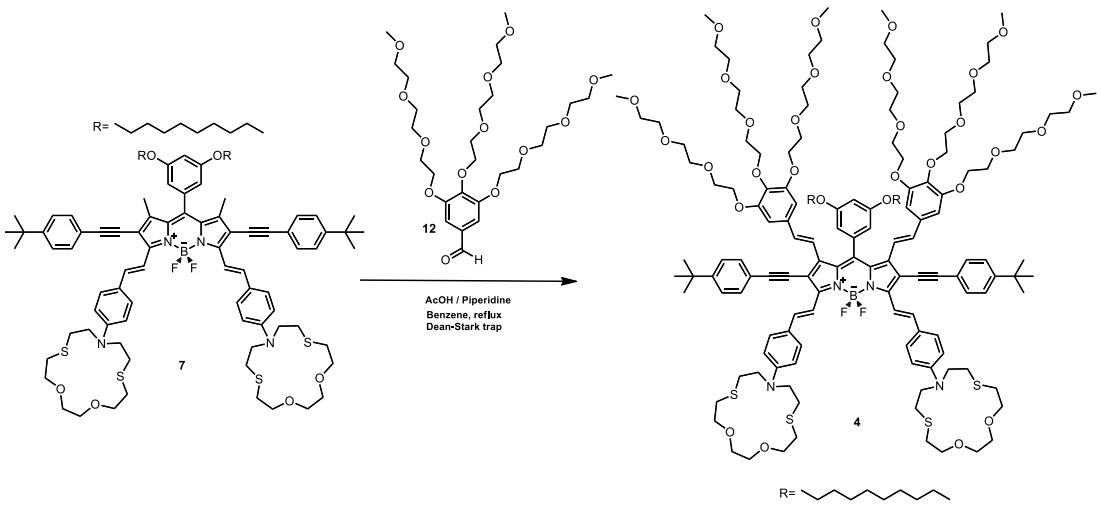
In a 100 ml round-bottomed flask containing 50 ml benzene, compound **10** (0.081 mmol, 100 mg) and compound **6** (0.24 mmol, 86 mg) piperidine (0.3 ml) and acetic acid (0.3 ml) were added. The mixture was heated under reflux by using a Dean Stark trap and progress of the reaction was monitored by TLC 3:1 Chloroform: Hexane. When all the starting material had been consumed, the mixture was cooled to room temperature and solvent was evaporated. Water (100 ml) added to the residue and the product was extracted into the chloroform (3 x 100 ml). Organic phase dried over Na_2SO_4, evaporated and residue was purified by silica gel column chromatography using 3:1 $CHCl_3$: Hexanes as the eluent. (94 mg, 60%). ^{1}H NMR (400 MHz, Chloroform-*d*) δ 8.54 (d, *J* = 15.9 Hz, 2H), 7.82 (t, *J* = 18.1 Hz, 4H), 7.76 – 7.62 (m, 6H), 7.55 (dd, *J* = 5.7, 3.3 Hz, 2H), 7.52 – 7.46 (m, 2H), 7.43 (d, *J* = 8.5 Hz, 4H), 7.09 (d, *J* = 8.9 Hz, 4H), 7.01 (d, *J* = 8.3 Hz, 4H), 6.82 (s, 1H), 6.65 (d, *J* = 2.3 Hz, 2H), 6.57 (s, 4H), 6.06 (s, 2H), 4.80 (d, *J* = 2.5 Hz, 4H), 4.23 (m,4H), 3.87 (m, 8H), 3.69 (s, 16H), 2.94 (m, 8H), 2.81 (t, *J* = 5.1 Hz, 8H), 2.60 (t, *J* = 2.4 Hz, 2H), 1.78 (m, 4H), 1.51 - 1.31 (m, 46H), 0.9 (t, *J* = 6.8 Hz, 6H).^{13}C NMR (100 MHz, $CDCl_3$) δ 169.7, 167.8, 161.6, 158.4, 151.5, 132.8, 132.5, 131.0, 130.9, 130.4, 129.2, 128.8, 128.6, 127.8, 125.7, 120.8, 117.6, 115.3, 115.1, 108.2, 103.4, 98.6, 86.1, 78.4, 75.8, 74.3, 70.8, 68.7, 68.2, 55.9, 52.4, 52.1, 38.7, 34.9, 31.9, 31.4, 31.2, 31.1, 29.7, 29.6, 29.6, 29.4, 29.0, 28.9, 25.9, 23.7, 22.9, 22.7. Calcd: 1928.962 [M+Na]+ , Found: 1928.968 [M+Na]+, Δ=3.07 ppm.

Synthesis of Compound 3:



To the solution of the compound **11** (0.017 mmol, 32 mg) in a 6:0.5:0.5 mixture of $CHCl_3$, EtOH and water; PEG_{2000}-N_3 (0.033 mmol, 67 mg), 0.16 mg sodium ascorbate, 0.1 mg CuSO4 and 3-4 drop Et3N are added and it was stirred at room temperature for 24 h. Water (50 ml) was added to the residue and the product was extracted into the chloroform (3 x 50 ml). (76 mg, 75%). ^{1}H NMR (400 MHz, Chloroform-*d*) δ 8.53 (d, *J* = 16.3 Hz, 2H), 7.92 (s, 2H), 7.83 (d, *J* = 8.5 Hz, 2H), 7.81 (d, *J* = 8.5 Hz, 2H), 7.77 – 7.65 (m, 6H), 7.54 (m, 2H), 7.5-7.4 (m, 6H), 7.12 (m, 4H), 6.99 (d, *J* = 8.4 Hz, 4H), 6.81 (s, 1H), 6.64 (s, 2H), 6.54 (s, 2H), 6.04 (d, *J* = 15.9 Hz, 2H), 5.35 (s, 4H), 4.59 (t, *J*= 5.0 Hz, 4H), 4.31 – 4.11 (m, 6H), 3.97 –3.39 (s, 225H), 2.92 (s, 8H), 2.80 (s, 8H), 2.24 (s, 4H), 1.65 (m, 4H), 1.49 – 1.01 (m, 40H), 1.01 – 0.70 (m, 6H). ^{13}C NMR (100 MHz, $CDCl_3$) δ 167.7, 161.6, 159.2, 151.5, 147.0, 130.9, 130.6, 130.4, 129.2, 128.8, 128.6, 125.7, 120.9, 115.3, 115.2, 111.7, 108.3, 98.5, 86.2, 74.2, 71.9, 70.6, 68.2, 62.1, 59.0, 51.9, 50.7, 50.4, 38.7, 31.9, 31.9, 31.3, 31.2, 29.7, 29.6, 29.6, 29.4, 29.4, 29.0, 28.9, 25.9, 23.7, 22.9, 22.69, 14.1, 14.0, 10.9. MALDI: Distribution around 6000 with separation of 45 corresponding to ethylene glycol unit.

Synthesis of Compound 4:



In a 100 ml round-bottomed flask containing 50 ml benzene, compound **7** (0.092 mmol, 150 mg) and compound **12** (0.27 mmol, 164 mg) piperidine (0.3 ml) and acetic acid (0.3 ml) were added. The mixture was heated under reflux by using a Dean Stark trap and progress of the reaction was monitored by TLC 10% Methanol: Dichloromethane. When all the starting material had been consumed, the mixture was cooled to room temperature and solvent was evaporated. Water (100 ml) added to the residue and the product was extracted into the chloroform (3 x 100 ml). Organic phase dried over Na_2SO_4, evaporated and residue was purified by silica gel column chromatography using 10% Methanol: Dichloromethane as the eluent. (87 mg, 34%). ^{1}H NMR (400 MHz, Chloroform-*d*) δ 8.58 (d, *J* = 16.1 Hz, 2H), 7.71 (d, *J* = 16.1 Hz, 2H), 7.63 (s, 4H), 7.46 (d, *J* = 8.2 Hz, 4H), 7.40 (d, *J* = 8.3 Hz, 4H), 6.74 (d, *J* = 8.4 Hz, 4H), 6.61 (s, 2H), 6.52 (s, 1H), 6.32 (s, 2H), 5.90 (d, *J* = 16.1 Hz, 2H), 5.66 (s, 4H), 4.16 (t, *J* = 5.2 Hz, 6H), 4.10 (s, 10H), 3.84-3.37 (m, 102H), 2.97 (t, *J* = 8.0 Hz, 8H), 2.80 (t, *J* = 5.2 Hz, 8H), 1.47-1.12 (m, 50H), 0.85 (t, *J* = 6.8 Hz, 6H). ^{13}C NMR (100 MHz, $CDCl_3$) δ 160.9, 153.5, 152.7, 151.6, 148.0, 141.3, 139.6, 138.6, 136.9, 135.3, 134.0, 132.8, 130.5, 129.8, 129.3, 128.4, 125.6, 124.0, 120.8, 120.3, 114.6, 112.0, 109.1, 108.1, 105.6, 98.6, 86.2, 74.2, 72.5, 71.9, 70.7, 70.6, 70.6, 69.8, 68.8, 59.0, 52.0, 34.9, 31.9, 31.4, 31.2, 29.6, 29.3, 29.0, 25.8, 22.7, 14.1. Calcd: 2793.4763 [M+Na]+ , Found: 2793.4909 [M+Na]+, Δ=5.23 ppm.

Computational Details

Density Functional Theory employing the unrestricted B3LYP[145,146] hybrid functional is used throughout. Geometries were fully optimized with CEP-31G basis.[147] The choice of basis can be justified considering the system size and extensive benchmarking from literature.[148] Excitation energy and characteristics were probed via TDDFT. Solvent environment was treated as a dielectric medium (εTHF=7.43) using polarizable continuum model (PCM) as implemented in Gaussian03. No restrictions on symmetry were imposed.

Styryl derivatives of BODIPY were modelled to study the effect of position of charge injection on the HOMO-LUMO gap. These species were optimized using Pople'sall electron 6-31G[149] basis including d-type polarization functions. Vibrational frequencies (all positive) confirmed the species to be true minima. Single point energy refinements were performed using Dunning type triple-ζ basis (cc-pVTZ).[150] All molecular orbitals are plotted at an isosurface value of 0.04 A.U. All calculations were carried out with Gaussian 03 (D.01).[150]

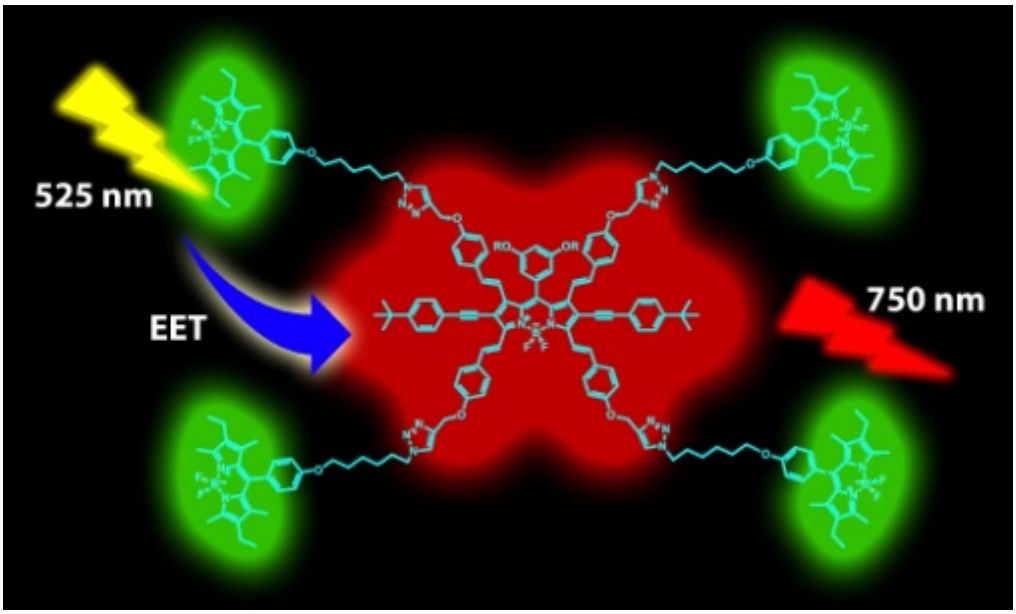
We are grateful to TUBITAK ULAKBIM (TR-Grid infrastructure) and to Gazi University Physics Department (pizag cluster) for computing resources.

CHAPTER 4

Dendritic Energy Transfer and Determination of Energy Transfer Based on Tetra-Styryl BODIPY Derivatives

This work is partially described in the following publication:

Kostereli, Z.; **Ozdemir, T.**; Buyukcakir, O.; Akkaya, E.U. *Org. Lett.*, **2012**, *14* , 3636–3639.



4.1. Objective

Versatile BODIPY dyes can be transformed into bright near-IR emitting fluorophores by quadruple-styryl substitutions. We demonstrated that by leaving clickable functionalities on the styryl moieties, an efficient synthesis of a light harvester is possible. In addition, we present clear spectral evidence showing that in dendritic light harvesters, calculations very commonly based on quantum yield or emission lifetime changes of the donor are bound to yield large overestimations of energy transfer efficiency.

4.2. Introduction

Efficient harvesting of solar radiation requires judiciously designed absorbers, considering the fact that it would be difficult to have a single molecule with strong absorptions in the entire visible spectrum and near-IR (perfect black dye). Therefore, it makes more sense to seek for multichromophoric dye ensembles. Different chromophoric units can be brought together either by covalent linkages or by non-covalent interactions. In either case, energy transfer from shorter wavelength emitter dyes to the longer wavelength emitting core unit is expected. The efficiency of energy transfer from the antenna chromophores to the central core is very important. In such multichromophoric light harvesters, energy transfer can be either through space[151] or through bond.[18] Through space energy transfer is also possible between two or more free chromophoric units. This kind of energy transfer has been studied very carefully and in fact, Forster (through space) energy transfer model is built on this kind of freely interacting chromophoric pairs. This energy transfer model was later on applied to covalently linked multichromophoric light harvesters. In this way, energy transfer efficiency is calculated assuming that the bimolecular model system can be directly related to energy transfer process in a large covalently linked light harvesting system. It has been recognized for some time that these values for energy transfer efficiency represent an upper limit and in most cases a significant overestimation.

We have been interested in light harvesting systems for some time.[152,153] In many examples, BODIPY chromophores have been utilized either as energy donors or energy acceptors. In recent years, brightly emitting BODIPY dyes are in the focus of renewed interest with an eye towards to practical applications and new derivatization opportunities.[154,155] One particular derivatization which already proved to be highly fruitful was Knoevenagel condensation of acidic methyl groups found in methyl-substituted BODIPYs with selected aromatic aldehydes. Mono and di-styryl BODIPY compounds were reported in 2001[156] and 2006,[157] respectively and in 2009, our research group reported[43] both tri and tetra-styryl BODIPY derivatives. Each styryl unit increases π- conjugation further, shifting the main absorption band ($S_0 \rightarrow S_1$ transition) to lower energy (longer wavelength region). By these simple sequences of reactions, absorption band of BODIPY dyes can be easily tuned in the range of 500-900 nm. Relative ease of this modification, alone, puts BODIPY derivatives in a very previlaged place among organic chromophores.

4.3. Result and Discussion

In order to investigate light harvesting properties of near- IR emitting tetra-styryl BODIPY dyes, we targeted modular harvesters **8** and **9**. The synthesis plan (Figure 72) makes us of common intermediate **7**. Compound **7** is a tetra-styryl dye obtained by quadruple Knoevenagel condensation of a previously reported 2,6-disubstituted intermediate with four 4-propynyloxybenzaldeyhde. Key intermediate, compound **7** carries four clickable terminal alkyne groups. This design conveniently allows modular attachment of essentially any azide functionalized chromophore. In the synthesis of compound **8**, we reacted intermediate **7** and **4**. For compound **9**, modular units **6** and **7** were joined together by click chemistry.

Our light harvesting design involves attachment of four shorter wavelength antenna units and one central core. Absorbance spectra of compound **4**, **6**, **7**, **8** and **9** are shown in Figure 1. As expected, both light harvesters show two major absorption bands corresponding to two different chromophores. In compound **8**, absorption

bands with peaks at 545 and 730 nm are apparent and in compound **9**, the two bands are centered around 652 and 732 nm. An experimental confirmation of energy

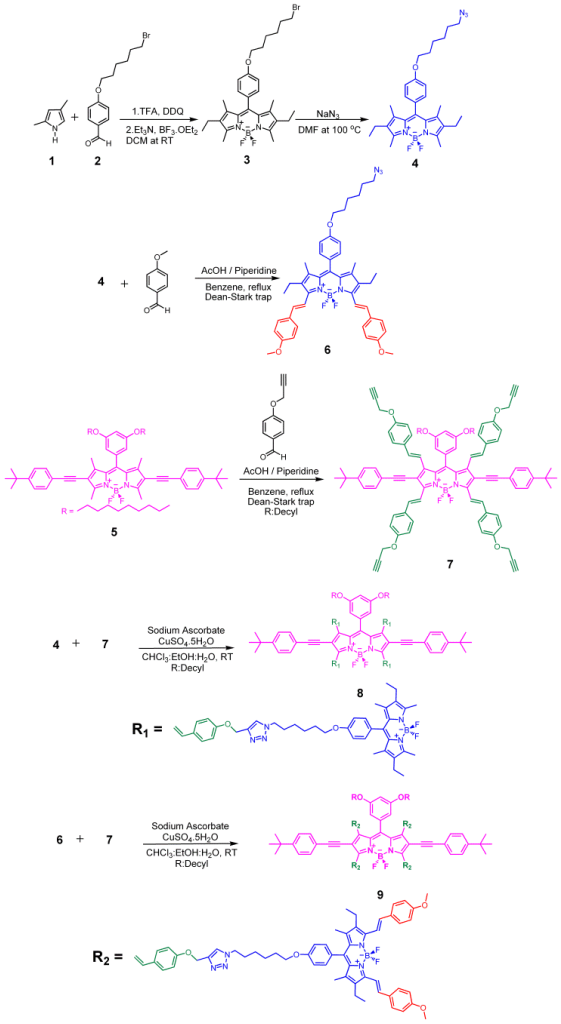


Figure 72. Reaction pathway of target compounds (Copyright © 2012, American Chemical Society, Reprinted with permission from ref (158)).[158]

transfer is readily obtained by comparing reference modules and the covalently assembled light harvesters. Figure 2 and 3 shows such comparisons. Emission spectra at equal concentrations of compounds **4** and **8** reveal a significant quenching of shorter wavelength BODIPY emission in compound **8**. Similar quenching of shorter wavelength emission is apparent in compound **9**, as well. This is no doubt and indicator of energy transfer efficiency. Another commonly employed demonstration of energy transfer is based on "enhanced core emission"[159] which is essentially obtained by exciting longer wavelength emitting modules at a common shorter wavelength used for exciting light harvesting system. As an example, **7**/**8** and

7/9 emissions excited at a shorter wavelength peak of **8** or **9**, respectively can be compared (Figures 73 and 74). It is clear, but also not surprising that emission from core is stronger in light harvester **8** and **9** compared to core module **7**. Quantitative

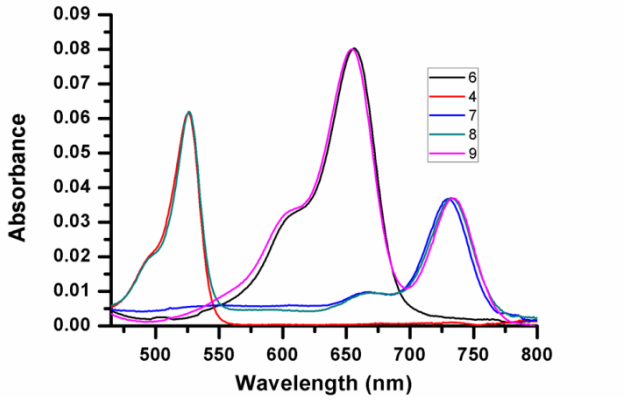


Figure 73. Absorbance spectra of compounds **4**, **6**, **7**, **8** and **9** at equal absorbances in $CHCl_3$, at 525 nm for **4** and **8**, at 655 nm for **6** and **9**, at 730 nm for **7**, **8** and **9** (Copyright © 2012, American Chemical Society, Reprinted with permission from ref (158)).

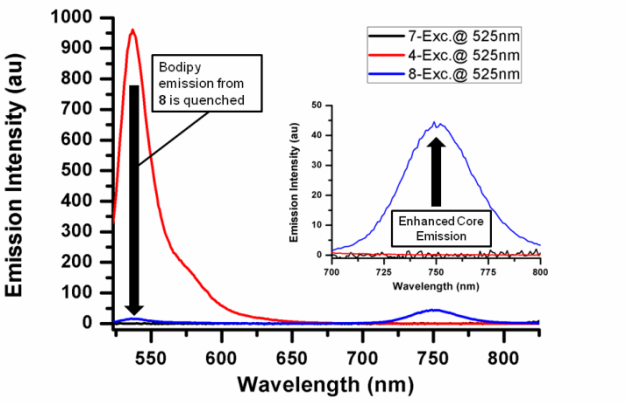


Figure 74. The emission spectra of **4**, **7**, and **8** at equal absorbances at 525 nm in $CHCl_3$. Inset: Energy transfer from peripheral BODIPY units **4** to tetrastyryl-BODIPY core **7** in light harvesting dendrimer **8** (Copyright © 2012, American Chemical Society, Reprinted with permission from ref (158)).

calculations of energy transfer can be based on the changes in lifetime or quantum yield.[4] This is again valid, only if bimolecular energy transfer arguments can be easily carried to larger and flexible unimolecular dendritic light harvesters. Spectral data and energy transfer rate/efficiencies are presented at Table 4 and Table 5, respectively. In light harvesters **8** and **9**, again, as expected shorter wavelength absorption is stronger with larger extinction coefficients over 300,000.

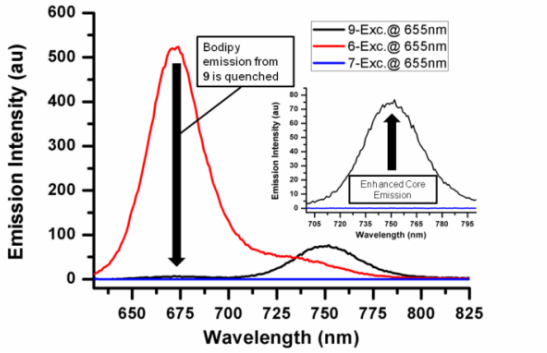


Figure 75. The emission spectra of **6**, **7**, and **9** at equal absorbances at 655 nm in $CHCl_3$. Inset: Energy transfer from di-styryl BODIPY units **4** to tetrastyryl-BODIPY core **7** in light harvesting dendrimer **9** (Copyright © 2012, American Chemical Society, Reprinted with permission from ref (158)).

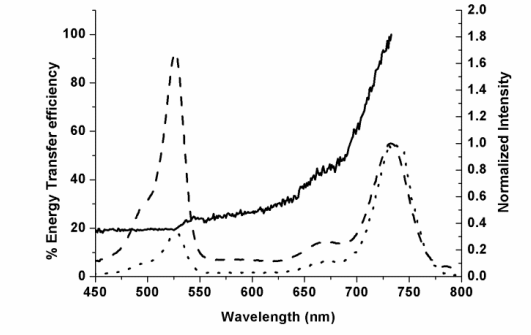


Figure 76 . Percent energy transfer efficiency of **8** (black solid). Excitation spectrum of **8** (dot line) and absorption spectrum of **8** (dashed) (normalized at 735 nm) (Copyright © 2012, American Chemical Society, Reprinted with permission from ref (158)).

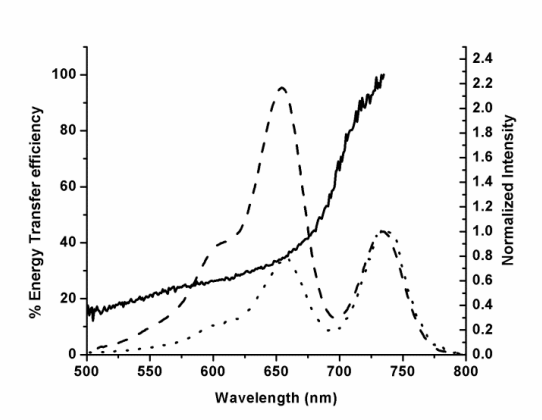


Figure 77. Percent energy transfer efficiency of **9** (black solid). Excitation spectrum of **9** (dot line) and absorption spectrum of **9** (dashed) (normalized at 735 nm) (Copyright © 2012, American Chemical Society, Reprinted with permission from ref (158)).

Emissions from both compounds **8** and **9** are bi-exponential as expected since there is always residual emission from the shorter wavelength chromophores in addition to longer wavelength emission from the central core (Table 5). Based on the significantly reduced emission lifetimes of the donor moieties, we can calculate 90 and 92% energy transfer efficiency values for light harvesters **8** and **9**, respectively. Calculations based on quantum yields, also, result in comparable efficiency values. However, a simple inspection of excitation spectra suggests that these efficiency values are largely overestimated. Same methodology has been used in assessing energy transfer efficiencies in a large number of light harvesting molecules, energy cascades and energy transfer cassettes.[160-162] Recently, in a dendritic light harvester designed for solar concentration, we have experimentally demonstrated that in such floppy light harvesting arrangements, Förster theory which was originally developed for bimolecular energy transfer is not applicable.[163] Deviation between energy transfer efficiencies calculated by the application of Förster theory and calculations

Table 4. Spectral data for BODIPY, distyryl-BODIPY and tetrastyryl-BODIPY dyes and light harvesting dendrimers (Copyright © 2012, American Chemical Society, Reprinted with permission from ref (158)).

Compound[a]	λ_{abs} (nm)	λ_{em} (nm)	Φ_f[b]	ε_{max}[c]
4	525	537	0.97[d]	76000
6	655	672	0.67[e]	48000
7	730	748	0.31[f]	143000
8	525 733	750	0.089[d]	349000 202000
9	655 734	750	0.058[e]	396000 186000

[a] Data acquired in $CHCl_3$ in dilute solutions. [b] relative quantum yields. [c] unit: $cm^{-1}M^{-1}$. [d] Rhodamine 6G in ethanol (Φ_f = 0.95). [e] Sulforhodamine 101 in ethanol (Φ_f = 0.90). [f] tetra-styryl[7]

based on excitation spectra can be very large. One simple way of presenting energy transfer efficiency as a function of wavelength was proposed by Wittmershaus in 1998;[164] it is a comparison of absorption and excitation spectra, normalized at the peak wavelength of absorption of the putative energy acceptor.

Table 5. Energy Transfer rate and efficiencies of Light harvesting dendrimers **8** and **9** (Copyright © 2012, American Chemical Society, Reprinted with permission from ref (158)).

Compounds [a]	λ_{ems}[nm]	τ[ns]	k_{en}(Förster) [s^{-1}]	Efficiency
8	537	0.13(40%)	$1.97x10^9$	90 %
		4.84(60%)	($1.39x10^8$)	(41%)
9	672	0.23(24%)	$2.05x10^9$	92 %
		4.10(76%)	($9.56x10^7$)	(30%)
4	537	5.02		
6	672	4.55		
7	748	3.41		

[a] Data acquired in $CHCl_3$ in dilute solutions.

In this way, the ratio of excitation to absorption values yields a plot of energy transfer efficiency as a function of excitation wavelength. Figure 76 and Figure 77 show two such operations done for the light harvesters **8** and **9**. From these ratios plotted as a function of wavelength, it is clear that in the region which corresponds to the absorption of energy donor (antenna chromophores) energy transfer efficiency is actually closer to 20-30%. This discrepancy, as mentioned previously is due to availability of additional vibrational and collisional non-radiative decay pathways in larger molecules incorporating a number of chromophores tethered with flexible linkers.

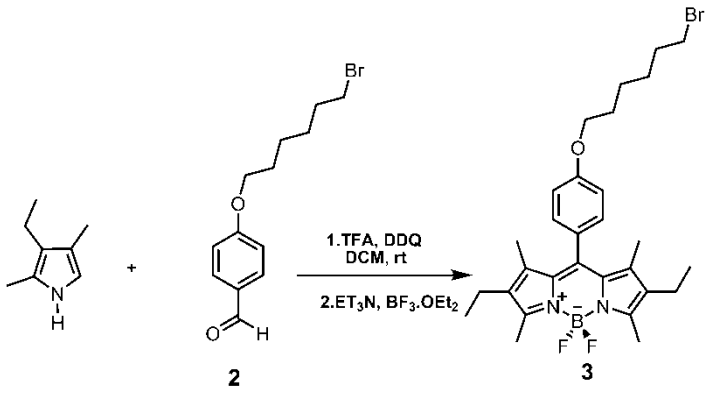
4.4. Conclusion

A thorough understanding of energy transfer process in large multichromophoric systems is quite important but before that is to be done, some persistent misunderstandings and mistakes in the literature have to be addressed and corrected. We are hoping that a clarification of energy transfer efficiency issue will facilitate the design and synthesis of novel and unequivocally more efficient light harvesters and solar concentrators. We are also confident that tetra-styryl BODIPY dyes or similarly tetra functionalized BODIPY dyes will continue to be at the core of these improved light harvesting assemblies.

4.5. Experimental Details

General: ^{1}H NMR and ^{13}C NMR spectra were recorded on Bruker DPX-400 (operating at 400 MHz for ^{1}H NMR and 100 MHz for ^{13}C NMR) in $CDCl_3$ with tetramethylsilane as internal standard. All spectra were recorded at $25^{0}C$ and coupling constants (*J values*) are given in Hz. Chemical shifts are given in parts per million (ppm). Absorption spectra were performed by using a Varian Cary-100 spectrophotometer. Fluorescence measurements were conducted on a Varian Eclipse spectrofluorometer. Mass spectra were recorded on Agilent Technologies 6530 Accurate-Mass Q-TOF LC/MS. MALDI mass spectra were recorded at the Izmir Institute of Technology, Izmir, Turkey and at the University of Sheffield, Mass Spectrometry Service Laboratory, Shieffield, U.K. Reactions were monitored by thin layer chromatography using Merck TLC Silica gel 60 F_{254}. Silica gel column chromatography was performed over Merck Silica gel 60 (particle size: 0.040-0.063 mm, 230-400 mesh ASTM). Compounds **1**[165], **2**[165] and **5**[43] were synthesized according to literature. Anhydrous tetrahydrofuran was obtained by refluxing over sodium/benzophenone prior to use. All other reagents and solvents were purchased from Aldrich and used without further purification.

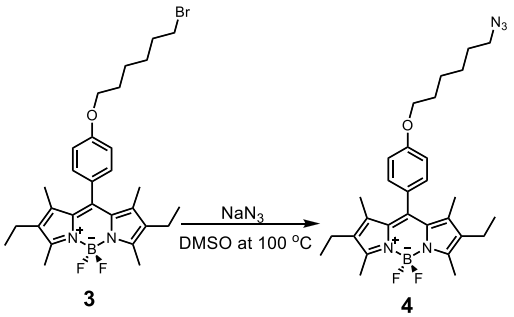
Synthesis of Compound 3:



Argon gas was bubbled through 200ml CH_2Cl_2 for 30 min then 3-ethyl-2,4-dimethyl pyrrole (1035 mg, 8.41 mmol) and compound **2** (1000 mg, 3.5 mmol) were dissolved in it under argon atmosphere. 1-2 drop of TFA was added and the solution stirred at room temperature nearly 3-4 h and Argon is removed. At this point, a solution of

DDQ (794.5 mg, 3.5 mmol) in 50 ml CH_2Cl_2 was added, stirring was continued for 30 min followed by the addition of 3 ml Et_3N and 3 ml $BF_3.OEt_2$. After stirring 30 min., the reaction mixture was washed three times with water and dried over Na_2SO_4. The solvent was evaporated and the residue was purified by column chromatography on silica gel using $CHCl_3$ as the eluent. Dark red solid (606.9 mg, 31%). ^{1}H NMR (400 MHz, $CDCl_3$): δ =1.0 (t, J= 7.52, 6H), 1.35 (s, 6H), 1.50-1.60 (m, 4H), 1.81-1.92 (m, 4H), 2.3 (q, J= 7.56, 4H), 2.55 (s, 6H), 3.59 (t, J= 6.64 Hz, 2H), 4.05 (t, J= 6.45 Hz, 2H), 7.0 (d, J= 8.56 Hz, 2H), 7.15 (d, J= 8. 56 Hz, 2H). ^{13}C NMR ($CDCl_3$, 100 MHz, δ ppm) 11.9, 12.5, 14.6, 17.1, 25.4, 26.7, 29.1, 32.5, 44.9, 67.9, 114.9, 127.8, 129.4, 130.1, 132.6, 138.4, 140.0, 153.5, 159.5

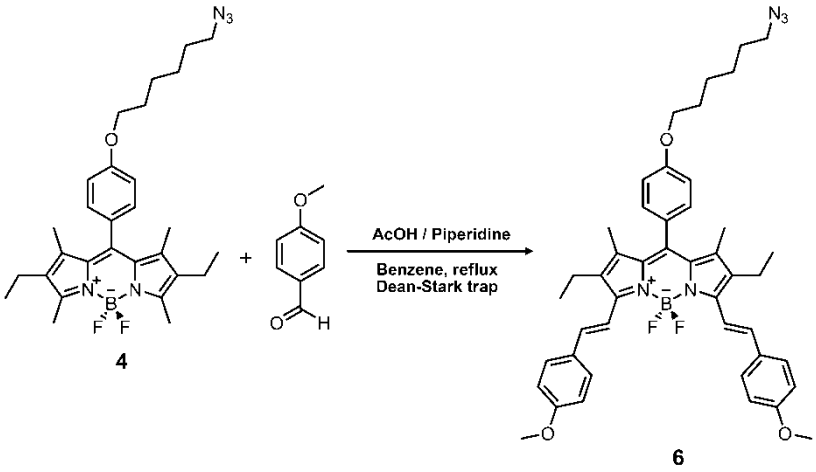
Synthesis of Compound 4:



3 4

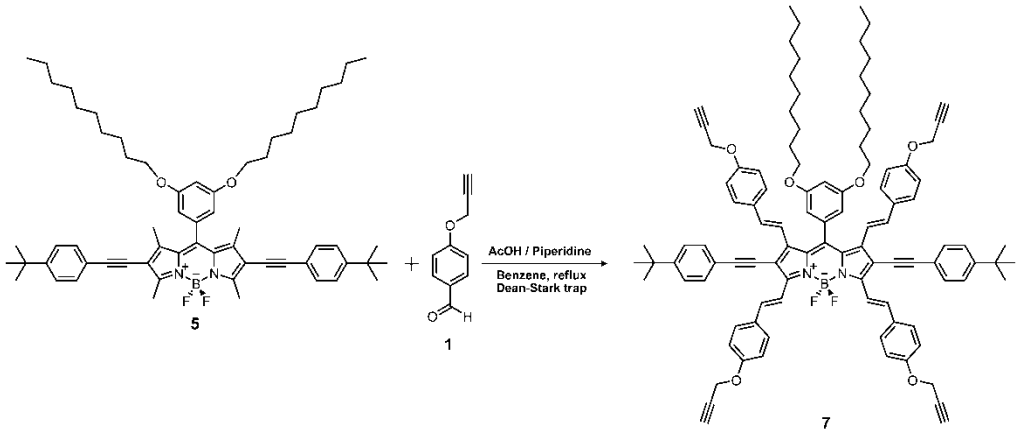
A mixture of compound **3** (800 mg, 1.43 mmol) and NaN_3 (232 mg, 3.576 mmol) in 20 ml DMSO was heated at 100 ^{o}C for 2h and controlled with TLC. When the reaction was completed, water (100 ml) was added to the residue and the product was extracted into the chloroform (3 x 100 ml). Organic phase dried over Na_2SO_4, evaporated and residue was used without further purification. Dark red solid (702.4 mg, 97 %). ^{1}H NMR ($CDCl_3$, 400 MHz, δ ppm) δ =1.0 (t, J= 7.52 Hz, 6H), 1.35 (s, 6H), 1.50-1.60 (m, 4H), 1.62-1.71 (m, 2H), 1.80-1.91 (m, 2H), 2.3 (q, J= 7.56 Hz, 4H), 2.55 (s, 6H), 3.32 (t, *J*= 6.64 Hz, 2H), 4.05 (t, *J*= 6.45 Hz, 2H), 7.0 (d, *J*= 8.56 Hz, 2H), 7.15 (d, *J*= 8.56 Hz, 2H). ^{13}C NMR ($CDCl_3$, 100 MHz, δ ppm) 11.8, 12.5, 14.6, 17.1, 25.7, 26.6, 28.8, 29,1, 51.4, 67.9, 115.0, 127.8, 129.4, 131.2, 132.6, 138.4, 140.3, 153.5, 159.5 MS (TOF- ESI): m/z: : Calcd: 521.3137 $[M]^+$, Found: 520.30651$[M-H]^+$, Δ=1.6 ppm.

Synthesis of Compound 6:



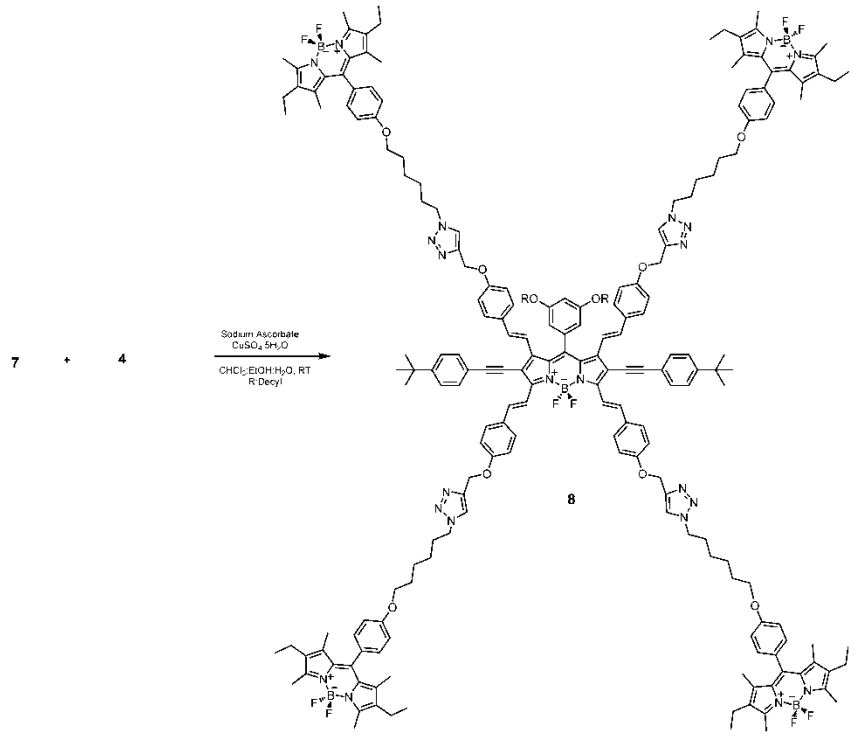
Compound **4** (200 mg, 0.384 mmol) and 4-Methoxybenzaldehyde (115 mg, 0.844 mmol) were added to a 100 ml round-bottomed flask containing 50 ml benzene and to this solution, piperidine (0.3 ml) and acetic acid (0.3 ml) were added. The mixture was heated under reflux by using a Dean Stark trap and it is monitored by TLC. When all the starting material had been consumed, the mixture was cooled to room temperature and solvent was evaporated. Water (100 ml) added to the residue and the product was extracted with the chloroform (3 x 100 ml). The organic phase dried over Na_2SO_4, evaporated The residue was poured into 2:1 EtOAc: Hexanes solution and dissolved by heating then it was cooled to 0 ^{0}C. Compound **6** precipitated at that temperature then it was filtered and obtained as pure product. Green solid (155.1 mg, 53%). ^{1}H NMR ($CDCl_3$, 400 MHz, δ ppm) 1.20 (t, J= 7.46 Hz, 6H), 1.40 (s, 6H), 1.50-1.60 (m, 4H), 1.65-1.75 (m, 2H), 1.85-1.95 (m, 2H), 2.65 (q, J= 7.62 Hz, 4H), 3.35 (t, *J*= 6.84 Hz, 2H), 3.89 (s, 6H), 4.10 (t, *J*= 6.40 Hz, 2H), 6.95 (d, *J*= 8.56 Hz, 2H), 7.05 (d, *J*= 8.44 Hz, 2H), 7.23 (d, *J*=8.44 Hz, 2H), 7.25 (d, *J*= 16.70 Hz, 2H), 7.62 (d, *J*= 8.60 Hz, 2H), 7.70 (d, *J*= 16.70 Hz, 2H). ^{13}C NMR ($CDCl_3$, 100 MHz, δ ppm) 11.7, 14.0, 18.4, 25.7, 26.5, 28.8, 29.1, 51.4, 55.3, 67.9, 114.2, 115.0, 118.2, 128.1, 128.7, 129.8, 130.3, 133.3, 133.4, 135.2, 138.1, 138.8, 150.3, 159.5, 160.1. MS (HRMS-ESI): m/z: : Calcd: 757.4 [M], Found: 757.5 $[M-H]^+$

Synthesis of Compound 7:



Compound **5** (400 mg, 0.42 mmol) and compound **1** (472 mg, 2.95 mmol) were added to a 100 ml round-bottomed flask containing 50 ml benzene and to this solution, piperidine (0.3 ml) and acetic acid (0.3 ml) were added. The mixture was heated under reflux by using a Dean Stark trap and it is monitored by TLC 3:2 Chloroform: Hexane. When all the starting material had been consumed, the mixture was cooled to room temperature and solvent was evaporated. Water (100 ml) added to the residue and the product was extracted into the chloroform (3 x 100 ml). Organic phase dried over Na_2SO_4, evaporated and residue was purified by silica gel column chromatography using 3:2 $CHCl_3$: Hexanes as the eluent. Dark green solid (416 mg, 65%). ^{1}H NMR (400 MHz, $CDCl_3$): δ = 0.88 (t; *J* = 6.8 Hz, 6H), 1.18-1.32 (m; 28H), 1.35 (s; 18H), 1.55-1.65 (m; 4H), 2.55 (t; *J* = 2.4 Hz, 1H), 2.60 (t; *J* = 2.4 Hz, 1H), 3.83 (t; *J* = 6.5 Hz, 4H), 4.70 (d; *J* = 2.4 Hz, 4H), 4.80 (d; *J* = 2.4 Hz, 4H), 6.10 (d; *J* = 16.2 Hz, 2H), 6.61 (d; *J* = 16.2 Hz, 2H), 6.72 (d; *J* = 2.2 Hz, 1H), 6.89 (d; *J* = 8.8 Hz, 4H), 7.02-7.10 (m; 8H), 7.42 (d; *J* = 8.7 Hz, 4H), 7.48 (d; *J* = 8.7 Hz, 4H), 7.70 (d; *J* = 8.8 Hz, 4H), 7.78 (d; *J* = 16.3 Hz, 2H), 7.82 (d; *J* = 17.0 Hz, 2H), 8.59 (d; *J* = 16.3 Hz, 2H). ^{13}C NMR (100 MHz, $CDCl_3$): δ =14.1, 22.7, 25.9, 29.0, 29.3, 29.6, 31.2, 31.9, 34.9, 55.8, 55.9, 68.7, 75.6, 75.9, 78.4, 78.5, 85.7, 98.9, 103.2, 108.3, 109.0, 114.9, 115.3, 117.4, 119.7, 120.7, 125.7, 128.0, 129.3, 130.5, 130.9, 131.2, 132.9, 133.7, 136.7, 137.6, 138.8, 142.1, 151.7, 153.4, 157.7, 158.6, 161.6. MS (HRMS-ESI): m/z: Calcd: 1516.819 [M^+], Found: 1516.798 [M^+] , Δ=14 ppm

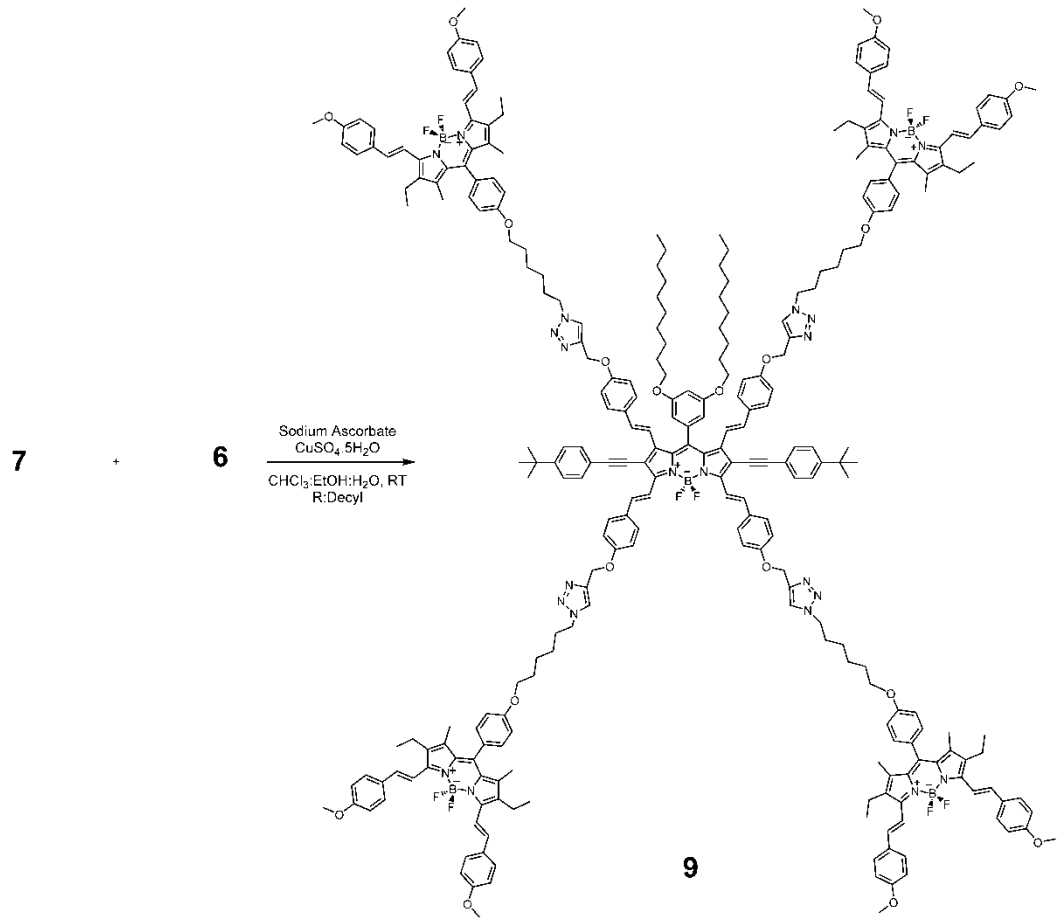
Synthesis of Compound 8:



To the solution of the compound **4** (124 mg, 0.238 mmol) in a 12:1:1 mixture of $CHCl_3$, EtOH and water (14 ml); compound **7** (60 mg, 0.040 mmol), sodium ascorbate (4.7 mg, 0.0237 mmol), $CuSO_4$ (2.9 mg, 0.0118 mmol) and 3-4 drop Et_3N are added and it was stirred at room temperature for 24 h. Water (50 ml) was added to the residue and the product was extracted into the chloroform (3 x 50 ml). After evaporation of the solvents, the crude product was purified by column chromatography ($CHCl_3$). Black solid (122 mg, 85%). ^{1}H NMR ($CDCl_3$, 400 MHz, δ ppm) 0.75 (t, J= 6.76 Hz, 6H), 0.89 (t, *J*= 8.3 Hz, 24H), 1.05-1.20 (m, 28H), 1.24 (s, 18H), 1.26 (s, 24H), 1.36 (p, *J*= 8.39 Hz, 4H), 1.43-1.55 (m, 16H), 1.74 (p, *J*= 7.01 Hz, 8H), 1.92 (p, *J*= 7.34 Hz, 8H), 2.16-2.26 (m, 16H), 2.44 (s, 24H), 3.75 (t, *J*= 6.42 Hz, 4H), 3.91 (t, *J*= 6.24 Hz, 8H), 4.31 (t, *J*= 6.66 Hz, 8H), 5.14 (s, 4H), 5.22 (s, 4H), 6.00 (d, *J*= 16.20 Hz, 2H), 6.53 (s, 2H), 6.62 (s, 1H), 6.80 (d, *J*= 8.64 Hz, 4H), 6.89 (d, *J*= 8.52 Hz, 8H), 6.96 (d, *J*= 8.72 Hz, 4H), 6.99 (d, *J*= 8.64 Hz, 4H), 7.02-7.08 (m, 8H), 7.32 (d, *J*= 8.60 Hz, 4H), 7.37 (d, *J*= 8.48 Hz, 4H), 7.52 (s, 2H), 7.56 (s, 2H), 7.58 (d, *J*= 8.68 Hz, 4H), 7.69 (d, *J*= 16.12 Hz, 4H), 8.46 (d, *J*= 16.40, 2H). ($CDCl_3$, 100 MHz, δ ppm) 11.8, 12.4, 14.1, 14.2, 14.6, 17.0, 21.0, 22.6, 25.6, 25.6,

25.9, 26.3, 26.4, 28.9, 29.0, 29.1, 29.3, 29.5, 30.2, 30.2, 31.2, 31.9, 50.3, 60.4, 62.2, 62.2, 67.7, 68.6, 98.9, 114.8, 114.9, 115.2, 120.5, 122.4, 122.5, 125.7, 127.7, 127.8, 128.1, 129.3, 129.4, 130.4, 131.2, 132.6, 132.6, 136.6, 137.4, 138.3, 138.4, 138.6, 138.8, 140.3, 140.3, 142.0, 144.0, 153.4, 153.4, 158.4, 159.3, 159.4, 161.6. MS (MALDI): m/z: Calcd: 3602.074 $[M]^+$, Found: 3711.572 $[M-Ag]^+$

Synthesis of Compound 9:



To the solution of the compound **6** (335 mg, 0.237 mmol) in a 12:1:1 mixture of $CHCl_3$, EtOH and water (14 ml); compound **7** (60 mg, 0.0396 mmol), sodium ascorbate (4.7 mg, 0.0237 mmol), $CuSO_4$ (2.9 mg, 0.0118 mmol) and 3-4 drop Et_3N were added and it was stirred at room temperature for 24 h. Water (50 ml) was added to the residue and the product was extracted into the chloroform (3 x 50 ml). After evaporation of the solvents, the crude product was purified by column

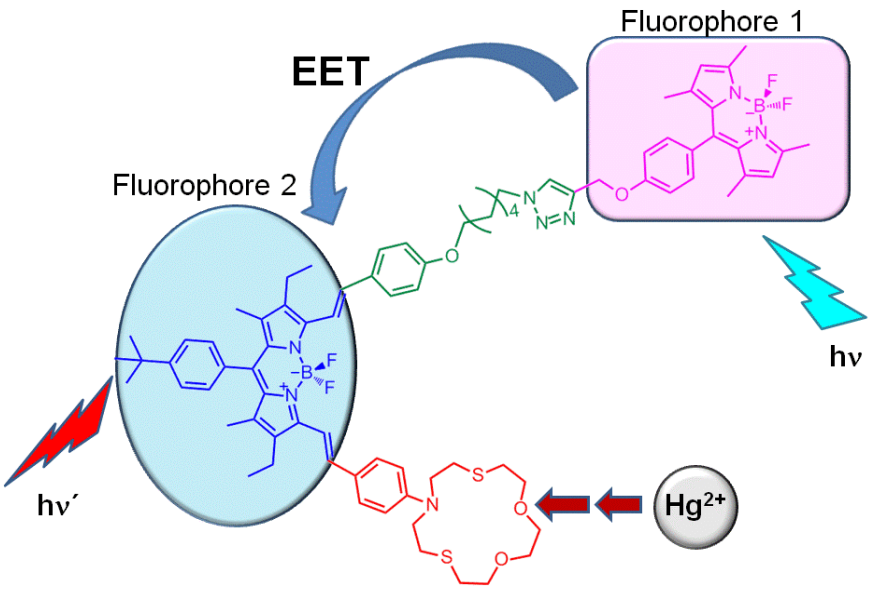
chromatography ($CHCl_3$). Black solid (144 mg, 80%). ^1H NMR ($CDCl_3$, 400 MHz, δ ppm) 0.90 (t, J= 6.90 Hz, 6H), 1.18 (t, *J*= 7.60 Hz, 24H), 1.19-1.30 (m, 28H), 1.37 (s, 18H), 1.40 (s, 24H), 1.41-1.50 (m, 4H), 1.52-1.69 (m, 16H), 1.79-1.90 (m, 8H), 1.95-2.07 (m, 8H), 2.55-2.65 (m, 16H), 3.86-3.90 (m, 28H), 4.09 (t, *J*= 6.20 Hz, 8H), 4.42 (t, *J*= 7.00 Hz, 8H), 5.25 (s, 4H), 5.32 (s, 4H), 6.11 (d, *J*= 16.13 Hz, 2H), 6.65 (d, *J*= 2.04 Hz, 2H), 6.75 (s, 1H), 6.92 (d, *J*= 8.56 Hz, 4H), 6.95 (d, *J*= 8.84 Hz, 16H), 7.01 (d, *J*= 8.50 Hz, 8H), 7.06 (d, *J*= 8.72 Hz, 4H), 7.10 (d, *J*= 8.00 Hz, 4H), 7.16-7.25 (m, 16H), 7.43 (d, *J*= 8.52 Hz, 4H), 7.48 (d, *J*= 8.52 Hz, 4H), 7.59 (d, *J*= 8.72 Hz, 16H), 7.63-7.74 (m, 16H), 7.78 (s, 2H), 7.83 (s, 2H), 8.58 (d, *J*= 16.13, 2H). ($CDCl_3$, 100 MHz, δ ppm) 11.7, 14.0, 14.1, 18.4, 22.7, 25.6, 25.6, 25.9, 26.3, 26.4, 28.9, 29.1, 29.3, 29.5, 30.2, 30.2, 31.2, 31.9, 34.9, 50.3, 55.4, 62.1, 62.2, 62.2, 67.7, 68.6, 85.7, 98.9, 108.2, 114.2, 114.8, 114.9, 114.9, 115.3, 118.1, 118.2, 119.5, 120.6, 122.4, 122.6, 122.7, 125.7, 128.0, 128.1, 128.1, 128.7, 129.3, 129.8, 130.3, 130.4, 133.2, 133.4, 133.8, 135.3, 138.2, 138.9, 142.1, 144.0, 150.3, 151.8, 153.3, 158.4, 159.1, 159.5, 160.2, 161.6. MS (MALDI): m/z: Calcd: 4546.4 [M^+], Found: 4547.0 [M^+]

CHAPTER 5

Coupling ICT Process to Excitation Energy Transfer: Improved Stokes Shift for Selective Hg (II) Sensing

This work is partially described in the following publication:

Atilgan, S.; **Ozdemir, T.**; Akkaya, E.U. *Org. Lett,*. 2010, *12*, 4792-4795.



5.1. Objective

Versatile chemistry of the BODIPY chromophore allows modular assembly of an excitation energy donor, acceptor and a cation selective ligand in just a couple of steps. The new approach should be applicable in other designs which target molecular sensors with large Stokes shift and red to NIR emission.

5.2. Introduction

Ion sensing and signaling continues to be a vibrant field of study.[166-168] The signal transduction phenomenon, which is at the core of signal generation, is a binding event which changes the spectral signature of a particular chromophore or fluorophore. In designing a molecular sensor, typically an ion selective ligand is incorporated into the structure. The ion binding is then expected to alter either ground state or excited state properties to yield a quantifiable signal. This signal in many cases will be in the form of a shift in the absorbance spectra or changes in the emission characteristics (intensity, lifetime, or position of the emission maximum). While some of the selective ion sensors are actually serendipitous discoveries of selective interactions of a particular receptor with the analyte in question, it is indeed possible to rationally design molecular sensors. To that end, ion-induced changes in internal charge transfer (ICT)[169,170] or photoinduced electron transfer (PET)[171,172] appear to be very useful. However, other fluorophore characteristics such as Stokes shift or brightness (usually defined as the product of quantum yield and the molar extinction coefficient) are more difficult to modulate.

We recently proposed[173] a systematic solution addressing this particular problem via coupling of excitation energy transfer to standard signal transduction processes. In this way, as long as the energy transfer is efficient, large pseudo-Stokes shifts are essentially guaranteed. As a bonus, if the excitation energy transfer (EET) efficiency itself can be modulated by ion binding, changes in intensity ratios take place at a wider range, thus increasing the dynamic range of the molecular sensor.[152] In our previous work,[174] we demonstrated the utility of this approach by the synthesis of fluorophores linked through phenylethynyl groups. In this work, our intention was to move the operation wavelengths more into the red/ near IR region and make use of

unique BODIPY chemistry[157,175,176] together with Huisgen type "Click" chemistry[159,177] to emphasize the modularity of our approach.

5.3. Result and Discussion

The synthesis (Figure 78) of the target molecule starts with the placement of a terminal alkyne moiety at the *meso* position of a BODIPY dye **4**. Azido-tethered aromatic aldehyde **7** was also prepared by a series of straightforward reactions. The core BODIPY unit **8** was functionalized through Knoevenagel reaction to yield **10**. A second condensation then places the azido linkage on the other side of the BODIPY core (**11**). Finally, the two chromophores are "clicked" together. Double styryl condensation not only creates opportunities for additional functionalization but also pushes the absorption and emission wavelengths of the BODIPY chromophore at least 150 nm into the red.[13,37,143,144,165,178]

The target compound **12** is freely soluble in most organic solvents, absorption spectrum in THF in the absence and presence of various metal ions is highly informative (Figure 79). In the absence of any metal ions, there are two clearly identifiable peaks in the visible region, one around 500 nm (energy donor, shorter wavelength absorbing BODIPY) and one for the core distyryl-BODIPY centered at 690 nm. The addition of metal ions at 10 μM concentration results in essentially no change, except for the Hg (II) ions. The ligand under the conditions of the study, displays a remarkable selectivity. Thus, in the presence of mercuric ions, the longer wavelength absorption peak shifts hypsochromically to 650 nm. This is perfectly understandable considering charge transfer nature of the dialklyamino substituent

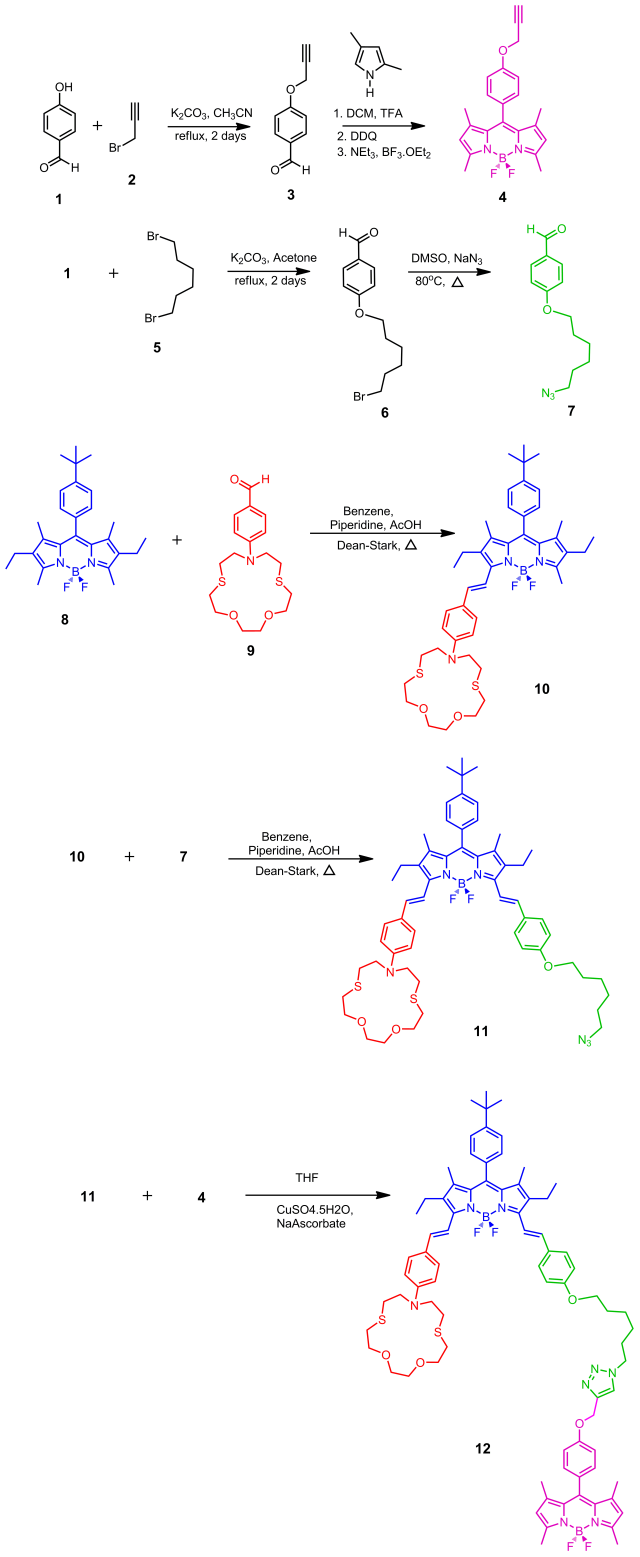


Figure 78. Synthesis of the target compound (Copyright © 2010, American Chemical Society, Reprinted with permission from ref (165)).[165]

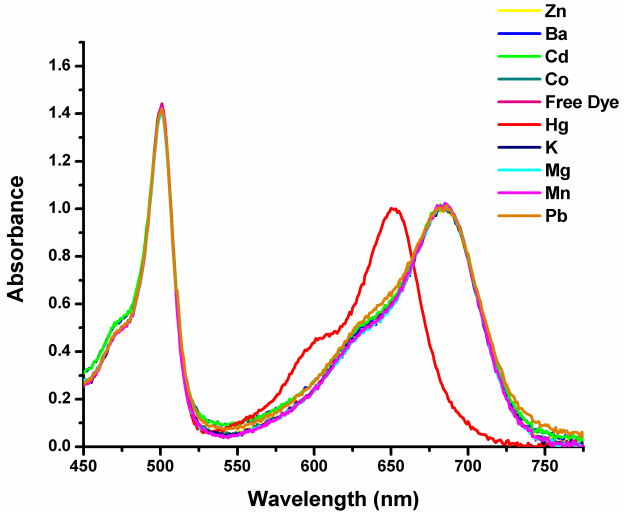


Figure 79. Absorbance spectra of the chemosensor compound **12** (1.5 μM) in THF in the absence and presence of various metal ions. Added metal ion concentrations were 10 μM (Copyright © 2010, American Chemical Society, Reprinted with permission from ref (165)).

being subdued by the binding of a Hg(II) ion. Fluorescence spectra are equally useful (Figure 7), free chemosensor shows two emission peaks at 518 nm, and at 725 nm. Other metal ions are essentially ineffective, but the addition of Hg (II) ions result in a blue shift in the emission together with a large increase in intensity. The decrease in the emission intensity of shorter wavelength emitting BODIPY is also noteworthy, as it indicates increased energy transfer efficiency due to larger spectral overlap between the donor and acceptor chromophore once the mercuric ion is tightly bound to the dithiaazacrown ligand.

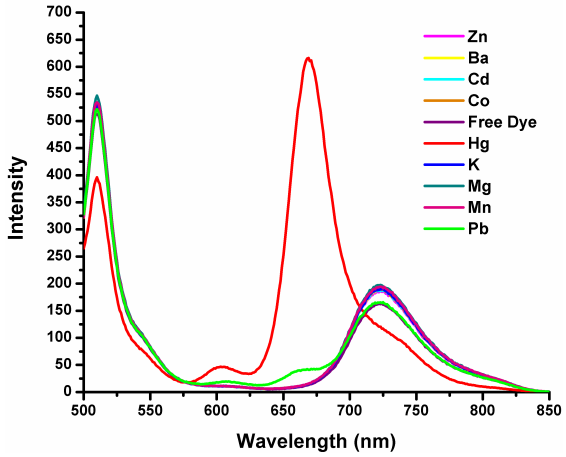


Figure 80. Emission spectra of compound **12** in THF (1.5 μM) in THF in the absence and presence of various metal ions. Added metal ion concentrations were 10.0×10^{-6} M. Excitation wavelength is 480 nm (Copyright © 2010, American Chemical Society, Reprinted with permission from ref (165)).

Excitation spectrum of compound **12** compared to that of the model compound **4** at equal concentrations shows the efficiency of energy transfer within the target molecule (Figure 81). When excited at 495 nm, emission can be collected from the longer wavelength emitting chromophore. The emission intensity from the energy donor chromophore is significantly quenched.

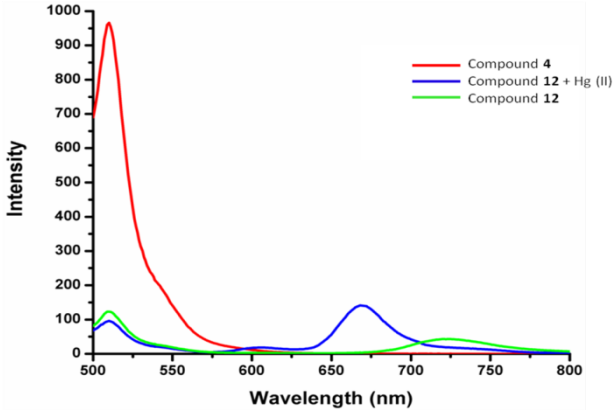


Figure 81. Excitation spectra of a model compound (**4**) and compound **12** with and without 10 μM Hg(II). For compound **4**, the emission data was collected at 518 nm, and for the longer wavelength peak the data was collected at the isoemissive point 710 nm (Copyright © 2010, American Chemical Society, Reprinted with permission from ref (165)).

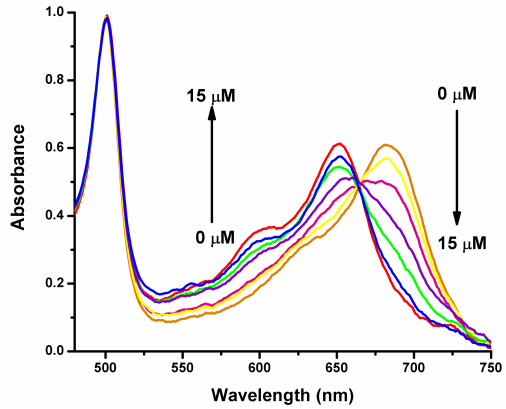


Figure 82. Hg(II) titration of the chemosensor compound **12**. Hg (II) concentration is varied between 0 to 15 μM in THF. The concentration of **12** was 1.5 μM (Copyright © 2010, American Chemical Society, Reprinted with permission from ref (165)).

We then proceeded with the titration of chemosensor compound **12** with Hg(II) ions. As expected, the shorter wavelength peak is not altered, but the longer wavelength peak is clearly shifted hypsochromically, resulting a clean isosbestic point at 662 nm (Figure 82). The absorption spectra, thus present multiple opportunities of ratiometric sensing of ions, in this case mercuric ions. When the titration process is

followed fluorometrically, (Figure 83) the results clearly validate our design principles. Shorter wavelength peak diminishes somewhat when the concentration of Hg (II) increases due to increased spectral overlap, hence more efficient energy transfer. Titration shows a clean equilibration between the two states, metal-free and metal bound, with a single identifiable isoemissive point. Time resolved

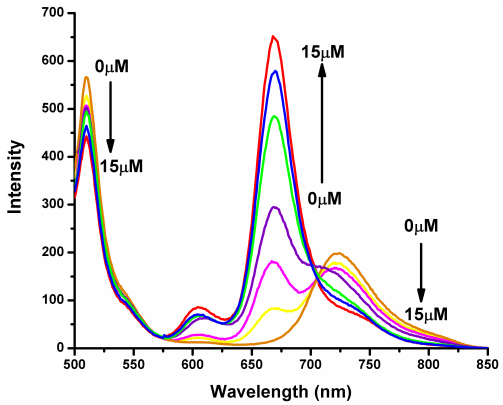


Figure 83. Hg (II) titration of the chemosensor **12** in THF. Ion concentration was varied between 0 to 15 μM. The chemosensor concentration was held at 1.5 μM (Copyright © 2010, American Chemical Society, Reprinted with permission from ref (165)).

Table 6. Lifetimes, FRET rate constants and efficiencies of Compound **4**, **12**, **12**+ Hg(II) (Copyright © 2010, American Chemical Society, Reprinted with permission from ref (165)).

Compound	τ (ns)	$k_{FRET}(s^{-1})$	ε_{FRET}
	λ_{em}(495 nm)		
4	3.34	-	-
12	2.97	3.76×10^{7}	11%
12 + Hg (II)	1.83	2.47×10^{8}	45%

Φ = 0.43 for Compound **12** (in THF) for excitation at 488 nm, Rhodamine 6G in water (Φ_f= 0.95) was used as reference. Φ = 0.11 for Compound **12** (in THF) for excitation at 683 nm, Compound **13**[43] in $CHCl_3$ (Φ_f= 0.35) was used as reference

fluorescence spectroscopy provides more quantitative data on the EET process. For compound **12** in THF, without Hg (II) the emission lifetime is 3.34 ns, but when Hg (II) is added in the micromolar quantities, the lifetime is reduced to 2.97 ns. Corresponding energy transfer efficiencies are 11 % and 45 % respectively (Table 6).

The selectivity of the chemosensor was further studied in completion experiments with other metal ions (Figure 84). Thus, an excess of the comPeTing ion was added (100 μM) in addition to 10.0 μM Hg (II). The data shows that the presences of large excesses of comPeTing ions have practically no effect on the emission intensity at 660 nm.

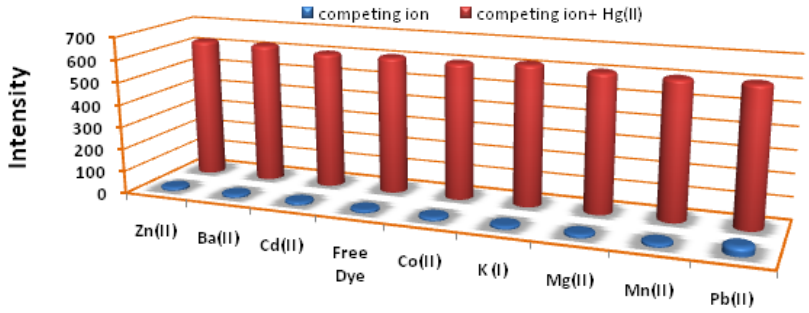


Figure 84. The free dye **12** (chemosensor) concentration was set at 1.5 μM, the concentration of the comPeTing cation 100 mM and concentration of Hg^{2+} was 10 mM. Excitation was at 500 nm with a slit width 5.0 nm (Copyright © 2010, American Chemical Society, Reprinted with permission from ref (165)).

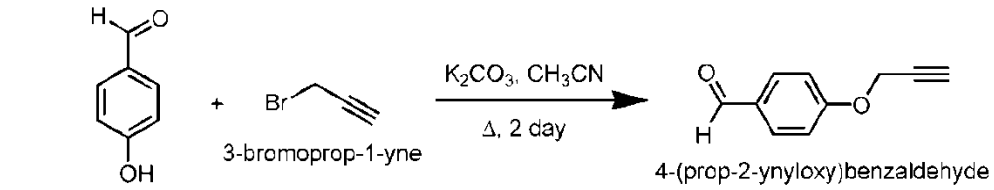
5.4. Conclusion

The principal outcomes of energy transfer coupled to internal charge transfer were obtained in a simple modular design. These are large pseudo-Stokes shift (approximately 300 to 250 nm), multiple ratiometric measurement opportunities. The applicability of radiometry can be clearly demonstrated by recording the emission wavelength ratios at 760 nm to 723 nm (I_{760}/I_{723}) as a function of Hg (II) concentrations. Naturally, radiometry can be clearly demonstrated by recording the emission wavelength ratios at 760 nm to 723 nm (I_{760}/I_{723}) as a function of Hg (II) concentrations. Additionally, selectivity is conserved here as well.

5.5. Experimental Details

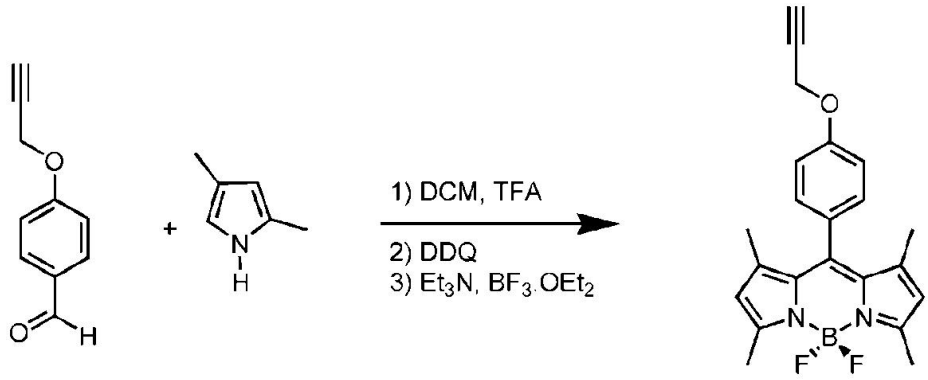
General: All chemicals and solvents purchased from Aldrich were used without further purification. ^{1}H NMR and ^{13}C NMR spectra were recorded using a Bruker DPX-400 in CDCl3 or DMSO-d6 with TMS as internal reference. Absorption spectrometry was performed using a Varian spectrophotometer. Steady state fluorescence and time-resolved fluorescence measurements were conducted using a Varian Eclipse spectrofluorometer and a Fluorolog Horiba Jobin-Yvon (Horiba Jobin Yvon Single Photon Counting Controller (FluoroHub) system), respectively. Column chromatography of all products was performed using Merck Silica Gel 60 (particle size: 0.040–0.063 mm, 230–400 mesh ASTM). Reactions were monitored by thin layer chromatography using fluorescent coated aluminum sheets. Solvents used for spectroscopy experiments were spectrophotometric grade. Mass spectra were recorded on Agilent Technologies 6530 Accurate-Mass Q-TOF LC/MS.

Synthesis of Compound 3:



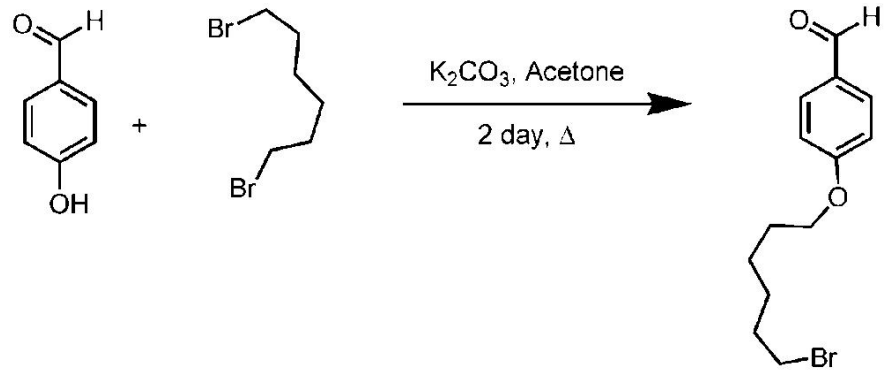
1.50 g of K_2CO_3 (7.3 mmol) was added into 100 ml of CH_3CN and then to this solution a mixture of 4-hydroxybenzaldehyde, **1**, (100 mg, 0.82 mmol), and 3-bromoprop-1-yne, 2, (106 mg, 0.90 mmol) in 5 ml CH_3CN was added in a dropwise manner for an hour. After addition the solution was heated until reflux temperature. After stirring for 2 days at this temperature the solution was filtered and filtrate was concentrated by rotary evaporation under vacuum. The crude product was purified by column chromatography using $CHCl_3$ as the eluent to afford product **3** as a white solid (98.4 mg, 74%).[159] ^{1}H NMR (400 MHz, $CDCl_3$) δ; 9.84 (s, 1H), 7.79 (d, *J*=8.8 Hz, 2H), 7.02 (d, *J*=8.8 Hz, 2H), 4.71 (d, *J*=2.4 Hz, 2H), 2.50 (t, *J*=2.4 Hz, 1H).

Synthesis of Compound 4:



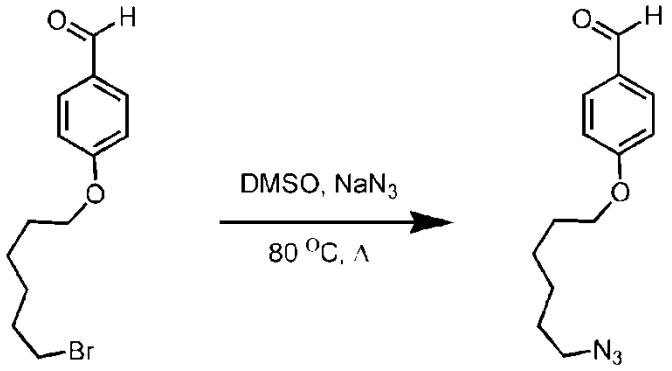
To a deoxygenated solution of aldehyde, **3**, (1.25 mmol, 200 mg) and 2,4-dimethylpyrrole (2.5 mmol, 237 mg) in CH_2Cl_2 (500 ml), TFA (125 mg, 1.1 mmol) was added and the mixture was stirred overnight. The red solution was treated with DDQ (284 mg, 1.25 mmol), stirred for 30 min, then 5 ml of Et_3N and 3 ml of $BF_3.Et_2O$ were added, and the mixture was stirred at rt for further 40 min. The organic phase was separated, dried ($MgSO_4$), filtered, and concentrated. The residue was purified by column chromatography ($CHCl_3$), collecting the first green fluorescent fraction afforded the expected BODIPY dye, **4**, 47 mg (10% yield), orange-red solid. ^1H NMR (400 MHz, $CDCl_3$) δ; 7.12 (d, *J*=8.8 Hz, 2H), 7.01 (d, *J*=8.8 Hz, 2H), 5.90 (s, 2H), 4.68 (d, *J*=2.0 Hz, 2H), 2.52 (d, *J*=2.0 Hz, 1H), 2.48 (s, 6H), 1.35 (s, 6H). ^{13}C NMR (100 MHz, $CDCl_3$) δ; 158.1, 155.4, 143.1, 141.5, 131.8, 130.4, 129.3, 128.0, 121.2, 115.6, 78.0, 75.9, 56.0, 14.7, 14.6

Synthesis of Compound 6:



To a solution of K_2CO_3 (200 mg, 1.45 mmol) in 100 ml freshly distilled acetone was added 4-hydroxybenzaldehyde, 1, (100 mg, 0.82 mmol) and 1,6 -dibromo hexane, **5**, (219 mg, 0.90 mmol) and the mixture was stirred at the reflux temperature for 2 days. After removal of the solid part by filtration, organic solvent was removed under reduced pressure. The crude product was dissolved in $CHCl_3$ to extract it with water. Organic layer was evaporated and resulting residue chromatographed (3:1 Hexane/EtOAc) to give yellow oil. (94 mg, yield 40%)[159] ^{1}H NMR (400 MHz, $CDCl_3$) δ; 9.87 (s, 1H), 7.82 (d, *J*=8.8 Hz, 2H), 6.98 (d, *J*=8.8 Hz, 2H), 4.03 (t, *J*=6.4 Hz, 2H), 3.42 (t, *J*=6.8 Hz, 2H), 1.93-1.80 (m, 4H), 1.52-1.49 (m, 4H). ^{13}C NMR (100 MHz, $CDCl_3$) δ; 189.1, 162.5, 130.3, 128.2, 113.1, 66.5, 32.1, 31.0, 27.2, 26.2, 23.6.

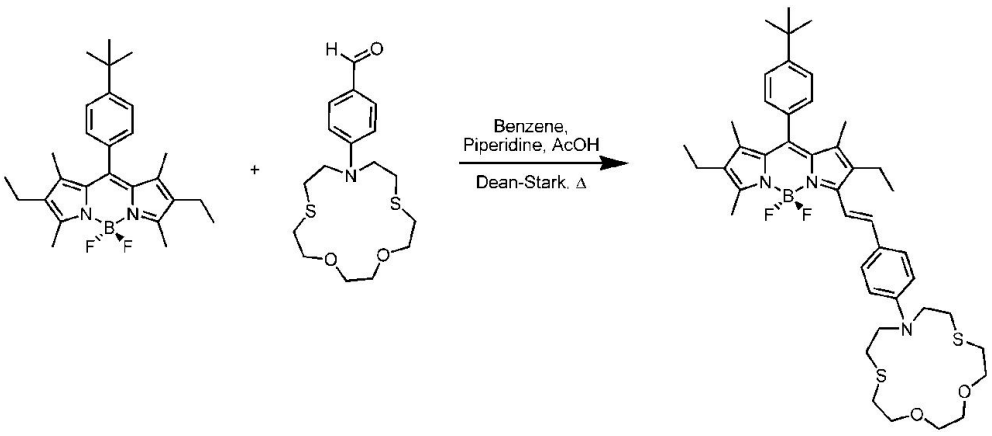
Synthesis of Compound 7:



4-(6-bromohexyloxy) benzaldehyde, **6**, (80 mg, 0.32 mmol) and NaN_3 (24 mg, 0.37 mmol) was added to DMSO and stirred vigorously. This suspension was then heated to 80 ^{o}C and stirred at this temperature for 3 hours. When TLC analysis showed complete consumption of the starting material the reaction was cooled to room temperature and then the crude product was poured onto brine solution and extracted three times with $CHCl_3$. The organic layer was removed by rotary evaporator. And the residue was purified with column chromatography, EtOAc as an eluent, to give the product, **7**, as a brown oil. (75 mg, 95% yield) [159] ^{1}H NMR (400 MHz, $CDCl_3$) δ; 9.78 (s, 1H), 7.74 (d, *J*=8.8 Hz, 2H), 6.90 (d, *J*=8.8 Hz, 2H), 3.95 (t, *J*=6.4 Hz, 2H), 3.20 (t, *J*=6.8 Hz, 2H), 1.78-1.71 (m, 2H), 1.59-1.52 (m, 2H), 1.47-1.33 (m, 4H)

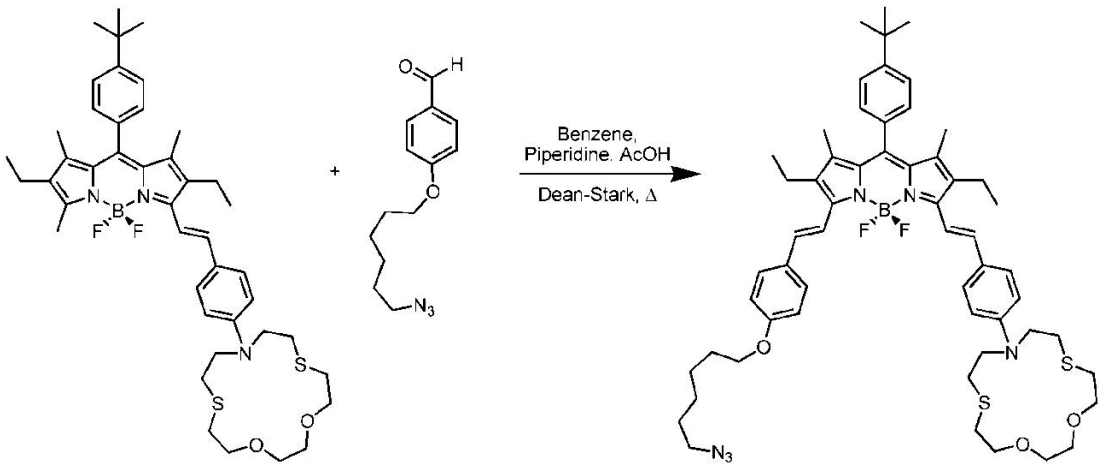
^{13}C NMR (100 MHz, $CDCl_3$) δ; 190.7, 164.1, 131.9, 129.8, 114.7, 68.1, 51.3, 28.9, 28.7, 26.4, 25.6.

Synthesis of Compound 10:



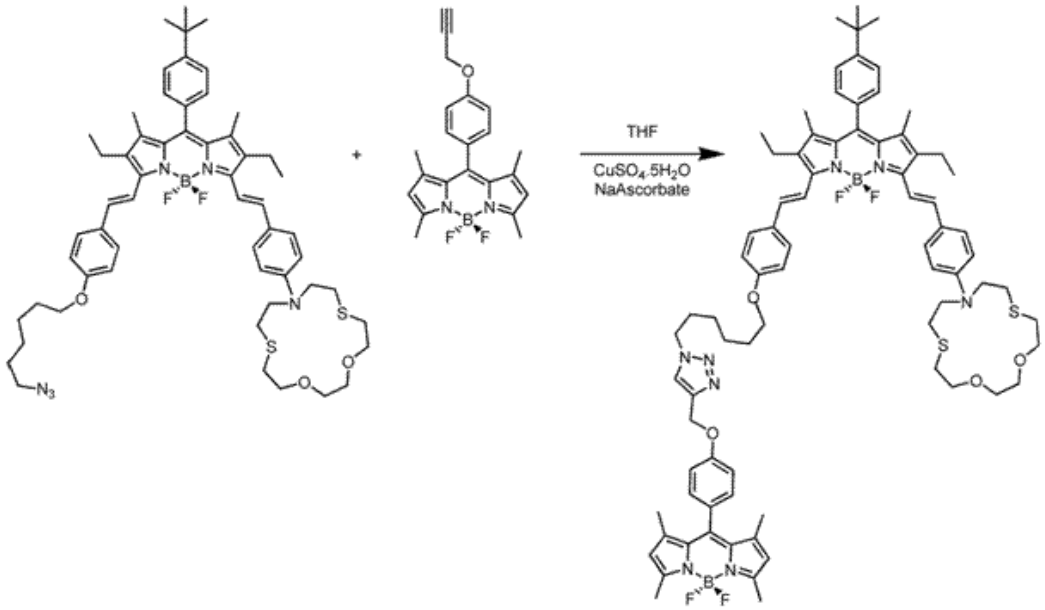
Tert-Butyl BODIPY, **8**, (200 mg, 0.46 mmol), compound **9** (160 mg, 0.46 mmol), were refluxed in a mixture of benzene (20 ml), glacial acetic acid (0.5 ml) and piperidine (1.0 ml). Any water formed during the reaction was removed azeotropically by heating overnight in a Dean–Stark apparatus. Crude product was then concentrated under vacuum, and purified by silica gel column chromatography ($CHCl_3$). The blue colored fraction was collected and the solvent was removed under reduced pressure to yield the bright red fluorescent compound **10** (35 mg, 10%). ^{1}H NMR (400 MHz, $CDCl_3$) δ; 7.49 (d, *J*=16.4 Hz, 1H), 7.43-7.40 (m, 4H), 7.12 (d, *J*=8.4 Hz, 2H), 7.08 (d, *J*=16.4 Hz, 1H), 6.57 (d, *J*=8.8 Hz, 2H), 3.74 (t, *J*=4.8 Hz, 4H), 3.63-3.58 (m, 8H), 2.84 (t, *J*=8.0 Hz, 4H), 2.71 (t, *J*=4.8 Hz, 4H), 2.50 (q, *J*=7.2 Hz, 2H), 2.23 (q, *J*=7.6 Hz, 2H), 1.50 (s, 3H), 1.30 (s, 9H), 1.23 (s, 3H), 1.21(s, 3H), 1.06 (t, *J*=7.2 Hz, 3H), 0.91 (t, *J*=7.6 Hz, 3H). ^{13}C NMR (100 MHz, $CDCl_3$) δ; 153.2, 137.7, 137.4, 136.6, 135.2, 134.7, 132.1, 131.8, 131.0, 130.5, 128.0, 127.9, 127.6, 125.3, 115.6, 114.9, 111.7, 74.2, 71.7, 51.1, 35.2, 31.4, 31.3, 29.6, 18.4, 16.3, 13.6, 13.0, 11.6, 10.6, 10.3.

Synthesis of Compound 11:



To a freshly distilled benzene Mono-styryl-BODIPY, **10**, (blue-BODIPY) (25 mg, 0.032 mmol) and 4-(6-azidohexyloxy)benzaldehyde, **7**, (16 mg, 0.064 mmol) were added. After vigorously stirring glacial acetic acid (0.5 ml), piperidine (1.0 ml) was added to this solution, heated to reflux temperature and kept at this temperature until TLC observation showed complete consumption of the blue BODIPY and formation of the green red fluorescent di-styryl BODIPY. At this point organic layer was removed under reduced pressure and the crude product re-dissolved in $CHCl_3$ and extracted three times with brine solution. The organic layer was removed and final residue was purified with column chromatography, $CHCl_3$ as an eluent. The red fluorescent compound was isolated, **11**. (24 mg, 75% yield). ^{1}H NMR (400 MHz, $CDCl_3$) δ; 7.60 (d, *J*=16.4 Hz, 1H), 7.55 (d, *J*=16.8 Hz, 1H), 7.49 (d, *J*=8.4 Hz, 2H), 7.46 (d, *J*=8.8 Hz, 2H), 7.41 (d, *J*=8.0 Hz, 2H), 7.15-7.06 (m, 4H), 6.86 (d, *J*=8.8 Hz, 2H), 6.60 (d, *J*=8.8 Hz, 2H), 3.94 (t, *J*=6.4 Hz, 2H), 3.75 (t, *J*=4.8 Hz, 4H), 3.65-3.59 (m, 8H), 3.21 (t, *J*=6.8 Hz, 2H), 2.88-2.84 (m, 4H), 2.71 (t, *J*=4.8 Hz, 4H), 2.54-2.51 (m, 4H), 1.80-1.72 (m, 2H), 1.63-1.56 (m, 2H), 1.48-1.47 (m, 4H), 1.30 (s, 9H), 1.24 (s, 6H), 1.07 (t, *J*=7.6 Hz, 6H) ^{13}C NMR (100 MHz, $CDCl_3$) δ; 159.4, 152.1, 151.4, 149.0, 147.4, 139.0, 137.9, 137.5, 136.3, 134.4, 133.6, 133.3, 133.2, 133.0, 132.7, 130.5, 130.0, 129.2, 128.6, 128.3, 125.9, 125.7, 118.4, 115.9, 114.7, 111.9, 74.3, 70.8, 67.9, 52.0, 51.4, 34.8, 31.4, 31.3, 29.6, 29.2, 28.8, 26.6, 25.7, 18.5, 18.4, 14.1, 14.0, 11.4, 11.3.

Synthesis of Compound 12:



To a freshly distilled THF, 1.0 equiv of BODIPY-acetylene, **4**, (9.01 mg, 0.023 mmol) and 1.1.equiv. of di styryl-BODIPY-N_3, **11**, (24 mg, 0.024 mmol) was added. Then TEA (10–30 mol% per triple bond) was added to this mixture, and stirred for 5 min, 10-30 mol% per triple bond of sodium ascorbate was added, followed by 5–15 mol% of $CuSO_4 \cdot 5H_2O$ per triple bond. (A stock solution of sodium ascorbate and $CuSO_4 \cdot 5H_2O$ in water was prepared in concentration 100 mg/ml) The THF/H_2O ratio must be 1/1 (v/v). The heterogeneous mixture was stirred vigorously until TLC analysis indicated complete consumption of the starting material. The reaction mixture was diluted with water and extracted with CH_2Cl_2. The combined organic layers were dried with Na_2SO_4, and concentrated in vacuo. Purification by column chromatography ($CHCl_3$, as an eluent) gave the desired product. (13.6 mg, 90% yield) ^{1}H NMR (400 MHz, $CDCl_3$) δ; 7.61 (d, *J*=16.8 Hz, 1H), 7.58 (s, 1H), 7.53 (d, *J*=16.8 Hz, 1H), 7.50-7.40 (m, 6H), 7.15-7.01 (m, 8H), 6.84 (d, *J*=8.8 Hz, 2H), 6.59 (d, *J*=8.8 Hz, 2H), 5.89 (s, 2H), 5.16 (s, 2H), 3.94 (t, *J*=6.4 Hz, 2H), 3.74 (t, *J*=4.8 Hz, 4H), 3.67-3.57 (m, 8H), 3.47-3.45 (m, 1H), 3.42-3.40 (m, 1H), 2.87-2.83 (m, 4H), 2.70 (t, *J*=4.8 Hz, 4H), 2.47 (s, 6H), 2.55-2.51 (m, 4H), 1.95-1.88 (m, 2H), 1.76-1.70 (m, 2H), 1.54-1.46 (m, 4H), 1.34 (s, 6H), 1.31 (s, 9H), 1.24 (s, 6H), 1.07 (t,

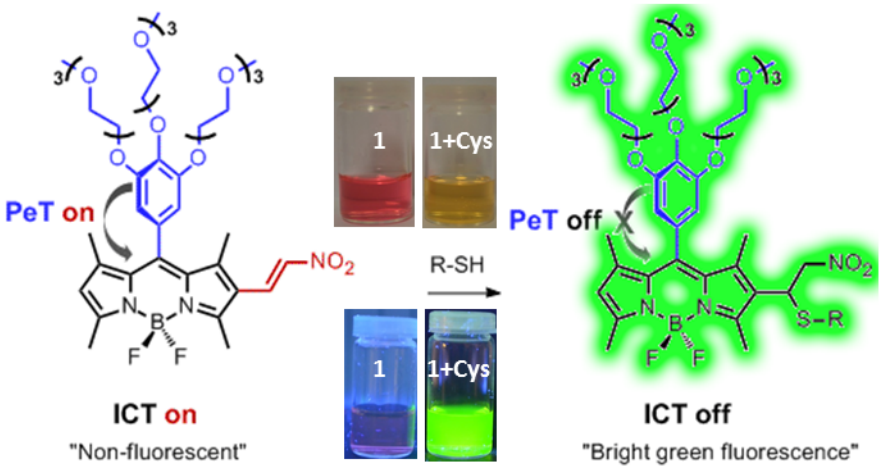
J=7.6 Hz, 3H), 1.07 (t, J= 7.6 Hz, 3H). ^{13}C NMR (100 MHz, $CDCl_3$) δ; 159.3, 158.9, 155.3, 152.2, 151.6, 148.9, 147.5, 143.6, 143.1, 141.6, 139.1, 137.9, 137.6, 136.4, 134.3, 133.7, 133.3, 133.2, 133.0, 132.7, 131.8, 130.6, 130.4, 129.3, 129.2, 128.6, 128.4, 127.6, 127.5, 126.3, 126.0, 125.0, 123.5, 123.2, 122.6, 121.6, 121.2, 118.5, 114.8, 114.6, 111.9, 74.3, 71.7, 71.0, 70.7, 67.7, 62.1, 61.9, 52.0, 50.4, 34.8, 31.9, 31.7, 31.4, 31.3, 30.2, 29.7, 29.6, 29.4, 28.9, 14.5, 14.1, 14.0, 13.9. MS (TOF-ESI): m/z: Calcd: 1381.704 $[M+H]^+$, Found: 1381.7114 [M+H]+ , Δ=5.35 ppm.

CHAPTER 6

Chromogenic and Fluorogenic Sensing of Biological Thiols in Aqueous Solutions Using BODIPY-Based Reagent

This work is partially described in the following publication:

Isik, M.; **Ozdemir, T.**; Simsek Turan, I.; Kolemen, S.; Akkaya, E.U. *Org. Lett.*, **2013**, *11*, 216-219.



6.1. Objective

Judicious design of BODIPY dyes carrying nitroethenyl substituents in conjugation with the BODIPY core, yields dyes which respond to biological thiols by both absorbance and emission changes. Incorporation of solubilizing ethylene glycol units ensures water solubility. The result is bright signaling of biologically relevant thiols in the longer wavelength region of the visible spectrum and in aqueous solutions.

6.2. Introduction

Sensing and signaling of biological thiols is at the focus of recent flurry of work.[179,180] These reaction based probes take advantage of high nucleophilicity of thiol functions found in biologically relevant species such as Cystein (Cys), Homocystein (Hcy) and Glutathione (GSH). These biothiols are vital for the maintenance of cellular redox status and alterations in their levels is linked to a number of debilitating diseases such as AIDS, cancer and Alzheimer's.[181-183] Consequently, probes which respond to these thiols by color change, emision change or both, are highly valued. If they are made to function in aqueous solutions, naturally, they are deemed to be more desirable considering potential applications.

We now present a nitroethenyl-BODIPY conjugate **1**, having both chromogenic and fluorescence turn-on responses for fast, selective and sensitive detection of biological thiols in aqueous media. The roles of three separate modules of the thiol probe **1** are displayed in Figure 85 and can be described as follows: (1) Boron dipyrromethene (BODIPY)[40,184] fluorophore was chosen as the signaling unit for its widely-accepted superiority (e.g. high molar absorptivity, high photostability, visible wavelength absorption and its modular nature for facile functionalization etc.) over more conventional alternatives. Due to these unique features, a plethora of fluorescent sensors/labels,[185-187] light harvesting systems,[25,188,189] photodynamic therapy agents[102,190,191] and molecular logic gate systems[192,193] are built around BODIPY cores and these received considerable attention of the chemical community. (2) Incorporation of a nitroalkene unit to the parent dye would transform it into a strong

Michael acceptor, which would be highly susceptible to sulfhydryl nucleophiles.[194,195] Indeed, Michael reaction based thiol sensing

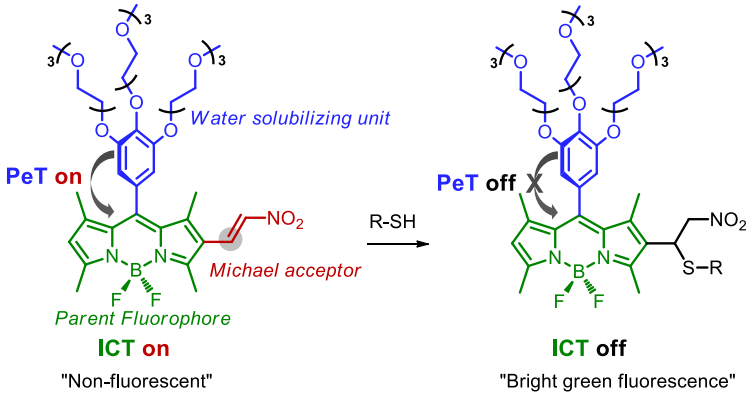


Figure 85. Design elements of the nitroethenyl-BODIPY conjugate thiol probe **1** (Copyright © 2010, American Chemical Society, Reprinted with permission from ref (196)).[196]

protocols[197-199] clearly emerge as the favorite among other strategies.[64,200,201] Nucleophilic attack of the thiol to the *β*-position of nitroethene is expected to disrupt the π-conjugation and block the Intramolecular Charge Transfer (ICT) process, which is expected to induce a blue shift in absorbance. (3) Gallic acid derived unit placed at the *meso*-position of BODIPY core plays two crucial functions: i) Photoinduced-electron-Transfer (PeT) based modulation of the emission, as the electron rich trimethoxyphenyl moiety could quench excited state of the electron deficient (due to conjugated nitroethenyl group) BODIPY core by an electron transfer ii) ethyleneglycolic entities anchored on phenolic hydroxyl functionalities should facilitate water solubility, enhancing the chances for practical applications of the probe **1**.

6.3. Results and Discussion

To test the aforementioned hypothesis, we set out to synthesize of a simpler analog of **1**, and studied its 1,4-addition reactivity with thiols. Thiol sensor **2** was prepared from the readily available 2-formylBODIPY[191] precursor via tandem Henry/elimination reaction. Once *β*-mercaptoethanol (**ME**), chosen as the simple biothiol model compound, reacted with the thiol sensor **2** an apparent color change from red to orange was noticed. This bright green fluorescing adduct **3** was presumed

to be the 1,4-conjugate addition product (Figure 86). Due to poor solubility of **2** in common polar organic solvents, absorption and emission spectra were not recorded. Michael reaction of **2** and **ME** was amenable to ^{1}H-NMR spectroscopy analysis. Comparison of ^{1}H-NMR spectra of **2** and **3** clearly shows that the addition of **ME** to

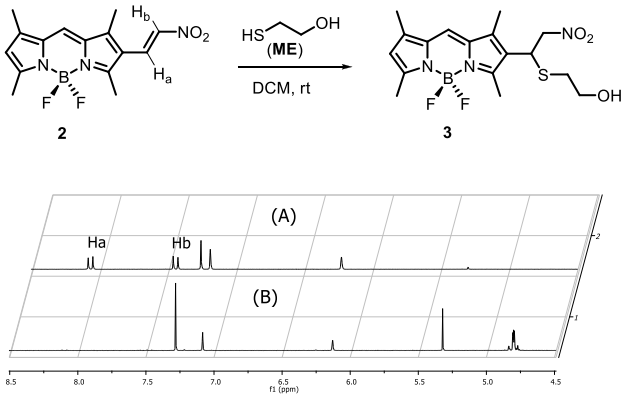


Figure 86. Stacked partial ^{1}H-NMR spectra of thiol probe **2** (A) and conjugate addition product **3** (B) in $CDCl_3$ at 25 °C (Copyright © 2010, American Chemical Society, Reprinted with permission from ref (196)).

the sensor **2** leads to the disappearance of the vinylic protons (H_a and H_b) resonating at 8.07 and 7.44 ppm with the concomitant appearance of α-protons of the newly formed nitroalkane showing at 4.80 ppm. About 0.1 ppm upfield shift of aromatic hydrogens (*meso*-H and 6-H) of BODIPY core is an indication of an increase in the electron density of the BODIPY core (the signaling unit) upon conjugate addition.

Once we demonstrated the Michael acceptor reactivity of the nitroethenyl-BODIPY derivative **2** towards the thiol **ME**, we have turned our attention to the water soluble derivative **1**. Synthetic route followed is depicted in Figure 87.

Gallic acid derived aldehyde **4** was prepared according to our previous report[37] and reacted with 2,4-dimethylpyrrole to furnish **5**. Fluorescent dye **5** was formylated via Vilsmeier-Haack reaction in good yield and subsequent condensation in nitromethane in the presence of catalytic amount of NH_4OAc (20 mol%) provided the thiol probe **1** in reasonable overall yields (14%).

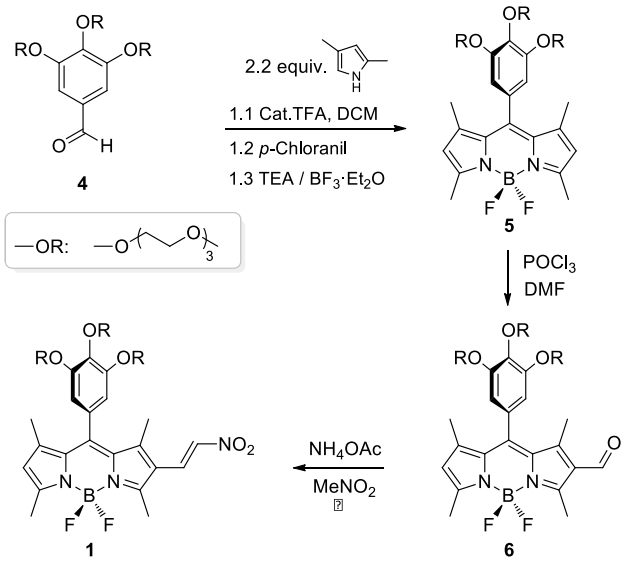


Figure 87. Synthetic route for the target Thiol Probe **1** (Copyright © 2010, American Chemical Society, Reprinted with permission from ref (196)).

Figure 88 shows the electronic absorption and fluorescence emission response of the thiol probe **1** (4 μM) in 50 mM HEPES:CH_3CN (80:20, v/v, pH=7.20) to increasing Cysteine (Cys) concentrations (0-400 equiv.).

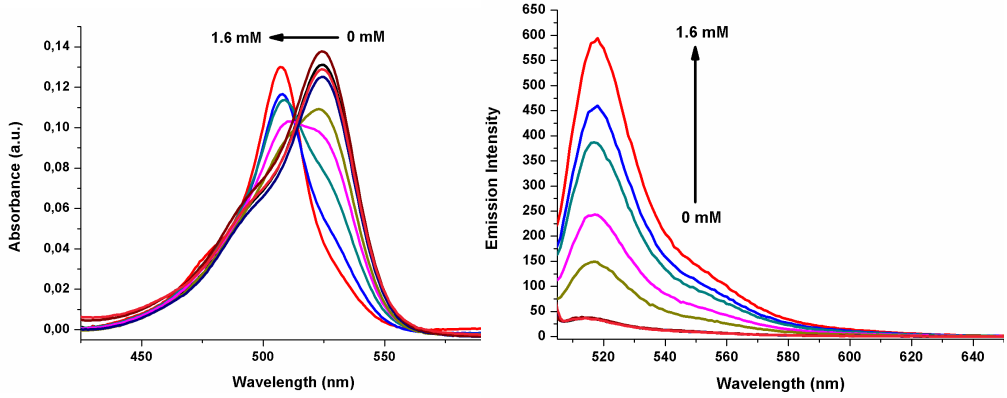


Figure 88. UV-vis absorption spectra (A) and fluorescence spectra (B) of the thiol probe **1** (4 μM) upon increased Cys concentrations (0-400 equiv.) in 50 mM HEPES:CH_3CN (80:20, v/v, pH=7.20, λ_{ex} 500 nm at 25 °C) (Copyright © 2010, American Chemical Society, Reprinted with permission from ref (196)).

Upon addition of Cys, absorption band of free dye **1** centered at 525 nm gradually decreased and a new band appeared with a maximum at 510 nm. A 15 nm blue shift with a well-defined isosbestic point at 518 nm is apparent from the absorption spectrum (Figure 88, left). This Cys-induced hypsochromic shift reveals the

suppression of ICT process that occurs between donor BODIPY core and acceptor nitroalkene unit, as predicted. Probe **1** is essentially nonfluorescent (Φf = 0.056) as evidenced by emission spectrum (Figure 88, right). Fluorescence intensity increases up to 20-fold (Figure 88) upon increasing Cys concentrations (0-400 equiv) with an emission band centered at 515 nm (λex 500 nm). In agreement with our design expectations, this fluorescence enhancement is at least partly due to a reduction in the efficiency of the PeT process upon the attack of the Cys thiol on probe **1** resulting an increase in the energy level of the BODIPY centered LUMO. Under identical conditions, other biological thiols, such as Homocysteine (Hcy) and Glutathione (GSH), afforded similar turn on fluorescence responses as well (Figure 89).

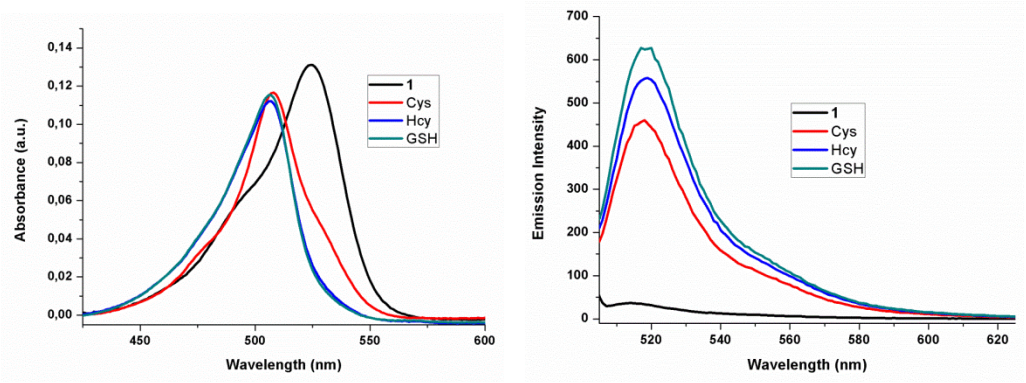


Figure 89. Absorption and fluorescence spectra of Thiol Probe **1** (4 μM) upon addition of 200 eqv. of Cys, Hcy and GSH in 50 mM HEPES:CH_3CN (80:20, v/v, pH=7.2, λex 500 nm at 25 °C) (Copyright © 2010, American Chemical Society, Reprinted with permission from ref (196)).

However, the response to Cys is much faster than that to Hcy and GSH. Thus, by controlling the reaction time, exquisite selectivity for Cys can be obtained (Figure 90 and inset in Figure 92).

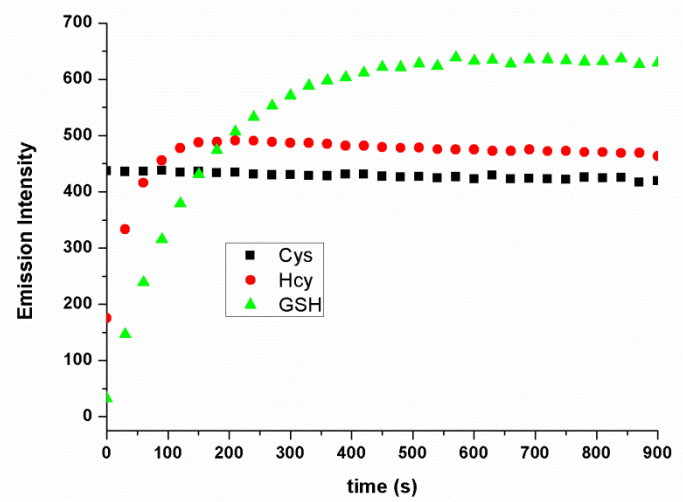


Figure 90. Kinetic measurements of Thiol Probe **1** upon addition of 200 eqv. of Cys, Hcy and GSH in 50 mM HEPES:CH_3CN (80:20, v/v, pH=7.2, λex 518 nm at 25 °C, time interval: 30s) (Copyright © 2010, American Chemical Society, Reprinted with permission from ref (196)).

Sensing experiments were also carried out in HEPES: CH3CN (60:40, v/v) and 100% HEPES buffer solutions (pH 7.2 in both).While 40% acetonitrile solution produces essentially the same responses as that of 20% acetonitrile solution, fluorescence response of **1** toward biological thiols was halved in 100% HEPES solution (Figure 90), but the signal is still strong enough for sensitive and selective detection of thiols (vide infra).

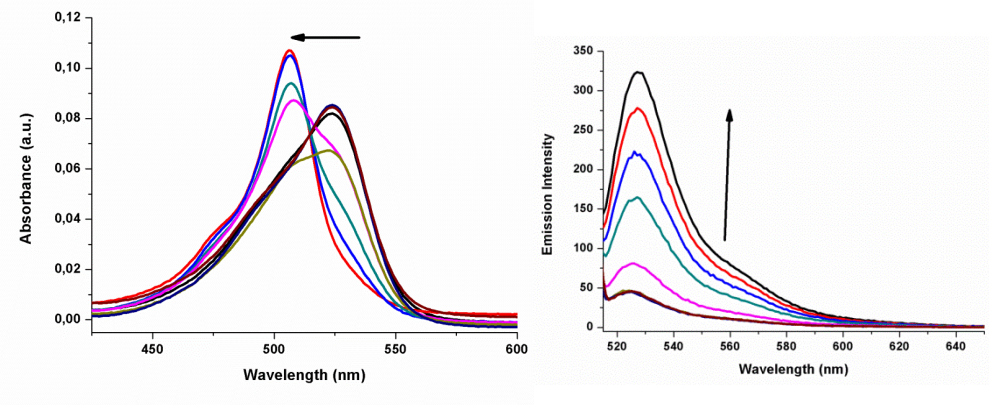


Figure 91. UV-vis absorption and fluorescence spectra of the Thiol Probe **1** (4 μM) upon increased Cys concentrations (0-400 equiv.) in 50 mM HEPES (pH=7.2, λex 500 nm at 25 °C) (Copyright © 2010, American Chemical Society, Reprinted with permission from ref (196)).

As a natural extension of this study, we have investigated the selectivity of probe **1** toward Cys, Hys and GSH over potentially comPeTing biologically relevant natural

aminoacids in HEPES: CH_3CN (80:20, v/v) at physiological pH (7.20). No significant change was observed in both absorption and fluorescence emission (Figure 92) spectra when natural amino acids other than cysteine were treated with the probe **1**.

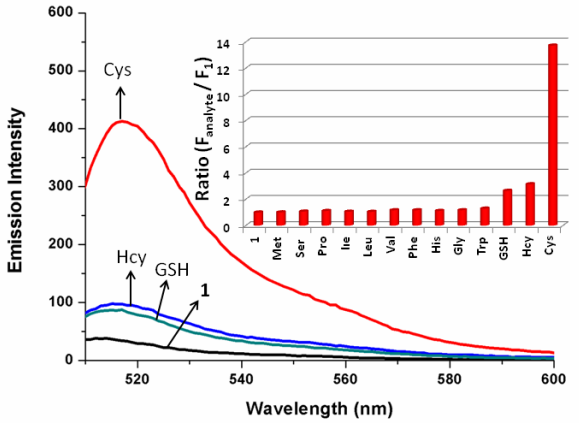


Figure 92. Fluorescence response of the thiol probe **1** (4 μM) towards biothiols (Cys, Hcy and GSH; 200 equiv. each)) and other natural amino acids (400 equiv.) in 50 mM HEPES:CH_3CN (80:20, v/v, pH=7.20, λ_{ex} 500 nm at 25 °C) (Copyright © 2010, American Chemical Society, Reprinted with permission from ref (196)).

Extending the sensing range of the probe into the red and near IR would be highly advantageous. To that end, we made use of now established protocols for Knoevenagel condensation of the methyl substituted BODIPYs and aldehydes. As probe **1** was derivatized by reacting with a trialkoxybenzaldehyde, the absorbance and fluorescence maxima moved into far red (λ_{abs} 623 nm and λ_{em} 650 nm) with enhanced water solubility as a bonus (Figure 93 and Table 7).

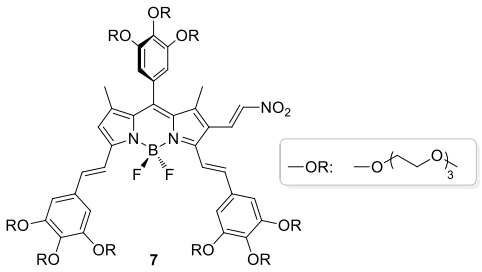


Figure 93. Red-emitting nitroolefin-BODIPY conjugate thiol probe **7** (Copyright © 2010, American Chemical Society, Reprinted with permission from ref (196)).

Table 7. Optical properties of the probes **1** and **7** (Copyright © 2010, American Chemical Society, Reprinted with permission from ref (196)).

Compound[a]	λ_{abs} (nm)	λ_{em} (nm)	Φ_f[b]	ε_{max}[c]
1	525	540	0.056[d]	58,500
7	623	655	0.016[e]	51,800

[a] Data acquired in 50 mM HEPES:CH_3CN (80:20, v/v, pH=7.20, in dilute solutions. [b] Relative quantum yields. [c] unit: $cm^{-1}M^{-1}$. [d] Reference dye: Rhodamine 6G in water (Φ_f= 0.95). [e] Reference dye: Cresyl violet in methanol (Φ_f= 0.90).

Synthesis of distyryl-BODIPY **7** was achieved in 3 steps starting from compound **5** (Figure 94). Optical properties of **1** and **7** are given below in Table 6. Compared to **1**, dye **7** has an extended π-conjugation which causes significant bathochromic shift (≈100 nm in absorption and ≈125 nm in emission peaks). However, this extension of conjugation diminished the fluorescence quantum yield of **7** to approx. one-third of probe **1**.

Sensor **7** displayed good water solubility due to the presence of nine triethyleneglycolic arms on the styryl and *meso* substituents.

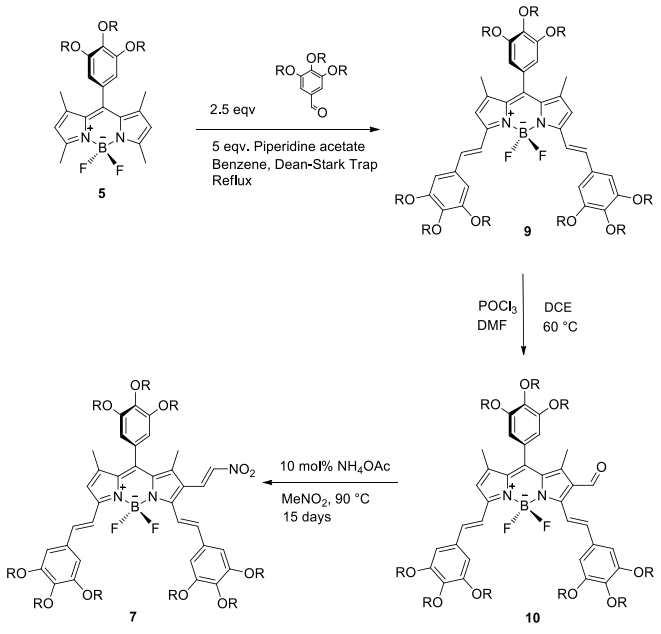


Figure 94. Synthetic route for the target Thiol Probe **7** (Copyright © 2010, American Chemical Society, Reprinted with permission from ref (196)).

Absorption and fluorescence response (Figure 95) of this red-emitting chromophore **7** were also examined. An equal magnitude of enhancement response was observed with the probe **7** and **1** upon incremental Cys additions (0-400 equiv.).

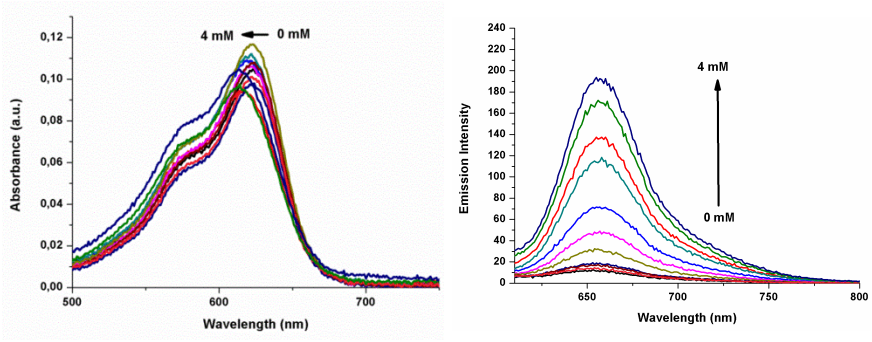


Figure 95. UV-vis absorption and fluorescence spectra of the Thiol Probe **7** (4 μM) upon increased Cys concentrations (0-1000 equiv.) in 50 mM HEPES:CH_3CN (80:20, v/v, pH=7.2, λex 600 nm at 25 °C) (Copyright © 2010, American Chemical Society, Reprinted with permission from ref (196)).

6.4. Conclusion

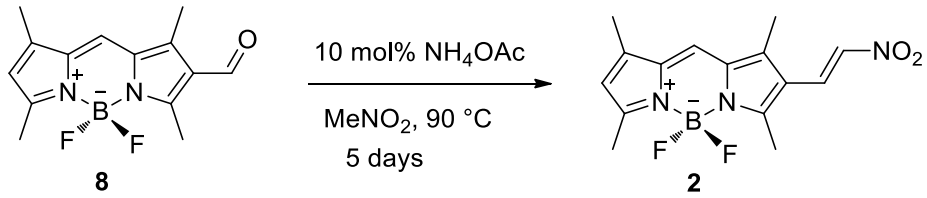
Two nitroethenyl-BODIPY derivatives (**1** and **7**) operating at different wavelengths were designed, synthesized and evaluated for biological thiol (Cys, Hcy and GSH) sensing in aqueous solutions. Both probes showed very fast and sensitive responses with color changes and "turn-on" fluorescence. We are confident that an understanding of BODIPY photophysics in relation to PeT efficiency and Internal Charge Transfer, would produce newer and more capable sensors for analytes of interest. Compounds **1** and **7** are two examples along that promising road.

6.5. Experimental Details

General: ^{1}H NMR and ^{13}C NMR spectra were recorded on Bruker Spectrospin Avance DPX 400 spectrometer using $CDCl_3$ as the solvent. Chemical shifts values are reported in ppm from tetramethylsilane as internal standard. Spin multiplicities are reported as the following: s (singlet), d (doublet), m (multiplet). HRMS data were acquired on an Agilent Technologies 6530 Accurate-Mass Q-TOF LC/MS. UV-Vis Absorption spectra were taken on a Varian Cary-100 spectrophotometer.

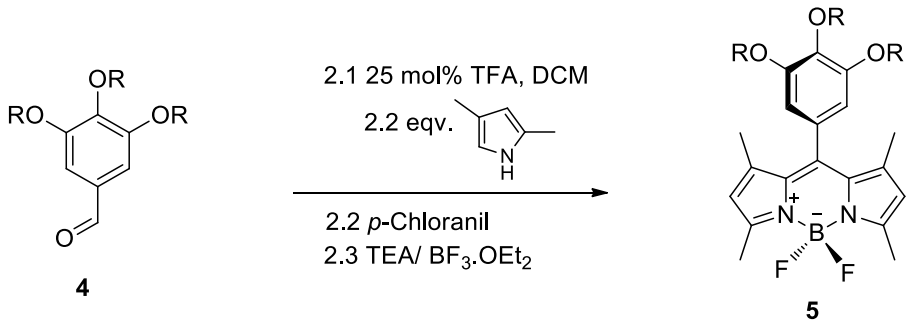
Fluorescence measurements were conducted on a Varian Eclipse spectrofluorometer. Flash column chromatography (FCC) was performed by using glass columns with a flash grade silica gel (Merck Silica Gel 60 (40–63 μm)). Reactions were monitored by thin layer chromatography (TLC) using precoated silica gel plates (Merck Silica Gel PF-254), visualized by UV-Vis light and DNP stains as appropriate. All organic extracts were dehydrated over anhydrous Na_2SO_4 and concentrated by using rotary evaporator before being subjected to FCC. 2-FormylBODIPY **8** was synthesized following reported literature procedure (see manuscript). All other chemicals and solvents were supplied from commercial sources and used as received.

Synthesis of Compound 2:



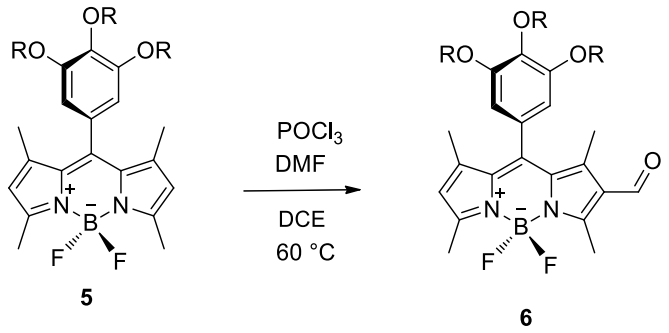
NH_4OAc (2.8 mg, 0.036 mmol) was added to a nitromethane (3,5 ml) solution of compound **8** (100 mg, 0.36 mmol) and the solution was left to stir at 90 ^oC for 5 days. Product formation was monitored with TLC using DCM as the eluent. At the end of reaction, nitromethane was removed in vacuo and obtained crude mixture was subjected to silica gel FCC using DCM as the eluent. Compound **2** was obtained as an orange crystalline solid (36 mg, 31.3% yield). ^1H NMR (400 MHz, $CDCl_3$) δ 8.065 (d, J = 13.68 Hz, 1H), 7.44 (d, J = 13.68 Hz, 1H), 7.19 (s, 1H), 6.22 (s, 1H), 2.66 (s, 3H), 2.60 (s, 3H), 2.39 (s, 3H), 2.31 (s, 3H). Due to the low solubility of the compound, ^{13}C-NMR spectrum could not be obtained. MS (TOF-ESI): m/z: Calcd: 318.1304 $[M-H]^-$, Found: 317.1277 $[M-H]^-$, Δ= 3.09 ppm.

Synthesis of Compound 5:



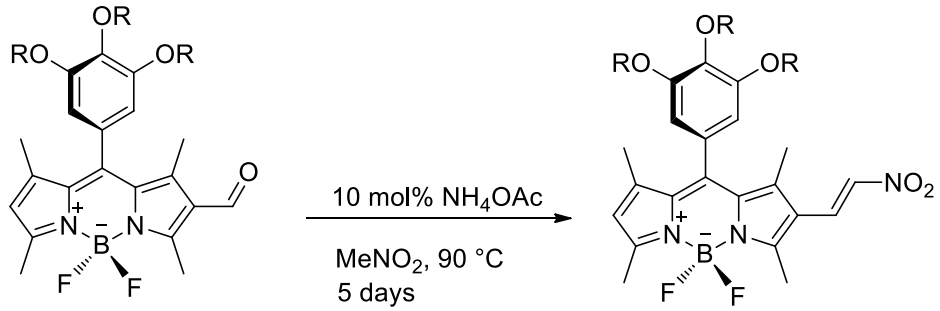
Trifluoroacetic acid (TFA; 1 drop) was added dropwise to a vigorously stirring solution of 3,4,5-tris(2-(2-(2-methoxyethoxy)ethoxy)benzaldehyde (1000 mg, 1.7 mmol) and 2,4-dimethylpyrrole (352 mg, 3.7 mmol) in 350 ml Ar-deaerrated dichloromethane (DCM). The resulting red solution was stirred at room temperature in the dark for 1 day. *p*-Chloranil (415 mg, 1.7 mmol) was then added in one portion and reaction was stirred for an additional hour. Triethylamine (TEA) (5.0 ml) was then added dropwise to this mixture over a period of 15 min, and the resulting dark brown solution was allowed to stir for an additional 15 min. BF_3•OEt_2 (5.0 ml) was then added dropwise over a period of 15 min. and the resulting dark red solution was allowed to stir further for 2h at rt. The slurry reaction mixture was washed with water (3 × 300 ml) and dried over anhydrous Na_2SO_4. The solvent was evaporated and the residue was purified by silica gel flash column chromatography (FCC) using DCM:MeOH (95:5) as the eluent. Standing on air, compound **5** was solidified as a dark orange solid (780 mg, 56% yield). ^{1}H NMR (400 MHz, $CDCl_3$) δ 6.55 (2, 2H), 5.99 (s, 2H), 4.22 (t, J= 4.97 Hz, 2H), 4.12 (t, J= 4.72 Hz, 4H), 3.84 (t, J= 5.29 Hz, 6H), 3.51-3.76 (m, 25H), 3.38 (s, 2H), 3.36 (s, 6H), 2.54 (s, 6H), 1.52 (s, 6H). ^{13}C NMR (100 MHz, $CDCl_3$) δ 155.8, 153.7, 142.9, 141.1, 139.0, 131.1, 129.9, 121.1, 107.7, 2.7, 71.9, 71.9, 70.8, 70.7, 70.6, 70.5, 69.7, 69.2, 58.8, 29.6 14.4, 14.2. MS (TOF-ESI): m/z: Calcd: 809.4286 $[M-H]^-$, Found: 808.4299 $[M-H]^-$, Δ= 6.16 ppm.

Synthesis of Compound 6:



$POCl_3$ (1 ml) was added dropwise to a vigorously stirring anhydrous DMF (1 ml) which was kept in ice bath under N_2. Resulting pale yellow viscous liquid was allowed to stir at room temperature for additional 30 min. To this, 1,2-dichloroethane (DCE) (50 ml) solution of compound **5** (810.43 mg, 1.0 mmol) was then slowly introduced and the resultant brown solution was heated at 60 °C for 3 h. (Attention!: 60 °C is critical to get mono-formylated product **6** as the major, side product formation was observed otherwise at higher temperatures.) Reaction was cooled to room temperature, and poured into ice-cold saturated $NaHCO_3$ solution. This mixture was extracted twice with DCM (100 ml portions) and dried over anhydrous Na_2SO_4. Solvent was evaporated in vacuo and compound was purified by silica gel FCC using 98:2 / DCM: MeOH as the eluent to obtain target compound **6** as orange crystalls (769mg, 91.7% yield). ^{1}H NMR (400 MHz, $CDCl_3$) δ 9.98 (s,1H), 6.53 (s, 2H), 6.15 (s, 1H), 4.23 (d, J= 4.34 Hz, 2H), 4.12 (d, J= 4.29 Hz, 4H), 3.83 (d, J= 4.81 Hz, 6H), 3.75-3.49 (m, 25H), 3.37 (s, 2H), 3.34 (s, 6H), 2.80 (s, 3H), 2.59 (s, 3H), 1.78 (s, 3H), 1.57 (s, 3H). ^{13}C NMR (100 MHz, $CDCl_3$) δ 185.8, 161.6, 156.4, 154.0, 147.1, 143.0, 142.6, 139.5, 133.9, 129.6, 128.8, 126.2, 123.9, 107.0, 72.7, 71.9, 71.8, 70.8, 70.6, 70.6, 70.5, 70.5, 69.6, 69.3, 58.9, 14.7, 11.5. MS (TOF-ESI): m/z: Calcd: 837.4235 $[M-H]^-$, Found: 836.4186 $[M-H]^-$, Δ= 1.47 ppm.

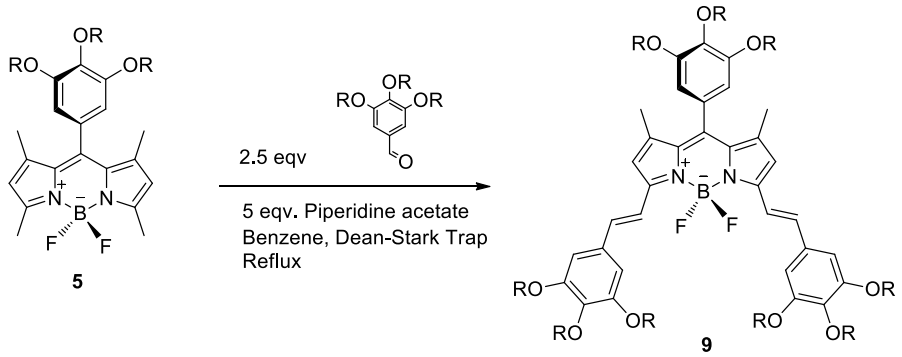
Synthesis of Compound 1:



6 **1**

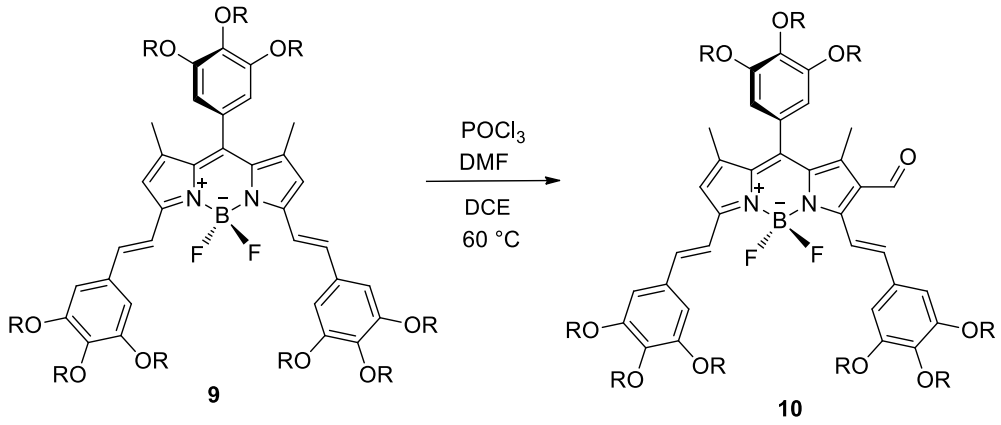
NH_4OAc (1.3 mg, 0.017 mmol) was added to a nitromethane (2 ml) solution of compound **6** (139 mg, 0.17 mmol) and the solution was left to stir at 90 ^oC for 5 days. Product formation was monitored with TLC using DCM: MeOH (98:2) as the eluant. At the end of reaction, nitromethane was removed in vacuo and obtained crude mixture was subjected to silica gel FCC using DCM: MeOH (98:2) as the eluent. Compound **1** was obtained as a wine-red waxy solid (40 mg, 27% yield). ^1H NMR (400 MHz, $CDCl_3$) δ 8.05 (d, J= 13.8 Hz, 1H), 7.37 (d, J= 13.63 Hz, 1H9, 6.56 (s, 2H), 6.18 (s, 1H), 4.26 (t, J= 4.64 Hz, 2H), 4.14 (t, J= 4.52 Hz, 4H), 3.86 (t, J=5.15Hz, 6H), 3.52- 3.76 (m, 25H), 3.40 (s, 2H), 3.37 (s, 6H), 2.72 (s, 3H), 2.63 (s, 3H), 1.64 (s, 3H), 1.59 (s, 3H). ^{13}C NMR (100 MHz, $CDCl_3$) δ 161.5, 154.2, 154.0, 147.1, 147.2, 140.1, 139.6, 134.6, 133.7, 130.7, 130.6, 128.8, 123.9, 120.0, 107.4, 72.8,71.9, 71.9, 70.8, 70.7, 70.7, 70.6, 70.6, 69.7, 69.3, 65.3, 59.0, 29.6, 14.7, 12.8,11.0. MS (TOF-ESI): m/z: Calcd: 880.7612 $[M-H]^-$, Found: 879.4238 $[M-H]^-$, Δ= 2.09 ppm.

Synthesis of Compound 9:



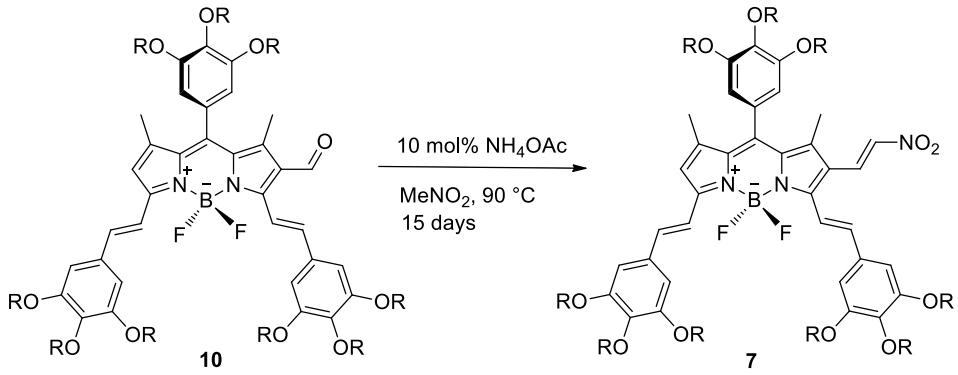
3,4,5-tris(2-(2-(2-methoxyethoxy)ethoxy)benzaldehyde (365 mg, 0.62 mmol) was added to a solution of 25 ml of compound **5** (200mg, 0.247mmol) in benzene containing piperidine acetate (179mg, 1.23mmol). Mixture was refluxed until all the starting material consumed and the product formation was monitored by TLC using DCM: MeOH (95:5) as the eluent. At the end of the reaction, obtained crude mixture was subjected to silica gel FCC using DCM: MeOH (95:5) as the eluent. Compound **9** was obtained as a dark-blue waxy solid (200mg, 41.4% yield). ^{1}H NMR (400 MHz, $CDCl_3$) δ 7.53 (d, J=16.04 Hz, 2H), 7.17 (d, J=15.91 Hz, 2H), 6.85 (s, 4H), 6.64 (s, 2H), 6.61 (s, 2H), 4.21-4.27 (m, 14H), 4.13-4.17 (m, 5H), 3.86-3.90 (m, 13H), 3.82-3.84 (m, 5H), 3.73-3.78 (m, 19H), 3.63-3.71 (m, 39H), 3.53-3.60 (m, 19H), 3.41 (s, 2H), 3.40 (s, 5H), 3.38 (s, 15H), 1.60 (s, 6H). ^{13}C NMR (100 MHz, $CDCl_3$) δ 153.6, 152.8, 152.6, 141.8, 139.9, 139.1, 138.2, 136.3, 133.2, 132.0, 129.9, 118.4, 117.8, 108.1, 107.6, 72.7, 72.4, 71.9, 71.8, 70.8, 70.8, 70.6, 70.6, 70.6, 70.5, 70.5, 69.7, 69.2, 69.1, 58.9, 58.9, 14.5. MS (TOF-ESI): m/z: Calcd: 1958.0264 $[M-H]^-$, Found: 1956.9858 $[M-H]^-$, Δ= 18.91 ppm.

Synthesis of Compound 10:



$POCl_3$ (0.1 ml) was added dropwise to a vigorously stirring anhydrous DMF (0.1 ml) which was kept in ice bath under N_2. Resulting pale yellow viscous liquid was allowed to stir at room temperature for additional 30 min. To this, 1,2-dichloroethane (DCE) (50 ml) solution of compound **9** (200 mg,0.102mmol) was then slowly introduced and the resultant brown solution was heated at 60 °C for 3 h. (Attention!: 60 °C is critical to get mono-formylated product **10** as the major, side product formation was observed otherwise at higher temperatures.) Reaction was cooled to room temperature, and poured into ice-cold saturated $NaHCO_3$ solution. This mixture was extracted twice with DCM (100 ml portions) and dried over anhydrous Na_2SO_4. Solvent was evaporated in vacuo and compound was purified by silica gel FCC using 95:5 / DCM: MeOH as the eluent. Product **10** was obtained as dark blue oily compound (178 mg, 87.7% yield). ^{1}H NMR (400 MHz, $CDCl_3$) δ 10.05 (s, 1H), 7.52 (dd, *J*= 16.28 Hz, 2H), 7.31 (d, *J*=17.93 Hz, 1H), 7.03 (d, *J*=16.16 Hz, 1H), 6.90 (d, *J*= 4.65 Hz, 4H), 6.77 (s, 1H), 6.59 (s, 2H), 4.13-4.27 (m, 19H), 3.81-3.89 (m, 18H), 3.70-3.75 (m, 18H), 3.61-3.69 (m, 37H), 3.51-3.57 (m, 19H), 3.35-3.39 (m, 24H), 1.85 (s, 3H), 1.64 (s, 3H). ^{13}C NMR (100 MHz, $CDCl_3$) δ 187.1, 157.1, 153.9, 153.4, 152.9, 152.8, 146.1, 141.4, 141.2, 141.0, 140.5, 140.3, 139.9, 139.5, 136.1, 131.7, 131.18, 131.10, 129.1, 126.9, 120.4, 117.5, 116.5, 108.2, 107.8, 107.5, 72.7, 72.5, 72.4, 71.9, 71.9, 70.8, 70.8, 70.8, 70.7, 70.6, 70.6, 70.5, 70.5, 69.7, 69.3, 69.2, 69.0, 59.0, 59.0, 58.9, 15.0, 12.3. MS (TOF-ESI): m/z: Calcd: 1986.0213 $[M-H]^-$, Found: 1984.9894 $[M-H]^-$, Δ= 14.25 ppm.

Synthesis of Compound 7:



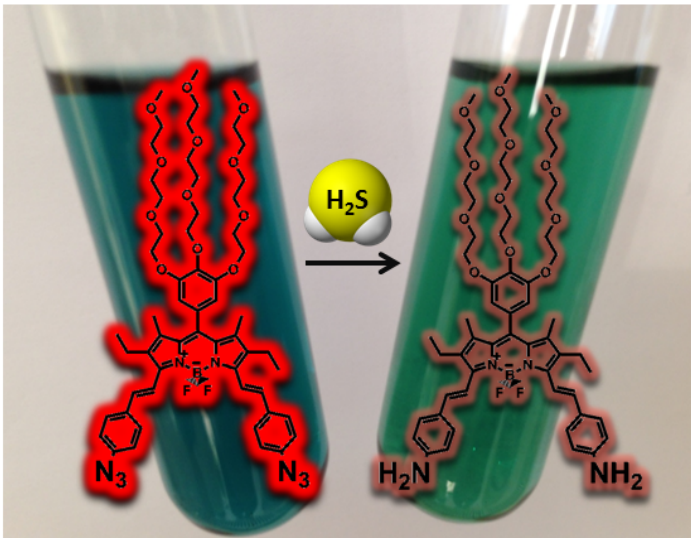
NH_4OAc (0.05 mg, 0.0065 mmol) was added to a nitromethane (1 ml) solution of compound **10** (130 mg, 0.065 mmol) and the solution was left to stir at 90 ^oC for 15 days. Product formation was monitored with TLC using DCM: MeOH (95:5) as the eluent. At the end of reaction, nitromethane was removed in vacuo and obtained crude mixture was subjected to silica gel FCC using DCM: MeOH (95:5) as the eluent. Compound **7** was obtained as a dark blue waxy solid (25 mg, 19% yield). ^1H NMR (400 MHz, $CDCl_3$) δ 8.16 (d, *J*=13.6 Hz, 1H), 7.51 (d, *J*=16.3 Hz, 2H), 7.38 (d, *J*=13.6 Hz, 1H), 7.32 (d, *J*=16.3 Hz, 2H), 6.87 (s, 2H), 6.85 (s, 2H), 6.78 (s, 1H), 6.61 (s,2H), 3.3-4.29 (m, 135H), 1.69 (s, 3H), 1.65 (s, 3H). MS (TOF-ESI): m/z: Calcd: 2028.0235 $[M-H]^-$, Found: 2028.0288 $[M-H]^-$, Δ=2.63 ppm.

CHAPTER 7

Fast Responding and Selective Near- IR BODIPY Dyes for Hydrogen Sulfide Sensing

This work is partially described in the following publication:

Ozdemir, T.; Sozmen, F.; Mamur, S.; Tekinay, T.; Akkaya, E.U. *Chem. Commun.*, **2014**, *50*, 5455-5457.



7.1. Objective

A BODIPY based, highly selective probe for hydrogen sulfide has been designed, synthesized and demonstrated to detect H_2S in living cells. In this design, the reduction of two arylazido groups change the charge transfer characteristics of the 3,5-distyryl substituents on the BODIPY core, producing a 20 nm bathochromic spectral shift in the absorption band, and quenching of the emission by 85% compared to the original intensity, through photoinduced electron transfer.

7.2. Introduction

Hydrogen sulfide (H_2S) has a characteristic repulsive odor of rotten eggs, and plays crucial roles in biological processes; as a result, many groups worldwide are interested in potential agents that will allow its real-time monitoring.[5,166,202,203] Like the other two gaseous signaling molecules, carbon monoxide (CO)[204-206] and nitric oxide (NO),[207-209] hydrogen sulfide is a biosynthetic gasotransmitter. These small gaseous molecules are different from the other messenger molecules regarding their production and function. Furthermore, because of their small size and charge neutrality, they can easily pass through the cellular membranes without affecting any cell signaling response.[210] The important roles of H_2S in many metabolic processes, such as cardiovascular protection, neuroprotective effect, arrangement of cell growth, calcium homeostasis and regulation of neurotransmission are well established in the literature.[71,211-213]

H_2S is an example of reactive sulfur species such as, thiols, *S*-nitrosothiols, sulfenic acids and sulfite, produced enzymatically from cysteine with a series of reactions, mainly catalyzed by two pyridoxal 5′-phosphate-dependent enzymes, cystathionine β-synthase (CBS) and cystathionine γ-lyase (CSE) and independently from pyridoxal 5′-phosphate by another enzyme, 3-mercaptopyruvate sulfur transferase (3MST).[214-216] Also elemental sulfur is another endogenous H_2S source.[217,218]

Biological imaging probes working in the near-IR region have attracted considerable attention in recent years, since the light used for excitation causes much less

photodamage to cells compared to ultraviolet or visible light used in exciting other probes. In addition, with near IR probes, cell autofluorescence is not an issue. On the other hand, BODIPY dyes which are difluoroboron-chelated dipyrromethene derivatives seem to be very good choices for designing novel H_2S probes due to their desirable properties such as; high quantum yields, chemical and photochemical stability, high molar absorption coefficients, and the fact that they allow straightforward access to near-IR emitting derivatives.[41,43,184,219]

7.3. Results and Discussion

In this work, Knoevenagel type chemistry has been used to obtain a near-IR emissive BODIPY derivative **1** with extended conjugation (Figure 96). Initially, we synthesized BODIPY **5** having three triethyleneglycol groups. To that end, compound **3** and **4** were prepared according to literature reports. Then, BODIPY **5** was constructed by the reaction of the aldehyde **4** and 3-ethyl-2,4-dimethylpyrrole. Finally, following recently established protocols,[220] condensation reaction of *p*-azidobenzaldehyde **3** yielded the probe **1** (Φ_f= 0.38, cresyl violet in ethanol as a reference dye) in analytically pure state following chromatographic purifications. This reaction allowed not only the formation of target probe in good yields, but also emission and absorption wavelengths of the probe were shifted to near-IR.

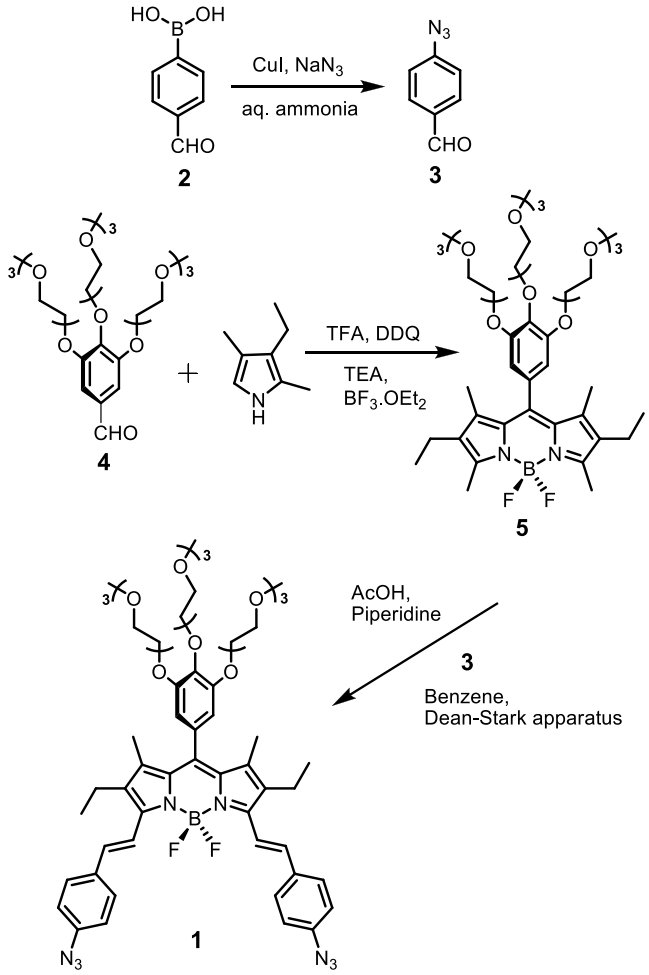


Figure 96. Synthesis of target probe **1** (Copyright © 2014, Royal Society of Chemistry, Reprinted with permission from ref (220)).[220]

H_2S probes functioning through the reduction of azido group to amines are available in the literature.[78,221-223] However, most of them do not respond fast enough. On the other hand, the probe proposed in this study (compound **1**) responds to H_2S with no time delay, practically immediately as the reagents are mixed.

Upon titration of probe **1** with various concentrations of Na_2S at room temperature in acetonitrile-buffer mixture (20 mM HEPES/CH_3CN, 40:60, v/v, pH=7.20, 25 °C), the red shift about 20 nm was observed in the electronic absorption spectrum (Figure 97a), the color change was easily noticeable with naked eye. The actual ratio of S^{2-}/HS^-/H_2S concentrations (speciation) is dictated by the pH of the buffer.

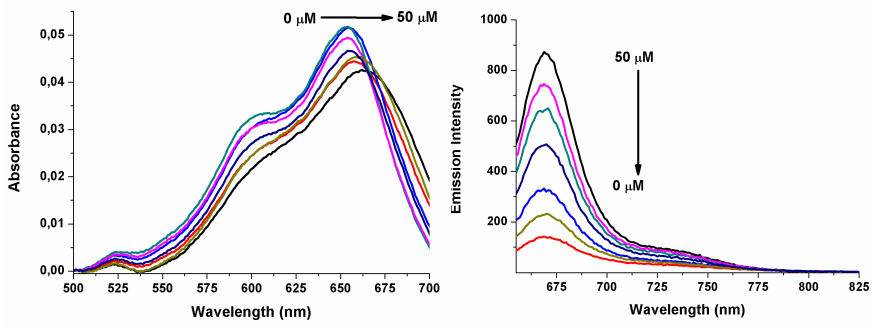


Figure 97. Absorption and emission spectra of **1** (2.0 μM) in 20 mM HEPES:CH_3CN (40:60, v/v, pH=7.20, 25 °C) in increasing Na_2S concentrations. Excitation wavelength is 650 nm. Experiments were done in triplicate (Copyright © 2014, Royal Society of Chemistry, Reprinted with permission from ref (220)).

As shown in the fluorescence spectra (Figure 97b), the emission of probe **1** was quenched with increased Na_2S concentrations at room temperature in 20 mM HEPES/CH_3CN solutions (40:60, v/v, pH=7.20, 25 °C). The detection limit was determined (ESI) to be 0.34 μM.

The reduction of azido to amine group provides an alternative excited state process (photoinduced electron transfer, PeT) which is responsible for quenching the of fluorescence emission.

Selectivity of the probe **1** for sulfide species was also investigated. To that end, fluorescence and electronic absorption spectral data were collected with other reactive sulfur species (RSS), reactive oxygen species (ROS) and reactive nitrogen species (RNS). Emission data provides clear evidence that the probe **1** offers very good selectivity for sulfide in (Figure 98a).

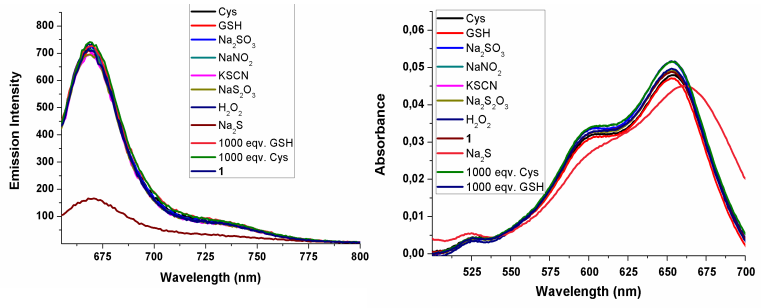


Figure 98. Absorption and emission spectra of probe 1 (2.0 μM) in 20 mM HEPES:CH_3CN (40:60, v/v, pH=7.20, 25 °C) in absence and presence of various anions. Added Na_2S concentration is 50 μM and anion concentrations were 100 μM. Excitation wavelength is 650 nm. Experiments were done in triplicate (Copyright © 2014, Royal Society of Chemistry, Reprinted with permission from ref (220)).

No other species were able to reduce the two azido groups to amine groups, so not change in fluorescence emission was observed. ComPeTition experiments in the presence of a number of comPeTing anions were also done (Figure 99), again corroborating the selectivity of the probe. The electronic absorption spectra were unchanged as well. We also note that, 1000 equivalents of glutathione or cysteine do not cause any changes in the emission intensity or absorbance spectrum of the probe **1** (Figure 98).

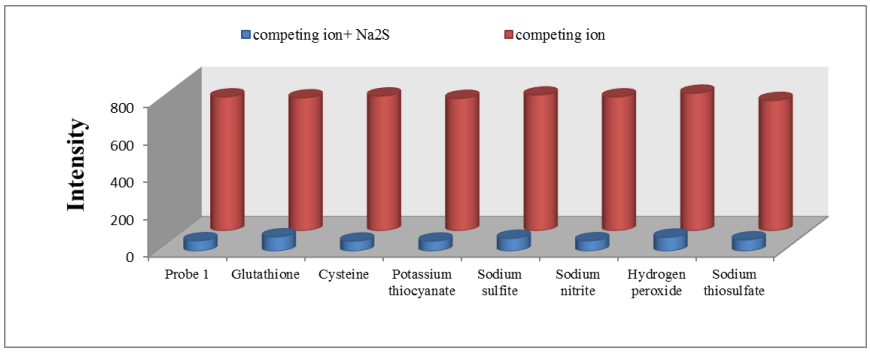


Figure 99. Emission intensity response of probe 1 (2.0 μM) with 50 equiv. of a comPeTing anions followed by addition of 50 equiv. Na_2S in 20 mM HEPES:CH_3CN (40:60, v/v, pH=7.20, 25 °C). Excitation wavelength was 650 nm with a slit width of 5-5 nm (Copyright © 2014, Royal Society of Chemistry, Reprinted with permission from ref (220)).

An NMR titration experiment was performed in order to investigate the changes in the chemical shifts of the aromatic protons during the reduction. Figure 100 shows the partial ^1H NMR spectra of the probe before (Figure 100a) and after (Figure 100b) Na_2S addition in CD_3CN. The NMR spectrum clearly shows that, all the aromatic protons of probe **1** were shifted upfield due to the formation of electron donor amine group as expected.

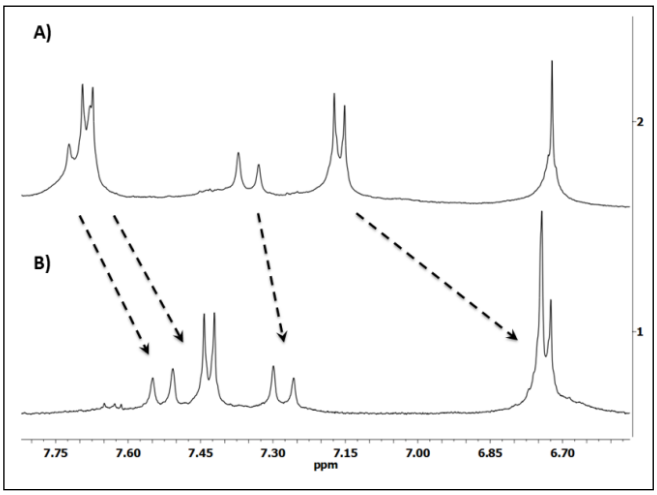


Figure 100. Stacked partial ^{1}H-NMR spectra probe **1** (A) and the same spectrum after the addition of Na_2S (B) in acetonitrile-D_3 at 25 ^{o}C (Copyright © 2014, Royal Society of Chemistry, Reprinted with permission from ref (220)).

In addition, mass spectral (Figure 101) data following sulfide treatment of the probe **1**, supports our structure assignment for the reduction product).

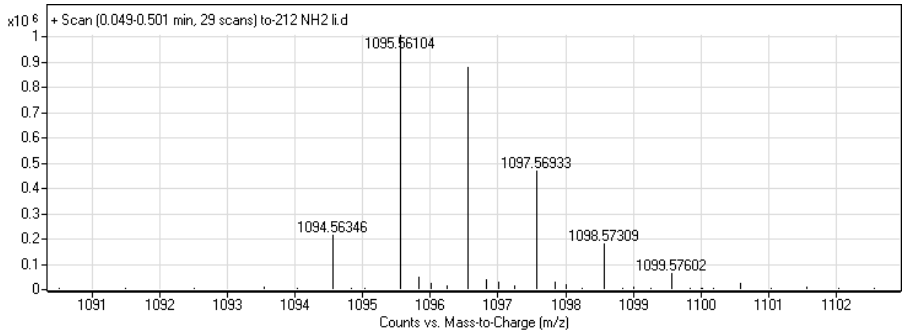


Figure 101. Mass spectrum of Compound **1** after addition the addition of Na_2S (Calcd: 1094.568 $[M+Na]^+$, Found:1094.563 $[M+Na]^+$, Δ=4.52 ppm.) (Copyright © 2014, Royal Society of Chemistry, Reprinted with permission from ref (220)).

We also wanted to demonstrate the utility of the probe **1** in living cells (Figure 102). Human breast adenocarcinoma cells (MCF-7) were grown to confluence at 37°C under 5% CO_2 in Dulbecco's Modified Eagle Serum (DMEM) containing 1% penicillin/streptomycin, 10% fetal bovine serum (FBS) and 2 mM L-glutamine. MCF-7 cells were incubated with 4.0 μM probe **1** for 30 min. at 37 ^{o}C and then washed with physiological saline to remove any excess amount of the probe. Under these conditions, confocal microscope image shows intense intracellular red fluorescence emission upon excitation at 633 nm. The cells which were treated with

probe **1**, were then incubated with 400 μM Na_2S in HEPES buffer for 2 hours at 37 ^oC. Under microscope, the quenching of intracellular fluorescence intensity of the probe **1** was clearly visible for the sulfide treated cells. Again, as noted for the spectroscopic experiments, the quenching seems to be only limited by the duration of incubation, the reaction seems to be very fast. Confocal microscope imaging was performed with a Leica TCS SP2 laser scanning microscope with an oil-immersion 40x objective lens.

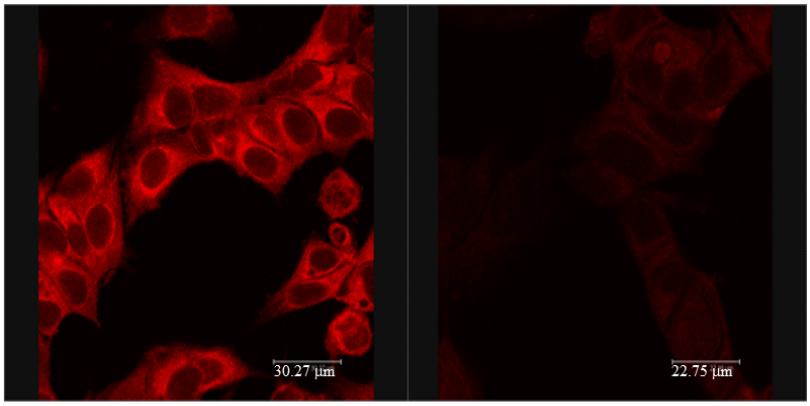


Figure 102. Confocal microscopy images of showing the H_2S response of probe **1** in MCF-7 cells. (Left) MCF-7 cells incubated with probe **1** (4 μM) for 30 min. at 37 ^oC (Right) MCF-7 cells incubated with probe **1** (4 μM) for 2 h, after which 100 eqv. Na_2S was added. The cells were imaged after additional incubation for 30 min. at 37 ^oC (Copyright © 2014, Royal Society of Chemistry, Reprinted with permission from ref (220)).

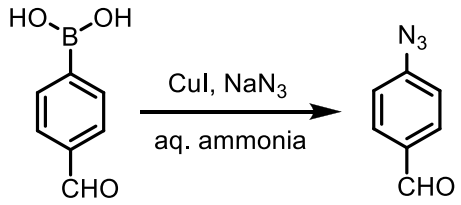
7.4. Conclusion

We developed a sensitive H_2S detection probe which is operating much faster compared to existing H_2S probes. Azide based probe **1** gives response the H_2S through reduction of two azido groups, resulting instant quenching of the emission and noticeable red shift in absorbance. The highly selective and sensitive nature of the probe **1** for H_2S over other reactive species demonstrates the potential utility of the probe **1**. Moreover, due to the presence of hydrophilic moieties in its structure, the probe is water soluble and thus appropriate for biological applications. Thus, added H_2S was successfully imaged inside the cells, suggesting a possibility of imaging endogenously produced H_2S in real-time and in the near IR region of the spectrum.

7.5. Experimental Details

General: ^{1}H NMR and ^{13}C NMR spectra were recorded on Bruker DPX-400 (operating at 400 MHz for ^{1}H NMR and 100 MHz for ^{13}C NMR) in $CDCl_3$ with tetramethylsilane as internal standard. All spectra were recorded at $25^{0}C$ and coupling constants (*J* values) are given in Hz. Chemical shifts are given in parts per million (ppm). Absorption spectra were performed by using a Varian Cary-100 spectrophotometer. Fluorescence measurements were conducted on a Varian Eclipse spectrofluorometer. Mass spectra were recorded on Agilent Technologies 6530 Accurate-Mass Q-TOF LC/MS. Reactions were monitored by thin layer chromatography using Merck TLC Silica gel 60 F254. Silica gel column chromatography was performed over Merck Silica gel 60 (particle size: 0.040-0.063 mm, 230-400 mesh ASTM). Compound **4** was synthesized according to literature.[13] All other reagents and solvents were purchased from Aldrich and used without further purification.

Synthesis of Compound 3:

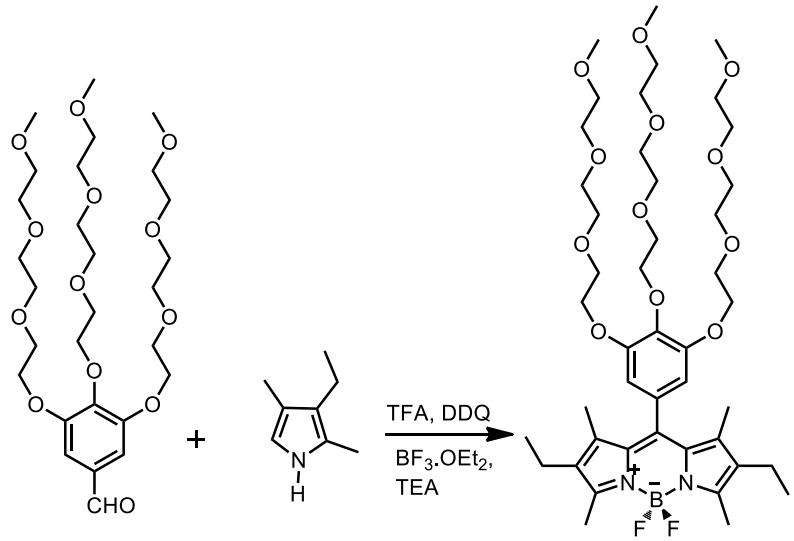


2 **3**

Compound **3** was synthesized according to literature with slight modifications.[224] CuI (95 mg, 0.5 mmol), 25% aqueous ammonia (0.95 ml, 12.5 mmol of NH_3), and water (2.5 ml) were stirred in a round bottomed flask at room temperature. After 30 min., 4- formylphenylboronic acid (**2**) (745 mg, 5 mmol), NaN_3 (1,625 g, 25 mmol), and water (5.5 ml) were added to the reaction mixture. The solution was stirred for 24 h at room temperature in an open atmosphere to allow the air to get into the reaction medium. Aqueous NaOH (2N, 7.5 ml) was added and extraction was performed with ethylacetate three times. Organic phase was gathered, dried over Na_2SO_4 and evaporated in *vacuo*. Column chromatography was performed using with the eluent

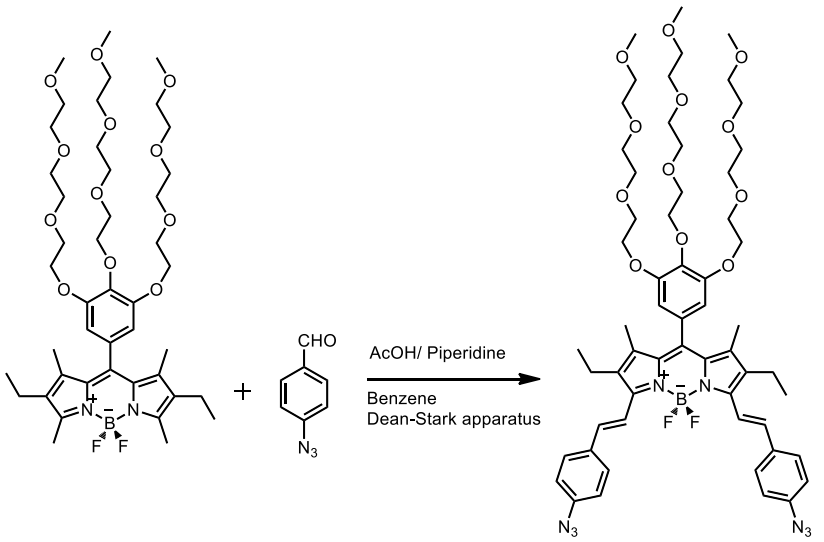
DCM: Hexane (1:1) to get the desired product. ^{1}H NMR (400 MHz, Chloroform-*d*) δ 9.92 (s, 1H), 7.86 (d, *J* = 8.5 Hz, 1H), 7.13 (d, *J* = 8.5 Hz, 1H). ^{13}C NMR (100 MHz, Chloroform-*d*) δ 190.56, 146.28, 133.26, 131.54, 119.49.

Synthesis of Compound 5:



Compound **4** (0.6 g, 1.01 mmol) was dissolved in 400 ml Ar-degassed DCM in a 1 L round bottom flask and 2,4-dimethyl-3-ethyl-pyrrole (0.3 ml, 2.22 mmol) was added. This was followed by the addition of 1-2 drops of TFA. The mixture was stirred about 3 hrs at room temperature. After TLC showed no starting material, p-chloroanil (297 mg, 1.21 mmol) was poured into the reaction vessel. After 1 hr stirring, 6 ml TEA was added dropwise to the solution over a period of 5 min. The color turned out to be brown and it was stirred for an additional 30 min. Lastly, 6 ml BF_3.OEt2 was added to the reaction in a dropwise manner over a period of 5 min, as well. The mixture was left to stir overnight at room temperature. Extraction was performed with water (3x300 ml) and the organic layer was dried over anhydrous Na_2SO_4. After concentrating the organic layer in *vacuo*, it was purified by flash column chromatography with the eluent 5% TEA: DCM. The product was obtained as red solid (367 mg, 42%). ^{1}H NMR (400 MHz, Chloroform-*d*) δ 6.56 (s, 2H), 4.24 (t, *J* = 5.0 Hz, 2H), 4.15 – 4.05 (m, 4H), 3.85 (t, *J* = 5.0 Hz, 4H), 3.79 – 3.48 (m, 26H), 3.40 (s, 3H), 3.37 (s, 6H), 2.54 (s, 6H), 2.31 (dd, *J* = 9.5, 5.2 Hz, 4H), 1.43 (s, 6H), 1.01 (t, *J* = 7.3 Hz, 6H).

Synthesis of Compound 1:



In a 100 ml round-bottomed flask containing 50 ml benzene, compound **5** (150 mg, 0.17 mmol) and 4-azidobenzaldehyde (56 mg, 0.38 mmol), piperidine (0.3 ml) and acetic acid (0.3 ml) were added. The mixture was heated under reflux by using a Dean Stark trap and progress of the reaction was monitored by TLC. When all the starting material had been consumed, the mixture was cooled to room temperature and solvent was evaporated. Water (100 ml) added to the residue and the product was extracted into the DCM (2 x 100 ml). Organic phase was dried over Na_2SO_4, evaporated and residue was purified by silica gel column chromatography using DCM as the eluent. (67 mg, 35%). ^{1}H NMR (400 MHz, Chloroform-*d*) δ 7.73 (d, *J* = 16.6 Hz, 2H), 7.62 (d, *J* = 8.6 Hz, 4H), 7.22 (d, *J* = 16.8 Hz, 2H), 7.07 (d, *J* = 8.5 Hz, 4H), 6.59 (s, 2H), 4.26 (dd, *J* = 5.8, 3.9 Hz, 2H), 4.15 (dd, *J* = 5.8, 3.8 Hz, 4H), 3.87 (t, *J* = 4.8 Hz, 4H), 3.80 – 3.44 (m, 26H), 3.40 (s, 3H), 3.36 (s, 6H), 2.67 – 2.59 (m, 4H),1.49 (s, 6H), 1.19 (t, *J* = 7.6 Hz, 6H). ^{13}C NMR (100 MHz, CDCl3) δ 153.90, 153.83, 140.01, 138.98, 134.66, 134.27, 133.98, 128.95, 128.77, 127.50, 124.19, 119.55, 119.39, 108.25, 72.77, 71.92, 70.88, 70.72, 70.66, 70.57, 69.76, 69.26, 58.99, 18.36, 14.02, 11.46, 1.00. Calcd: 1147.54 [M+Na]+ , Found: 1147.528 [M+Na]+, Δ=10.45 ppm.

NMR Data of Compound 1 after addition the addition of Na_2S:

^{1}H NMR (400 MHz, CD_3CN) δ 7.53 (d, *J* = 16.6 Hz, 2H), 7.43 (d, *J* = 8.5 Hz, 4H), 7.28 (d, *J* = 16.7 Hz, 2H), 6.73 (d, *J* = 7.5 Hz, 6H), 4.56 (d, *J* = 9.1 Hz, 2H), 4.25 – 4.20 (m, 4H), 4.19 – 4.11 (m, 4H), 3.87 – 3.43 (m, 26H), 3.34 (s, 3H), 3.31 (s, 6H), 2.69 (m, 4H), 1.54 (s, 6H), 1.18 (t, *J* = 7.4 Hz, 6H).

UV-Vis Titration Experiments:

Titrations of probe **1** with Na_2S: 60 μL portions of 100 μM stock solution of probe **1** in acetonitrile were added aliquots of 20 mM Na_2S solutions (in 20 mM HEPES, pH=7.20, 25 °C), (30, 15, 7.5, 3, 1.5, 0.75 μL). Volumes of these solutions were adjusted to 3 ml (HEPES: CH_3CN, 40:60, v/v). UV-vis absorption spectra were recorded at room temperature.

Detection Limit:

Fluorescence titrations were employed to determine detection limit of probe **1**. According to reported method,[225,226] by measuring of emission intensity of probe **1** in absence of Na_2S by 7 times, standard deviation of blank measurements were recorded. A linear relationship between the fluorescence intensity and Na_2S concentration was acquired and according to equation,

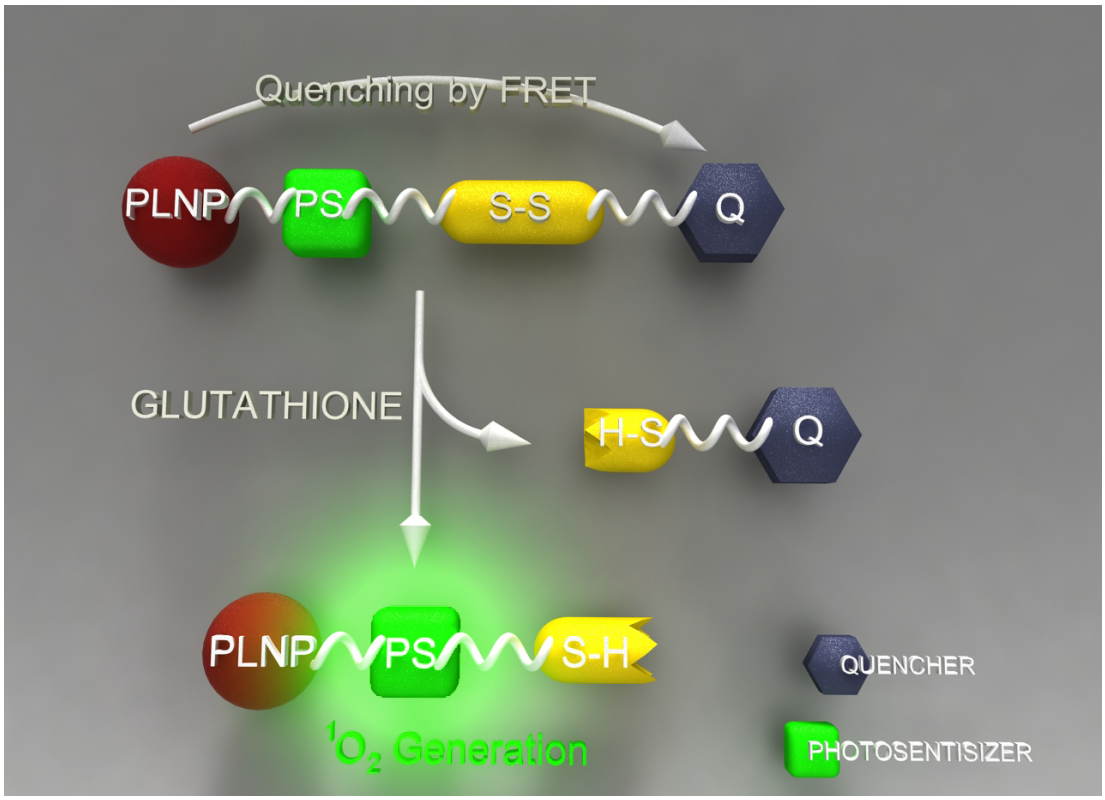
$$\text{detection limit} = 3s/m,$$

where *s* is the standard deviation of 7 blank measures, *m* is the slope of emission intensity versus Na_2S concentration graph. This calculation gives the detection limit of probe **1** as 0.34 μM.

CHAPTER 8

Persistent Luminescent Nanoparticles (PLNP) Mediated Activation of Photosensitizers for Photodynamic Therapy

Ozdemir, T.; Kolemen, S.; Tanriverdi- Ecik, E.; Yan, X.-P.; Akkaya, E. U., *in preparation*



8.1. Objective

PLNP-BODIPY nanoconstruct is designed to be activated in cancer cells and generated singlet oxygen and being a selective agent, it is predicted to destroy tumors the way PDT does, but without any need for external excitation. This project holds great potential to offer a solution to one of the most critical obstacle for the prevalent application of photodynamic therapy.

8.2. Introduction

Photodynamic therapy is based on the activation of a nontoxic photosensitizer by an appropriate light source in the presence of molecular oxygen. In other words, there are three main components of photodynamic therapy: photosensitizer, light, and O_2. The combination of these components generates the cytotoxic reactive oxygen species. One of the important points that should be addressed is the selectivity of the photosensitizers. The selective accumulation of photosensitizers can be achieved with several approaches including bioconjugation of tumor-specific agents like monoclonal antibodies, epidermal growth factors and encapsulation in nanocarriers such as silica-based nanoparticles.[227-229] In this respect, up-to-date approach is the "smart" photosensitizing agents.[114] These agents offer the selective activation through the tumor-specific parameters. In this approach, photosensitizer can be designed to be self-quenched via aggregation or its activity is reduced with the quenchers. The activation process is triggered due to the acidic or reducing characteristics of tumor's medium, thus, disaggregation or separation of quenchers take place and photodynamic action is achieved.[122] With this approach, specific activation of photosensitizers brings important advantages compared to non-specific phototoxicity. Another important parameter that affects the efficacy of photodynamic action is the light. Light used in photodynamic therapy should be in the visible region, practically 600-900 nm to be able to pass deeply in the tissue, to prevent self-absorption of tissues and to lower the light scattering.[230] However, the penetration of light through mammalian tissue reaches only a few millimeters.[231] Thus, to eliminate this problem, we aimed to incorporate persistent luminescent nanoparticles (PLNP). Persistent Luminescent Nanoparticles (PLNP) is a comparatively new technology to

construct long lasting luminescent nanoparticles which emits in the red to near-infrared range. These type of materials can emit in visible region for hours after the irradiation source has been switched off.[123] Visible light or UV can be used to irradiate the material. The storage of the excitation energy by traps and its slow release via thermal energy is the reason of the long decay time. This new technology can permit optical excitation before *in vivo* local or systemic injection.[131] Also, its luminescence can last several hours and helps the reduction of autofluorescence.[232] Therefore, the significant signal-to-noise ratio improvement allows detection in rather deep organs. Activation of PLNP-photosensitizer conjugate will be achieved by high glutathione concentration present in cancer cells. Glutathione is a thiol containing tripeptide and its concentration in tumor cells is higher up to 1000-fold. In tumor cells, the irregular blood flow causes hypoxic state, decreased oxygen level and so the activity of reductive enzymes increases (high glutathione concentrations).[118] In previous studies, it was well-stated that GSH is elevated in breast cancer,[119] colon cancer,[120] *etc.* In the presence of high intracellular concentration of glutathione, disulfide bonds are broken. On the other hand, disulfide bonds are thermodynamically stable and provide reasonably good stability in the bloodstream in the absence of sulfhydryl groups.

In this design, functionalized PLNP is attached to photosensitizer which is di-styryl BODIPY unit having two iodine atoms in its 2 and 6 positions to enhance the intersystem crossing (heavy-atom effect) for effective singlet oxygen generation.

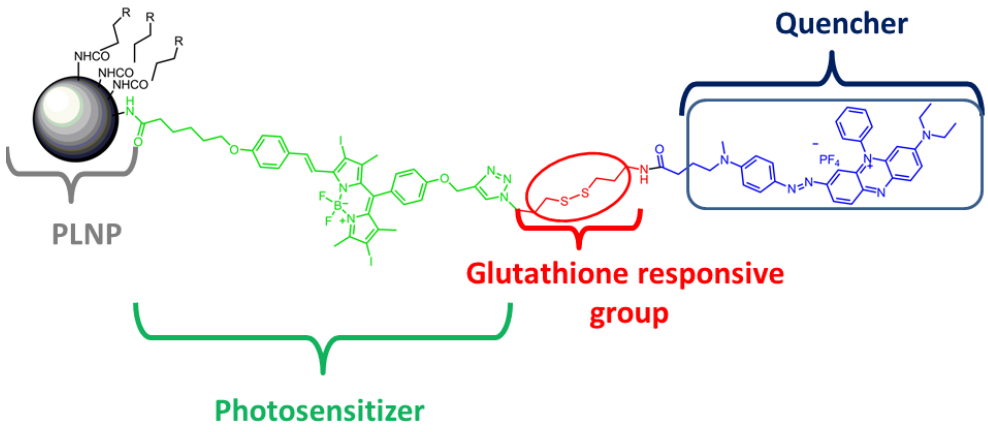


Figure 103. The chemical structure and the functions of the groups attached.

In the absence of glutathione, energy transfer process from PLNP to quencher part suppresses the activation of photosensitizer-BODIPY. It is known from studies in our laboratory that the energy transfer process is more feasible than passing through triplet state.[233] Therefore, singlet oxygen will not be produced. The singlet oxygen will be produced only if there is higher concentration of glutathione. In this case, disulfide linker is expected to be cleaved and detachment from the quencher will facilitate the irradiation of BODIPY so singlet oxygen will be generated (Figure 104).

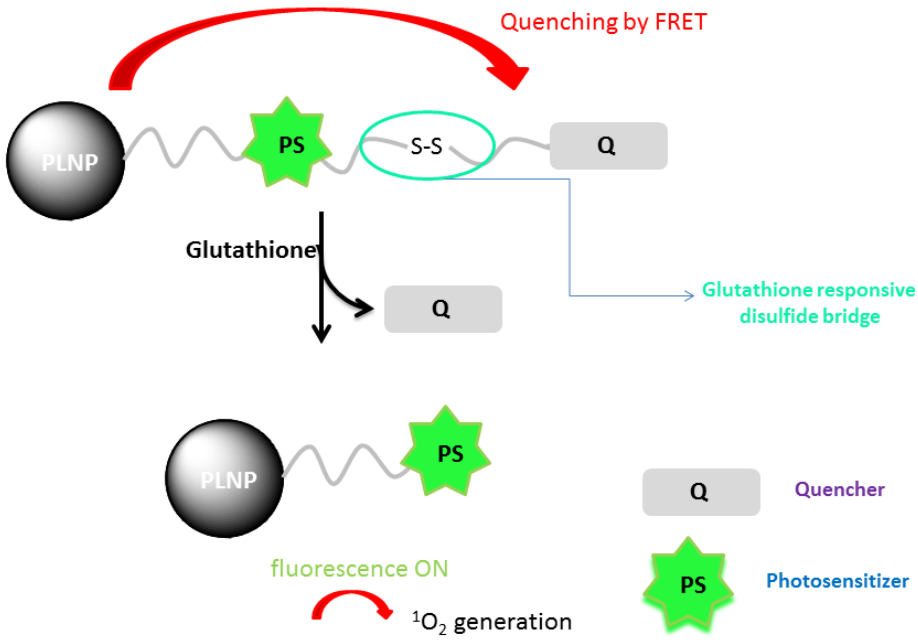


Figure 104. The working principle of the target.

8.3. Results and Discussion

In our first design, we thought to use $Ca_{0.2}Zn_{0.9}Mg_{0.9}Si_2O_6$ doped with Eu^{2+}, Dy^{3+}, Mn^{2+}, because afterglow emission maximum is at 690 nm and its persistent luminescence can longer more than 24 hour when kept in dark.[131] Addition of small amount of Dy^{3+}constitutes trap centers and Mn^{2+} is the ultimate emitting core getting energy from electron-hole pair recombination. It is proposed that the red and the near-IR emission is the result of the symmetry and the crystal field strength at the Mn^{2+} site. Also, rare-earth ions behave like primary acceptors of the energy that can

be given off thermally to Mn^{2+} for several hours. Long lasting afterglow emission is because of the persistence energy transfer from the rare earth ions. In summary, Eu^{2+} is used to generate electron trapped centers, Dy^{3+} is to form hole-trapped centers[15] and Mn^{2+} receives energy from the excitation of the electron-hole pairs.

The persistent luminescent nanoparticles were obtained by using sol-gel approach to get small particles as given below (Figure 105).[14]

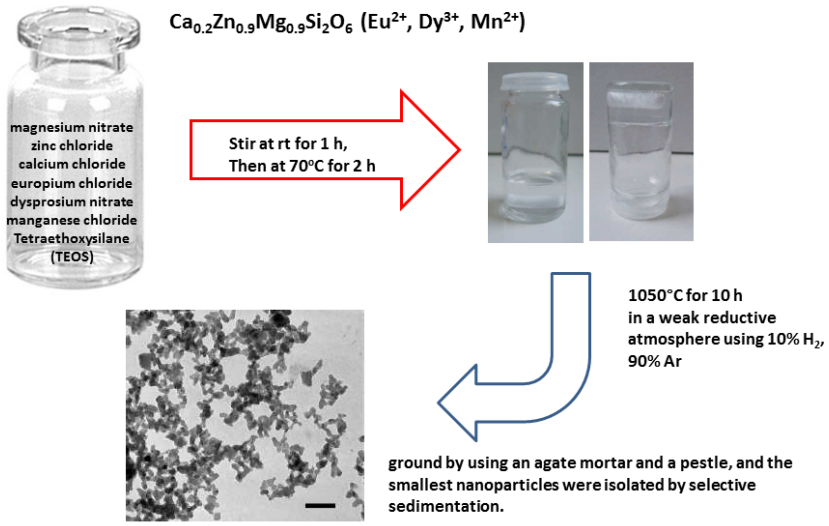


Figure 105. The synthetic route of the PLNP.

To be able to have small sized nanoparticles, sol-gel approach was performed since solid-state reaction gives micrometer sized particles. Adequate amounts of magnesium nitrate ($Mg(NO_3)_2.6H_2O$), zinc chloride ($ZnCl_2$), calcium chloride ($CaCl_2.2H_2O$), europium chloride ($EuCl_3$, $6H_2O$), dysprosium nitrate ($Dy(NO_3)_3$, $5H_2O$), manganese chloride ($MnCl_2$, $4H_2O$), tetraethoxysilane (TEOS) 4 ml of deionized water at pH 2 were stirred at room temperature for 1 hour. To see the sol-gel transition, reaction mixture was kept at 70 °C for additional 2 hours. To get rid of water and ethanol, the gel was dried in an oven at 110 °C.

By using quartz combustion boat, the opaque dry gel was warmed to 1050 °C in a weak reductive atmosphere using 5% H_2, 95% Ar for 10 h and then cool to room temperature. At the end of this procedure, white powder was obtained.

To acquire small particles, with the help of an agate mortar and a pestle, the powder was ground. Selective sedimentation was performed to isolate small particles. 5 mM NaOH solution at a concentration of 10 mg of PLNP per ml was used to disperse the powder by sonication. Distilled water at a concentration of 2.5 mg/ml was added to dilute the suspension. To eliminate the larger particles, centrifugation was done. To increase the isolation of small particles, acetone corresponding to 25% of the supernatant volume was added. Then, centrifugation process was appled one more time. With the removal of supernatant, the PLNP was hold in a vacuum oven to dry the particles.

To measure the size of the nanoparticles, dynamic light scattering was performed. This technique offers diffusion coefficient of small particles in a liquid and the light scattering intensity of the particles as a function of time gives this coefficient. According to DLS results seen in Figure 106, synthesized nanoparticles are in the range of 100 nm. The second and third runs show that small nanoparticles come together and size increases with time because of aggregation. Additionally, since surface has free hydroxyl groups, Zeta potential measurements showed that NPs have negative surface electric potential (Figure 106).

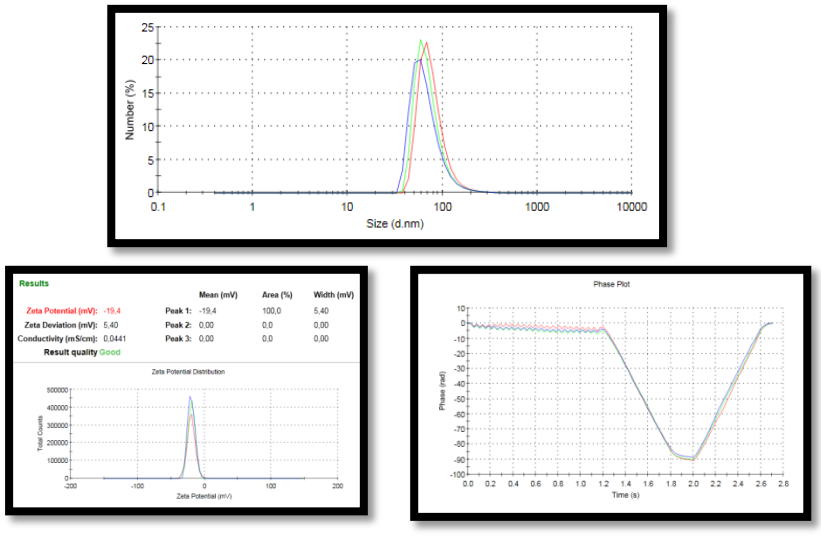


Figure 106. Size of the different nanoparticles determined by DLS (top) and Zeta potential measurements (bottom) of synthesized PLNP.

Moreover, the transmission electronic microscopy (TEM) analysis (Figure 107A) indicated that our nanoparticles represented a reasonable narrow size distribution, with particles diameter ranging from 50 to 100 nm. Also, when we compare our TEM image with the one in literature, similar patterns can be interpreted.

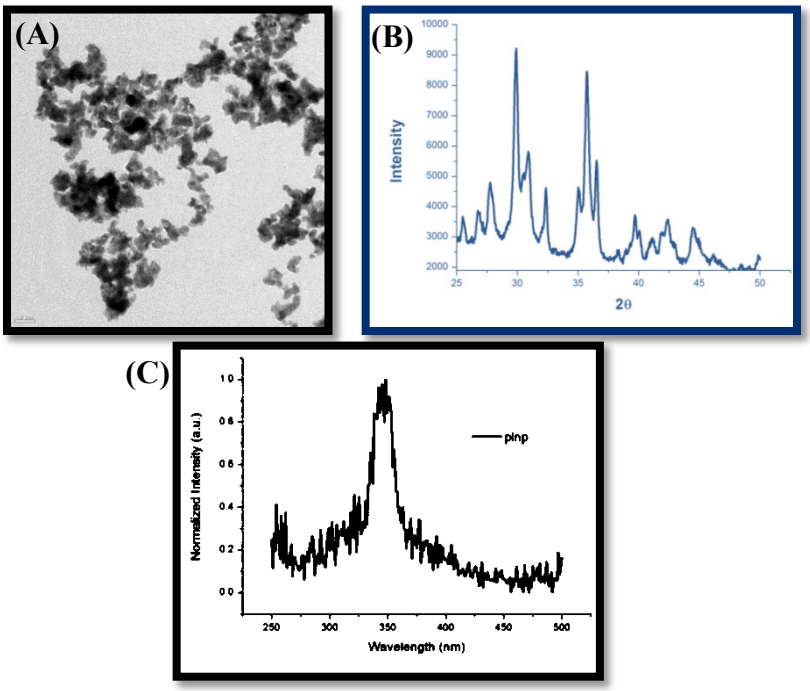


Figure 107. Transmission electron microscopy image (scale bar = 200 nm) (A), XRD pattern (B) and excitation spectrum (C) of synthesized PLNP.

Furthermore, The X-ray diffraction (XRD) results (Figure 107B) indicated the similar peaks with the literature.[9] Excitation spectra of our PLNP (Figure 107C) showed almost the same pattern as shown below.

The photosensitizer part is given in Figure 108. 3-chloropropanol was treated with sodium azide in DMSO at 60 °C to get 3-azidopropan-1-ol. Since tosyl group is a good leaving group, 3-azidopropyl 4-methylbenzenesulfonate was obtained with the tosylchloride in triethylamine. After getting S-(3-azidopropyl) ethanethioate, disulfide bridges with two azido functionality was obtained. To acquire the 3-((3-azidopropyl)disulfanyl)propan-1-amine, Staudinger reaction was performed. Also, to have 6-(4-formylphenoxy)hexanoic acid, Williamson-ether synthesis was used.

4-(prop-2-yn-1-yloxy)benzaldehyde and 2,4-dimetylpyrrole were used to obtain desired BODIPY and this BODIPY was iodinated on 2 and 6 positions by electrophilic aromatic substitutions.

When we decided to use $Ca_{0.2}Zn_{0.9}Mg_{0.9}Si_2O_6$ doped with Eu^{2+}, Dy^{3+}, Mn^{2+} nanoparticles, to get effective spectral overlap between the emission of nanoparticle and absorbance of BODIPY derivative, we synthesized mono-styryl BODIPY

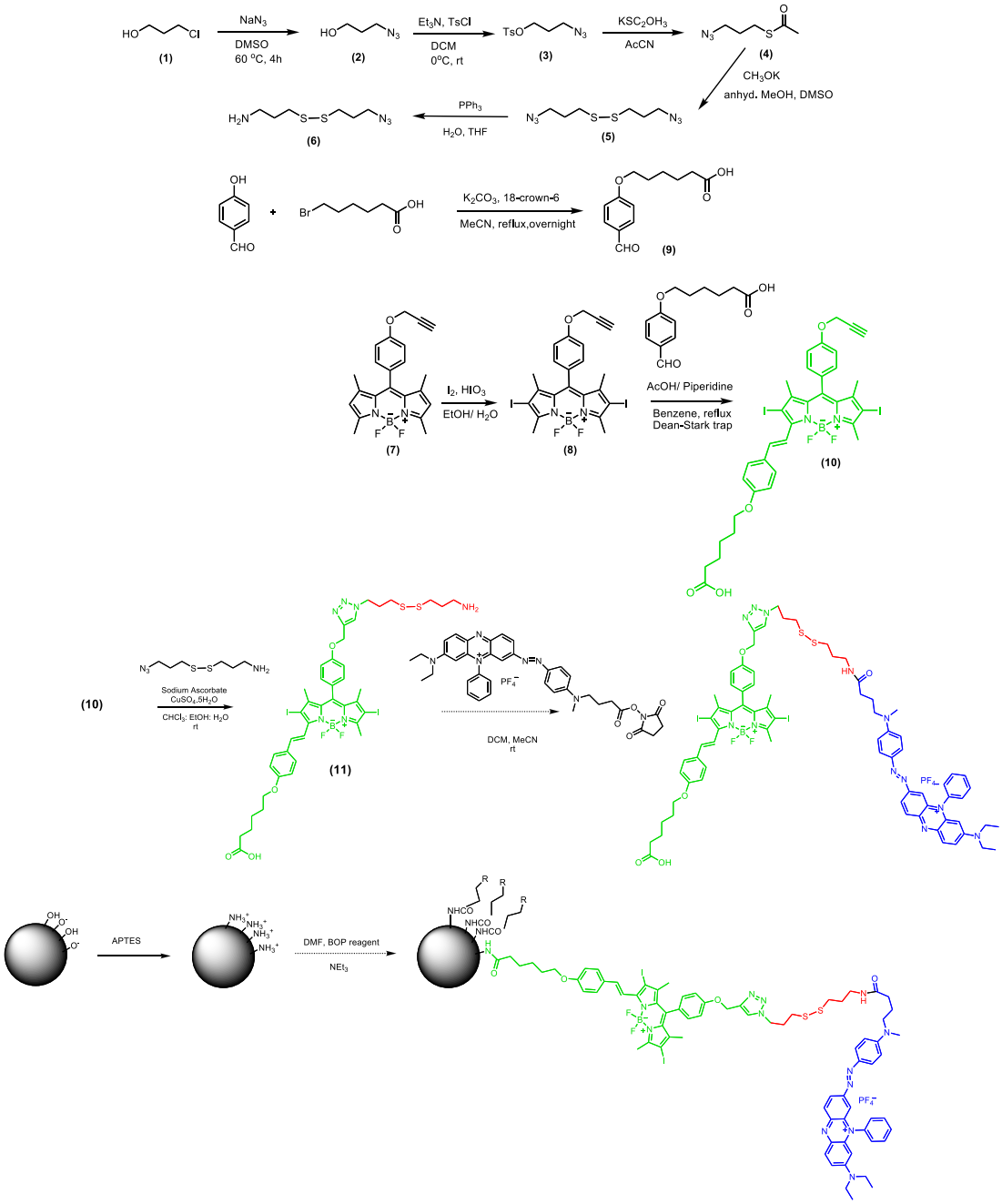


Figure 108. Previous reaction pathway of target compounds.

derivative. Then, click reaction with mono-styryl BODIPY and linker part was performed. Since we are not able to get reasonable amount of nanoparticles due to the difficulties in synthesis and obtaining small sized particles, we could not conjugate photosensitizer part with nanoparticles. The amount of nanoparticles was needed to be increased for further modification. However, not only the synthetic procedure is highly demanding but also the yield of the nanoparticles and the afterglow properties were not adequate so we had to change the type of nanoparticles.

Due to the highly demanding synthesis of persistent luminescent nanoparticles, **we collaborate with Prof. Xiu-Ping Yan at State Key Laboratory of Medicinal Chemical Biology (Nankai University) where the synthesis and characterization of nanoparticles that we used in the study were done.** The nanoparticles described in the paper "Functional Near Infrared-Emitting Cr^{3+}/Pr^{3+} Co-Doped Zinc Gallogermanate Persistent Luminescent Nanoparticles with Superlong Afterglow for in Vivo Targeted Bioimaging" were used.[234] These nanoparticles have very intense near-IR emission and their afterglow time is comparatively long. Also, these nanoparticles are compatible in biological medium and toxicity is very low. Thus, these mentioned features permit the long-term in vivo imaging.

The synthesis of this nanoparticle relies on the citrate-gel method together with reducing-atmosphere free calcination. The general composition of the long-persistent luminescent nanoparticles (LPLNPs) is $Zn_{2.94}Ga_{1.96}Ge_2O_{10}:Cr^{3+}$, Pr^{3+}. The persistent luminescence brightness and duration is dependent on several factors. One of them is pH of the starting solution. It was emphasized that pH 5 is a convenient value. Another factor is calcination temperature. If the calcination temperature is below 600 °C, emission is not observed. Also, higher calcination temperatures bring about higher emission intensity at 695 nm and a decrease in host emission was observed. The explanation for this is the creation of more vacancies of Ge^{4+}, Zn^{2+}, and oxygen. Codoping with Pr^{3+}/Cr^{3+} and introduction of Zn deficiency in zinc gallogermanate (ZGGO) host offers an increase in the intensity of persistent luminescence and afterglow time. To find optimum codoping composition, several experiments were conducted with varying contents. It was observed that the increase in the amount of

Cr^{3+} in ZGGO host is inversely proportional to intensity of persistent luminescence. The reason for this is the immediate release of energy of excitation storage and decay of afterglow emission.[127,235] The brightest afterglow emission is gained with $Zn_3Ga_{1.96}Ge_2O_{10}:Cr_{0.01}Pr_{0.03}$. The codoping with Pr^{3+} affects the duration of persistent luminescence by altering the trap density and depth since trivalent lanthanide ions with plentiful energy levels of 4f electron configurations allows more effective traps to increase the brightness and duration of the afterglow.[236,237] The introduction of Zn^{2+} improves the afterglow emission and enables the persistent energy transfer between host emission and Cr^{3+} by creating more cation vacancies as hole traps to improve afterglow intensity.[238]

The size of the nanoparticles were characterized by transmission electron microscopy (TEM) which gives 48.7 ± 15.3 nm (calculated from 100 randomly selected particles) and dynamic light scattering analysis which demonstrates a hydrodynamic diameter of 71.3 nm with a polydispersity index of 0.253.

Polyethylene groups were attached to persistent luminescent nanoparticles by using 3-amino propyltriethoxysilane (APTES)-functionalized LPLNPs and succinimidyl carbonate-poly (ethylene glycol)-carboxymethyl in order to develop biocompatibility, solubility, colloidal stability, and blood circulation time.

In Figure 109, emission and excitation properties of LPLNPs powder, undoped ZGGO and aqueous solution of LPLNPs are given. The emission band centered at 695 nm with excitation at 254 nm is because of $^2E \rightarrow {}^4A_2$ transition in distorted Cr^{3+} ions in gallogermanate.[235] There are four different peaks in the excitation spectrum. Peak at 260 nm is caused by the combination of the ZGGO host excitation and the O-Cr charge transfer band.[239] 3d intrashell transitions of Cr^{3+} lead to other peaks at 407 nm ($^4A_2 \rightarrow {}^4T_1$ (te^2) transition), 464 nm ($^4A_2 \rightarrow {}^4T_1$ (t^2e) transition), and 558 nm ($^4A_2 \rightarrow {}^4T_2$ transition). Also, electrons-holes recombination between the native defects (oxygen-defect, interstitial monovalent Zn, Ge-related centers, Zn-defect, and gallium−oxygen vacancy pair) of ZGGO host triggers a broad white emission band in the range of 350−660 nm with a maximum emission at 505 nm (Figure 109b).[240]

However, host emission is quenched with codoping with Pr^{3+}/Cr^{3+} because of nonradiative energy transfer between the host emission and the absorption of Cr^{3+}

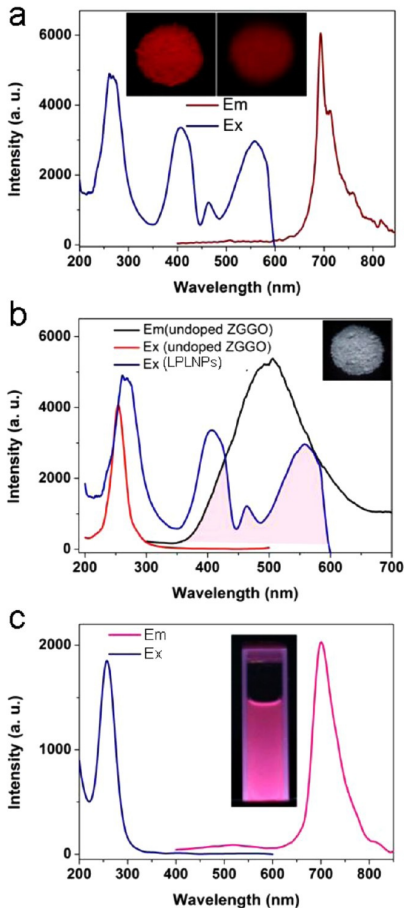


Figure 109. (a) Excitation (blue curve, at the emission of 695 nm) and emission (red curve, excitation at 254 nm) spectra of the LPLNPs powder. The inset shows the digital photos of LPLNPs powder under 254 nm UV excitation (left), and 5 s after stopping UV irradiation (right). (b) Excitation spectra of undoped ZGGO powder (red curve) and LPLNPs powder (blue curve) at the emission of 695 nm, and emission spectra of undoped ZGGO powder (black curve) under the excitation of 254 nm. The inset shows the digital photo of undoped ZGGO powder under 254 nm UV excitation. (c) Excitation (blue curve, emission at 700 nm) and emission (red curve, excitation at 254 nm) spectra of the aqueous dispersion of LPLNPs (1 mg ml−1). The inset shows the digital photo of the aqueous dispersion of LPLNPs under 254 nm UV excitation (Copyright © 2013, American Chemical Society, Reprinted with permission from ref (234)).

($^4A_2 \rightarrow {}^4T_1$ (te^2), $^4A_2 \rightarrow {}^4T_1$ (t^2e) and $^4A_2 \rightarrow {}^4T_2$ transition) resulting from their large spectral overlap (Figure 109b). The aqueous LPLNPs show a bright emission centered at 700 nm and very low emission at 521 nm upon excitation at 254 nm (Figure 109c) which is the demonstration of effective energy transfer in water. Other

excitation peaks disappeared in aqueous LPLNPs because of the presence O-H vibrations. Afterglow intensity is high and it is durable up to 24 hours after ceasing the excitation source. Thus, these long-lasting nanoparticles are suitable for *in vivo* imaging.

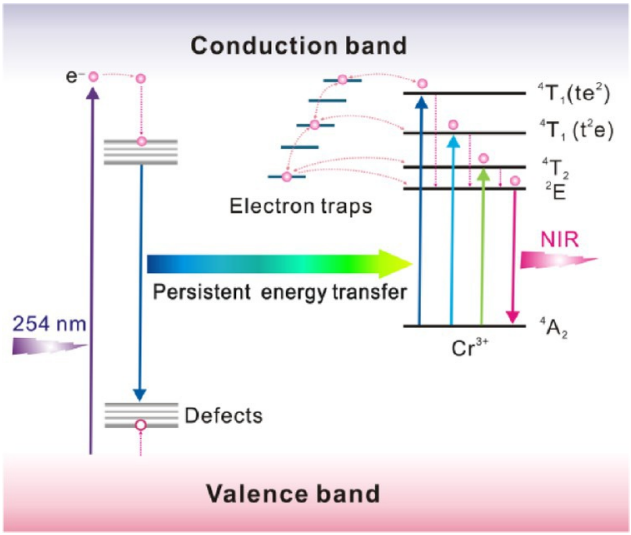


Figure 110. The proposed mechanism for persistent energy transfer between ZGGO and Cr^{3+} (Copyright © 2013, American Chemical Society, Reprinted with permission from ref (234)).

The proposed mechanism for energy transfer is given in Figure 110. With the excitation at 254 nm, ZGGO host electrons are excited from valence band to the conduction band. This is followed by the capturing of free excited electrons by native defects upon non-radiative relaxation. Ceasing the excitation source causes the recombination of electrons and holes from native defects causing broad afterglow emission. Due to the spectral overlap between the host emission and the three absorption band peak of Cr^{3+}, energy of host is given to the Cr^{3+} ion in a persistent manner.[241] This persistent energy transfer allows the concurrent raise of the 3d electrons of Cr^{3+} from ground state to ($^4A_2$) to three dissimilar energy levels of excited-states ($^4T_1$ (te^2), $^4T_1$ (t^2e) and $^4T_2$). The electrons in $^4T_1$ (te^2) are caught by shallow electron traps by conduction band and by non-radiative processes, they may go to deep traps.[127] By the way, the energy corresponding traps are occupied by $^4T_1$ (t^2e) and $^4T_2$ electrons upon tunneling.[242] When the energy transfer terminates, the released electrons from shallow traps are combined with ionized Cr^{3+} yielding a bright afterglow at first. Then, the gradual opposite tunneling recombination for deeper traps' electrons takes place afterwards and this arises the superlong afterglow.

However, since we changed the nanoparticles that we used the absorption and emission properties were altered. Hence, a new BODIPY dye was designed and synthesized via a multistep approach to have appropriate energy level match with the new nanoparticles' characteristics (Figure 111). Two successive Knoevenagel condensation of iodinated BODIPY on 2&6 positions with 4-methoxy benzaldehyde

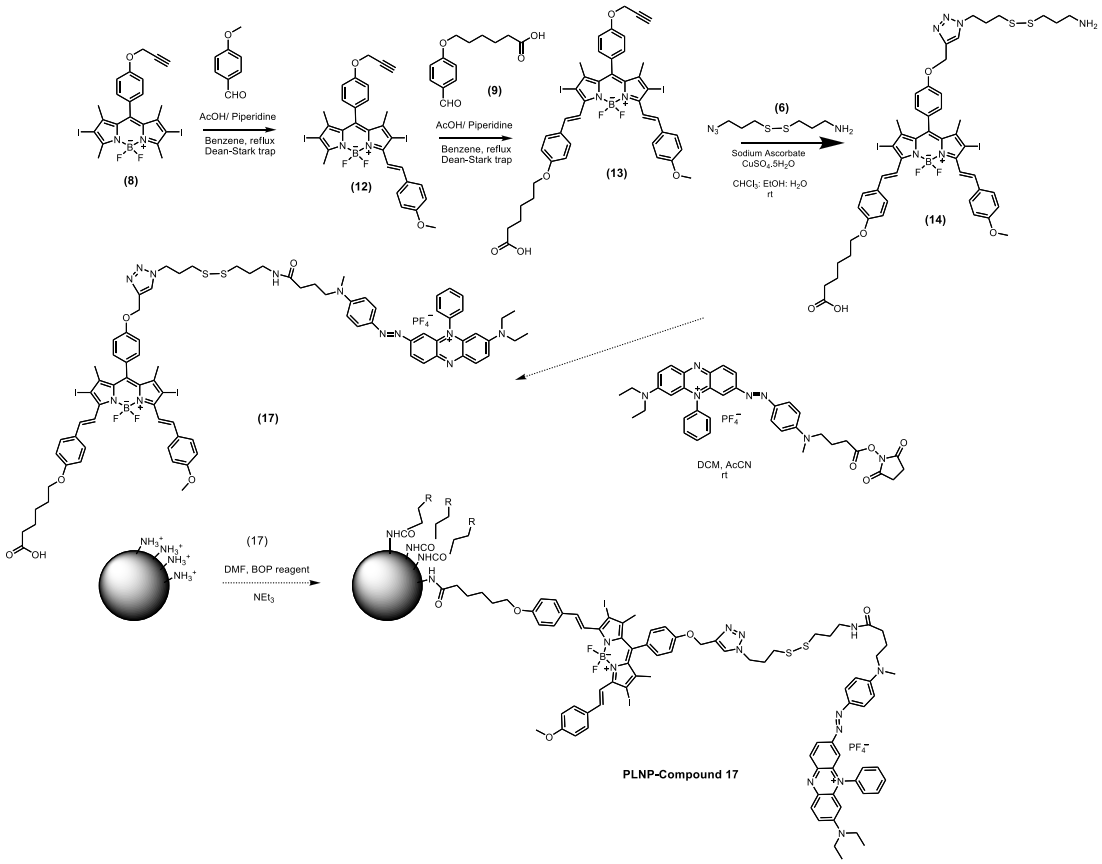


Figure 111. Current reaction pathway of target compounds.

and 6-(4-formylphenoxy)hexanoic acid were carried out. With the help of click reaction, 3-((3-azidopropyl)disulfanyl)propan-1-amine and distyryl BODIPY derivative were attached. We used 4-methoxy benzaldeyde to enhance the solubility in Knoevenagel condensation condition. Synthesis of the target molecule (PLNP-**17)** will be completed after the introduction of the quencher group and subsequent attachment of this compound to nanoparticles. The spectral investigation of PLNP and quencher units is in agreement to have effective quenching efficiency. Quenching range of BHQ-3 is between 620 and 730 nm and it is the preferred

quencher for dyes emitting in the range of 640-775 nm which is well-suited with the emission of PLNP.

We also synthesized compound **16** in order to validate our design principle (Figure 112). Cleavage of disulfide linker leaves free thiol groups and to account for this, free thiol group containing photosensitizer was attached successfully to nanoparticles.

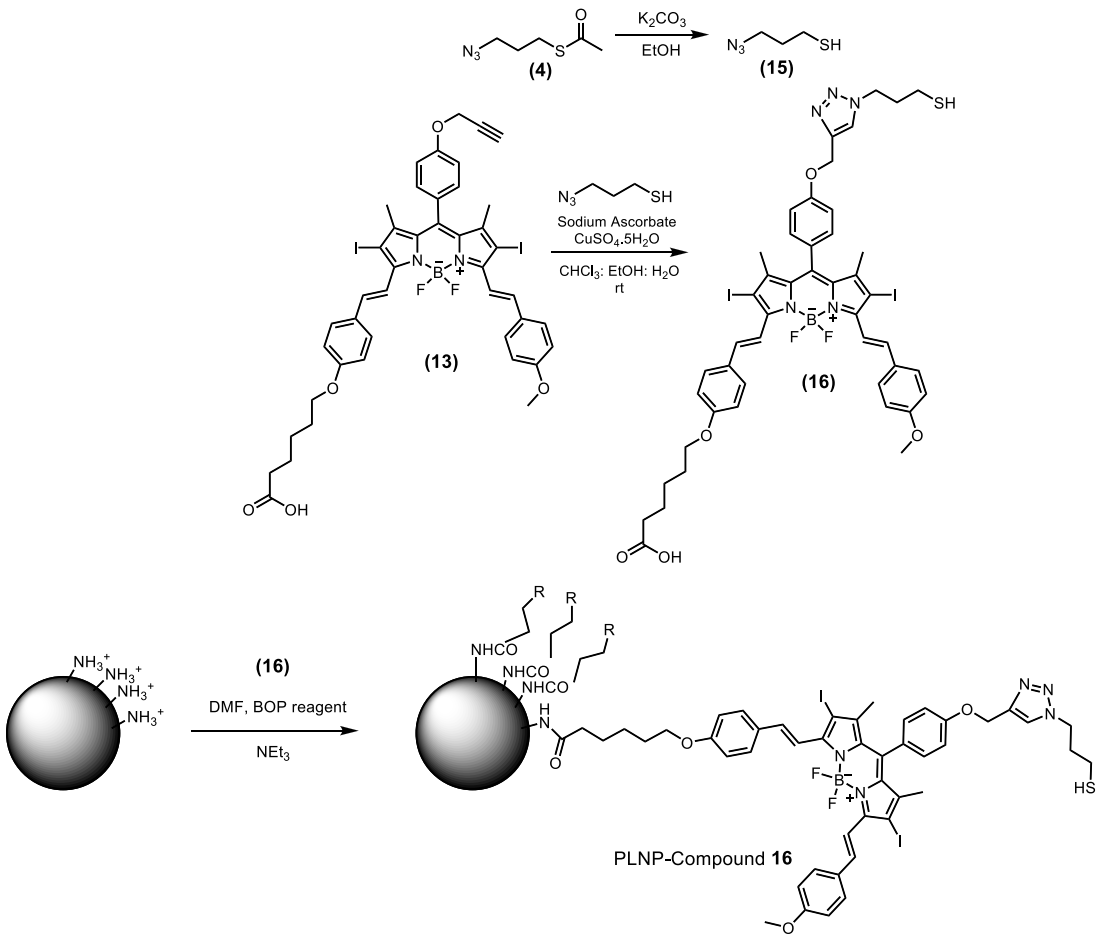


Figure 112. The synthetic pathway of compound **16** and PLNP-Compound **16** conjugate.

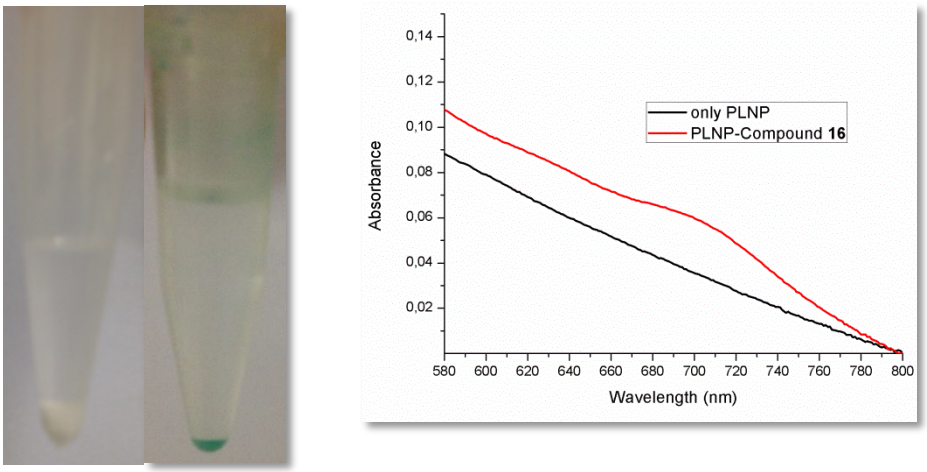


Figure 113. The (a) digital photograph and (b) absorbance spectra of only PLNP and PLNP-Compound 16 conjugate.

Figure 113 implies the attachment of compound **16** to nanoparticles. Both the digital photograph and absorbance spectra of only PLNP and PLNP-Compound **16** clearly show the conjugation between these units.

Singlet oxygen generation ability of PLNP-Compound **16** was investigated using photobleaching of water soluble singlet oxygen trap 2'-(Anthracene-9,10 diylbis (methylene))dimalonic acid (ADMDA). As given in Figure 114, ADMDA reacts with $^1O_2$ and absorbance at 376 nm decreases. Since the nanoparticles are activated at 254 nm so 254 nm UV lamp was used to irradiate the sample.

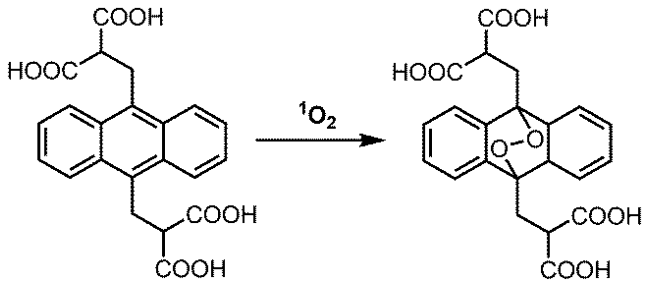


Figure 114. Reaction of singlet oxygen with 2,2'-(Anthracene-9,10-diylbis(methylene))dimalonic acid.

In control experiments, only trap and only nanoparticles containing solutions were monitored for 10 min intervals for 20 min in dark and 60 min under 254 nm irradiation. As expected, no remarkable decrease was observed (Figure 115). However, PLNP-Compound **16** conjugate demonstrated a significant decrease upon

irradiation which shows the ability of producing singlet oxygen and so the photodynamic action of the conjugate.

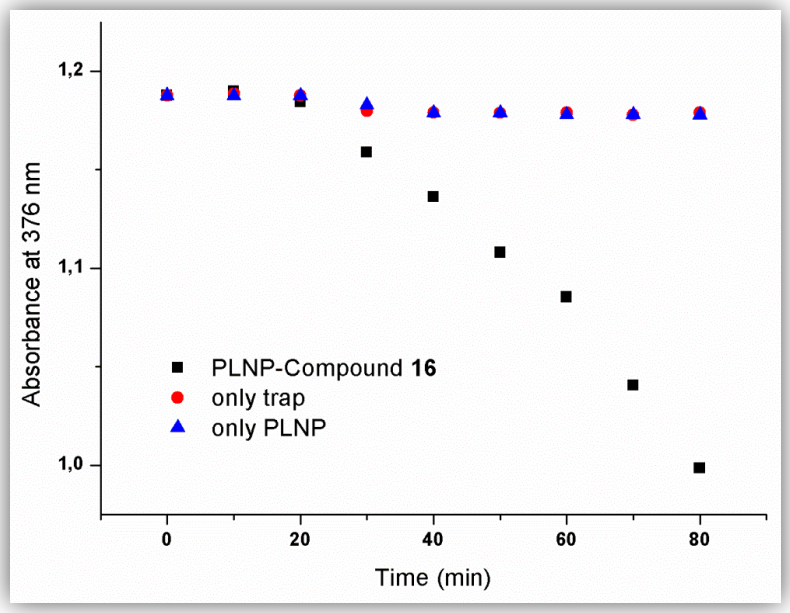


Figure 115. Relative singlet oxygen efficiency of only trap, only PLNP and PLNP-Compound **16** conjugate in aqueous solution detected by the absorbance decrease of 2'-(Anthracene-9,10 diylbis (methylene))dimalonic acid (ADMDA) at 376 nm with time. During 20 minutes, the samples were kept under dark and the following 60 min; the samples were irradiated with 254 nm light using UV lamp.

As stated above, for practical applications and potential use of this concept, quencher moiety will be attached as a control unit.

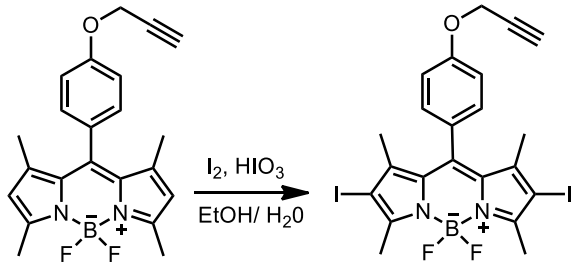
8.4. Conclusion

The design of the PLNP-BODIPY nanoconstruct is achieved and singlet oxygen generation experiments showed the efficiency of the photosensitizer activated through the energy transfer from PLNP to BODIPY. This construct is a promising candidate that signifies a solution to eliminate light issue in photodynamic therapy. Addition of control unit will enhance the use of these constructs for practical applications.

8.5. Experimental Details

General: ^{1}H NMR and ^{13}C NMR spectra were recorded on Bruker DPX-400 (operating at 400 MHz for ^{1}H NMR and 100 MHz for ^{13}C NMR) in $CDCl_3$ with tetramethylsilane as internal standard. All spectra were recorded at 25 °C and coupling constants (*J* values) are given in Hz. Chemical shifts are given in parts per million (ppm). Absorption spectra were performed by using a Varian Cary-100 spectrophotometer. Fluorescence measurements were conducted on a Varian Eclipse spectrofluorometer. Mass spectra were recorded on Agilent Technologies 6530 Accurate-Mass Q-TOF LC/MS. Reactions were monitored by thin layer chromatography using Merck TLC Silica gel 60 F254. Silica gel column chromatography was performed over Merck Silica gel 60 (particle size: 0.040-0.063 mm, 230-400 mesh ASTM). Compound **7** was synthesized according to literature.[243] All other reagents and solvents were purchased from Aldrich and used without further purification.

Synthesis of Compound 8:

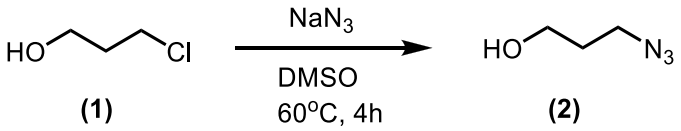


(7) (8)

In a 250 ml round-bottom flask, compound **7** (500 mg, 1.32 mmol) and I_2 (840 mg, 3.30 mmol) were dissolved in ethanol (150 ml). Iodic acid, HIO_3 (466 mg, 2.6 mmol) was dissolved in a few drops of water and was added into the previous solution. The reaction mixture was heated to 50 °C and stirred until the starting compounds were disappeared at this temperature. When the reaction was completed, saturated sodium thiosulfate solution was added (50 ml) and extraction with dichlorometane followed by a was with water was performed. Organic layer was dried with Na_2SO_4 and evaporated under reduced pressure. The final product was purified by silica gel column chromatography using DCM/Hexane (1:1, v/v). Fraction containing target

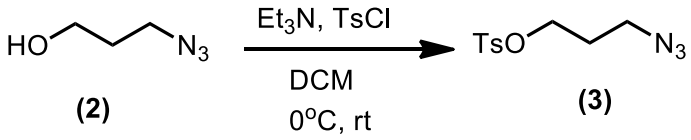
compound was collected, after removal of solvent under reduced pressure, final product was obtained (330 mg, 40%). ^{1}H NMR ($CDCl_3$, 400 MHz, δ ppm) 7.1 (d, *J*=8.8 Hz, 2H), 7.0 (d, *J*=8.8 Hz, 2H), 4.7 (s, 2H), 2.6 (s, 6H), 2.5 (s, 1H), 1.3 (s, 6H). Calcd: 629.96 [M]+ , Found: 629.76 [M]+

Synthesis of Compound 2:



Compound **1** (10.0 g, 106 mmol) was dissolved in 70 ml DMSO and NaN_3 (14.0 g, 212 mmol) was added. The reaction mixture was heated to 100 °C and stirred for overnight at this temperature. Then, water (100 ml) was added and the product was extracted with the ethylacetate (3 x 100 ml). Organic phases were combined, dried over Na_2SO_4 and the volatiles were evaporated under reduced pressure. The residue was used without further purification (4g, 37 %). ^{1}H NMR ($CDCl_3$, 400 MHz, δ ppm) 3.7 (t, *J*=6.0 Hz, 2H), 3.3 (t, *J*=6.6 Hz, 2H), 1.7 (m, 2H). ^{13}C NMR ($CDCl_3$, 100 MHz, δ ppm) 59.6, 48.4, 31.4.

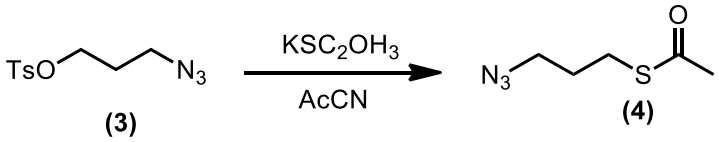
Synthesis of Compound 3:



In a 250 ml round-bottom flask, compound **2** (3.5 g, 35 mmol) was dissolved in 100 ml DCM and triethylamine (7.3 ml, 52 mmol) was added. Then, reaction mixture was cooled to 0 °C using ice bath and p-toluene sulfonyl chloride (7.9 g, 42 mmol) was added portion-wise. After stirring for 12 hours at room temperature, extraction was performed with water. Organic layer was dried over Na_2SO_4 and the solvent was evaporated under reduced pressure. The final product was purified by silica gel column chromatography using DCM/Hexane (1:1, v/v). Fraction containing target compound was collected, after removal of solvent under reduced pressure, final

product was obtained. (4.8 g, 55%) ^{1}H NMR ($CDCl_3$, 400 MHz, δ ppm) 7.8 (d, *J*=8.3 Hz, 2H), 7.3 (d, *J*=8.6 Hz, 2H), 4.1 (t, *J*=6.0 Hz, 2H), 3.3 (t, *J*=6.5 Hz, 2H), 2.4 (s, 3H), 1.84 (p, *J*=6.3, *J*=6.1 Hz, 2H). ^{13}C NMR ($CDCl_3$, 100 MHz, δ ppm) 145.1, 132.7, 130.3, 129.9, 127.9, 127.0, 67.1, 47.3, 28.4, 21.6.

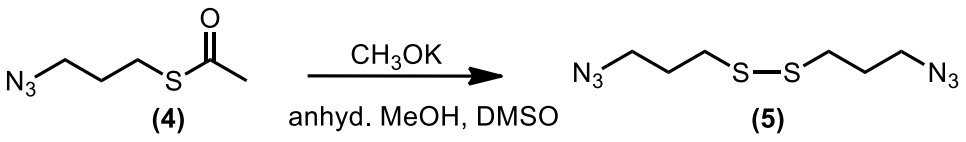
Synthesis of Compound 4:



(3) **(4)**

Compound **3** (4.8 g, 18 mmol) was dissolved in 60 ml acetonitrile and potassium thioacetate (4.3 g, 37 mmol) was added to resulting solution. The reaction mixture was heated to 60 °C and stirred for 12 hours at this temperature. Then, resulting mixture was filtered using suction filtration and acetonitrile was evaporated under reduced pressure. After extraction with DCM, organic phase was dried over Na_2SO_4 and the solvent was evaporated under reduced pressure. The residue was used without further purification (2.0 g, 67 %). ^{1}H NMR ($CDCl_3$, 400 MHz, δ ppm) 3.4 (t, *J*=6.6 Hz, 2H), 2.9 (t, *J*=7.1 Hz, 2H), 2.3 (s, 3H), 1.85 (p, 2H, *J*=6.8, *J*=6.9 Hz). ^{13}C NMR ($CDCl_3$, 100 MHz, δ ppm) 50.1, 30.6, 28.9, 26.1.

Synthesis of Compound 5:

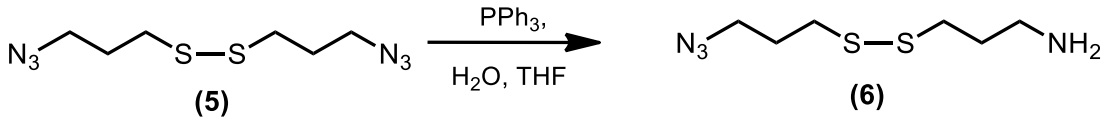


(4) **(5)**

Compound **4** (587 mg, 3.70 mmol) was dissolved in 25 ml dry methanol and potassium methoxide (1.5 ml, 7.4 mmol) was added. The reaction mixture was stirred for 2 hours at room temperature. Then, 0.6 ml DMSO was added and resulting mixture was stirred and for additional 20 hours at this temperature. Then the pH was adjusted to 7 by using amberlite CG-50-II and the reaction mixture was filtered using suction filtration and solvent was evaporated under reduced pressure. The residue was purified by silica gel column chromatography using DCM/Hexane (1:1, v/v). Fraction containing target compound was collected, after removal of solvent under

reduced pressure, the final product was obtained (300 mg, 35%). ^{1}H NMR ($CDCl_3$, 400 MHz, δ ppm) 3.4 (t, *J*=6.5 Hz, 4H), 2.8 (t, *J*=7.0 Hz, 4H), 1.9 (p, *J*=6.8, 6.7 Hz, 4H)

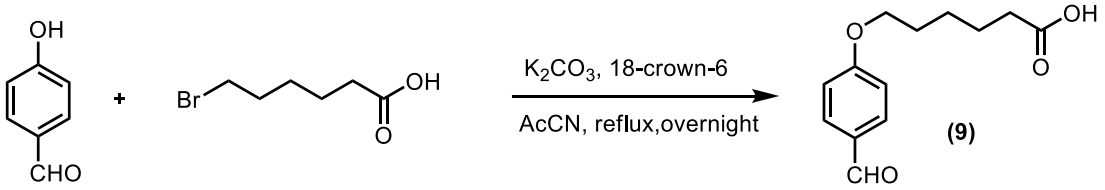
Synthesis of Compound 6:



(5) **(6)**

In a 250 ml round-bottom flask, compound **5** (500 mg, 2.2 mmol) was dissolved in 7 ml THF and 30 µl water was added. Then, reaction mixture was cooled to 0^{o}C using ice bath and triphenylphosphine (450 mg, 2.2 mmol) was added portion-wise. After stirring for 18 hours at room temperature, THF was evaporated under reduced pressure. The resulting mixture was dissolved in ethyl acetate and 1N HCl was added. Then, aqueous phase was separated and the treated with NaOH (10%, w/w) to adjust pH to 10-12. Ethyl acetate was used for extraction and organic phase was dried over Na_2SO_4 and the solvent was evaporated under reduced pressure. The final product was purified by silica gel column chromatography using DCM/methanol (10:1, v/v). Fraction containing target compound was collected, after removal of solvent under reduced pressure, final product was obtained. (100 mg, 23%) ^{1}H NMR ($CDCl_3$, 400 MHz, δ ppm) 3.7 (broad, 2H), 3.4 (t, *J*=6.4 Hz, 2H), 2.9 (t, *J*=6.8 Hz, 2H), 2.8 (t, *J*=7.3 Hz, 4H), 1.99-1.93 (m, 4H)

Synthesis of Compound 9:

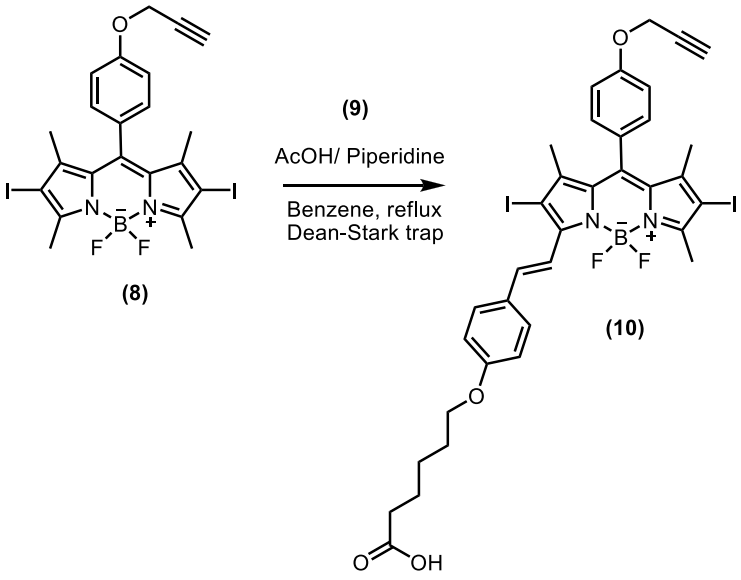


(9)

K_2CO_3 (3.2 g, 23 mmol) was added into 200 ml of acetonitrile and then to this solution, 4-hydroxybenzaldehyde (460 mg, 3.7 mmol) and 6-bromophenylhexanoic acid (1.1 g, 5.6 mmol) was added. After addition of catalytic amount of 18-crown-6 the resulting mixture was heated at reflux for 2 days. The solution was then filtered

and the residue was washed with acetonitrile two times. The residue was dissolved in water and neutralized with 4 M HCl. A white precipitate was formed. The mixture was filtered and the solution was concentrated by rotary evaporation under vacuum. The crude product was purified by column chromatography using MeOH: DCM (5:95, v/v) as the eluent to afford product **9** as a white solid (98.4 mg, 74%). ^{1}H NMR (400 MHz, $CDCl_3$) δ 9.90 (s, 1H), 7.85 (d, *J* = 8.9 Hz, 2H), 7.01 (d, *J* = 8.6 Hz, 2H), 4.07 (t, *J* = 6.4 Hz, 2H), 2.43 (t, *J* = 7.4 Hz, 2H), 1.95 – 1.81 (m, 2H), 1.76 (dt, *J* = 15.0, 7.5 Hz, 2H), 1.63 – 1.51 (m, 2H).

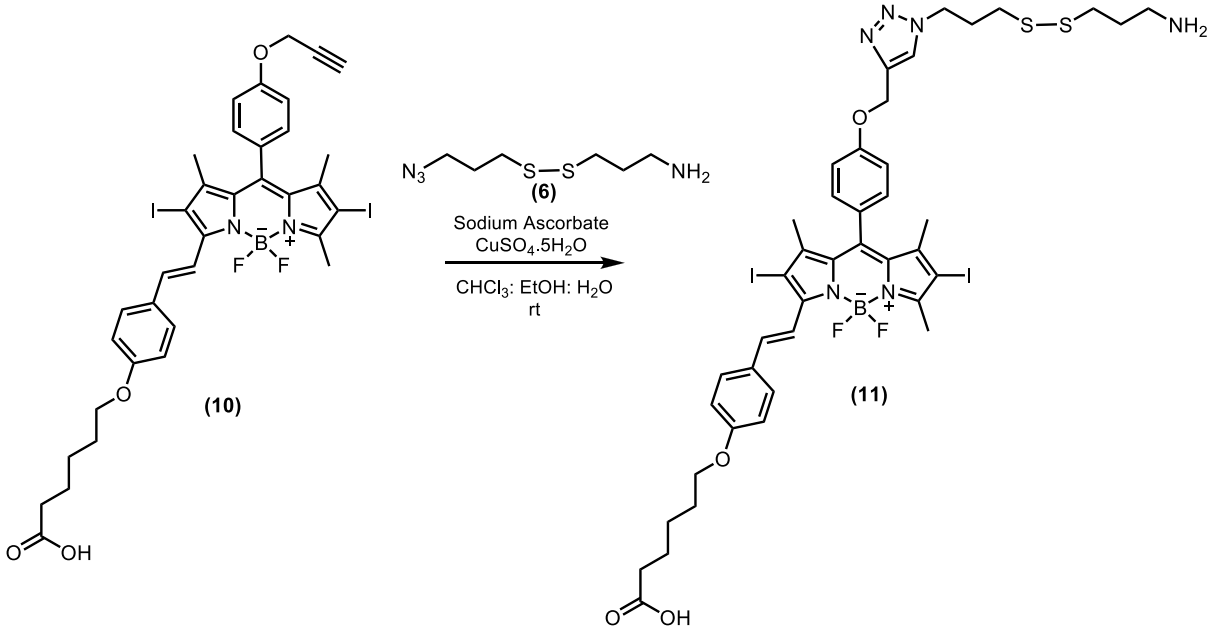
Synthesis of Compound 10:



In a 100 ml round-bottomed flask containing 50 ml benzene, compound **8** (225 mg, 0.36 mmol) and compound **9** (78.0 mg, 0.36 mmol) piperidine (0.15 ml) and acetic acid (0.15 ml) were added. The mixture was heated under reflux with a Dean Stark trap and progress of the reaction was monitored by TLC. When all the starting materials were consumed, the mixture was cooled to room temperature and the solvent was evaporated. Water (100 ml) added to the residue and the product was extracted into the DCM (1x 100 ml). Organic phase dried over Na_2SO_4 and the solvent was evaporated. The residue was purified by silica gel column chromatography using MeOH: DCM (5:95, v/v) as the eluent to give **10** (140 mg, 53%). ^{1}H NMR ($CDCl_3$, 400 MHz, δ ppm) 8.2 (d, *J*=17 Hz, 1H), 7.6 (d, *J*=8.8 Hz,

2H), 7.5 (d, *J*=17 Hz, 1H), 7.2 (d, *J*=8.8 Hz, 2H), 7.1 (d, *J*=8.7 Hz, 2H), 6.9 (d, *J*=8.8 Hz, 2H), 4.8 (s, 2H), 4.0 (t, *J*=6.8 Hz, 2H), 2.7 (s, 3H), 2.6 (s, 1H), 1.8-1.6 (M, 8H), 1.4 (s, 3H), 1.3 (s, 3H). ^{13}C NMR ($CDCl_3$, 100 MHz, δ ppm): 177.7, 160.2, 158.4, 156.5, 150.7, 146.1, 144.7, 139.7, 139.1, 132.1, 130.4, 129.43, 129.40, 129.3, 129.2, 129.1, 127.9, 116.4, 115.9, 115.0, 114.9, 114.8, 67.7, 56.1, 56.0, 53.4, 47.4, 42.5, 33.8, 31.5, 29.2, 26.4, 24.7, 21.4, 17.6, 17.1. Calcd: 849.29 [M+H]+ , Found: 848.11 [M+H]+

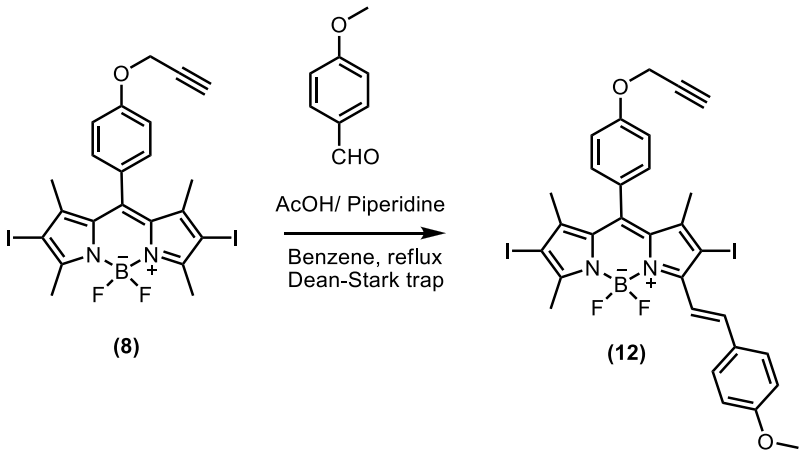
Synthesis of Compound 11:



To the solution of the compound **10** (138 mg, 0.18 mmol) in a 6:0.5:0.5 mixture of $CHCl_3$, EtOH and water; compound **6** (38 mg, 0.18 mmol), 7.3 mg sodium ascorbate, 4.6 mg $CuSO_4$ and 3-4 drop Et_3N were added and it was stirred at room temperature for three days. The crude product was purified by column chromatography using MeOH: DCM (5:95, v/v) as the eluent to afford product **11** (20 mg, 10%).^{1}H NMR ($CDCl_3$, 400 MHz, δ ppm) 8.2 (d, *J*=17 Hz, 1H), 7.6 (d, 2H, *J*=8.7 Hz), 7.5 (d, *J*=17 Hz, 1H), 7.2 (d, *J*=8.7 Hz, 2H), 7.1 (d, *J*=8.8 Hz, 2H), 6.9 (d, *J*=8.8 Hz, 2H), 4.5 (s, 2H),4.0 (t, *J*=6.7 Hz, 2H), 3.5 (m, 2H), 2.8 (t, *J*=6.7 Hz, 2H), 2.7 (s, 3H), 2.4-2.3 (m, 4H), 2.1-1.7 (m, 8H), 1.5 (s, 3H), 1.4 (s, 3H), 1.3 (m, 4H). ^{13}C NMR ($CDCl_3$, 100 MHz, δ ppm): 213.7, 178.3, 160.2, 159.1, 156.5, 150.6,

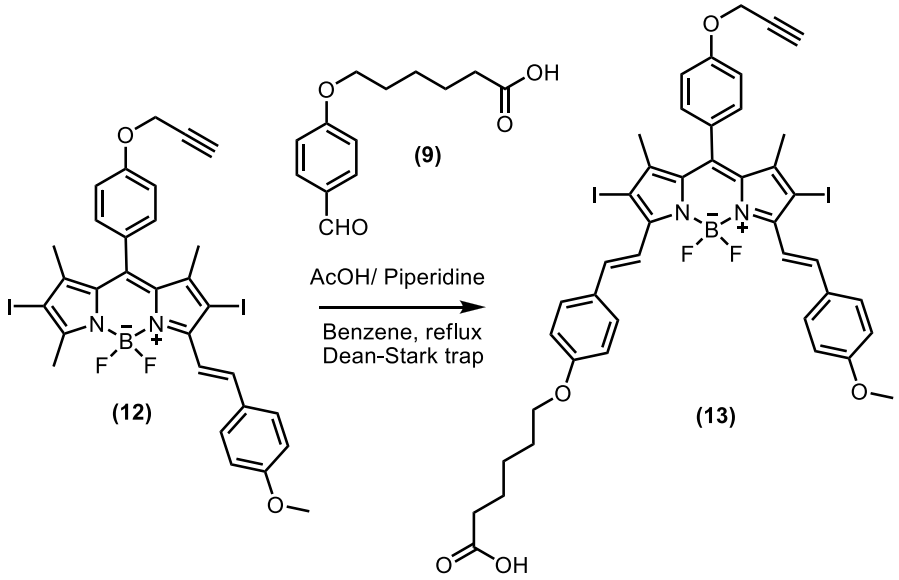
146.1, 144.7, 143.6, 139.8, 139.1, 132.5, 132.1, 129.5, 129.3, 129.1, 127.7, 123.0, 116.4, 115.7, 114.8, 85.9, 82.2, 67.7, 62.0, 49.6, 48.5, 35.1, 34.4, 33.7, 29.6, 29.4, 29.2, 28.8, 28.2, 24.7, 24.4, 22.6, 17.6, 17.1, 16.1, 14.1. Calcd: 1056 [M+H]+ , Found: 1060 [M+H]+

Synthesis of Compound 12:



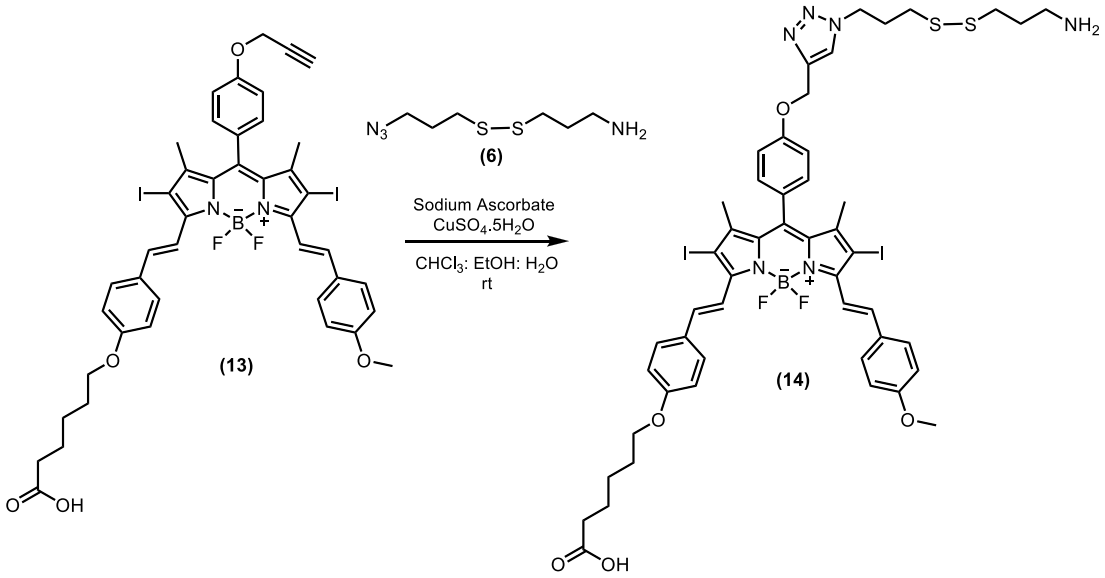
In a 100 ml round-bottomed flask containing 50 ml benzene, compound **8** (230 mg, 0.37 mmol), p-anisaldehyde (30.0 mg, 0.22 mmol), piperidine (0.20 ml) and acetic acid (0.20 ml) were added. The mixture was heated under reflux with a Dean Stark trap and progress of the reaction was monitored by TLC. When all the starting materials was consumed, the mixture was cooled to room temperature and solvent was evaporated. Water (100 ml) added to the residue and the product was extracted with DCM (1x 100 ml). Organic phase was dried over Na_2SO_4 and the solvent was evaporated. The residue was purified by silica gel column chromatography using DCM: hexane (1:1, v/v) as the eluent to give compound **12** (67 mg, 25%). ^{1}H NMR (400 MHz, $CDCl_3$) δ 8.15 (d, *J* = 16.6 Hz, 1H), 7.62 (d, *J* = 8.7 Hz, 2H), 7.56 (d, *J* = 16.6 Hz, 1H), 7.21 (d, *J* = 8.7 Hz, 2H), 7.15 (d, *J* = 8.7 Hz, 2H), 6.96 (d, *J* = 8.7 Hz, 2H), 4.81 (d, *J* = 2.4 Hz, 2H), 3.89 (s, 3H), 2.77 – 2.65 (m, 3H), 2.58 (s, 1H), 1.50 (s, 3H), 1.45 (s, 3H). ^{13}C NMR (100 MHz, $CDCl_3$) δ 160.7, 158.5, 156.64, 150.7, 146.1, 144.8, 139.8, 139.0, 129.5, 129.4, 129.2, 127.98, 116.6, 115.9, 114.3, 76.7, 76.1, 56.1, 55.4, 17.6, 17.2, 16.2. Calcd: 748.0067 [M]+ , Found: 748.0178 [M]+

Synthesis of Compound 13:



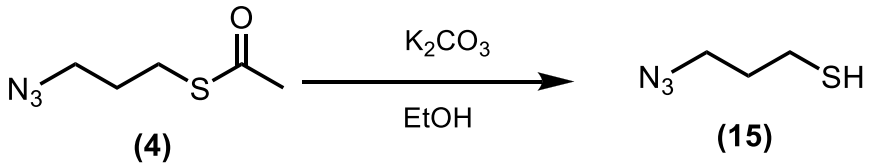
In a 100 ml round-bottomed flask containing 50 ml benzene, compound **12** (120 mg, 0.14 mmol) and compound **9** (33 mg, 0.14 mmol), piperidine (0.20 ml) and acetic acid (0.20 ml) were added. The mixture was heated under reflux with a Dean Stark trap and progress of the reaction was monitored by TLC. When all the starting materials were consumed, the mixture was cooled to room temperature and solvent was evaporated. Water (100 ml) added to the residue and the product was extracted with DCM (1x 100 ml). Organic phase was dried over Na_2SO_4 and the solvent was evaporated. The residue was purified by silica gel column chromatography using MeOH: DCM (2:98, v/v) as the eluent to give compound **13** (88 mg, 65%). ^{1}H NMR (400 MHz, $CDCl_3$) δ 8.15 (d, *J* = 16.6 Hz, 2H), 7.61 (dt, *J* = 13.3, 6.5 Hz, 6H), 7.22 (d, *J* = 8.7 Hz, 2H), 7.14 (d, *J* = 8.7 Hz, 2H), 6.96 (t, *J* = 9.0 Hz, 4H), 4.81 (d, *J* = 2.4 Hz, 2H), 4.03 (t, *J* = 6.3 Hz, 2H), 3.88 (s, 3H), 2.60 (s, 1H), 2.43 (t, *J* = 7.4 Hz, 2H), 1.95 – 1.79 (m, 2H), 1.75 (dd, *J* = 15.2, 7.6 Hz, 2H), 1.64 (dd, *J* = 9.4, 3.3 Hz, 2H), 1.58 -1.51 (m, 7H). ^{13}C NMR (100 MHz, $CDCl_3$) δ 177.9, 160.7, 160.2, 158.5, 150.6, 150.4, 145.7, 145.6, 139.20, 139.1, 138.2, 133.2, 132.0, 129.7, 129.6, 129.5, 129.3, 129.0, 128.3, 82.7, 67.8, 56.1, 55.4, 48.0, 33.8, 29.7, 28.9, 25.8, 25.6, 24.7, 24.5, 17.7. Calcd: 988.0938 [M+H]+ , Found: 988.0986 [M+H]+, Δ=4.84 ppm.

Synthesis of Compound 14:



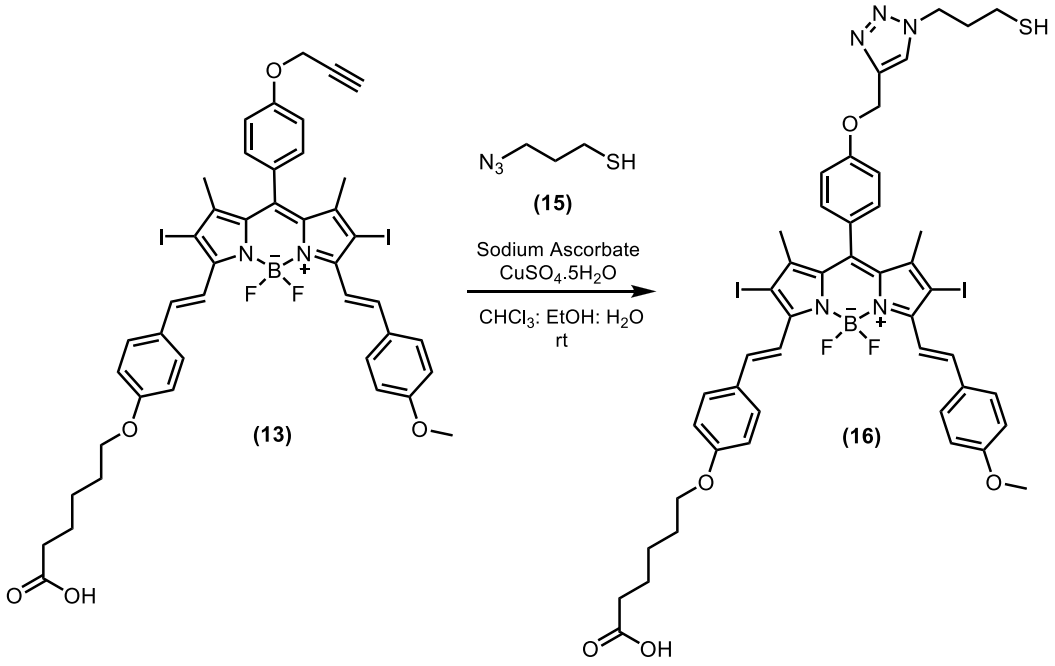
To the solution of the compound **13** (93 mg, 0.096 mmol) in a 6:0.5:0.5 mixture of $CHCl_3$, EtOH and water; compound **6** (200 mg, 0.096 mmol), 3.8 mg of sodium ascorbate, 2.4 mg of $CuSO_4$ and 3-4 drop of Et_3N were added and the mixture was stirred at room temperature for three days. The solvent was evaporated and the crude product was purified by column chromatography using MeOH: DCM (5:95, v/v) as the eluent to afford product **3** (17 mg, 15%). ^{1}H NMR (400 MHz, $CDCl_3$) δ 8.15 (d, *J* = 16.7 Hz, 2H), 7.75-7.7.55 (m, 7H), 7.22 (d, *J* = 7.8 Hz, 2H), 7.16 (d, *J* = 7.7 Hz, 2H), 6.96 (t, *J* = 8.3 Hz, 4H), 5.31 (s, 2H), 4.56 (t, *J* = 6.4 Hz, 2H), 4.04 (t, *J* = 5.6 Hz, 2H), 3.88 (s, 3H), 2.78 (t, *J* = 6.9 Hz, 2H), 2.71 (t, *J* = 6.5 Hz, 2H), 2.42 (dd, *J* = 16.7, 7.4 Hz, 4H), 2.06 – 1.91 (m, 2H), 1.86 (s, 2H), 1.75 (dd, *J* = 14.5, 6.8 Hz, 2H), 1.63 (d, *J* = 19.6 Hz, 2H), 1.58 (s, 2H), 1.51 (s, 6H). ^{13}C NMR (100 MHz, $CDCl_3$) δ 160.7, 160.3, 159.2, 139.1, 139.0, 133.2, 132.5, 129.8, 129.6, 129.5, 129.3, 128.0, 123.1, 116.6, 115.7, 114.9, 114.3, 67.8, 62.2, 55.4, 49.7, 48.5, 35.2, 34.5, 33.6, 31.9, 29.7, 29.3, 29.2, 29.2, 29.1, 28.9, 28.3, 25.6, 24.5, 17.7. Calcd: 1210.1337 [M+K]+ , Found: 1210.1180 [M+K]+, Δ=12.99 ppm.

Synthesis of Compound 15:



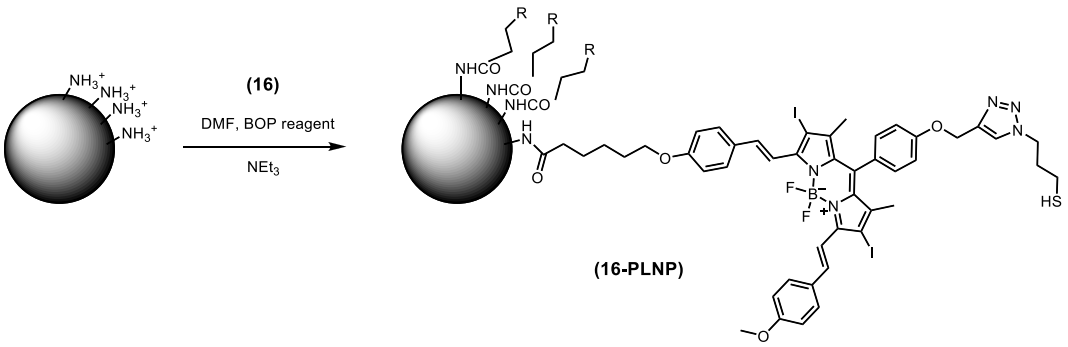
Compound **4** (100 mg, 0.62 mmol **)** was dissolved in 7 ml EtOH and K_2CO_3 (95 mg, 0.69 mmol) was added into solution. After stirring at room temperature for 4 hours, water was added and the mixture wasextracted with ethyl acetate. Organic phase dried over Na_2SO_4 and the solvent was evaporated. The residue was purified by silica gel column chromatography using DCM: Hexane (1:1, v/v) as the eluent to give compound **15** (25 mg, 35%). ^{1}H NMR (400 MHz, $CDCl_3$) δ 3.45 (t, *J* = 6.5 Hz, 2H), 2.78 (t, *J* = 7.0 Hz, 2H), 2.05 – 1.95 (m, 2H). ^{13}C NMR (100 MHz, $CDCl_3$) δ 49.72, 35.27, 28.26.

Synthesis of Compound 16:



To the solution of the compound **13** (35 mg, 0.036 mmol) in a 3 ml: 0.25 ml: 0.25 ml mixture of $CHCl_3$, EtOH and water; compound **15** (4.2 mg, 0.036 mmol), 1.5 mg of sodium ascorbate, 1.0 mg of $CuSO_4$ and 1-2 drop Et_3N are added and it was stirred at room temperature for three days. The crude product was purified by column chromatography using MeOH: DCM (5:95, v/v) as the eluent to afford product **16** (17 mg, 15%). ^{1}H NMR (400 MHz, $CDCl_3$) δ 8.06 (dd, *J* = 16.5, 12.0 Hz, 2H), 7.73 (s, 1H), 7.53 (dd, *J* = 16.2, 10.7 Hz, 6H), 7.14 (d, *J* = 8.1 Hz, 2H), 7.08 (d, *J* = 8.2 Hz, 2H), 6.89 (t, *J* = 8.5 Hz, 4H), 5.21 (s, 2H), 4.49 (t, *J* = 6.6 Hz, 2H), 3.96 (t, *J* = 6.3 Hz, 2H), 3.80 (s, 3H), 2.63 (t, *J* = 6.7 Hz, 2H), 2.31-2.7 (m, 4H), 1.85 – 1.71 (m, 2H), 1.66-1.58 (m, 2H), 1.56 – 1.31 (m, 8H).^{13}C NMR (100 MHz, $CDCl_3$) δ 160.7, 160.7, 160.3, 160.2, 159.1, 145.6, 145.5, 143.6, 140.9, 140.8, 139.2, 139.0, 138.9, 138.8, 138.5, 138.2, 133.1, 132.3, 129.8, 129.7, 129.5, 129.3, 129.2, 127.9, 127.5, 123.4, 67.8, 61.8, 55.3, 49.6, 49.4, 49.2, 49.0, 48.8, 48.5, 48.3, 34.3, 33.9, 29.1, 28.8, 25.5, 24.6, 17.6, 13.8. Calcd: 1105.1298 [M+Na]+ , Found: 1105.1658 [M+Na]+, Δ=32.5 ppm.

Synthesis of PLNP-Compound 16:



To the solution of the compound **16** (20 mg, 0.018 mmol) in 1 ml DMF, 5 mg of APTES-functionalized PLNP, (benzotriazol-1-yloxy)tris(dimethylamino)phosphonium hexafluorophosphate (10 mg, 0.022 mmol) and 1 drop of Et_3N was added. Resulting solution was stirred overnight in the dark at room temperature. The unreacted reagents were removed by centrifugation and the resulting PLNP-Compound **16** was washed with DMF with several times

PDT Measurements:

$^1O_2$ dependent degradation of water soluble trap, 2,2'-(anthracene-9,10-diylbis(methylene)dimalonic acid was used to measure photodynamic activity because the absorption of this compound at 376 nm decreases indicating the generation of $^1O_2$.

Measurements were performed using 254 nm UV lamp and samples were irradiated with the light source from a 40 cm distance. All samples were bubbled with O_2 for 5 min prior to experiments. D_2O was used for the solutions since the lifetime of $^1O_2$ in this solution is higher.

At first, several dark measurements were taken followed by irradiation of the mixture at absorption maximum of a sensitizer. Absorbance decrease of trap molecules was monitored suggesting singlet oxygen generation in the presence of light and sensitizers.

CHAPTER 9

CONCLUSION

This thesis is aimed to promote the improvement in the topic of the chemistry of BODIPY dyes, ion sensing and biologically meaningful molecules, energy transfer and as well as photodynamic therapy concepts. Along this way, six different studies were employed for those application areas. Of course, straightforward derivatization on BODIPY core allows getting functional dyes with desired properties. This is why BODIPY dyes have been implemented in distinct utilization and its popularity is continuing.

In the Chapter 3, with the help of tetra-styryl BODIPY derivatives, which are isomers, the ion-response properties of BODIPY dyes regarding with Hg (II) binding were explored. This study not only enlightens the importance of modification positions on BODIPY core, but also provides the near-IR fluorescent dyes which are highly important for biological aspects. In this study, Hg (II) selective crown ether moiety was incorporated to 1&7 positions and 3&5 positions. According to the attached positions, the optical properties of these two isomers demonstrate different signaling features. This difference is explained in terms of orbital analysis. Moreover, water-soluble equivalents were synthesized to make these dyes biologically applicable. In addition to absorbance and fluorescence measurements, ITC experiments gave information about binding characteristics.

Light harvesting concept is harnessed in Chapter 4. Light harvesting energy transfer cassettes were synthesized by a convergent synthesis methodology via “click chemistry” on versatile BODIPY dyes. Effective through-space energy transfer occurs from peripheral BODIPY and distryl-BODIPY units to a 1,3,5,7-tetrastyryl functionalized near IR emissive BODIPY core. The resulting cassettes are the first examples of tetrastyryl-BODIPY based light harvesting systems and highly promising candidates for design and synthesis of similar structures. Furthermore, the determination of energy transfer efficiency is performed as a plot of dividing

normalized absorption and excitation spectra as a function of wavelength. This calculation gives better result considering the large multichromophoric systems.

Chapter 5 is about the coupling of excitation energy transfer with internal charge transfer in the Hg (II) sensing. Internal charge transfer is a known signaling process which is highly utilized in the design of chemosensors. Incorporation of this mechanism with excitation energy transfer offers increment in pseudo-Stokes shifts and signaling characteristics can be observed in a broader range. Thus, in our design, two BODIPY dyes were designed as donor and acceptor moieties. Acceptor moiety involves the Hg (II) selective crown ether part. With the binding of Hg (II) ions, the acceptor moiety shows blue shift resulting increase in spectral overlap and so energy transfer.

Design and synthesis of BODIPY-based probe for biological thiols both chromogenically and fluorogenically in aqueous solution is described in Chapter 6. Biological thiols are cysteine, homocysteine and glutathione. The abnormal concentrations play crucial roles on different deficiencies and diseases. Hence, the fluorescent detection of biological thiols is highly important. With this sense, two BODIPY-based probes carrying thiol reactive nitro-ethenyl groups were designed and characterized with spectroscopic measurements. Results show that both probes demonstrate “turn on” fluorescence response to cysteine, homocysteine and glutathione due to the blocking PeT process with reaction between thiol group and nitroethenyl moiety. However, the controlling of reaction time facilitates the faster response

In Chapter 7, highly selective, fast responding near-IR BODIPY-based hydrogen sulfide probe is explained. Being a biosynthetic gasotransmitter, hydrogen sulfide has important roles on biological processes such as cardiovascular protection, neuroprotective effect, arrangement of cell growth, calcium homeostasis and regulation of neurotransmission. Due to the function of hydrogen sulfide in metabolic processes, the real-time monitoring of this small molecule becomes very important. Hence, we designed BODIPY-based probe having hydrogen sulfide reactive two arylazido groups and triethylene groups to enhance water solubility.

With the addition of hydrogen sulfide, 20 nm red shift is observed in absorption spectra and decrease in fluorescence intensity due to the PeT process. This selective and fast responding probe was utilized for in vitro imaging studies.

In Chapter 8, our aim is to conjugate persistent luminescent nanoparticles to get the activation of photodynamic action. To eliminate the use of external light problem in photodynamic therapy, we thought to use persistent luminescent nanoparticles capable of emitting light for hours without need for external irradiation once irradiated. A BODIPY derivative was incorporated to persistent luminescent nanoparticles to get photodynamic action. Singlet oxygen generation measurements showed efficiency of the design principle. This BODIPY part will be attached to quencher part via glutathione responsive disulfide bridge to be effective in cancer cells. In conclusion, this nanoassemble is a promising model for photodynamic therapy by suggesting solution to problem of light which limits the widespread usage of photodynamic therapy.

BIBLIOGRAPHY

(1) Tsien, R. Y. New calcium indicators and buffers with high selectivity against magnesium and protons: design, synthesis, and properties of prototype structures. *Biochemistry* **1980**, *19*, 2396-2404.

(2) Lakowicz, J. R.: *Principles of Molecular Fluorescence*; 3 rd ed.; Plenum: New York, 2009.

(3) Kim, S. K.; Yoon, J. A new fluorescent PET chemosensor for fluoride ions. *Chem. Commun.* **2002**, 770-771.

(4) Valeur, B.: *Molecular Fluorescence*; Wiley, WHC: Weinheim, 2002.

(5) Beer, P. D.; Gale, P. A. Anion recognition and sensing: The state of the art and future perspectives. *Angew. Chem. Int. Edit.* **2001**, *40*, 486-516.

(6) de Silva, A. P. Luminescent Photoinduced Electron Transfer (PET) Molecules for Sensing and Logic Operations. *J. Phys. Chem. Lett.* **2011**, *2*, 2865-2871.

(7) Koutaka, H.; Kosuge, J.; Fukasaku, N.; Hirano, T.; Kikuchi, K.; Urano, Y.; Kojima, H.; Nagano, T. A novel fluorescent probe for zinc ion based on boron dipyrromethene (BODIPY) chromophore. *Chem. & Pharm. Bull.* **2004**, *52*, 700-703.

(8) Fujikawa, Y.; Urano, Y.; Komatsu, T.; Hanaoka, K.; Kojima, H.; Terai, T.; Inoue, H.; Nagano, T. Design and Synthesis of Highly Sensitive Fluorogenic Substrates for Glutathione S-Transferase and Application for Activity Imaging in Living Cells. *J. Am. Chem. Soc.* **2008**, *130*, 14533-14543.

(9) Wang, X.; Cui, L.; Zhou, N.; Zhu, W.; Wang, R.; Qian, X.; Xu, Y. A highly selective and sensitive near-infrared fluorescence probe for arylamine N-acetyltransferase 2 in vitro and in vivo. *Chem. Sci.* **2013**, *4*, 2936-2940.

(10) Zhang, H.; Fan, J. L.; Wang, J. Y.; Zhang, S. Z.; Dou, B. R.; Peng, X. J. An Off-On COX-2-Specific Fluorescent Probe: Targeting the Golgi Apparatus of Cancer Cells. *J. Am. Chem. Soc.* **2013**, *135*, 11663-11669.

(11) Wada, M.; Ito, S.; Uno, H.; Murashima, T.; Ono, N.; Urano, T.; Urano, Y. Synthesis and optical properties of a new class of pyrromethene-BF2 complexes fused with rigid bicyclo rings and benzo derivatives. *Tetrahedron Lett.* **2001**, *42*, 6711-6713.

(12) Thoresen, L. H.; Kim, H.; Welch, M. B.; Burghart, A.; Burgess, K. Synthesis of 3,5-diaryl-4,4-difluoro-4-bora-3a,4a-diaza-s-indacene (BODIPY) dyes. *Synlett* **1998**, 1276-1278.

(13) Atilgan, S.; Kutuk, I.; Ozdemir, T. A near IR di-styryl BODIPY-based ratiometric fluorescent chemosensor for Hg(II). *Tetrahedron Lett.* **2010**, *51*, 892-894.

(14) Jyothikumar, V.; Sun, Y.; Periasamy, A. Label Free Fluorescence Lifetime FRET Imaging. *Biophys. J.* **2013**, *104*, 671a-671a.

(15) Webber, S. E. Photon-Harvesting Polymers. *Chem. Rev.* **1990**, *90*, 1469-1482.

(16) Balzani, V. C., A.; Venturi, M. : *Molecular Devices and Machines – A Journey into the Nano World*; Wiley-VCH, 2002.

(17) Turro, N. J.: *Modern Molecular Photochemistry*; University Science Books: Sausalito, 1991.

(18) Dexter, D. L. A Theory of Sensitized Luminescence in Solids. *J. Chem. Phys.* **1953**, *21*, 836-850.

(19) Papageorgiou, G. C.: *Chlorophyll a Fluorescence: A Signature of Photosynthesis*; Springer Netherlands, 2004.

(20) Harriman, A.; Mallon, L. J.; Elliot, K. J.; Haefele, A.; Ulrich, G.; Ziessel, R. Length Dependence for Intramolecular Energy Transfer in Three- and Four-Color Donor-Spacer-Acceptor Arrays. *J. Am. Chem. Soc.* **2009**, *131*, 13375-13386.

(21) Jares-Erijman, E. A.; Jovin, T. M. FRET imaging. *Nat. Biotechnol.* **2003**, *21*, 1387-1395.

(22) Miyawaki, A.; Llopis, J.; Heim, R.; McCaffery, J. M.; Adams, J. A.; Ikura, M.; Tsien, R. Y. Fluorescent indicators for Ca2+ based on green fluorescent proteins and calmodulin. *Nature* **1997**, *388*, 882-887.

(23) Khrapunov, S.; Brenowitz, M.; Rice, P. A.; Catalano, C. E. Binding then bending: A mechanism for wrapping DNA. *P. Natl. Acad. Sci. USA* **2006**, *103*, 19217-19218.

(24) Praveen, V. K.; Ranjith, C.; Bandini, E.; Ajayaghosh, A.; Armaroli, N. Oligo(phenylenevinylene) hybrids and self-assemblies: versatile materials for excitation energy transfer. *Chem. Soc. Rev.* **2014**, *43*, 4222-4242.

(25) Zhang, X. L.; Xiao, Y.; Qian, X. H. Highly efficient energy transfer in the light harvesting system composed of three kinds of boron-dipyrromethene derivatives. *Org. Lett.* **2008**, *10*, 29-32.

(26) Liu, Z. P.; He, W. J.; Guo, Z. J. Metal coordination in photoluminescent sensing. *Chem. Soc. Rev.* **2013**, *42*, 1568-1600.

(27) Guan, X. Y.; Lin, W. Y.; Huang, W. M. Development of a new rhodamine-based FRET platform and its application as a Cu2+ probe. *Org. Biomol. Chem.* **2014**, *12*, 3944-3949.

(28) Sreenath, K.; Allen, J. R.; Davidson, M. W.; Zhu, L. A FRET-based indicator for imaging mitochondrial zinc ions. *Chem. Commun.* **2011**, *47*, 11730-11732.

(29) Dittmer, P. J.; Miranda, J. G.; Gorski, J. A.; Palmer, A. E. Genetically Encoded Sensors to Elucidate Spatial Distribution of Cellular Zinc. *J. Biol. Chem.* **2009**, *284*, 16289-16297.

(30) Zhou, Y.; Zhu, C. Y.; Gao, X. S.; You, X. Y.; Yao, C. Hg2+-Selective Ratiometric and "Off-On" Chemosensor Based on the Azadiene-Pyrene Derivative. *Org. Lett.* **2010**, *12*, 2566-2569.

(31) Boens, N.; Leen, V.; Dehaen, W. Fluorescent indicators based on BODIPY. *Chem. Soc. Rev.* **2012**, *41*, 1130-1172.

(32) Escobedo, J. O.; Rusin, O.; Lim, S.; Strongin, R. M. NIR dyes for bioimaging applications. *Curr. Opin. Chem. Biol.* **2010**, *14*, 64-70.

(33) Nolting, D. D.; Gore, J. C.; Pham, W. Near-Infrared Dyes: Probe Development and Applications in Optical Molecular Imaging. *Curr. Org. Synth.* **2011**, *8*, 521-534.

(34) Schmitt, A.; Hinkeldey, B.; Wild, M.; Jung, G. Synthesis of the Core Compound of the BODIPY Dye Class: 4,4'-Difluoro-4-bora-(3a,4a)-diaza-s-indacene. *J. Fluoresc.* **2009**, *19*, 755-758.

(35) Wories, H. J.; Koek, J. H.; Lodder, G.; Lugtenburg, J.; Fokkens, R.; Driessen, O.; Mohn, G. R. A Novel Water-Soluble Fluorescent-Probe - Synthesis, Luminescence and Biological Properties of the Sodium-Salt of the 4-Sulfonato-3,3',5,5'-Tetramethyl-2,2'-Pyrromethen-1,1'-Bf2 Complex. *Recl. Trav. Chim. Pay. B* **1985**, *104*, 288-291.

(36) Pavlopoulos, T. G.; Boyer, J. H.; Shah, M.; Thangaraj, K.; Soong, M. L. Laser Action from 2,6,8-Position Trisubstituted 1,3,5,7-Tetramethylpyrromethene-Bf2 Complexes .1. *Appl. Opt.* **1990**, *29*, 3885-3886.

(37) Atilgan, S.; Ekmekci, Z.; Dogan, A. L.; Guc, D.; Akkaya, E. U. Water soluble distyryl-boradiazaindacenes as efficient photosensitizers for photodynamic therapy. *Chem. Commun.* **2006**, 4398-4400.

(38) Jiao, L. J.; Yu, C. J.; Li, J. L.; Wang, Z. Y.; Wu, M.; Hao, E. H. beta-Formyl-BODIPYs from the Vilsmeier-Haack Reaction. *J. Org. Chem.* **2009**, *74*, 7525-7528.

(39) Thivierge, C.; Bandichhor, R.; Burgess, K. Spectral dispersion and water solubilization of BODIPY dyes via palladium-catalyzed C-H functionalization. *Org. Lett.* **2007**, *9*, 2135-2138.

(40) Loudet, A.; Burgess, K. BODIPY dyes and their derivatives: Syntheses and spectroscopic properties. *Chem. Rev.* **2007**, *107*, 4891-4932.

(41) Rurack, K.; Kollmannsberger, M.; Daub, J. A highly efficient sensor molecule emitting in the near infrared (NIR): 3,5-distyryl-8-(p-dimethylaminophenyl)difluoroboradiaza-s-indacene. *New J. Chem.* **2001**, *25*, 289-292.

(42) Yu, Y. H.; Descalzo, A. B.; Shen, Z.; Rohr, H.; Liu, Q.; Wang, Y. W.; Spieles, M.; Li, Y. Z.; Rurack, K.; You, X. Z. Mono- and di(dimethylamino) styryl-substituted borondipyrromethene and borondiindomethene dyes with intense near-infrared fluorescence. *Chem.-Asian J.* **2006**, *1*, 176-187.

(43) Buyukcakir, O.; Bozdemir, O. A.; Kolemen, S.; Erbas, S.; Akkaya, E. U. Tetrastyryl-Bodipy Dyes: Convenient Synthesis and Characterization of Elusive Near IR Fluorophores. *Org. Lett.* **2009**, *11*, 4644-4647.

(44) Bura, T.; Retailleau, P.; Ulrich, G.; Ziessel, R. Highly Substituted Bodipy Dyes with Spectroscopic Features Sensitive to the Environment. *J. Org. Chem.* **2011**, *76*, 1109-1117.

(45) Zhu, S. L.; Zhang, J. T.; Vegesna, G.; Tiwari, A.; Luo, F. T.; Zeller, M.; Luck, R.; Li, H. H.; Green, S.; Liu, H. Y. Controlled Knoevenagel reactions of methyl groups of 1,3,5,7-tetramethyl BODIPY dyes for unique BODIPY dyes. *RSC Adv.* **2012**, *2*, 404-407.

(46) Nolan, E. M.; Lippard, S. J. Tools and tactics for the optical detection of mercuric ion. *Chem. Rev.* **2008**, *108*, 3443-3480.

(47) Gutknecht, J. Inorganic Mercury (Hg2+) Transport through Lipid Bilayer-Membranes. *J. Membr. Biol.* **1981**, *61*, 61-66.

(48) Kaur, P.; Aschner, M.; Syversen, T. Glutathione modulation influences methyl mercury induced neurotoxicity in primary cell cultures of neurons and astrocytes. *Neurotoxicology* **2006**, *27*, 492-500.

(49) Milaeva, E. R. The role of radical reactions in organomercurials impact on lipid peroxidation. *J. Inorg. Biochem.* **2006**, *100*, 905-915.

(50) Zhang, X. L.; Xiao, Y.; Qian, X. H. A Ratiometric Fluorescent Probe Based on FRET for Imaging Hg2+ Ions in Living Cells. *Angew. Chem. Int. Edit.* **2008**, *47*, 8025-8029.

(51) Wang, J. B.; Qian, X. H. A series of polyamide receptor based PET fluorescent sensor molecules: Positively cooperative Hg2+ ion binding with high sensitivity. *Org. Lett.* **2006**, *8*, 3721-3724.

(52) Yuan, M. J.; Li, Y. L.; Li, J. B.; Li, C. H.; Liu, X. F.; Lv, J.; Xu, J. L.; Liu, H. B.; Wang, S.; Zhu, D. A colorimetric and fluorometric dual-modal assay for mercury ion by a molecule. *Org. Lett.* **2007**, *9*, 2313-2316.

(53) Deneke, S. M. Thiol-based antioxidants. *Curr. Top. Cell. Regul.* **2000**, *36*, 151-180.

(54) Jocelyn, P. C.: *Biochemistry of the SH Group*; Academic Press: New York, 1972.

(55) Osman, L. P., Mitchell, S.C., Waring, R.H. Cysteine, its Metabolism and Toxicity. *Sulfur Rep.* , *20*, 155-172.

(56) Wang, K.; Peng, H.; Wang, B. Recent Advances in Thiol and Sulfide Reactive Probes. *J. Cell. Biochem.* **2014**, *115*, 1007–1022.

(57) Wu, G. Y.; Fang, Y. Z.; Yang, S.; Lupton, J. R.; Turner, N. D. Glutathione metabolism and its implications for health. *J. Nutr.* **2004**, *134*, 489-492.

(58) Koval, I. V. Reactions of thiols. *Russ. J. Org. Chem.* **2007**, *43*, 319-346.

(59) Kand, D.; Kalle, A. M.; Varma, S. J.; Talukdar, P. A chromenoquinoline-based fluorescent off-on thiol probe for bioimaging. *Chem. Commun.* **2012**, *48*, 2722-2724.

(60) Lin, W. Y.; Yuan, L.; Cao, Z. M.; Feng, Y. M.; Long, L. L. A Sensitive and Selective Fluorescent Thiol Probe in Water Based on the Conjugate 1,4-Addition of Thiols to alpha,beta-Unsaturated Ketones. *Chem.-Eur. J.* **2009**, *15*, 5096-5103.

(61) Wang, H. L.; Zhou, G. D.; Mao, C.; Chen, X. Q. A fluorescent sensor bearing nitroolefin moiety for the detection of thiols and its biological imaging. *Dyes Pigm.* **2013**, *96*, 232-236.

(62) Chen, X.; Ko, S. K.; Kim, M. J.; Shin, I.; Yoon, J. A thiol-specific fluorescent probe and its application for bioimaging. *Chem. Commun.* **2010**, *46*, 2751-2753.

(63) Maeda, H.; Matsuno, H.; Ushida, M.; Katayama, K.; Saeki, K.; Itoh, N. 2,4-dinitrobenzenesulfonyl fluoresceins as fluorescent alternatives to Ellman's reagent in thiol-quantification enzyme assays. *Angew. Chem. Int. Edit.* **2005**, *44*, 2922-2925.

(64) Rusin, O.; St Luce, N. N.; Agbaria, R. A.; Escobedo, J. O.; Jiang, S.; Warner, I. M.; Dawan, F. B.; Lian, K.; Strongin, R. M. Visual detection of cysteine and homocysteine. *J. Am. Chem. Soc.* **2004**, *126*, 438-439.

(65) Wang, W. H.; Rusin, O.; Xu, X. Y.; Kim, K. K.; Escobedo, J. O.; Fakayode, S. O.; Fletcher, K. A.; Lowry, M.; Schowalter, C. M.; Lawrence, C. M.; Fronczek, F. R.;

Warner, I. M.; Strongin, R. M. Detection of homocysteine and cysteine. *J. Am. Chem. Soc.* **2005**, *127*, 15949-15958.

(66) Cao, X. W.; Lin, W. Y.; Yu, Q. X. A Ratiometric Fluorescent Probe for Thiols Based on a Tetrakis (4-hydroxyphenyl)porphyrin-Coumarin Scaffold. *J. Org. Chem.* **2011**, *76*, 7423-7430.

(67) Jung, H. S.; Han, J. H.; Habata, Y.; Kang, C.; Kim, J. S. An iminocoumarin-Cu(II) ensemble-based chemodosimeter toward thiols. *Chem. Commun.* **2011**, *47*, 5142-5144.

(68) Duan, C. X.; Liu, Y. G. Recent Advances in Fluorescent Probes for Monitoring of Hydrogen Sulfide. *Curr. Med. Chem.* **2013**, *20*, 2929-2937.

(69) Pluth, M. D.; Bailey, T. S.; Hammers, M. D.; Montoya, L. A. Chemical Tools for Studying Biological Hydrogen Sulfide. *ACS Sym. Ser.* **2013**, *1152*, 15-32.

(70) Hyspler, R.; Ticha, A.; Indrova, M.; Zadak, Z.; Hysplerova, L.; Gasparic, J.; Churacek, J. A simple, optimized method for the determination of sulphide in whole blood by GC-MS as a marker of bowel fermentation processes. *J. Chromatogr. B Analyt. Technol. Biomed. Life Sci.* **2002**, *770*, 255-259.

(71) Baskar, R.; Bian, J. S. Hydrogen sulfide gas has cell growth regulatory role. *Eur. J. Pharmacol.* **2011**, *656*, 5-9.

(72) Szabo, G.; Veres, G.; Radovits, T.; Gero, D.; Modis, K.; Miesel-Groschel, C.; Horkay, F.; Karck, M.; Szabo, C. Cardioprotective effects of hydrogen sulfide. *Nitric Oxide-Biol. Ch.* **2011**, *25*, 201-210.

(73) Szabo, C.; PapaPeTropoulos, A. Hydrogen sulphide and angiogenesis: mechanisms and applications. *Brit. J. Pharmacol.* **2011**, *164*, 853-865.

(74) Jha, S.; Calvert, J. W.; Duranski, M. R.; Ramachandran, A.; Lefer, D. J. Hydrogen sulfide attenuates hepatic ischemia-reperfusion injury: role of antioxidant and antiapoptotic signaling. *Am. J. Physiol.-Heart. C* **2008**, *295*, H801-H806.

(75) Wang, R. Hydrogen Sulfide: The Third Gasotransmitter in Biology and Medicine. *Antioxid. Redox Sign.* **2010**, *12*, 1061-1064.

(76) Qian, Y.; Zhang, L.; Ding, S. T.; Deng, X.; He, C.; Zheng, X. E.; Zhu, H. L.; Zhao, J. A fluorescent probe for rapid detection of hydrogen sulfide in blood plasma and brain tissues in mice. *Chem. Sci.* **2012**, *3*, 2920-2923.

(77) Zhang, J. Y.; Sun, Y. Q.; Liu, J.; Shi, Y. W.; Guo, W. A fluorescent probe for the biological signaling molecule H2S based on a specific H2S trap group. *Chem. Commun.* **2013**, *49*, 11305-11307.

(78) Lippert, A. R.; New, E. J.; Chang, C. J. Reaction-Based Fluorescent Probes for Selective Imaging of Hydrogen Sulfide in Living Cells. *J. Am. Chem. Soc.* **2011**, *133*, 10078-10080.

(79) Yu, F. B. A.; Li, P.; Song, P.; Wang, B. S.; Zhao, J. Z.; Han, K. L. An ICT-based strategy to a colorimetric and ratiometric fluorescence probe for hydrogen sulfide in living cells. *Chem. Commun.* **2012**, *48*, 2852-2854.

(80) Zheng, K. B.; Lin, W. Y.; Tan, L. A phenanthroimidazole-based fluorescent chemosensor for imaging hydrogen sulfide in living cells. *Org. Biomol. Chem.* **2012**, *10*, 9683-9688.

(81) Chen, B. F.; Lv, C.; Tang, X. J. Chemoselective reduction-based fluorescence probe for detection of hydrogen sulfide in living cells. *Anal. Bioanal. Chem.* **2012**, *404*, 1919-1923.

(82) Zhou, G. D.; Wang, H. L.; Ma, Y.; Chen, X. Q. An NBD fluorophore-based colorimetric and fluorescent chemosensor for hydrogen sulfide and its application for bioimaging. *Tetrahedron* **2013**, *69*, 867-870.

(83) Das, S. K.; Lim, C. S.; Yang, S. Y.; Han, J. H.; Cho, B. R. A small molecule two-photon probe for hydrogen sulfide in live tissues. *Chem. Commun.* **2012**, *48*, 8395-8397.

(84) Wan, Q. Q.; Song, Y. C.; Li, Z.; Gao, X. H.; Ma, H. M. In vivo monitoring of hydrogen sulfide using a cresyl violet-based ratiometric fluorescence probe. *Chem. Commun.* **2013**, *49*, 502-504.

(85) Qian, Y.; Karpus, J.; Kabil, O.; Zhang, S. Y.; Zhu, H. L.; Banerjee, R.; Zhao, J.; He, C. Selective fluorescent probes for live-cell monitoring of sulphide. *Nat. Commun.* **2011**, *2-7*.

(86) Liu, C. R.; Peng, B.; Li, S.; Park, C. M.; Whorton, A. R.; Xian, M. Reaction Based Fluorescent Probes for Hydrogen Sulfide. *Org. Lett.* **2012**, *14*, 2184-2187.

(87) Liu, J.; Sun, Y. Q.; Zhang, J. Y.; Yang, T.; Cao, J. B.; Zhang, L. S.; Guo, W. A Ratiometric Fluorescent Probe for Biological Signaling Molecule H2S: Fast Response and High Selectivity. *Chem.-Eur. J.* **2013**, *19*, 4717-4722.

(88) Choi, M. G.; Cha, S.; Lee, H.; Jeon, H. L.; Chang, S. K. Sulfide-selective chemosignaling by a Cu2+ complex of dipicolylamine appended fluorescein. *Chem. Commun.* **2009**, 7390-7392.

(89) Wilson, B. C. Photodynamic therapy for cancer: Principles. *Can. J. Gastroenterol.* **2002**, *16*, 393-396.

(90) Dai, T. H.; Fuchs, B. B.; Coleman, J. J.; Prates, R. A.; Astrakas, C.; St Denis, T. G.; Ribeiro, M. S.; Mylonakis, E.; Hamblin, M. R.; Tegos, G. P. Concepts and principles of photodynamic therapy as an alternative antifungal discovery platform. *Front. Microbiol.* **2012**, *3,* 1-16.

(91) Sternberg, E. D.; Dolphin, D.; Bruckner, C. Porphyrin-based photosensitizers for use in photodynamic therapy. *Tetrahedron* **1998**, *54*, 4151-4202.

(92) Robertson, C. A.; Evans, D. H.; Abraharnse, H. Photodynamic therapy (PDT): A short review on cellular mechanisms and cancer research applications for PDT. *J. Photoch. Photobio. B* **2009**, *96*, 1-8.

(93) Castano, A. P.; Demidova, T. N.; Hamblin, M. R. Mechanisms in photodynamic therapy: part one-photosensitizers, photochemistry and cellular localization. *Photodiagn. Photodyn.* **2004**, *1*, 279-293.

(94) Ravanat, J. L.; Cadet, J. Reaction of Singlet Oxygen with 2'-Deoxyguanosine and DNA - Isolation and Characterization of the Main Oxidation-Products. *Chem. Res. Toxicol.* **1995**, *8*, 379-388.

(95) Plaetzer, K.; Krammer, B.; Berlanda, J.; Berr, F.; Kiesslich, T. Photophysics and photochemistry of photodynamic therapy: fundamental aspects. *Laser Med. Sci.* **2009**, *24*, 259-268.

(96) Moan, J.; Berg, K. The Photodegradation of Porphyrins in Cells Can Be Used to Estimate the Lifetime of Singlet Oxygen. *Photochem. Photobiol.* **1991**, *53*, 549-553.

(97) Mang, T. S. Lasers and light sources for PDT: past, present and future. *Photodiagn. Photodyn.* **2004**, *1*, 43-48.

(98) Huang, Z. A review of progress in clinical photodynamic therapy. *Technol. Cancer Res. T.* **2005**, *4*, 283-293.

(99) Wilson, B. C.; Jeeves, W. P.; Lowe, D. M. Invivo and Post-Mortem Measurements of the Attenuation Spectra of Light in Mammalian-Tissues. *Photochem. Photobiol.* **1985**, *42*, 153-162.

(100) Wainwright, M. Non-porphyrin photosensitizers in biomedicine. *Chem. Soc. Rev.* **1996**, *25*, 351-359.

(101) Zhuang, S. G.; Lynch, M. C.; Kochevar, I. E. Caspase-8 mediates caspase-3 activation and cytochrome c release during singlet oxygen-induced apoptosis of HL-60 cells. *Exp. Cell. Res.* **1999**, *250*, 203-212.

(102) Kamkaew, A.; Lim, S. H.; Lee, H. B.; Kiew, L. V.; Chung, L. Y.; Burgess, K. BODIPY dyes in photodynamic therapy. *Chem. Soc. Rev.* **2013**, *42*, 77-88.

(103) Yogo, T.; Urano, Y.; Ishitsuka, Y.; Maniwa, F.; Nagano, T. Highly efficient and photostable photosensitizer based on BODIPY chromophore. *J. Am. Chem. Soc.* **2005**, *127*, 12162-12163.

(104) Guldi, D. M.; Prato, M. Excited-state properties of C-60 fullerene derivatives. *Acc. Chem. Res.* **2000**, *33*, 695-703.

(105) Huang, L.; Yu, X. R.; Wu, W. H.; Zhao, J. Z. Styryl Bodipy-C-60 Dyads as Efficient Heavy-Atom-Free Organic Triplet Photosensitizers. *Org. Lett.* **2012**, *14*, 2594-2597.

(106) De Rosa, F. S.; Bentley, M. V. L. B. Photodynamic therapy of skin cancers: Sensitizers, clinical studies and future directives. *Pharm. Res.* **2000**, *17*, 1447-1455.

(107) Plaetzer, K.; Kiesslich, T.; Krammer, B.; Hammerl, P. Characterization of the cell death modes and the associated changes in cellular energy supply in response to AlPcS4-PDT. *Photoch. Photobio. Sci.* **2002**, *1*, 172-177.

(108) PeTtigrew, C. A.; Cotter, T. G. Deregulation of Cell Death (Apoptosis): Implications for Tumor Development. *Discov. Med.* **2009**, *8*, 61-63.

(109) Perfettini, J. L.; Kroemer, G. Caspase activation is not death. *Nat. Immunol.* **2003**, *4*, 308-310.

(110) Mroz, P.; Yaroslavsky, A.; Kharkwal, G. B.; Hamblin, M. R. Cell Death Pathways in Photodynamic Therapy of Cancer. *Cancers* **2011**, *3*, 2516-2539.

(111) Savill, J.; Fadok, V. Corpse clearance defines the meaning of cell death. *Nature* **2000**, *407*, 784-788.

(112) Castano, A. P.; Demidova, T. N.; Hamblin, M. R. Mechanisms in photodynamic therapy: part two-cellular signaling, cell metabolism and modes of cell death. *Photodiagn. Photodyn.* **2005**, *2*, 1-23.

(113) Castano, A. P.; Demidova, T. N.; Hamblin, M. R. Mechanisms in photodynamic therapy: Part three- Photosensitizer pharmacokinetics, biodistribution, tumor localization and modes of tumor destruction. *Photodiagn. Photodyn.* **2005**, *2*, 91-106.

(114) Lovell, J. F.; Liu, T. W. B.; Chen, J.; Zheng, G. Activatable Photosensitizers for Imaging and Therapy. *Chem. Rev.* **2010**, *110*, 2839-2857.

(115) Texier, I.; Heinrich, E. Inhibition of fluorescent dyes for the design of efficient activatable probes dedicated to non-invasive small animal imaging - art. no. 64490I. *P. Soc. Photo-Opt. Ins.* **2007**, *6449*, I4490-I4490.

(116) Razkin, J.; Josserand, V.; Boturyn, D.; Jin, Z. H.; Dumy, P.; Favrot, M.; Coll, J. L.; Texier, I. Activatable fluorescent probes for tumour-targeting imaging in live mice. *Chem. Med. Chem.* **2006**, *1*, 1069-1072.

(117) Wang, J.; You, M. X.; Zhu, G. Z.; Shukoor, M. I.; Chen, Z.; Zhao, Z. L.; Altman, M. B.; Yuan, Q.; Zhu, Z.; Chen, Y.; Huang, C. Z.; Tan, W. H. Photosensitizer-Gold Nanorod Composite for Targeted Multimodal Therapy. *Small* **2013**, *9*, 3678-3684.

(118) Ducry, L.; Stump, B. Antibody-Drug Conjugates: Linking Cytotoxic Payloads to Monoclonal Antibodies. *Bioconjugate Chem.* **2010**, *21*, 5-13.

(119) Yeh, C. C.; Hou, M. F.; Wu, S. H.; Tsai, S. M.; Lin, S. K.; Hou, L. A.; Ma, H.; Tsai, L. Y. A study of glutathione status in the blood and tissues of patients with breast cancer. *Cell Biochem. Funct.* **2006**, *24*, 555-559.

(120) Barranco, S. C.; Perry, R. R.; Durm, M. E.; Quraishi, M.; Werner, A. L.; Gregorcyk, S. G.; Kolm, P. Relationship between colorectal cancer glutathione levels and patient survival - Early results. *Dis. Colon Rectum.* **2000**, *43*, 1133-1140.

(121) Yang, J.; Chen, H.; Vlahov, I. R.; Cheng, J. X.; Low, P. S. Evaluation of disulfide reduction during receptor-mediated endocytosis by using FRET imaging. *P. Natl. Acad. Sci. USA* **2006**, *103*, 13872-13877.

(122) Lau, J. T. F.; Lo, P. C.; Jiang, X. J.; Wang, Q.; Ng, D. K. P. A Dual Activatable Photosensitizer toward Targeted Photodynamic Therapy. *J. Med. Chem.* **2014**, *57*, 4088-4097.

(123) Harvey, E. N.: *A history of luminescence : from the earliest times until 1900*; American Philosophical Society: Philadelphia,, 1957.

(124) Murayama, Y.: *in Phosphor Handbook*; CRC Press: Boca Raton, 1999.

(125) Hoogenstraaten, W.; Klasens, H. A. Some Properties of Zinc Sulfide Activated with Copper and Cobalt. *J. Electrochem. Soc.* **1953**, *100*, 366-375.

(126) Matsuzawa, T.; Aoki, Y.; Takeuchi, N.; Murayama, Y. New long phosphorescent phosphor with high brightness, SrAl2O4:Eu2+,Dy3+. *J. Electrochem. Soc.* **1996**, *143*, 2670-2673.

(127) Pan, Z. W.; Lu, Y. Y.; Liu, F. Sunlight-activated long-persistent luminescence in the near-infrared from Cr3+-doped zinc gallogermanates. *Nat. Mater.* **2012**, *11*, 58-63.

(128) Van den Eeckhout, K.; Smet, P. F.; Poelman, D. Luminescent Afterglow Behavior in the M2Si5N8: Eu Family (M = Ca, Sr, Ba). *Materials* **2011**, *4*, 980-990.

(129) Shah, N.; Cerussi, A.; Eker, C.; Espinoza, J.; Butler, J.; Fishkin, J.; Hornung, R.; Tromberg, B. Noninvasive functional optical spectroscopy of human breast tissue. *P. Natl. Acad. Sci. USA* **2001**, *98*, 4420-4425.

(130) Altinoglu, E. I.; Russin, T. J.; Kaiser, J. M.; Barth, B. M.; Eklund, P. C.; Kester, M.; Adair, J. H. Near-Infrared Emitting Fluorophore-Doped Calcium Phosphate Nanoparticles for In Vivo Imaging of Human Breast Cancer. *ACS Nano* **2008**, *2*, 2075-2084.

(131) de Chermont, Q. L.; Chaneac, C.; Seguin, J.; Pelle, F.; Maitrejean, S.; Jolivet, J. P.; Gourier, D.; Bessodes, M.; Scherman, D. Nanoprobes with near-infrared persistent luminescence for in vivo imaging. *P. Natl. Acad. Sci. USA* **2007**, *104*, 9266-9271.

(132) Maldiney, T.; Byk, G.; Wattier, N.; Seguin, J.; Khandadash, R.; Bessodes, M.; Richard, C.; Scherman, D. Synthesis and functionalization of persistent luminescence nanoparticles with small molecules and evaluation of their targeting ability. *Int. J. Pharm.* **2012**, *423*, 102-107.

(133) Wu, B. Y.; Wang, H. F.; Chen, J. T.; Yan, X. P. Fluorescence Resonance Energy Transfer Inhibition Assay for alpha-Fetoprotein Excreted during Cancer Cell Growth Using Functionalized Persistent Luminescence Nanoparticles. *J. Am. Chem. Soc.* **2011**, *133*, 686-688.

(134) Fabian, J.; Nakazumi, H.; Matsuoka, M. Near-Infrared Absorbing Dyes. *Chem. Rev.* **1992**, *92*, 1197-1226.

(135) Loudet, A.; Bandichhor, R.; Burgess, K.; Palma, A.; McDonnell, S. O.; Hall, M. J.; O'Shea, D. F. B,O-Chelated Azadipyrromethenes as Near-IR Probes. *Org. Lett.* **2008**, *10*, 4771-4774.

(136) Goeb, S.; Ziessel, R. Convenient synthesis of green diisoindolodithienylpyrromethene-dialkynyl borane dyes. *Org. Lett.* **2007**, *9*, 737-740.

(137) Ntziachristos, V.; Bremer, C.; Weissleder, R. Fluorescence imaging with near-infrared light: new technological advances that enable in vivo molecular imaging. *Eur. Radiol.* **2003**, *13*, 195-208.

(138) Young, S. W.; Woodburn, K. W.; Wright, M.; Mody, T. D.; Fan, Q.; Sessler, J. L.; Dow, W. C.; Miller, R. A. Lutetium texaphyrin (PCI-0123): A near-infrared, water-soluble photosensitizer. *Photochem. Photobiol.* **1996**, *63*, 892-897.

(139) Guliyev, R.; Coskun, A.; Akkaya, E. U. Design Strategies for Ratiometric Chemosensors: Modulation of Excitation Energy Transfer at the Energy Donor Site. *J. Am. Chem. Soc.* **2009**, *131*, 9007-9013.

(140) He, J. J.; Benko, G.; Korodi, F.; Polivka, T.; Lomoth, R.; Akermark, B.; Sun, L. C.; Hagfeldt, A.; Sundstrom, V. Modified phthalocyanines for efficient near-IR sensitization of nanostructured TiO2 electrode. *J. Am. Chem. Soc.* **2002**, *124*, 4922-4932.

(141) Weissleder, R. A clearer vision for in vivo imaging. *Nat. Biotechnol.* **2001**, *19*, 316-317.

(142) Ozdemir, T.; Kostereli, Z.; Guliyev, R.; Yalcin, S.; Dede, Y.; Akkaya, E. U. Ion responsive near-IR BODIPY dyes: two isomers, two different signals. *RSC Adv.* **2014**, *4*, 14915-14918.

(143) Erbas, S.; Gorgulu, A.; Kocakusakogullari, M.; Akkaya, E. U. Non-covalent functionalized SWNTs as delivery agents for novel Bodipy-based potential PDT sensitizers. *Chem. Commun.* **2009**, 4956-4958.

(144) Bozdemir, O. A.; Guliyev, R.; Buyukcakir, O.; Selcuk, S.; Kolemen, S.; Gulseren, G.; Nalbantoglu, T.; Boyaci, H.; Akkaya, E. U. Selective Manipulation of ICT and PET Processes in Styryl-Bodipy Derivatives: Applications in Molecular Logic and Fluorescence Sensing of Metal Ions. *J. Am. Chem. Soc.* **2010**, *132*, 8029-8036.

(145) Lee, C. T.; Yang, W. T.; Parr, R. G. Development of the Colle-Salvetti Correlation-Energy Formula into a Functional of the Electron-Density. *Phys. Rev. B* **1988**, *37*, 785-789.

(146) Stevens, W. J.; Basch, H.; Krauss, M. Compact Effective Potentials and Efficient Shared-Exponent Basis-Sets for the 1st-Row and 2nd-Row Atoms. *J. Chem. Phys.* **1984**, *81*, 6026-6033.

(147) Duman, S.; Cakmak, Y.; Kolemen, S.; Akkaya, E. U.; Dede, Y. Heavy Atom Free Singlet Oxygen Generation: Doubly Substituted Configurations Dominate S-1 States of Bis-BODIPYs. *J. Org. Chem.* **2012**, *77*, 4516-4527.

(148) Hehre, W. J.; Ditchfield, R.; Pople, J. A. Self—Consistent Molecular Orbital Methods. XII. Further Extensions of Gaussian—Type Basis Sets for Use in Molecular Orbital Studies of Organic Molecules *J. Chem. Phys.* **1972**, *56*, 2257-2261.

(149) Dunning, T. H. Gaussian-Basis Sets for Use in Correlated Molecular Calculations .1. The Atoms Boron through Neon and Hydrogen. *J. Chem. Phys.* **1989**, *90*, 1007-1023.

(150) Frish, M. J. e. a. Gaussian 03, revision c. 02; Gaussian. *Inc., Wallingford, CT* **2004**, *4*.

(151) Förster, T. Z. *Naturforsch. Teil A.* **1949**, *4*, 321-342.

(152) Coskun, A.; Akkaya, E. U. Signal ratio amplification via modulation of resonance energy transfer: Proof of principle in an emission ratiometric Hg(II) sensor. *J. Am. Chem. Soc.* **2006**, *128*, 14474-14475.

(153) Kolemen, S.; Bozdemir, O. A.; Cakmak, Y.; Barin, G.; Erten-Ela, S.; Marszalek, M.; Yum, J. H.; Zakeeruddin, S. M.; Nazeeruddin, M. K.; Gratzel, M.; Akkaya, E. U. Optimization of distyryl-Bodipy chromophores for efficient panchromatic sensitization in dye sensitized solar cells. *Chem. Sci.* **2011**, *2*, 949-954.

(154) Burghart, A.; Thoresen, L. H.; Chen, J.; Burgess, K.; Bergstrom, F.; Johansson, L. B. A. Energy transfer cassettes based on BODIPY (R) dyes. *Chem. Commun.* **2000**, 2203-2204.

(155) Wan, C. W.; Burghart, A.; Chen, J.; Bergstrom, F.; Johansson, L. B. A.; Wolford, M. F.; Kim, T. G.; Topp, M. R.; Hochstrasser, R. M.; Burgess, K. Anthracene-BODIPY cassettes: Syntheses and energy transfer. *Chem.-Eur. J.* **2003**, *9*, 4430-4441.

(156) Coskun, A.; Akkaya, E. U. Difluorobora-s-diazaindacene dyes as highly selective dosimetric reagents for fluoride anions. *Tetrahedron Lett.* **2004**, *45*, 4947-4949.

(157) Dost, Z.; Atilgan, S.; Akkaya, E. U. Distyryl-boradiazaindacenes: facile synthesis of novel near IR emitting fluorophores. *Tetrahedron* **2006**, *62*, 8484-8488.

(158) Kostereli, Z.; Ozdemir, T.; Buyukcakir, O.; Akkaya, E. U. Tetrastyryl-BODIPY-Based Dendritic Light Harvester and Estimation of Energy Transfer Efficiency. *Org. Lett.* **2012**, *14*, 3636-3639.

(159) Yilmaz, M. D.; Bozdemir, O. A.; Akkaya, E. U. Light harvesting and efficient energy transfer in a boron-dipyrrin (BODIPY) functionalized perylenediimide derivative. *Org. Lett.* **2006**, *8*, 2871-2873.

(160) Bozdemir, O. A.; Yilmaz, M. D.; Buyukcakir, O.; Siemiarczuk, A.; Tutas, M.; Akkaya, E. U. Convergent synthesis and light harvesting properties of dendritic boradiazaindacene (BODIPY) appended perylenediimide dyes. *New J. Chem.* **2010**, *34*, 151-155.

(161) Li, F. R.; Yang, S. I.; Ciringh, Y. Z.; Seth, J.; Martin, C. H.; Singh, D. L.; Kim, D. H.; Birge, R. R.; Bocian, D. F.; Holten, D.; Lindsey, J. S. Design, synthesis, and photodynamics of light-harvesting arrays comprised of a porphyrin and one, two, or eight boron-dipyrrin accessory pigments. *J. Am. Chem. Soc.* **1998**, *120*, 10001-10017.

(162) Hawker, C. J.; Frechet, J. M. J. Preparation of Polymers with Controlled Molecular Architecture - a New Convergent Approach to Dendritic Macromolecules. *J. Am. Chem. Soc.* **1990**, *112*, 7638-7647.

(163) Bozdemir, O. A.; Erbas-Cakmak, S.; Ekiz, O. O.; Dana, A.; Akkaya, E. U. Towards Unimolecular Luminescent Solar Concentrators: Bodipy-Based Dendritic Energy-Transfer Cascade with Panchromatic Absorption and Monochromatized Emission. *Angew. Chem. Int. Edit.* **2011**, *50*, 10907-10912.

(164) Roberts, D. V.; Wittmershaus, B. P.; Zhang, Y. Z.; Swan, S.; Klinosky, M. P. Efficient excitation energy transfer among multiple dyes in polystyrene microspheres. *J. Lumin.* **1998**, *79*, 225-231.

(165) Atilgan, S.; Ozdemir, T.; Akkaya, E. U. Selective Hg(II) Sensing with Improved Stokes Shift by Coupling the Internal Charge Transfer Process to Excitation Energy Transfer. *Org. Lett.* **2010**, *12*, 4792-4795.

(166) de Silva, A. P.; Gunaratne, H. Q. N.; Gunnlaugsson, T.; Huxley, A. J. M.; McCoy, C. P.; Rademacher, J. T.; Rice, T. E. Signaling recognition events with fluorescent sensors and switches. *Chem. Rev.* **1997**, *97*, 1515-1566.

(167) Xu, Z. C.; Yoon, J.; Spring, D. R. Fluorescent chemosensors for Zn2+. *Chem. Soc. Rev.* **2010**, *39*, 1996-2006.

(168) Kim, J. S.; Quang, D. T. Calixarene-derived fluorescent probes. *Chem. Rev.* **2007**, *107*, 3780-3799.

(169) Bourson, J.; Valeur, B. Ion-Responsive Fluorescent Compounds .2. Cation-Steered Intramolecular Charge-Transfer in a Crowned Merocyanine. *J. Phys. Chem.* **1989**, *93*, 3871-3876.

(170) Oguz, U.; Akkaya, E. U. A squaraine-based sodium selective fluorescent chemosensor. *Tetrahedron Lett.* **1998**, *39*, 5857-5860.

(171) De Silva, A. P.; Gunaratne, H. Q. N.; Sandanayake, K. R. A. S. A New Benzo-Annelated Cryptand and a Derivative with Alkali Cation-Sensitive Fluorescence. *Tetrahedron Lett.* **1990**, *31*, 5193-5196.

(172) Ozmen, B.; Akkaya, E. U. Infrared fluorescence sensing of submicromolar calcium: pushing the limits of photoinduced electron transfer. *Tetrahedron Lett.* **2000**, *41*, 9185-9188.

(173) Coskun, A.; Akkaya, E. U. Ion sensing coupled to resonance energy transfer: A highly selective and sensitive ratiometric fluorescent chemosensor for Ag(I) by a modular approach. *J. Am. Chem. Soc.* **2005**, *127*, 10464-10465.

(174) Cakmak, Y.; Akkaya, E. U. Phenylethynyl-BODIPY Oligomers: Bright Dyes and Fluorescent Building Blocks. *Org. Lett.* **2009**, *11*, 85-88.

(175) Rohand, T.; Baruah, M.; Qin, W. W.; Boens, N.; Dehaen, W. Functionalisation of fluorescent BODIPY dyes by nucleophilic substitution. *Chem. Commun.* **2006**, 266-268.

(176) Ulrich, G.; Goze, C.; Guardigli, M.; Roda, A.; Ziessel, R. Pyrromethene dialkynyl borane complexes for "cascatelle" energy transfer and protein labeling. *Angew. Chem. Int. Edit.* **2005**, *44*, 3694-3698.

(177) Rostovtsev, V. V.; Green, L. G.; Fokin, V. V.; Sharpless, K. B. A stepwise Huisgen cycloaddition process: Copper(I)-catalyzed regioselective "ligation" of azides and terminal alkynes. *Angew. Chem. Int. Edit.* **2002**, *41*, 2596-2599.

(178) Deniz, E.; Isbasar, G. C.; Bozdemir, O. A.; Yildirim, L. T.; Siemiarczuk, A.; Akkaya, E. U. Bidirectional switching of near IR emitting boradiazaindacene fluorophores. *Org. Lett.* **2008**, *10*, 3401-3403.

(179) Chen, X.; Zhou, Y.; Peng, X. J.; Yoon, J. Fluorescent and colorimetric probes for detection of thiols. *Chem. Soc. Rev.* **2010**, *39*, 2120-2135.

(180) Jun, M. E.; Roy, B.; Ahn, K. H. "Turn-on" fluorescent sensing with "reactive" probes. *Chem. Commun.* **2011**, *47*, 7583-7601.

(181) Zhang, S.; Ong, C. N.; Shen, H. M. Critical roles of intracellular thiols and calcium in parthenolide-induced apoptosis in human colorectal cancer cells. *Cancer Lett.* **2004**, *208*, 143-153.

(182) Pastore, A.; Piemonte, F.; Locatelli, M.; Lo Russo, A.; Gaeta, L. M.; Tozzi, G.; Federici, G. Determination of blood total, reduced, and oxidized glutathione in pediatric subjects. *Clin. Chem.* **2001**, *47*, 1467-1469.

(183) Townsend, D. M.; Tew, K. D.; Tapiero, H. The importance of glutathione in human disease. *Biomed. Pharmacother.* **2003**, *57*, 145-155.

(184) Ziessel, R.; Ulrich, G.; Harriman, A. The chemistry of Bodipy: a new El Dorado for fluorescence tools. *New J. Chem.* **2007**, *31*, 496-501.

(185) Sunahara, H.; Urano, Y.; Kojima, H.; Nagano, T. Design and synthesis of a library of BODIPY-based environmental polarity sensors utilizing photoinduced electron-transfer-controlled fluorescence ON/OFF switching. *J. Am. Chem. Soc.* **2007**, *129*, 5597-5604.

(186) Baruah, M.; Qin, W. W.; Vallee, R. A. L.; Beljonne, D.; Rohand, T.; Dehaen, W.; Boens, N. A highly potassium-selective ratiometric fluorescent indicator based on BODIPY azacrown ether excitable with visible light. *Org. Lett.* **2005**, *7*, 4377-4380.

(187) Qi, X.; Kim, S. K.; Han, S. J.; Xu, L.; Jee, A. Y.; Kim, H. N.; Lee, C.; Kim, Y.; Lee, M.; Kim, S. J.; Yoon, J. New BODIPY-triazine based tripod fluorescent systems. *Tetrahedron Lett.* **2008**, *49*, 261-264.

(188) Iehl, J.; Nierengarten, J. F.; Harriman, A.; Bura, T.; Ziessel, R. Artificial Light-Harvesting Arrays: Electronic Energy Migration and Trapping on a Sphere and between Spheres. *J. Am. Chem. Soc.* **2012**, *134*, 988-998.

(189) Bozdemir, O. A.; Cakmak, Y.; Sozmen, F.; Ozdemir, T.; Siemiarczuk, A.; Akkaya, E. U. Synthesis of Symmetrical Multichromophoric Bodipy Dyes and Their Facile Transformation into Energy Transfer Cassettes. *Chem.-Eur. J.* **2010**, *16*, 6346-6351.

(190) Gallagher, W. M.; Allen, L. T.; O'Shea, C.; Kenna, T.; Hall, M.; Gorman, A.; Killoran, J.; O'Shea, D. F. A potent nonporphyrin class of photodynamic therapeutic agent: cellular localisation, cytotoxic potential and influence of hypoxia. *Brit. J. Cancer* **2005**, *92*, 1702-1710.

(191) Cakmak, Y.; Kolemen, S.; Duman, S.; Dede, Y.; Dolen, Y.; Kilic, B.; Kostereli, Z.; Yildirim, L. T.; Dogan, A. L.; Guc, D.; Akkaya, E. U. Designing Excited States: Theory-Guided Access to Efficient Photosensitizers for Photodynamic Action. *Angew. Chem. Int. Edit.* **2011**, *50*, 11937-11941.

(192) Guliyev, R.; Ozturk, S.; Kostereli, Z.; Akkaya, E. U. From Virtual to Physical: Integration of Chemical Logic Gates. *Angew. Chem. Int. Edit.* **2011**, *50*, 9826-9831.

(193) Coskun, A.; Deniz, E.; Akkaya, E. U. Effective PET and ICT switching of boradiazaindacene emission: A unimolecular, emission-mode, molecular half-subtractor with reconfigurable logic gates. *Org. Lett.* **2005**, *7*, 5187-5189.

(194) Sun, Y. Q.; Chen, M. L.; Liu, J.; Lv, X.; Li, J. F.; Guo, W. Nitroolefin-based coumarin as a colorimetric and fluorescent dual probe for biothiols. *Chem. Commun.* **2011**, *47*, 11029-11031.

(195) Zhang, M.; Wu, Y. C.; Zhang, S. Z.; Zhu, H. N.; Wu, Q.; Jiao, L. J.; Hao, E. H. A nitroolefin functionalized BODIPY chemodosimeter for biothiols driven by an unexpected conjugated addition mechanism. *Chem. Commun.* **2012**, *48*, 8925-8927.

(196) Isik, M.; Ozdemir, T.; Turan, I. S.; Kolemen, S.; Akkaya, E. U. Chromogenic and Fluorogenic Sensing of Biological Thiols in Aqueous Solutions Using BODIPY-Based Reagents. *Org. Lett.* **2013**, *15*, 216-219.

(197) Lim, S.; Escobedo, J. O.; Lowry, M.; Xu, X. Y.; Strongin, R. Selective fluorescence detection of cysteine and N-terminal cysteine peptide residues. *Chem. Commun.* **2010**, *46*, 5707-5709.

(198) Ros-Lis, J. V.; Garcia, B.; Jimenez, D.; Martinez-Manez, R.; Sancenon, F.; Soto, J.; Gonzalvo, F.; Valldecabres, M. C. Squaraines as fluoro-chromogenic probes for thiol-containing compounds and their application to the detection of biorelevant thiols. *J. Am. Chem. Soc.* **2004**, *126*, 4064-4065.

(199) Hong, V.; Kislukhin, A. A.; Finn, M. G. Thiol-Selective Fluorogenic Probes for Labeling and Release. *J. Am. Chem. Soc.* **2009**, *131*, 9986-9994.

(200) Sibrian-Vazquez, M.; Escobedo, J. O.; Lim, S.; Samoei, G. K.; Strongin, R. M. Homocystamides promote free-radical and oxidative damage to proteins. *P. Natl. Acad. Sci. USA* **2010**, *107*, 551-554.

(201) Guo, Z. Q.; Nam, S.; Park, S.; Yoon, J. A highly selective ratiometric near-infrared fluorescent cyanine sensor for cysteine with remarkable shift and its application in bioimaging. *Chem. Sci.* **2012**, *3*, 2760-2765.

(202) Xuan, W. M.; Sheng, C. Q.; Cao, Y. T.; He, W. H.; Wang, W. Fluorescent Probes for the Detection of Hydrogen Sulfide in Biological Systems. *Angew. Chem. Int. Edit.* **2012**, *51*, 2282-2284.

(203) Kumar, N.; Bhalla, V.; Kumar, M. Recent developments of fluorescent probes for the detection of gasotransmitters (NO, CO and H2S). *Coord. Chem. Rev.* **2013**, *257*, 2335-2347.

(204) Clark, J. E.; Naughton, P.; Shurey, S.; Green, C. J.; Johnson, T. R.; Mann, B. E.; Foresti, R.; Motterlini, R. Cardioprotective actions by a water-soluble carbon monoxide-releasing molecule. *Circ. Res.* **2003**, *93*, E2-E8.

(205) Bilban, M.; Haschemi, A.; Wegiel, B.; Chin, B. Y.; Wagner, O.; Otterbein, L. E. Heme oxygenase and carbon monoxide initiate homeostatic signaling. *J. Mol. Med.* **2008**, *86*, 267-279.

(206) Amersi, F.; Shen, X. D.; Anselmo, D.; Melinek, J.; Iyer, S.; Southard, D. J.; Katori, M.; Volk, H. D.; Busuttil, R. W.; Buelow, R.; Kupiec-Weglinski, J. W. Ex vivo exposure to carbon monoxide prevents hepatic ischemia/reperfusion injury through p38 MAP kinase pathway. *Hepatology* **2002**, *35*, 815-823.

(207) Culotta, E.; Koshland, D. E. No News Is Good-News. *Science* **1992**, *258*, 1862-1865.

(208) Ignarro, L. J.; Cirino, G.; Casini, A.; Napoli, C. Nitric oxide as a signaling molecule in the vascular system: An overview. *J. Cardiovasc. Pharmacol.* **1999**, *34*, 879-886.

(209) Ignarro, L. J. Nitric oxide: A unique endogenous signaling molecule in vascular biology (Nobel lecture). *Angew. Chem. Int. Edit.* **1999**, *38*, 1882-1892.

(210) Predmore, B. L.; Lefer, D. J.; Gojon, G. Hydrogen Sulfide in Biochemistry and Medicine. *Antioxid. Redox Sign.* **2012**, *17*, 119-140.

(211) Lefer, D. J. A new gaseous signaling molecule emerges: Cardioprotective role of hydrogen sulfide. *P. Natl. Acad. Sci. USA* **2007**, *104*, 17907-17908.

(212) PapaPeTropoulos, A.; Pyriochou, A.; Altaany, Z.; Yang, G. D.; Marazioti, A.; Zhou, Z. M.; Jeschke, M. G.; Branski, L. K.; Herndon, D. N.; Wang, R.; Szabo, C. Hydrogen sulfide is an endogenous stimulator of angiogenesis. *P. Natl. Acad. Sci. USA* **2009**, *106*, 21972-21977.

(213) Gadalla, M. M.; Snyder, S. H. Hydrogen sulfide as a gasotransmitter. *J. Neurochem.* **2010**, *113*, 14-26.

(214) Singh, S.; Padovani, D.; Leslie, R. A.; Chiku, T.; Banerjee, R. Relative Contributions of Cystathionine beta-Synthase and gamma-Cystathionase to H2S Biogenesis via Alternative Trans-sulfuration Reactions. *J. Biol. Chem.* **2009**, *284*, 22457-22466.

(215) Chiku, T.; Padovani, D.; Zhu, W. D.; Singh, S.; Vitvitsky, V.; Banerjee, R. H2S Biogenesis by Human Cystathionine gamma-Lyase Leads to the Novel Sulfur Metabolites Lanthionine and Homolanthionine and Is Responsive to the Grade of Hyperhomocysteinemia. *J. Biol. Chem.* **2009**, *284*, 11601-11612.

(216) Shibuya, N.; Tanaka, M.; Yoshida, M.; Ogasawara, Y.; Togawa, T.; Ishii, K.; Kimura, H. 3-Mercaptopyruvate Sulfurtransferase Produces Hydrogen Sulfide and Bound Sulfane Sulfur in the Brain. *Antioxid. Redox Sign*. **2009**, *11*, 703-714.

(217) Searcy, D. G.; Lee, S. H. Sulfur reduction by human erythrocytes. *J. Exp. Zool.* **1998**, *282*, 310-322.

(218) Whiteman, M.; Moore, P. K. Hydrogen sulfide and the vasculature: a novel vasculoprotective entity and regulator of nitric oxide bioavailability ? *J. Cell. Mol. Med.* **2009**, *13*, 488-507.

(219) Ulrich, G.; Ziessel, R.; Harriman, A. The chemistry of fluorescent bodipy dyes: Versatility unsurpassed. *Angew. Chem. Int. Edit.* **2008**, *47*, 1184-1201.

(220) Ozdemir, T.; Sozmen, F.; Mamur, S.; Tekinay, T.; Akkaya, E. U. Fast responding and selective near-IR Bodipy dye for hydrogen sulfide sensing. *Chem. Commun.* **2014**, *50*, 5455-5457.

(221) Montoya, L. A.; Pluth, M. D. Selective turn-on fluorescent probes for imaging hydrogen sulfide in living cells. *Chem. Commun.* **2012**, *48*, 4767-4769.

(222) Thorson, M. K.; Majtan, T.; Kraus, J. P.; Barrios, A. M. Identification of Cystathionine -Synthase Inhibitors Using a Hydrogen Sulfide Selective Probe. *Angew. Chem. Int. Edit.* **2013**, *52*, 4641-4644.

(223) Sun, W.; Fan, J. L.; Hu, C.; Cao, J. F.; Zhang, H.; Xiong, X. Q.; Wang, J. Y.; Cui, S.; Sun, S. G.; Peng, X. J. A two-photon fluorescent probe with near-infrared emission for hydrogen sulfide imaging in biosystems. *Chem. Commun.* **2013**, *49*, 3890-3892.

(224) Yang, H. J.; Li, Y.; Jiang, M.; Wang, J. M.; Fu, H. General Copper-Catalyzed Transformations of Functional Groups from Arylboronic Acids in Water. *Chem.-Eur. J.* **2011**, *17*, 5652-5660.

(225) Saha, T.; Kand, D.; Talukdar, P. A colorimetric and fluorometric BODIPY probe for rapid, selective detection of H2S and its application in live cell imaging. *Org. Biomol. Chem.* **2013**, *11*, 8166-8170.

(226) Wang, R.; Yu, F. B.; Chen, L. X.; Chen, H.; Wang, L. J.; Zhang, W. W. A highly selective turn-on near-infrared fluorescent probe for hydrogen sulfide detection and imaging in living cells. *Chem. Commun.* **2012**, *48*, 11757-11759.

(227) Bugaj, A. M. Targeted photodynamic therapy - a promising strategy of tumor treatment. *Photoch. Photobio. Sci.* **2011**, *10*, 1097-1109.

(228) Schmitt, F.; Juillerat-Jeanneret, L. Drug Targeting Strategies for Photodynamic Therapy. *Anti-Cancer Agent Me.* **2012**, *12*, 500-525.

(229) Lim, C. K.; Heo, J.; Shin, S.; Jeong, K.; Seo, Y. H.; Jang, W. D.; Park, C. R.; Park, S. Y.; Kim, S.; Kwon, I. C. Nanophotosensitizers toward advanced photodynamic therapy of Cancer. *Cancer Lett.* **2013**, *334*, 176-187.

(230) Cheong, W. F.; Prahl, S. A.; Welch, A. J. A Review of the Optical-Properties of Biological Tissues. *Ieee J. Quantum Elect.* **1990**, *26*, 2166-2185.

(231) Moan, J.; Iani, V.; Ma, L. W. Choice of the proper wavelength for photochemotherapy. *P. Soc. Photo-Opt. Ins.* **1996**, *2625*, 544-549.

(232) Frangioni, J. V. In vivo near-infrared fluorescence imaging. *Curr. Opin. Chem. Biol.* **2003**, *7*, 626-634.

(233) Erbas-Cakmak, S.; Bozdemir, O. A.; Cakmak, Y.; Akkaya, E. U. Proof of principle for a molecular 1:2 demultiplexer to function as an autonomously switching theranostic device. *Chem. Sci.* **2013**, *4*, 858-862.

(234) Abdukayum, A.; Chen, J. T.; Zhao, Q.; Yan, X. P. Functional Near Infrared-Emitting Cr3+/Pr3+ Co-Doped Zinc Gallogermanate Persistent Luminescent Nanoparticles with Superlong Afterglow for in Vivo Targeted Bioimaging. *J. Am. Chem. Soc.* **2013**, *135*, 14125-14133.

(235) Bessiere, A.; Jacquart, S.; Priolkar, K.; Lecointre, A.; Viana, B.; Gourier, D. ZnGa2O4:Cr3+: a new red long-lasting phosphor with high brightness. *Opt. Express* **2011**, *19*, 10131-10137.

(236) Maldiney, T.; Lecointre, A.; Viana, B.; Bessiere, A.; Bessodes, M.; Gourier, D.; Richard, C.; Scherman, D. Controlling Electron Trap Depth To Enhance Optical Properties of Persistent Luminescence Nanoparticles for In Vivo Imaging. *J. Am. Chem. Soc.* **2011**, *133*, 11810-11815.

(237) Jia, D.; Lewis, L. A.; Wang, X. J. Cr3+-Doped Lanthanum Gallogermanate Phosphors with Long Persistent IR Emission. *Electrochem. Solid St.* **2010**, *13*, J32-J34.

(238) Aitasalo, T.; Deren, P.; Holsa, J.; Jungner, H.; Krupa, J. C.; Lastusaari, M.; Legendziewicz, J.; Niittykoski, J.; Strek, W. Persistent luminescence phenomena in materials doped with rare earth ions. *J. Solid State Chem.* **2003**, *171*, 114-122.

(239) Kim, J. S.; Kim, J. S.; Park, H. L. Optical and structural properties of nanosized ZnGa2O4 : Cr3+ phosphor. *Solid State Commun.* **2004**, *131*, 735-738.

(240) Binet, L.; Gourier, D. Origin of the blue luminescence of beta-Ga2O3. *J. Phys. Chem. Solids* **1998**, *59*, 1241-1249.

(241) Kuang, J. Y.; Liu, Y. L. Observation of energy transfer from host to rare earth ions in Pr3+-doped USA long-lasting phosphor. *Chem. Phys. Lett.* **2006**, *424*, 58-62.

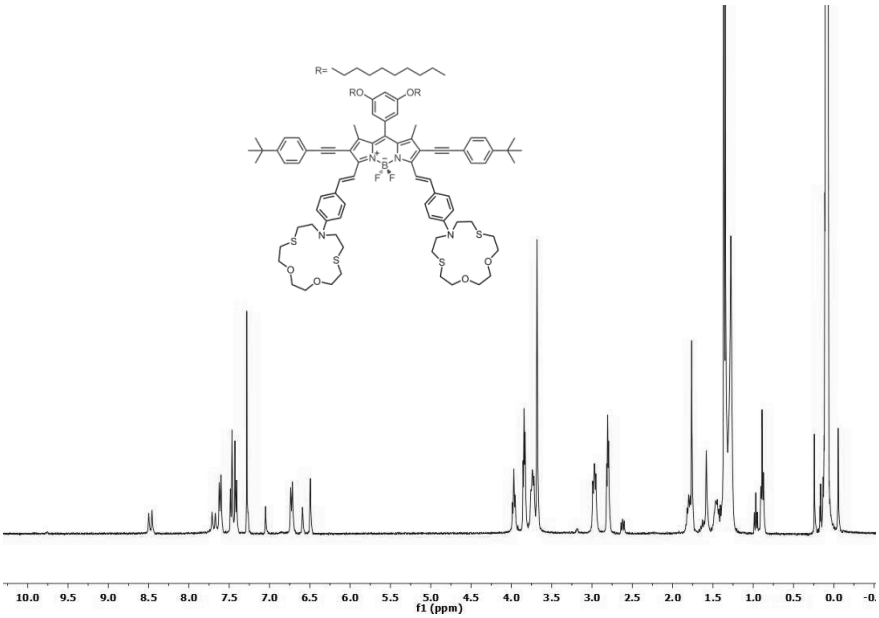
(242) Lecointre, A.; Bessiere, A.; Bos, A. J. J.; Dorenbos, P.; Viana, B.; Jacquart, S. Designing a Red Persistent Luminescence Phosphor: The Example of YPO4:Pr3+,Ln(3+) (Ln = Nd, Er, Ho, Dy). *J. Phys. Chem. C* **2011**, *115*, 4217-4227.

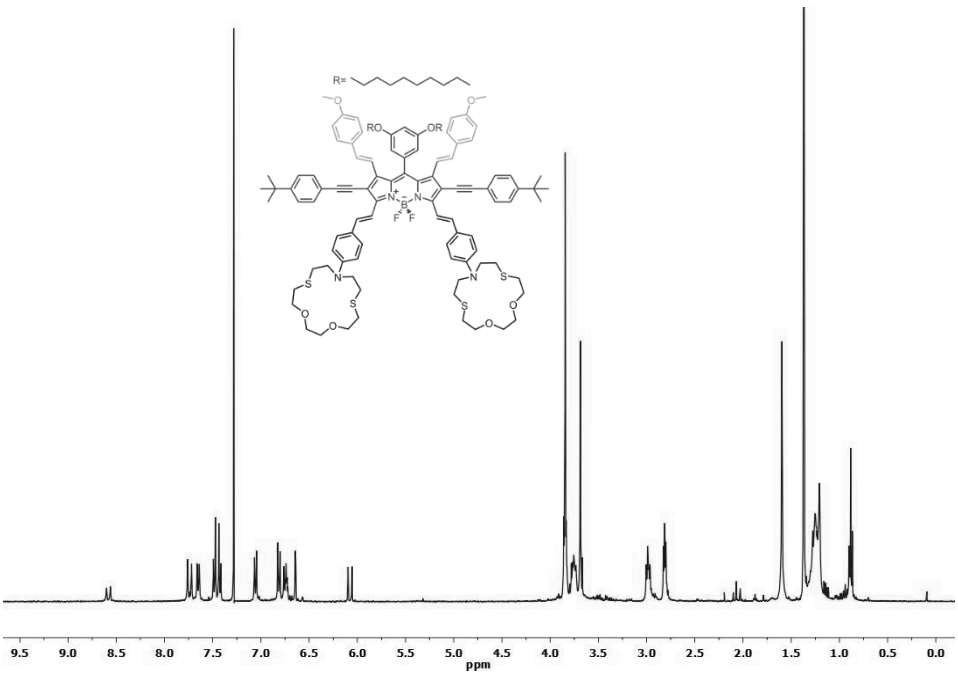
(243) Atilgan, S.; Ozdemir, T.; Akkaya, E. U. A sensitive and selective ratiometric near IR fluorescent probe for zinc ions based on the distyryl-bodipy fluorophore. *Org. Lett.* **2008**, *10*, 4065-4067.

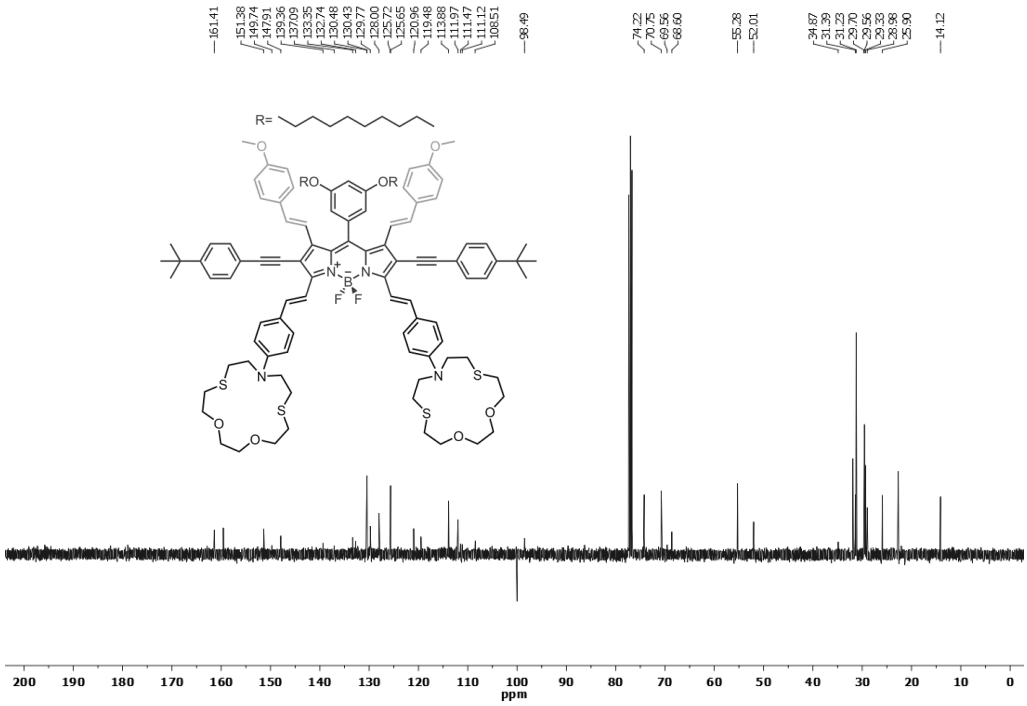
APPENDIX

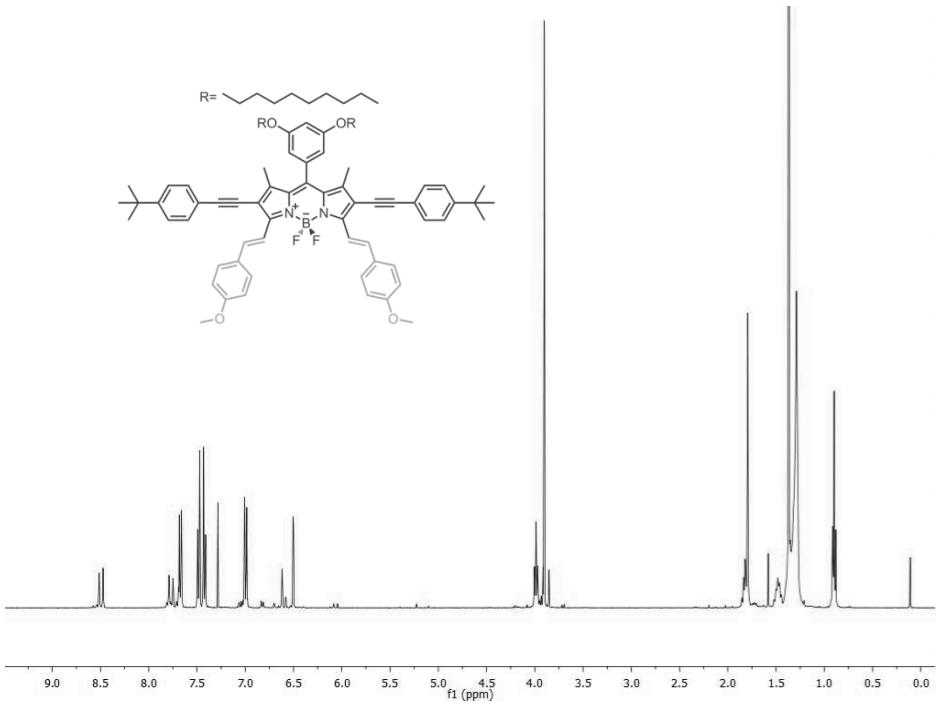
A1. Rational Design of Ion Responsive, Isomeric Near- IR BODIPY Dyes

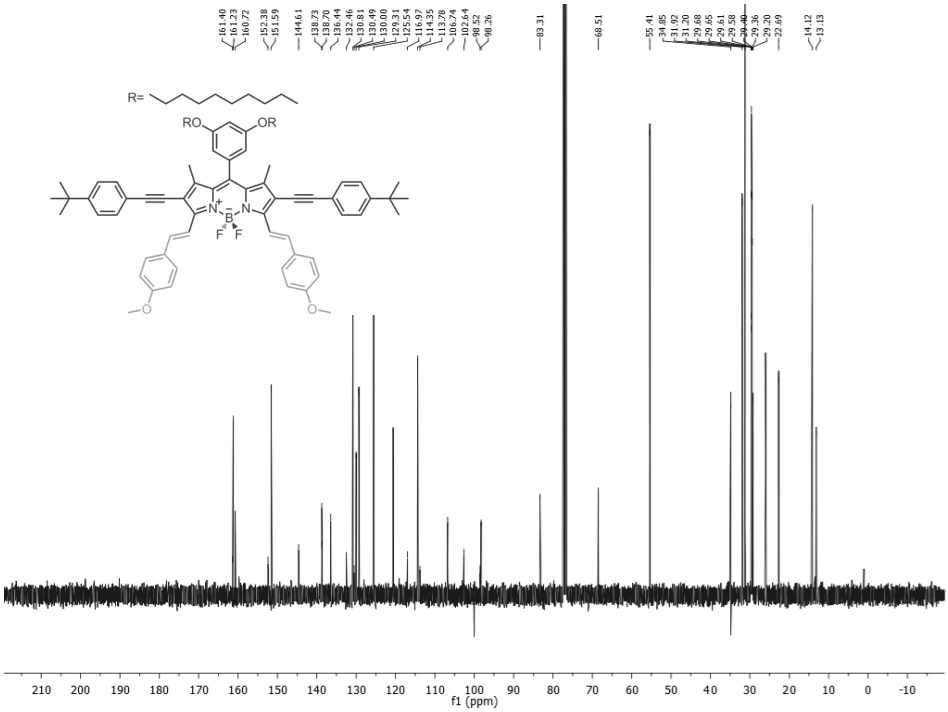
A1.1. ^{1}H, ^{13}C and Mass Spectra

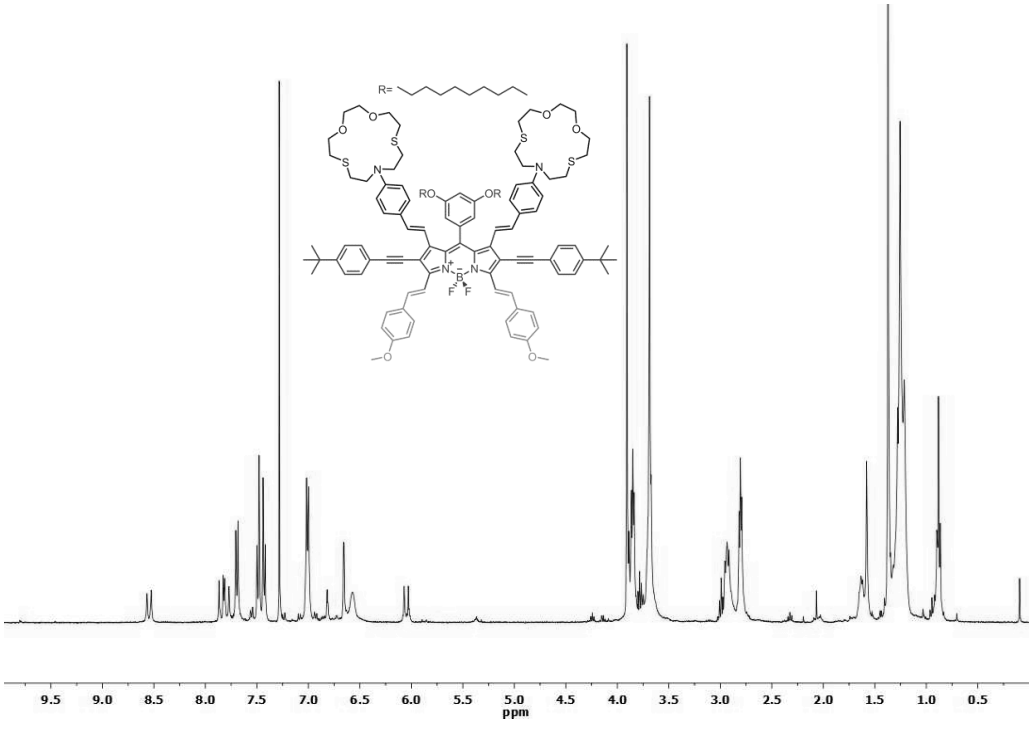


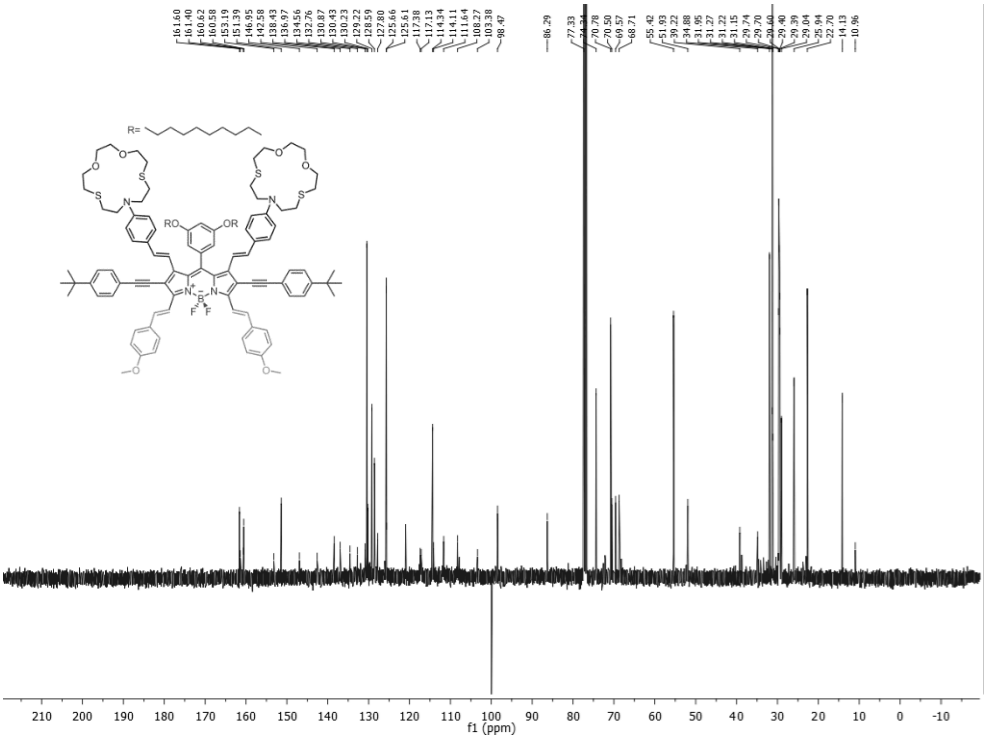


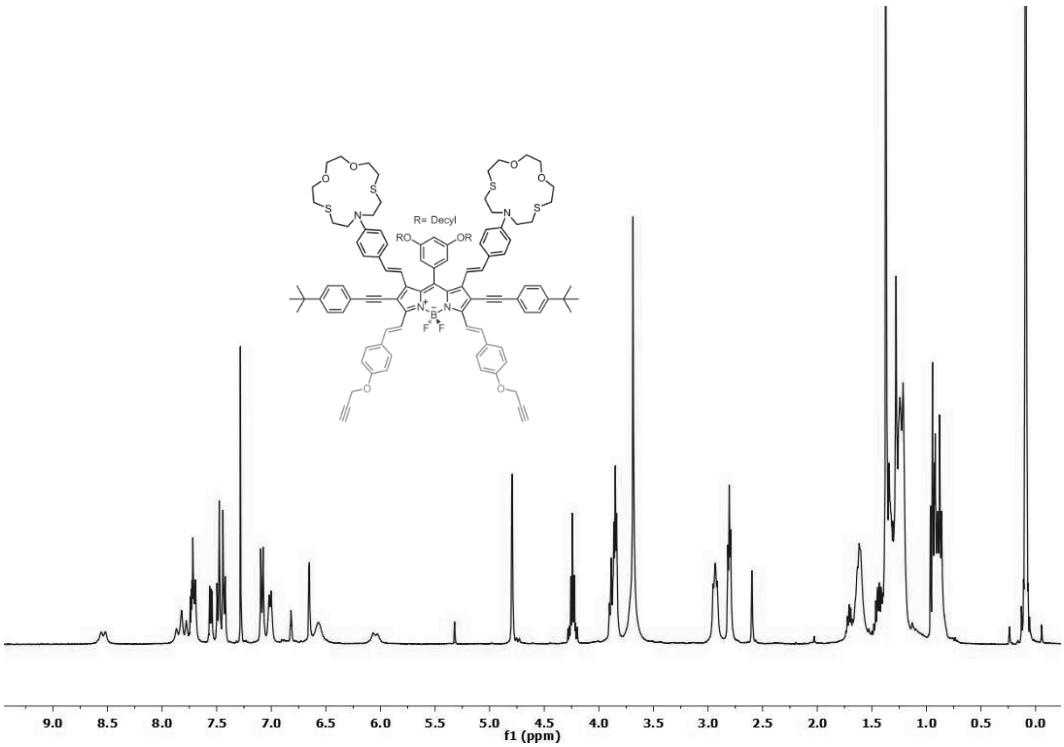

161.41
151.38
149.74
147.91
139.56
137.09
132.35
132.74
130.48
130.43
129.77
128.00
125.72
125.65
120.96
119.48
113.88
111.97
111.47
111.12
108.51
98.49
74.22
70.75
69.56
68.60
55.28
52.01
34.87
31.39
31.23
30.70
29.56
29.33
28.98
25.90
14.12
R=
RO
OR
ppm

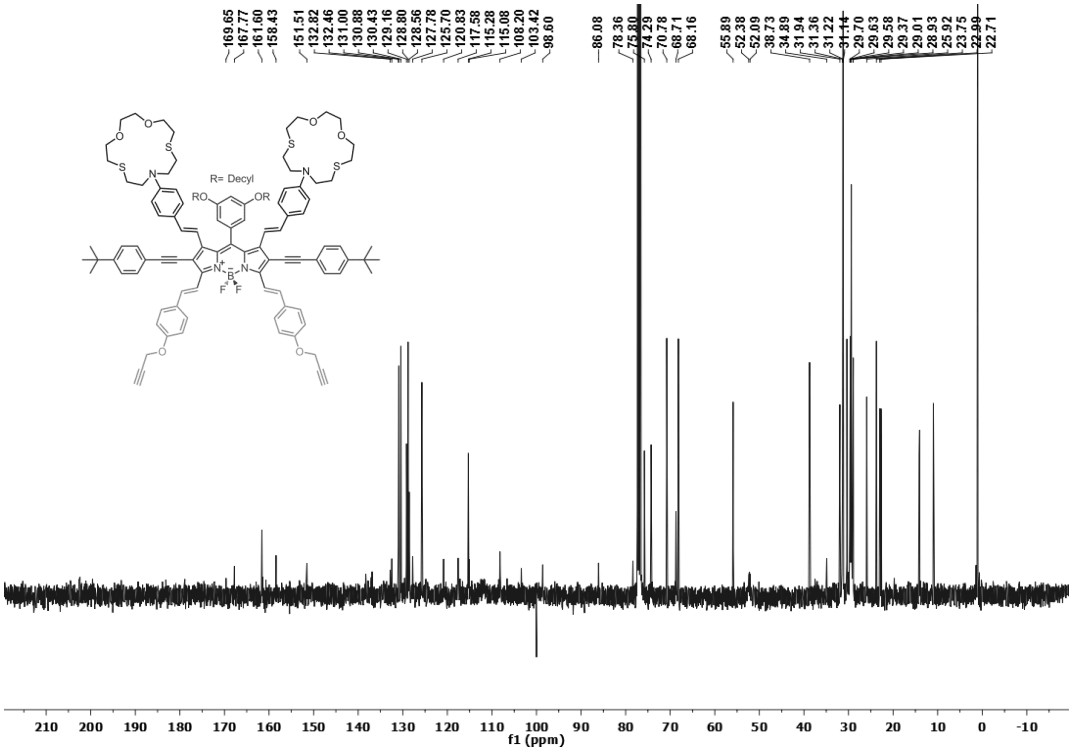

R=
RO
OR
f1 (ppm)

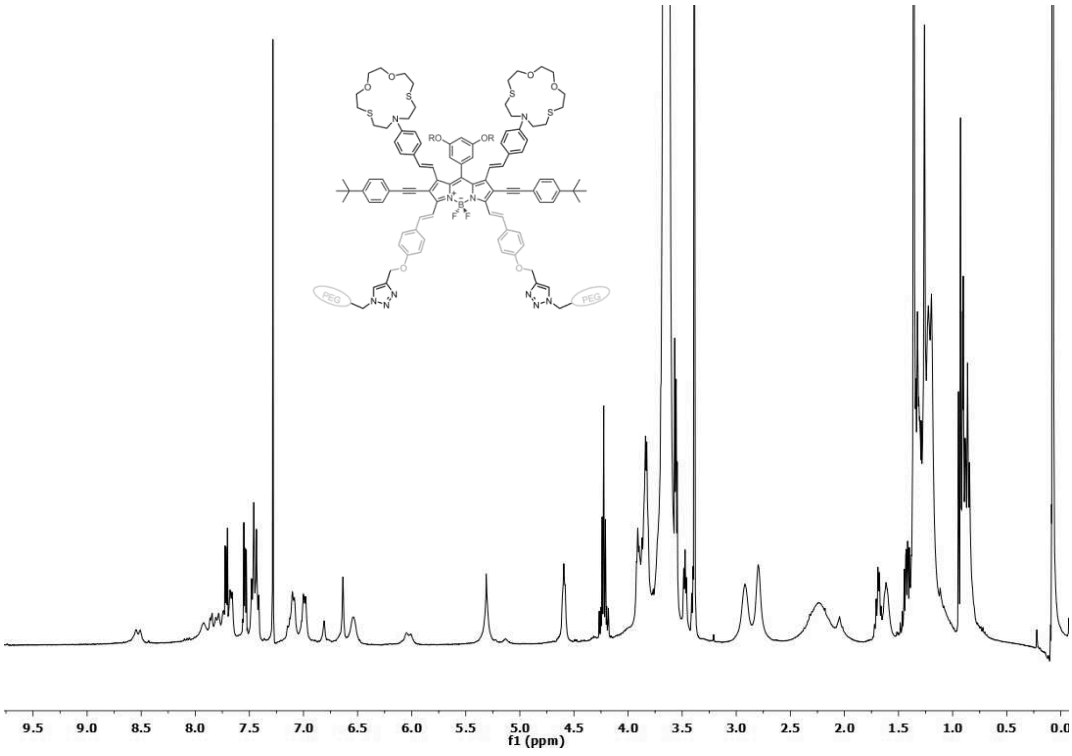

R=
RO
OR
f1 (ppm)

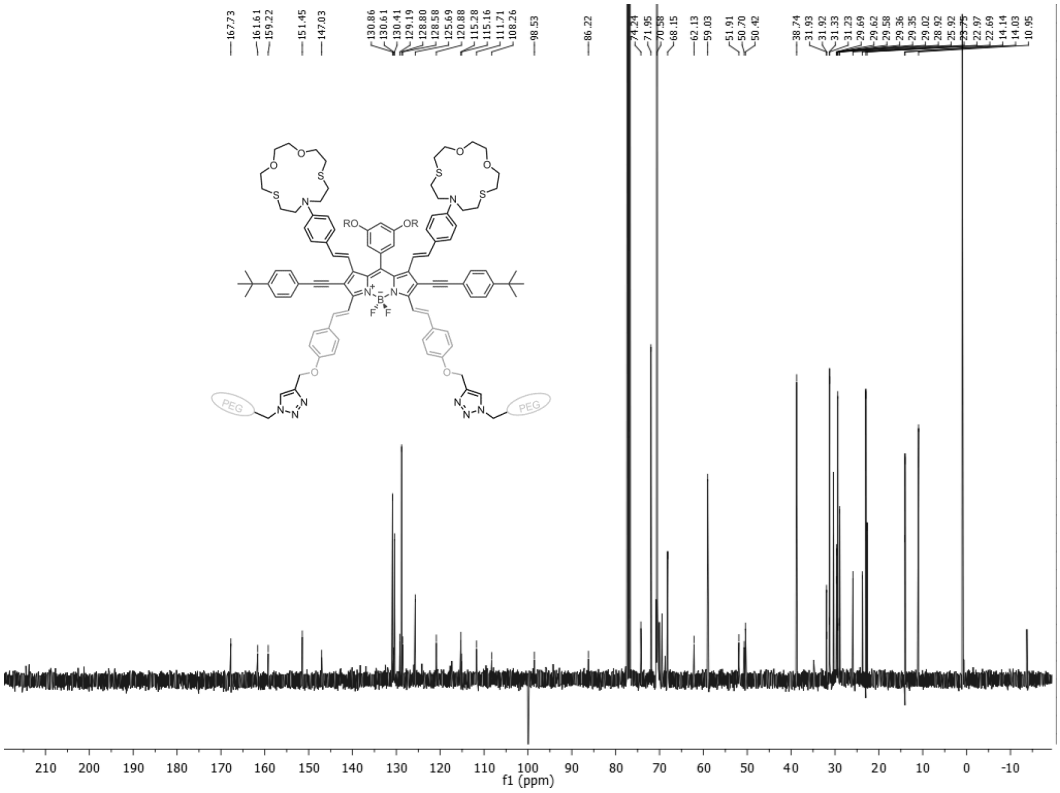

R=
RO
OR
ppm

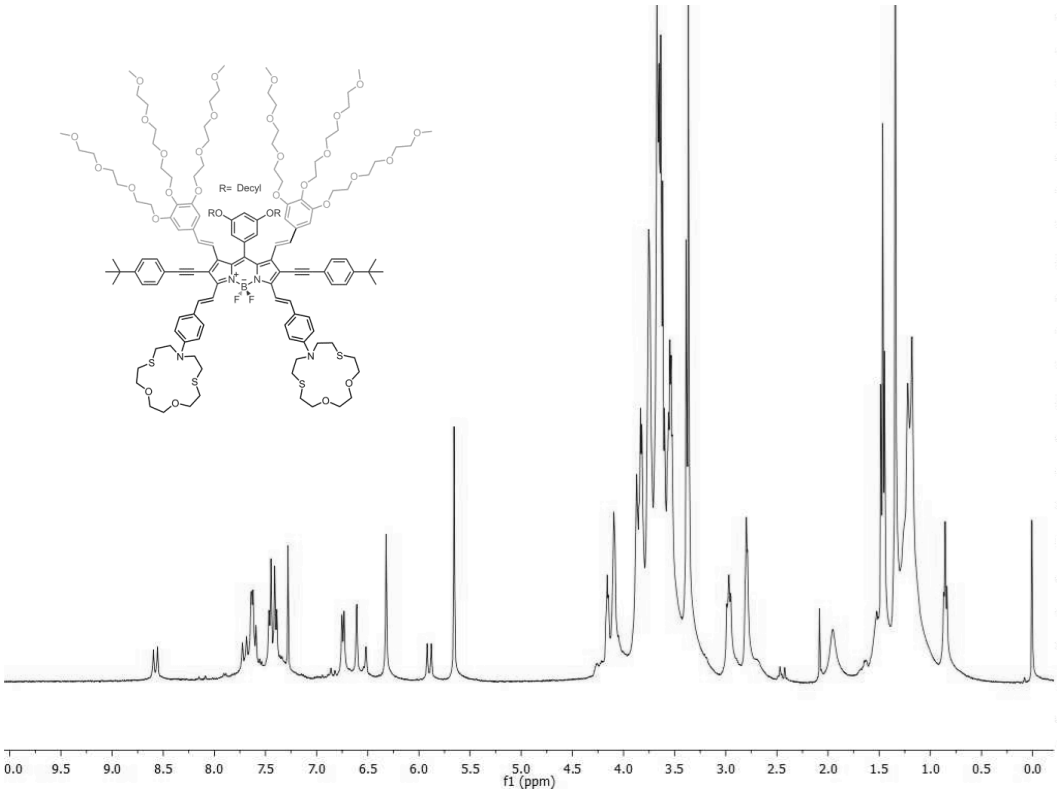

R=
RO
OR
f1 (ppm)

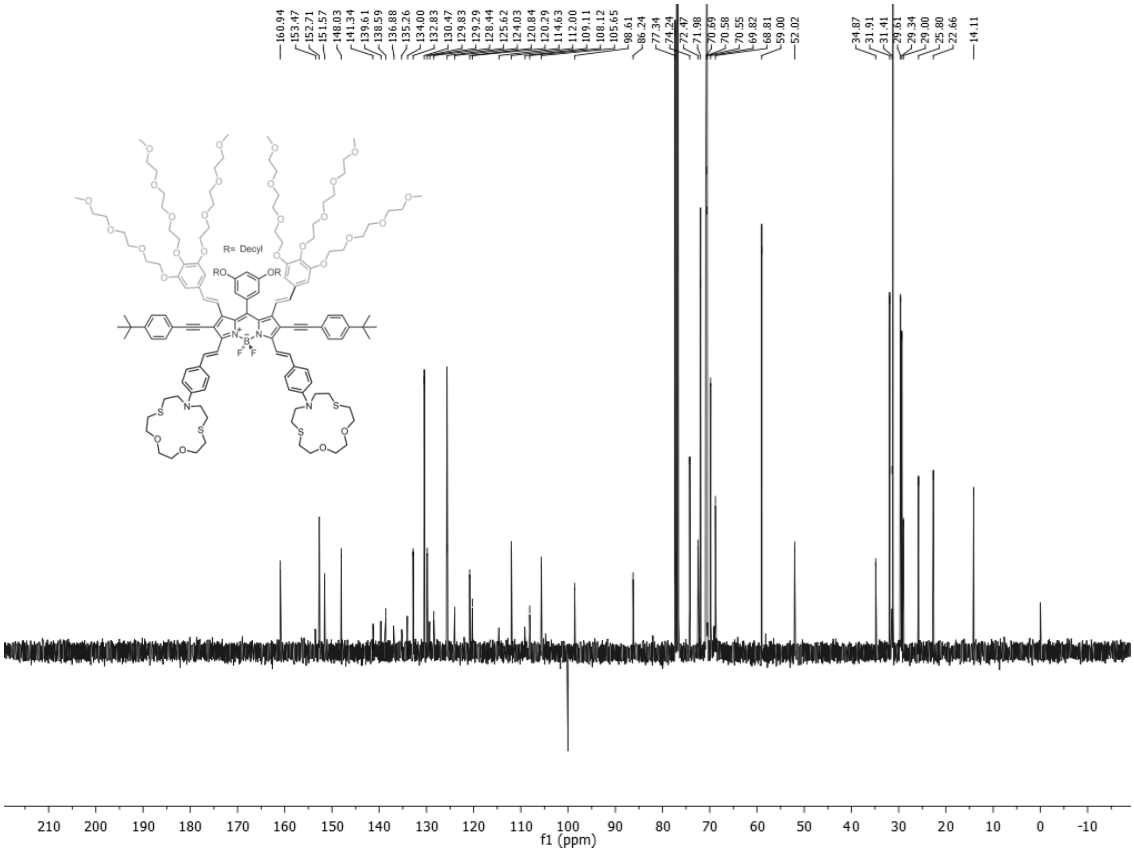

R= Decyl
RO
OR
f1 (ppm)

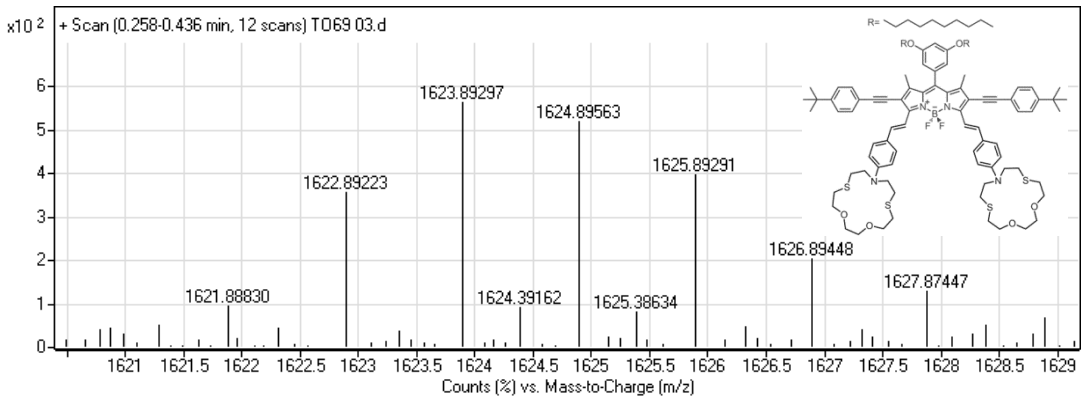

169.65
167.77
161.60
158.43
151.51
132.82
132.46
131.00
130.88
130.43
129.16
128.80
128.56
127.78
125.70
120.83
117.58
115.28
115.08
108.20
103.42
98.60
86.08
78.36
75.80
74.29
70.78
68.71
68.16
55.89
52.38
52.09
38.73
34.89
31.94
31.36
31.22
31.11
29.70
29.63
29.58
29.37
29.01
28.93
25.92
23.75
22.99
22.71
R= Decyl
RO
OR
f1 (ppm)

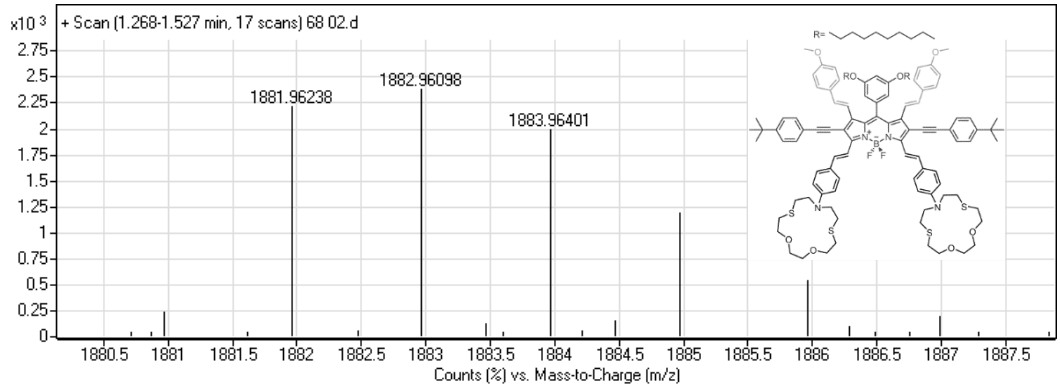

RO
OR
PEG
PEG
f1 (ppm)

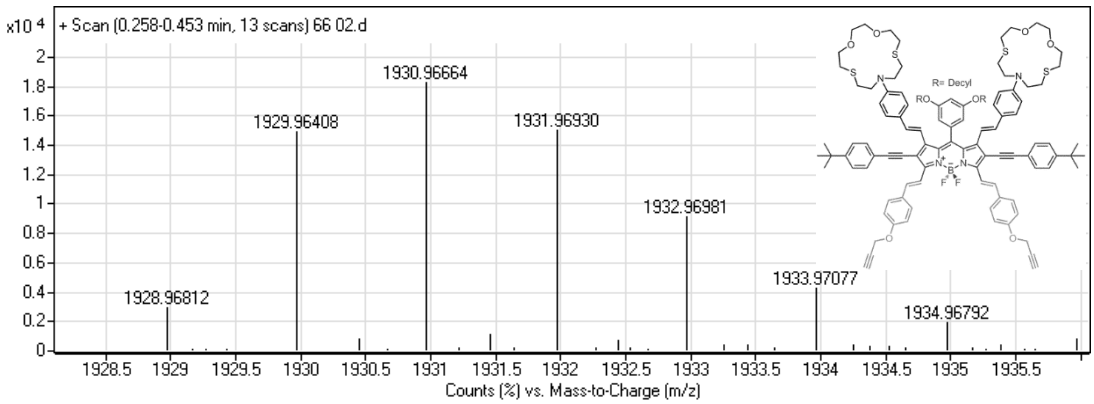

167.73
161.61
159.22
151.45
147.03
130.86
130.61
130.41
129.19
128.80
128.58
125.69
120.88
115.28
115.16
111.71
108.26
98.53
86.22
74.24
71.95
70.38
68.15
62.13
59.03
51.91
50.70
50.42
38.74
31.93
31.92
31.33
31.23
29.69
29.62
29.58
29.36
29.35
29.02
28.92
25.92
23.75
22.97
22.69
14.14
14.03
10.95
RO
OR
PEG
PEG
f1 (ppm)

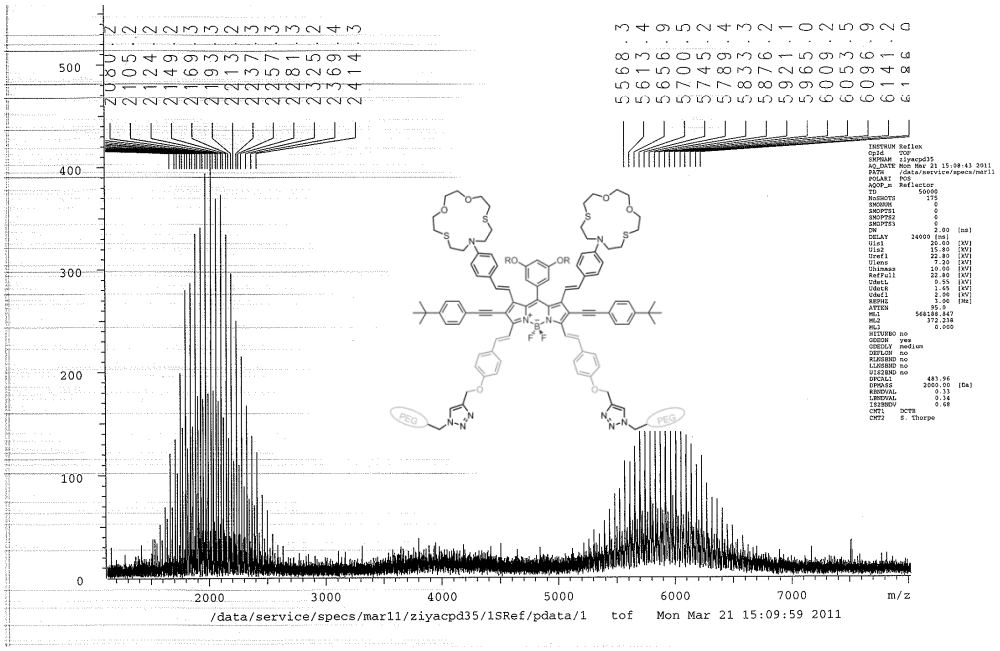

R= Decyl
RO
OR
f1 (ppm)

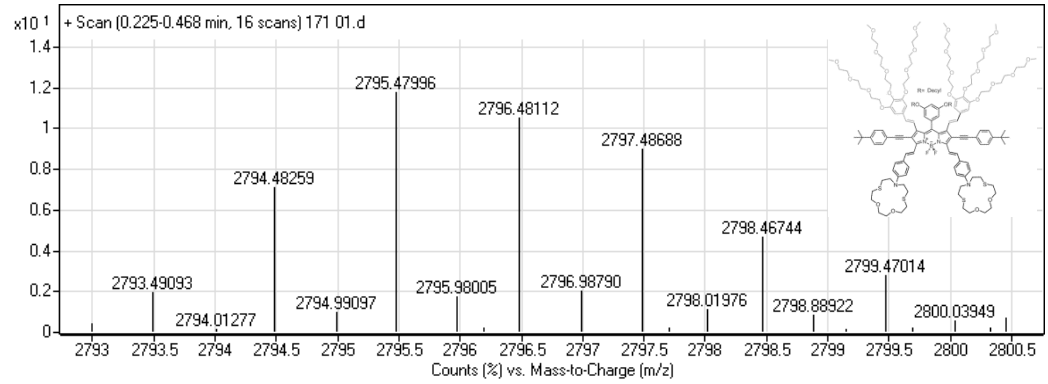

160.94
153.47
152.71
151.57
148.03
141.34
139.61
138.59
136.88
135.26
134.00
132.83
130.47
129.83
129.29
128.44
125.62
124.03
120.84
120.29
114.63
112.00
109.11
108.12
105.65
98.61
86.24
77.34
77.24
72.47
71.98
70.69
70.58
70.55
69.82
68.81
59.00
52.02
34.87
31.91
31.41
29.61
29.34
29.00
25.80
22.66
14.11
R= Decyl
RO
OR
210 200 190 180 170 160 150 140 130 120 110 100 90 80 70 60 50 40 30 20 10 0 -10
f1 (ppm)

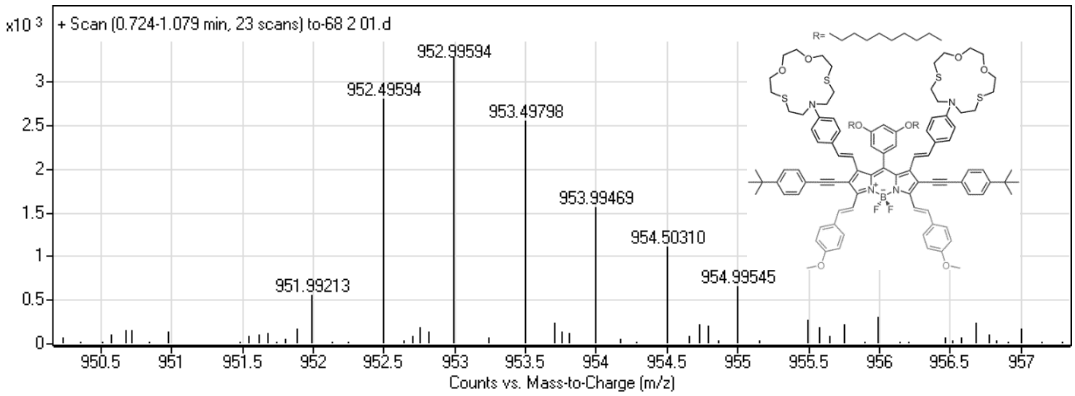

x10 2
+ Scan (0.258-0.436 min, 12 scans) TO69 03.d
1623.89297
1624.89563
1622.89223
1625.89291
1626.89448
1627.87447
1621.88830
1624.39162
1625.38634
R=
RO
OR
0 1 2 3 4 5 6
1621 1621.5 1622 1622.5 1623 1623.5 1624 1624.5 1625 1625.5 1626 1626.5 1627 1627.5 1628 1628.5 1629
Counts (%) vs. Mass-to-Charge (m/z)


x10 3
+ Scan (1.268-1.527 min, 17 scans) 68 02.d
1881.96238
1882.96098
1883.96401
Counts (%) vs. Mass-to-Charge (m/z)


x10 4
+ Scan (0.258-0.453 min, 13 scans) 66 02.d
1928.96812
1929.96408
1930.96664
1931.96930
1932.96981
1933.97077
1934.96792
R= Decyl
Counts (%) vs. Mass-to-Charge (m/z)

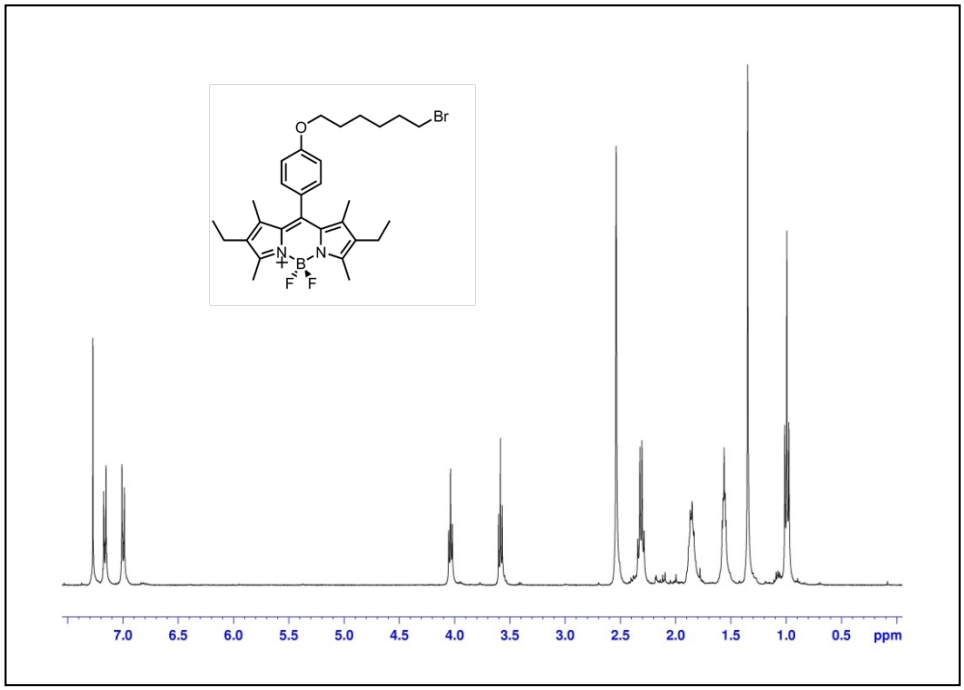

m/z
/data/service/specs/mar11/ziyacpd35/1SRef/pdata/1 tof Mon Mar 21 15:09:59 2011

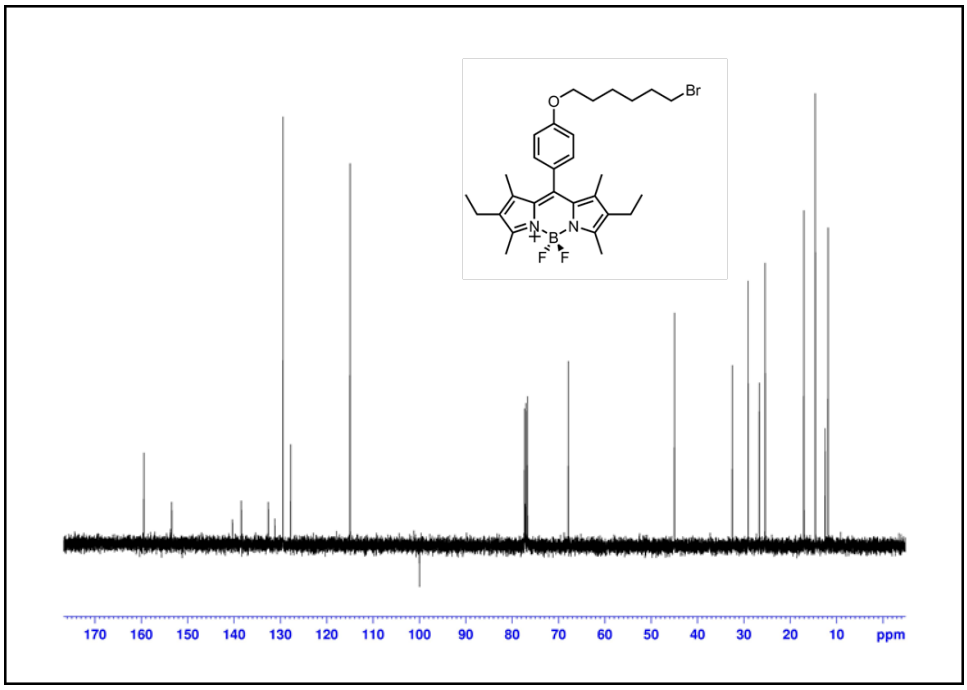

x10 1
+ Scan (0.225-0.468 min, 16 scans) 171 01.d
2795.47996
2796.48112
2797.48688
2794.48259
2798.46744
2799.47014
2793.49093
2795.98005
2796.98790
2798.01976
2798.88922
2794.99097
2794.01277
2800.03949
Counts (%) vs. Mass-to-Charge (m/z)

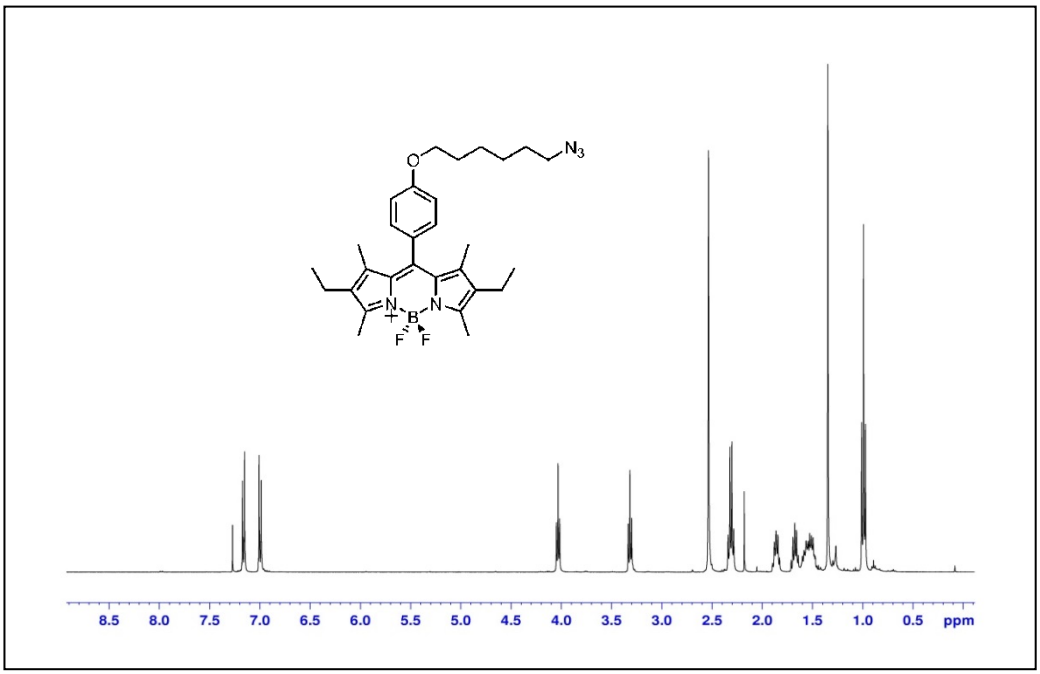

x10 3
+ Scan (0.724-1.079 min, 23 scans) to-68 2 01.d
952.99594
952.49594
953.49798
953.99469
954.50310
954.99545
951.99213
Counts vs. Mass-to-Charge (m/z)

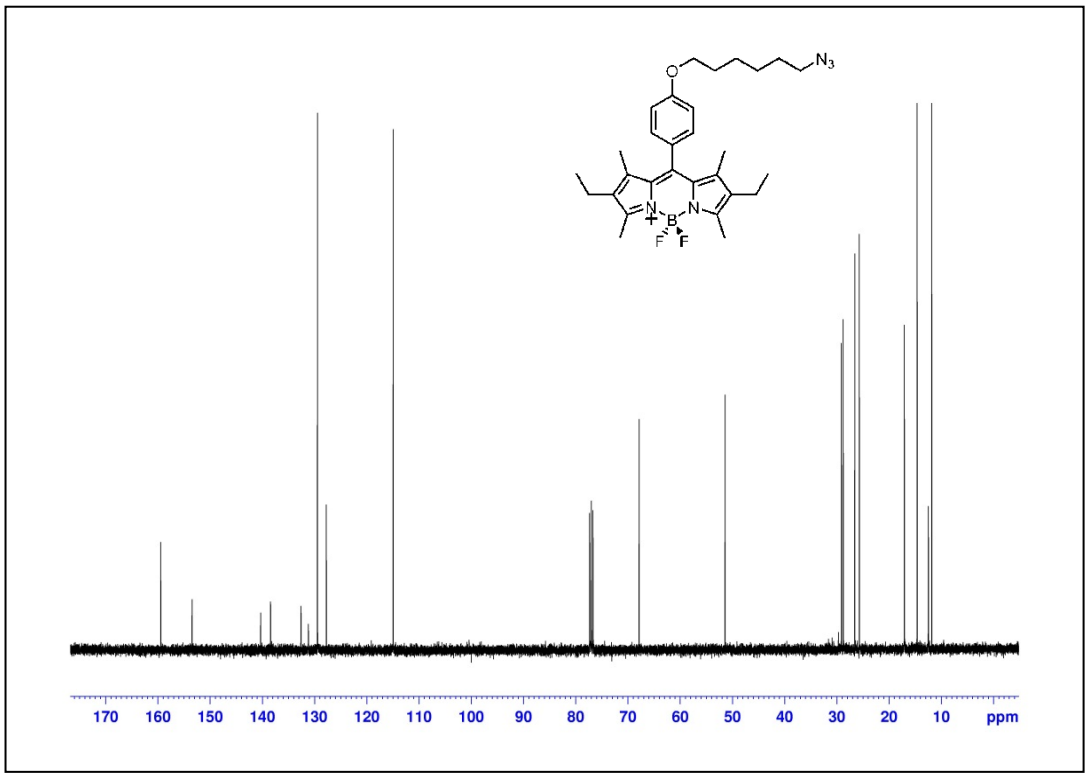
A2. Dendritic Energy Transfer and Determination of Energy Transfer Based on Tetra-Styryl BODIPY Derivatives

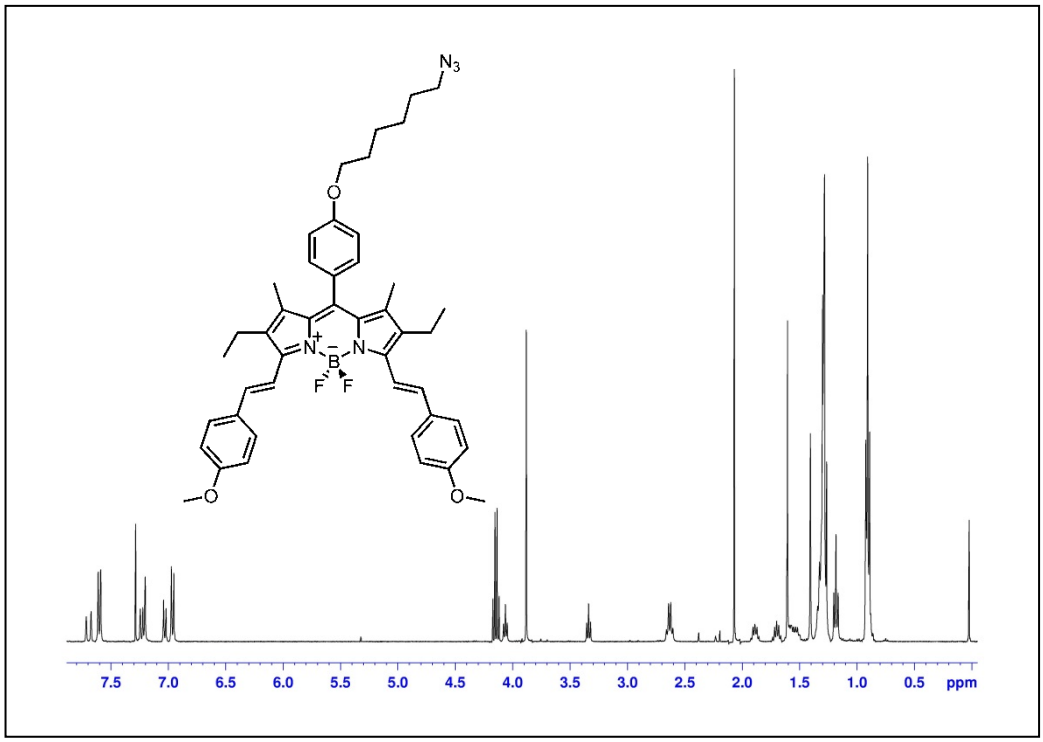
A2.1. ^{1}H, ^{13}C and Mass Spectra

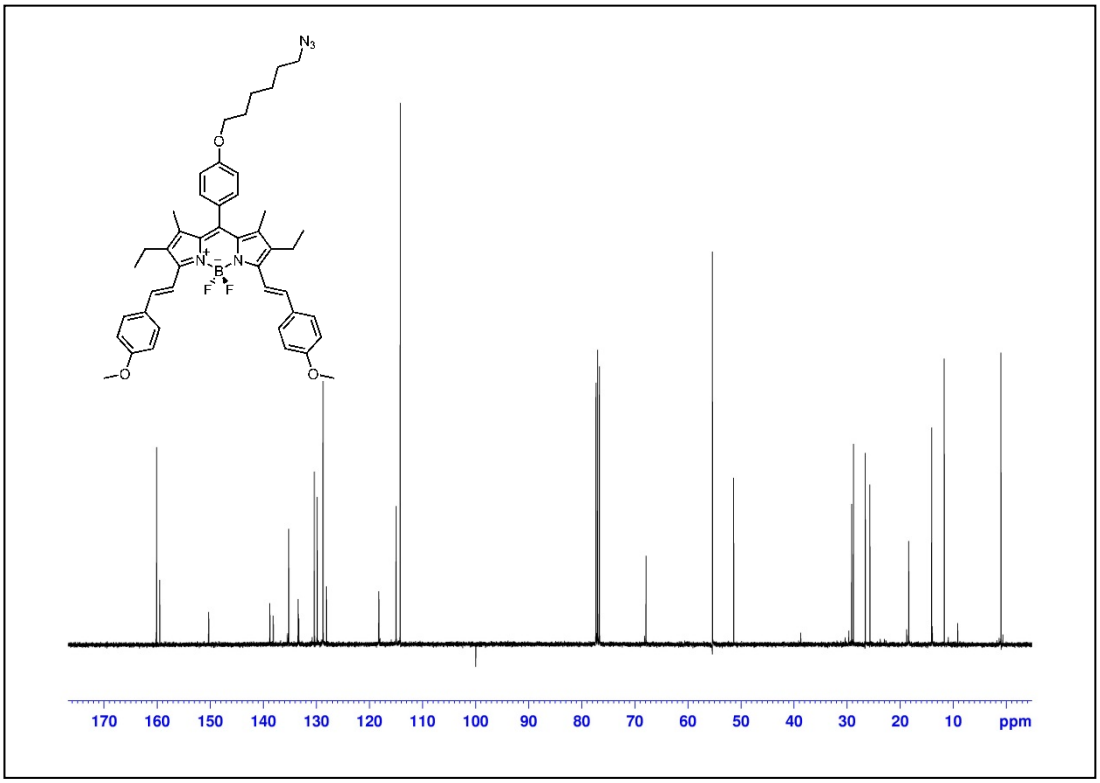


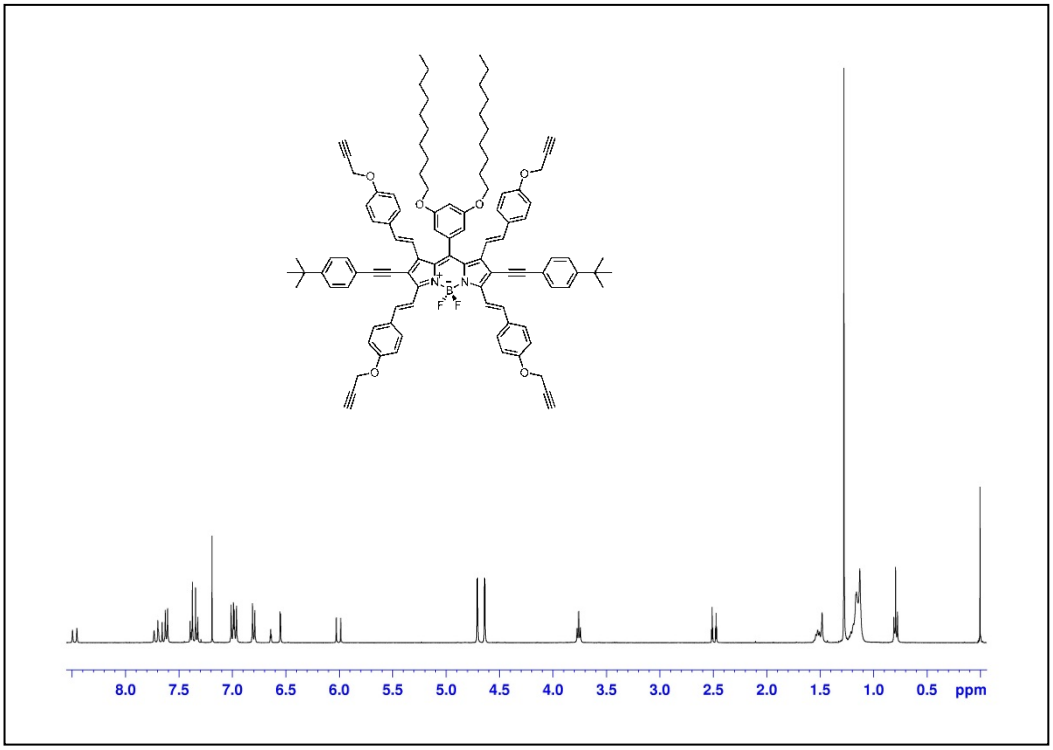


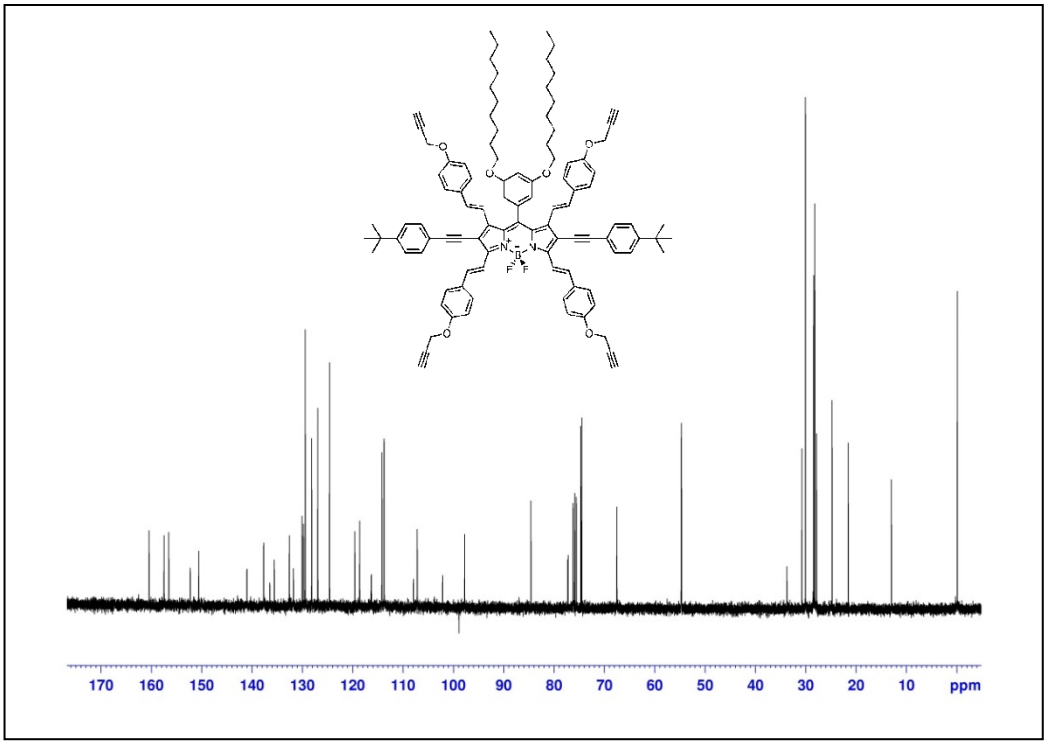

O
N3
N
B
F
F
8.5 8.0 7.5 7.0 6.5 6.0 5.5 5.0 4.5 4.0 3.5 3.0 2.5 2.0 1.5 1.0 0.5 ppm

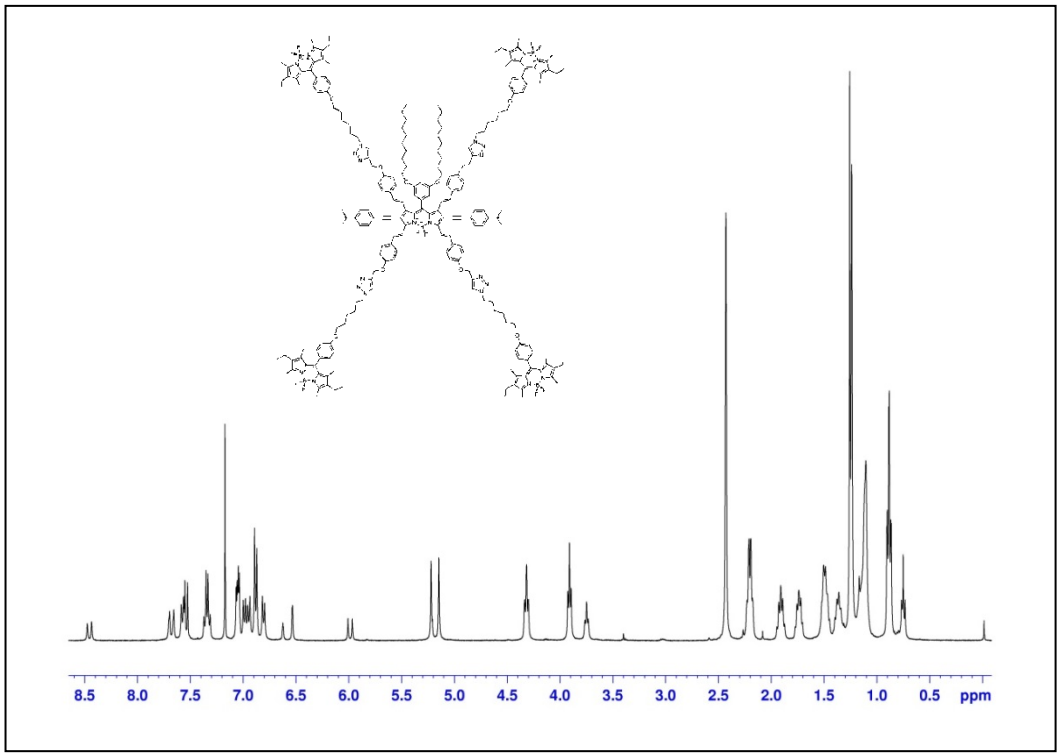

O
N3
N
B
F
F
170 160 150 140 130 120 110 100 90 80 70 60 50 40 30 20 10 ppm

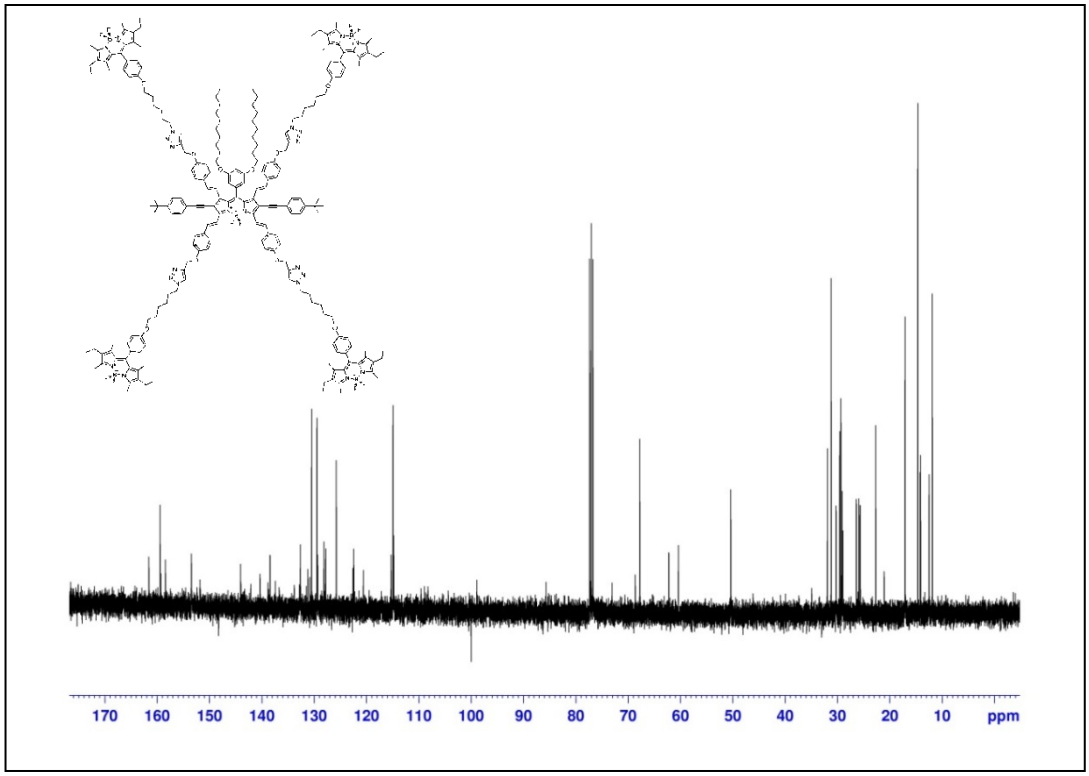

N3
O
N+
B
N
F
F
O
O
7.5
7.0
6.5
6.0
5.5
5.0
4.5
4.0
3.5
3.0
2.5
2.0
1.5
1.0
0.5
ppm

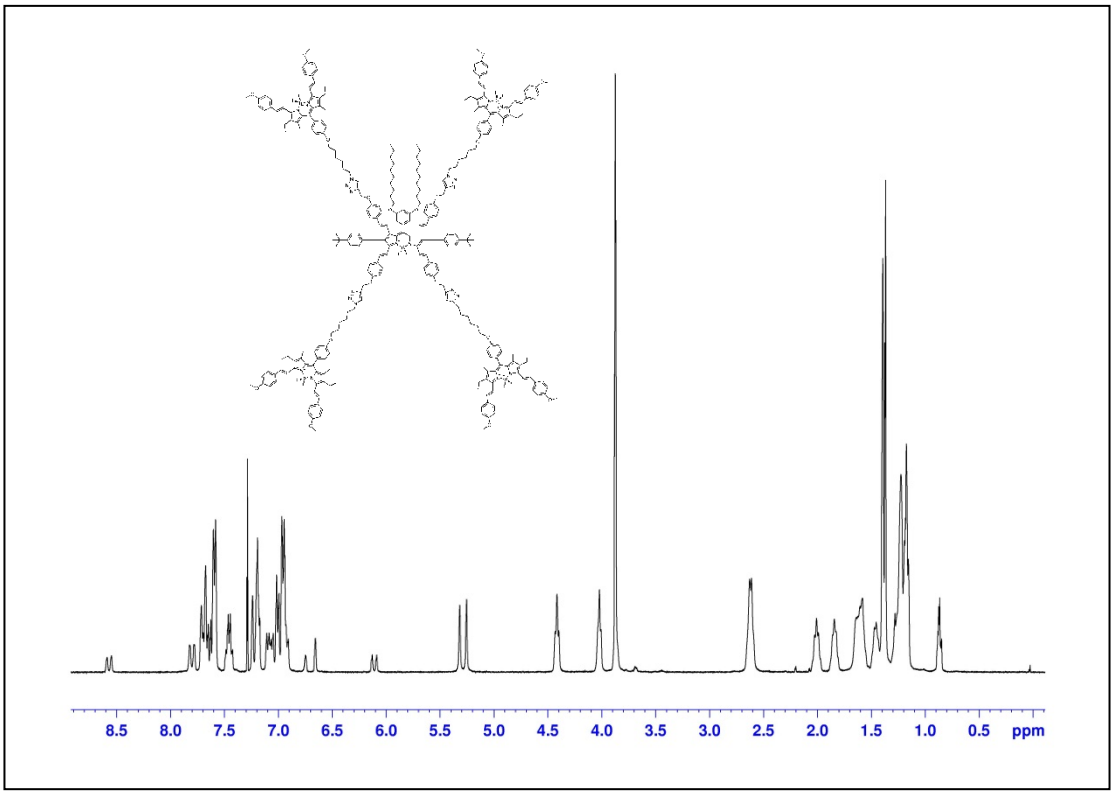

N3
O
N+
B
N
F
F
O
O
170
160
150
140
130
120
110
100
90
80
70
60
50
40
30
20
10
ppm

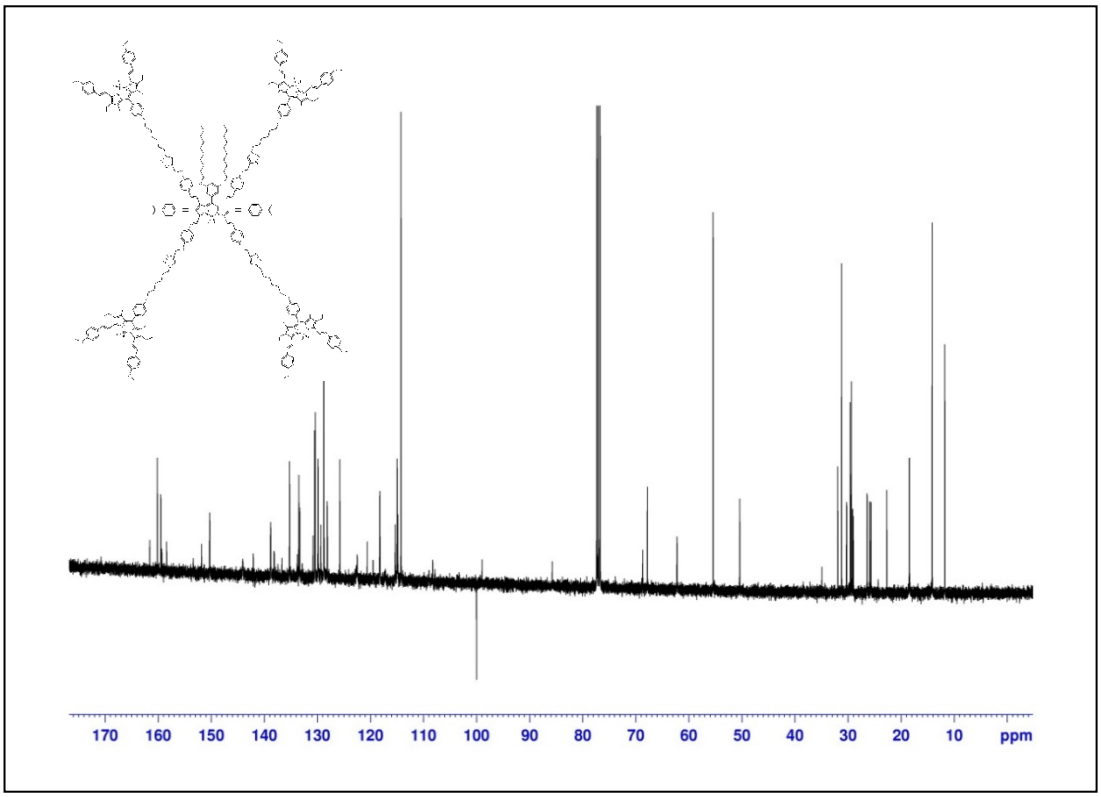

8.0
7.5
7.0
6.5
6.0
5.5
5.0
4.5
4.0
3.5
3.0
2.5
2.0
1.5
1.0
0.5
ppm

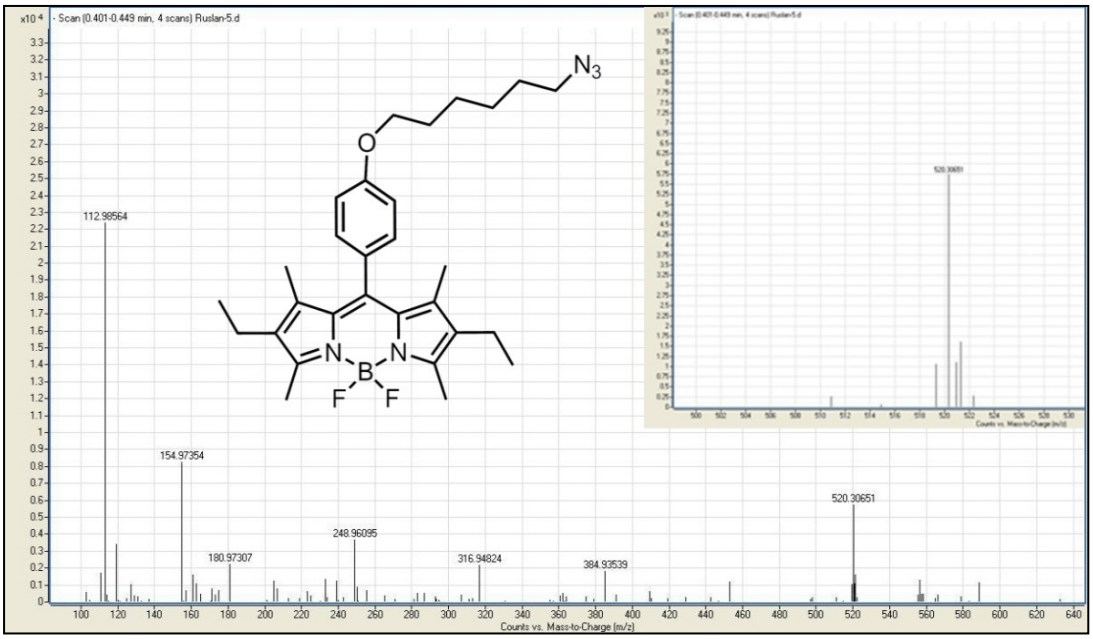

170
160
150
140
130
120
110
100
90
80
70
60
50
40
30
20
10
ppm

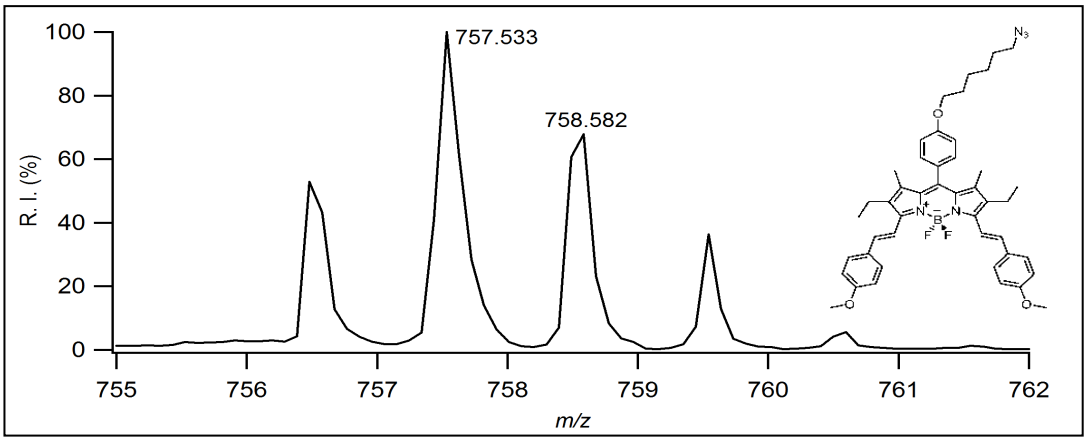

8.5
8.0
7.5
7.0
6.5
6.0
5.5
5.0
4.5
4.0
3.5
3.0
2.5
2.0
1.5
1.0
0.5
ppm

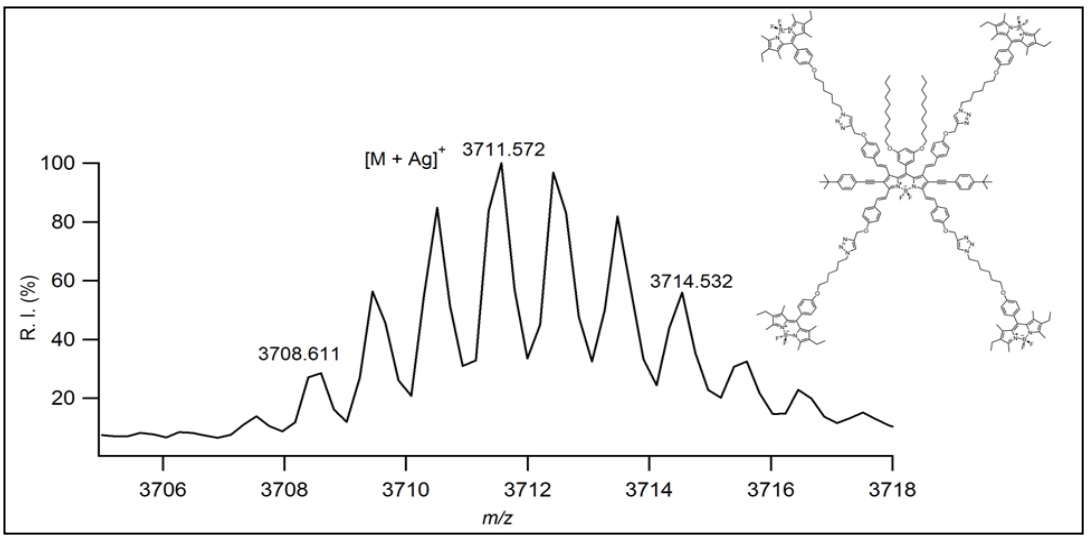

170
160
150
140
130
120
110
100
90
80
70
60
50
40
30
20
10
ppm

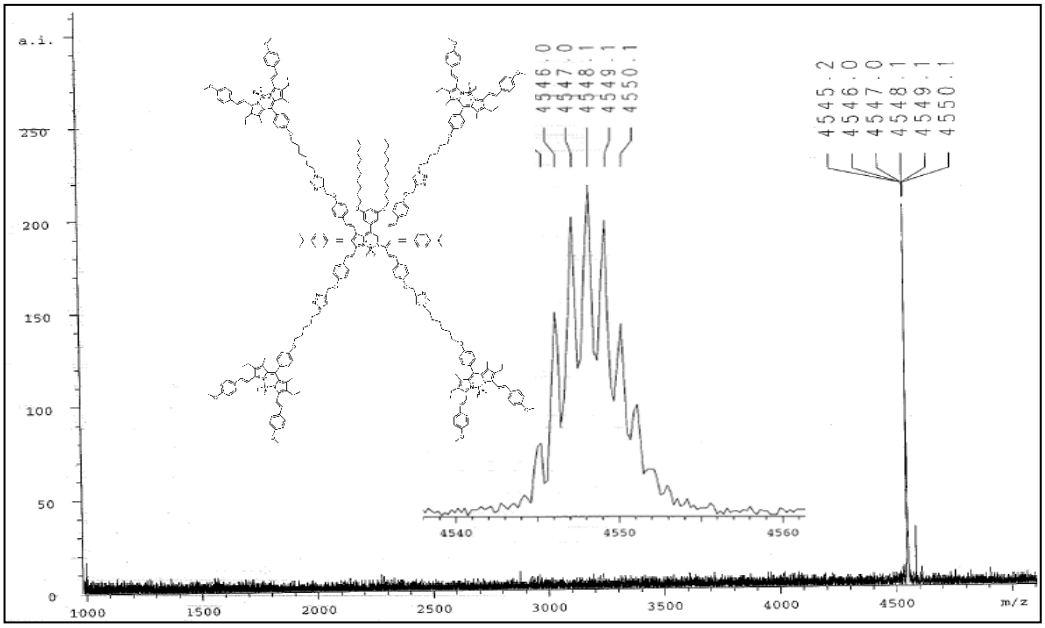

8.5
8.0
7.5
7.0
6.5
6.0
5.5
5.0
4.5
4.0
3.5
3.0
2.5
2.0
1.5
1.0
0.5
ppm


170
160
150
140
130
120
110
100
90
80
70
60
50
40
30
20
10
ppm


Scan (0.401-0.449 min, 4 scans) Ruslan-5.d
112.98564
154.97354
180.97307
248.96095
316.94824
384.93539
520.30651
Counts vs. Mass-to-Charge [m/z]

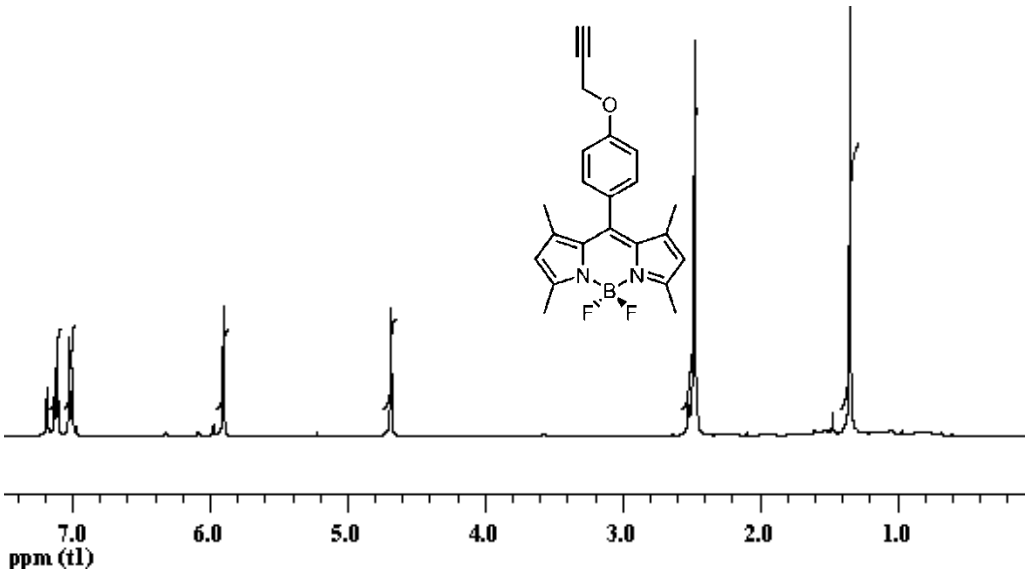

757.533
758.582
R. I. (%)
m/z

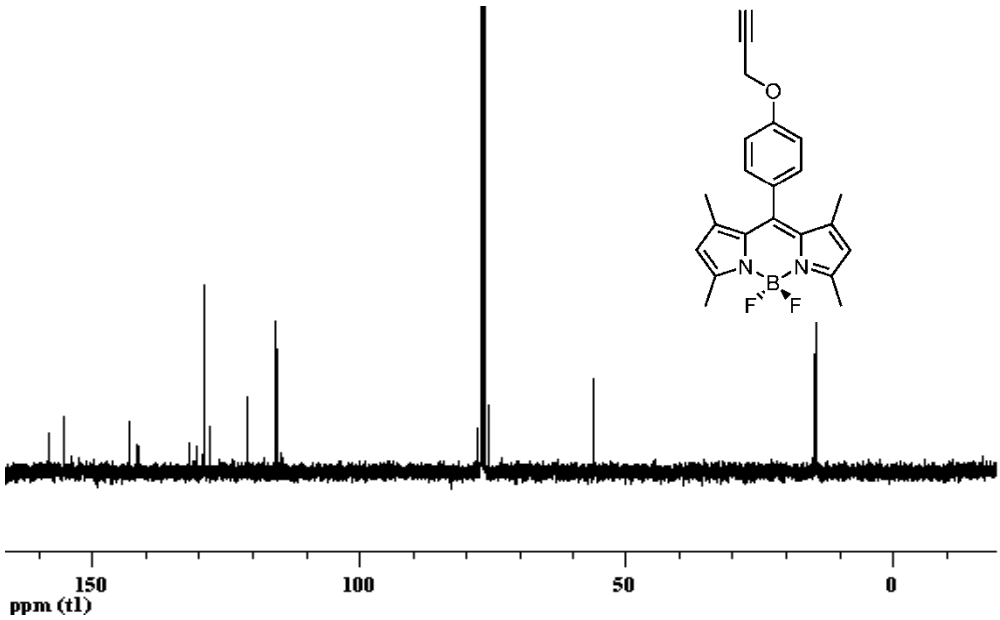

[M + Ag]+
3711.572
3714.532
3708.611
R. I. (%)
m/z

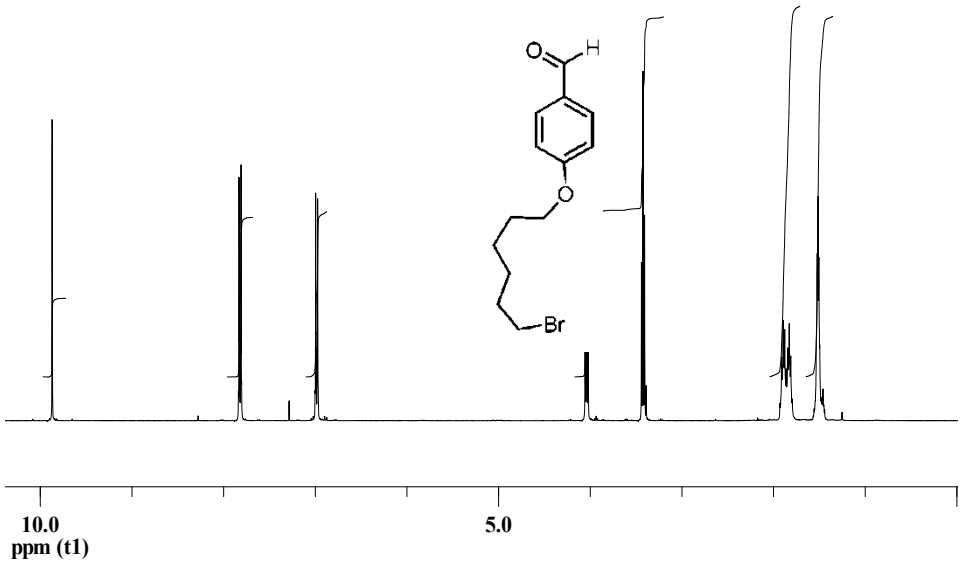

a.i.
250
200
150
100
50
0
1000
1500
2000
2500
3000
3500
4000
4500
m/z
4546.0
4547.0
4548.1
4549.1
4550.1
4540
4550
4560
4545.2
4546.0
4547.0
4548.1
4549.1
4550.1

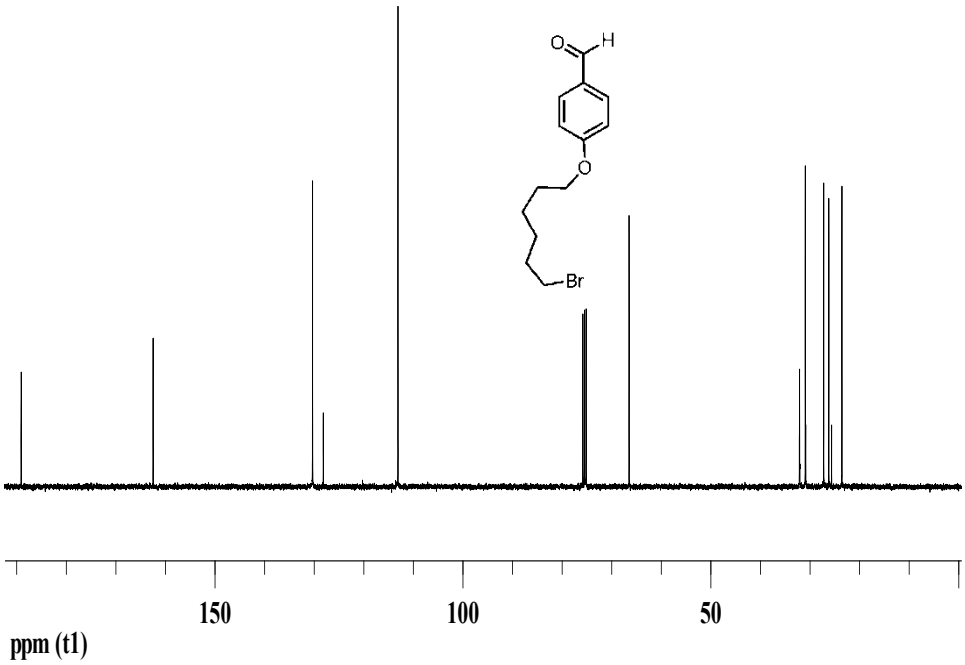
A3. Coupling ICT Process to Excitation Energy Transfer: Improved Stokes Shift for Selective Hg(II) Sensing

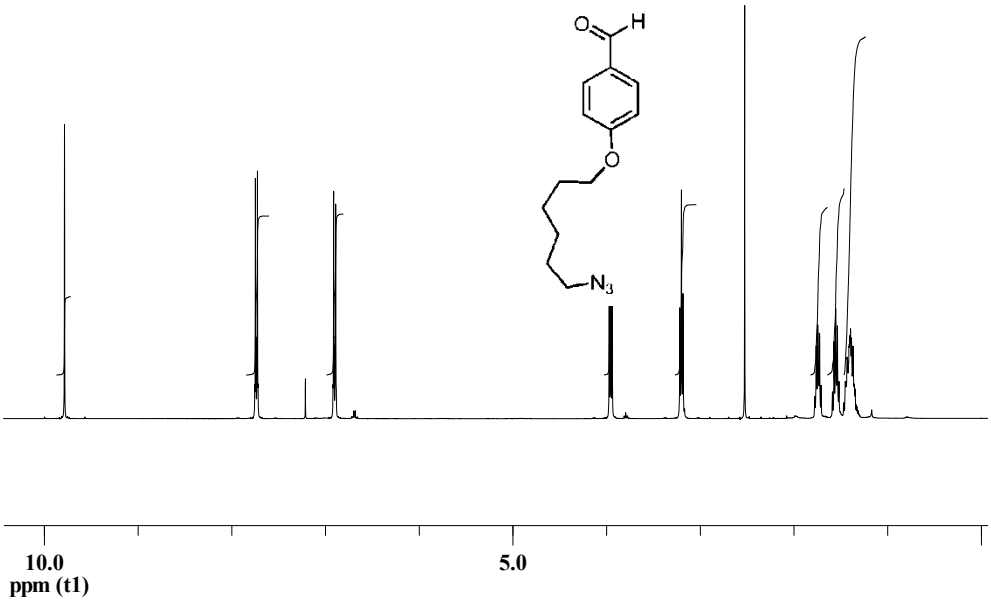
A3.1. ^{1}H, ^{13}C and Mass Spectra

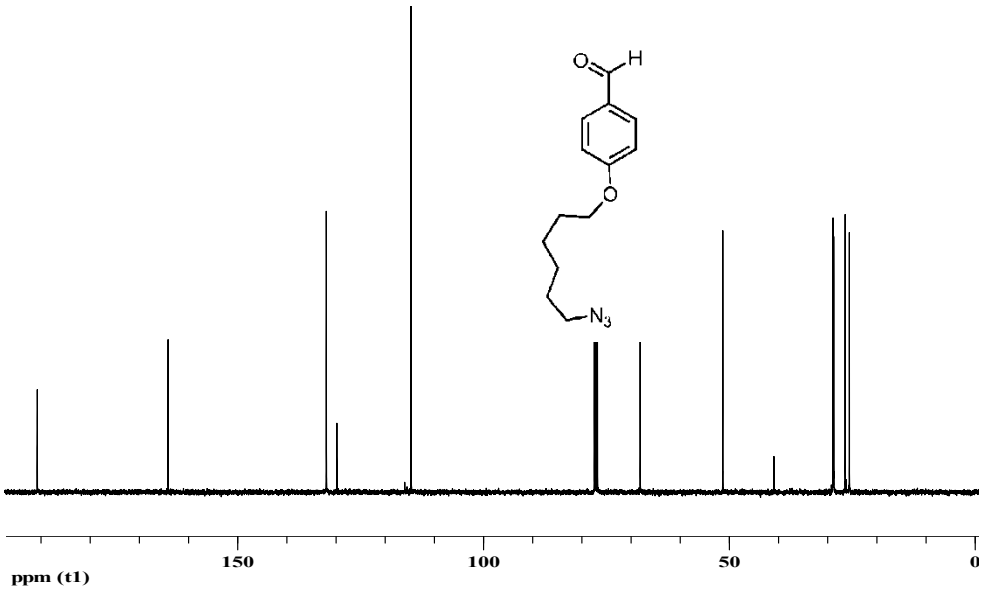


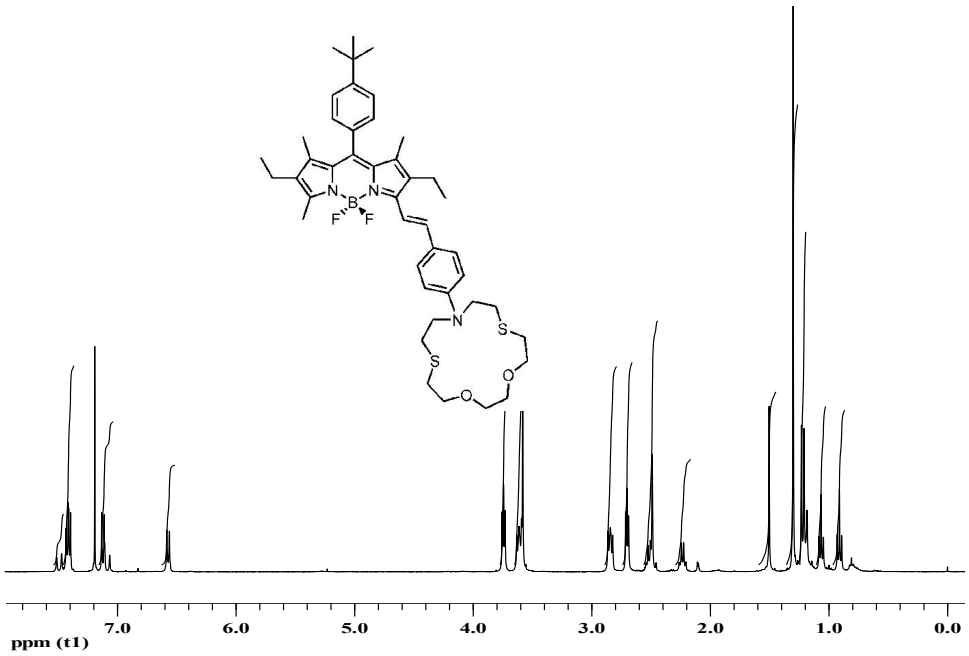


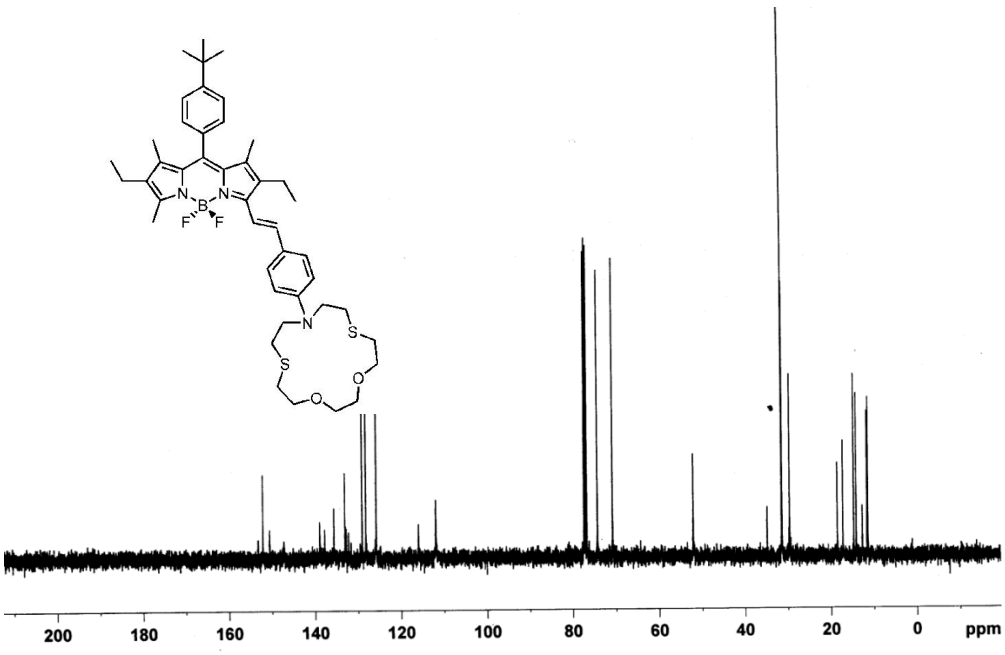

O
H
O
Br
10.0
ppm (t1)
5.0

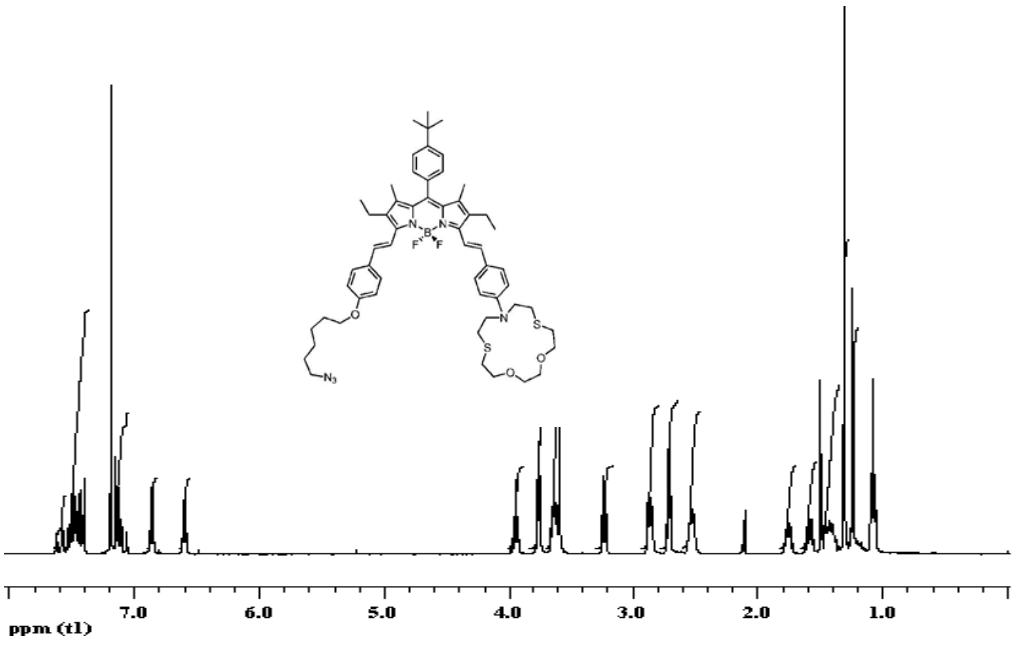

O
H
O
Br
150
100
50
ppm (t1)

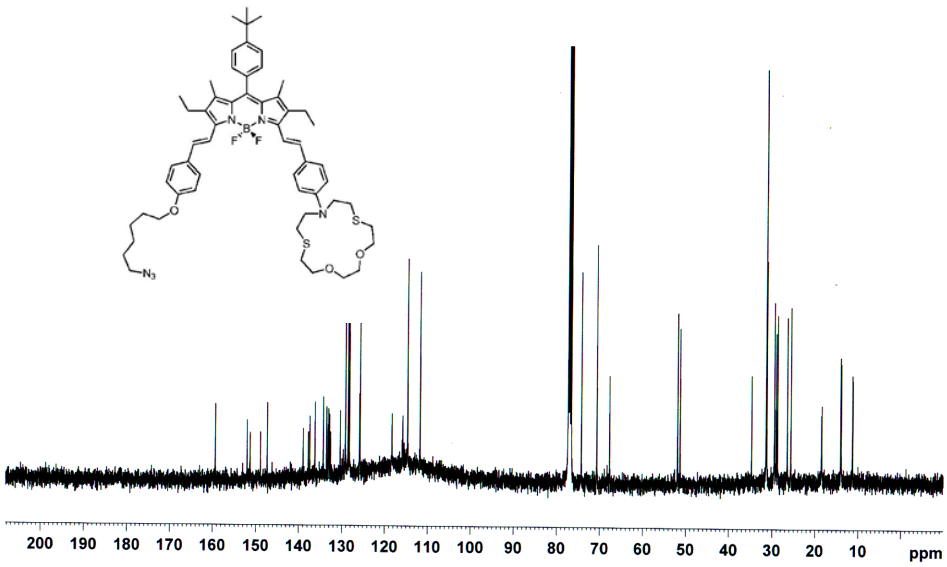

O
H
O
N3
10.0
ppm (t1)
5.0

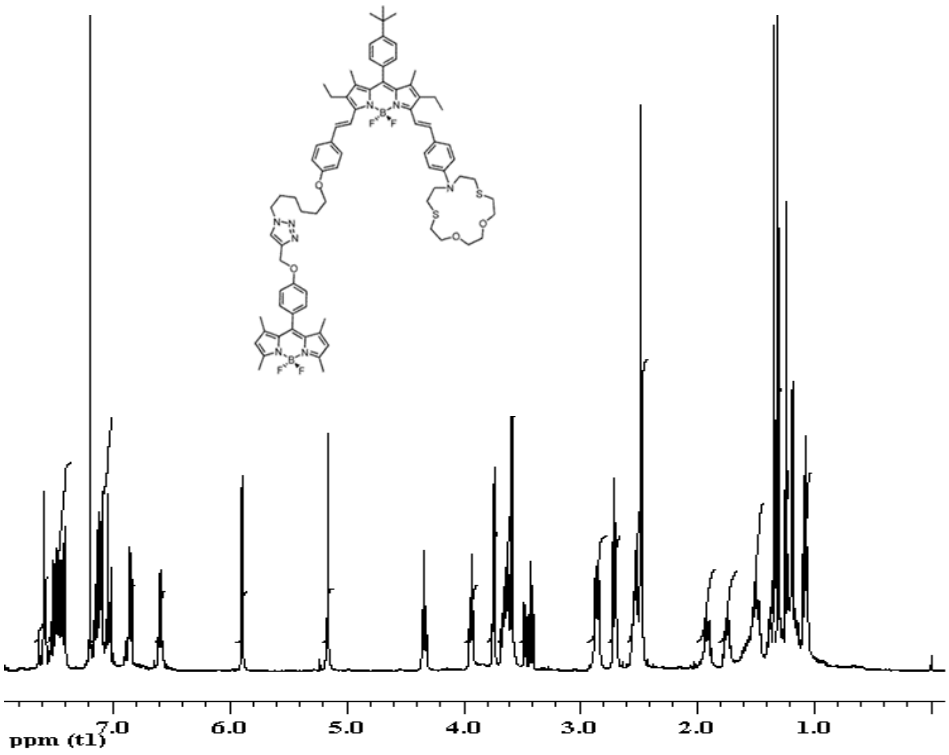

O
H
O
N3
150
100
50
0
ppm (t1)

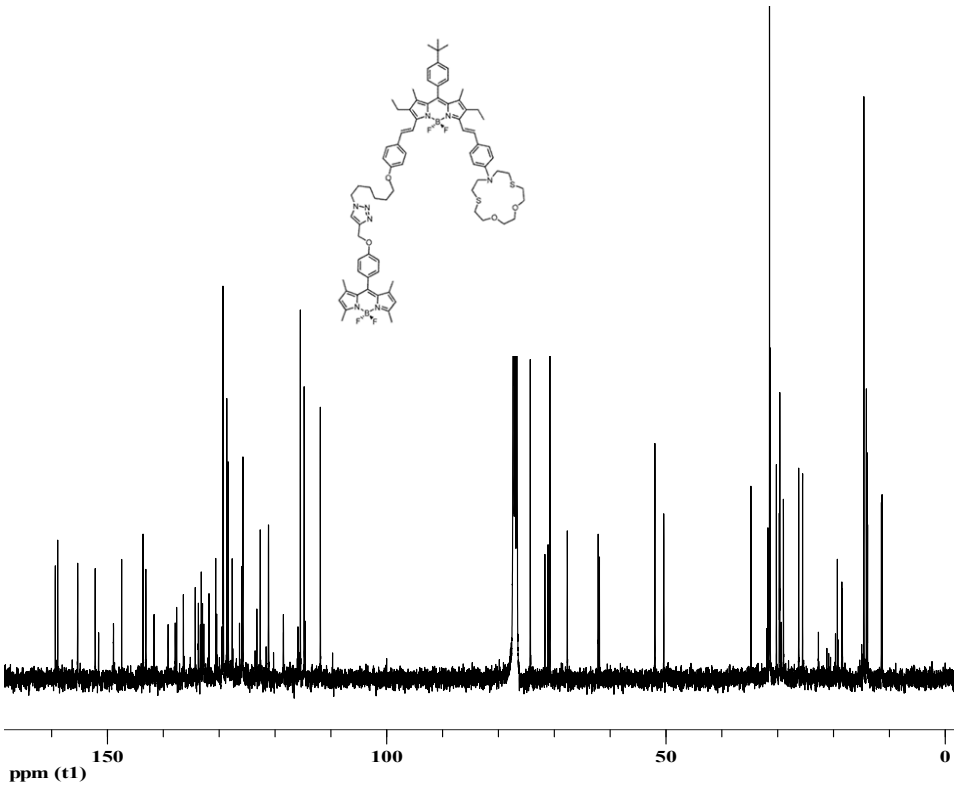

ppm (t1)
7.0
6.0
5.0
4.0
3.0
2.0
1.0
0.0

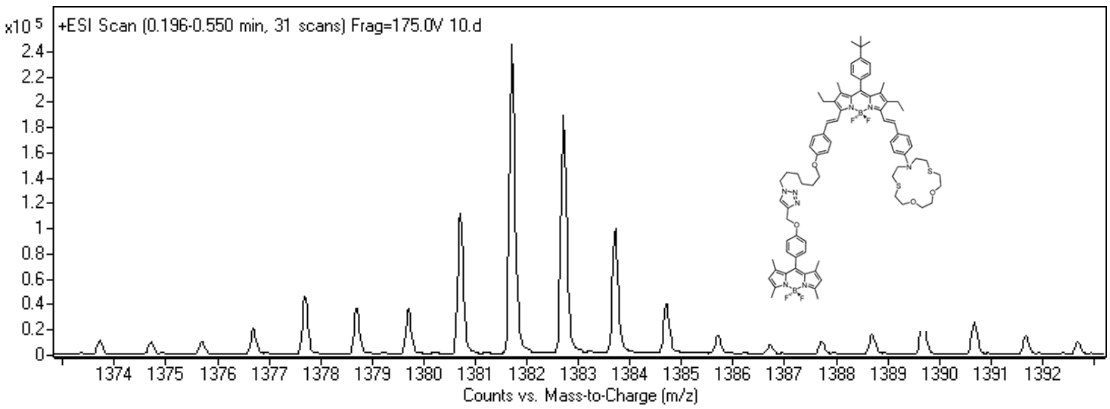

200
180
160
140
120
100
80
60
40
20
0
ppm


7.0
6.0
5.0
4.0
3.0
2.0
1.0
ppm (t1)


200 190 180 170 160 150 140 130 120 110 100 90 80 70 60 50 40 30 20 10
ppm

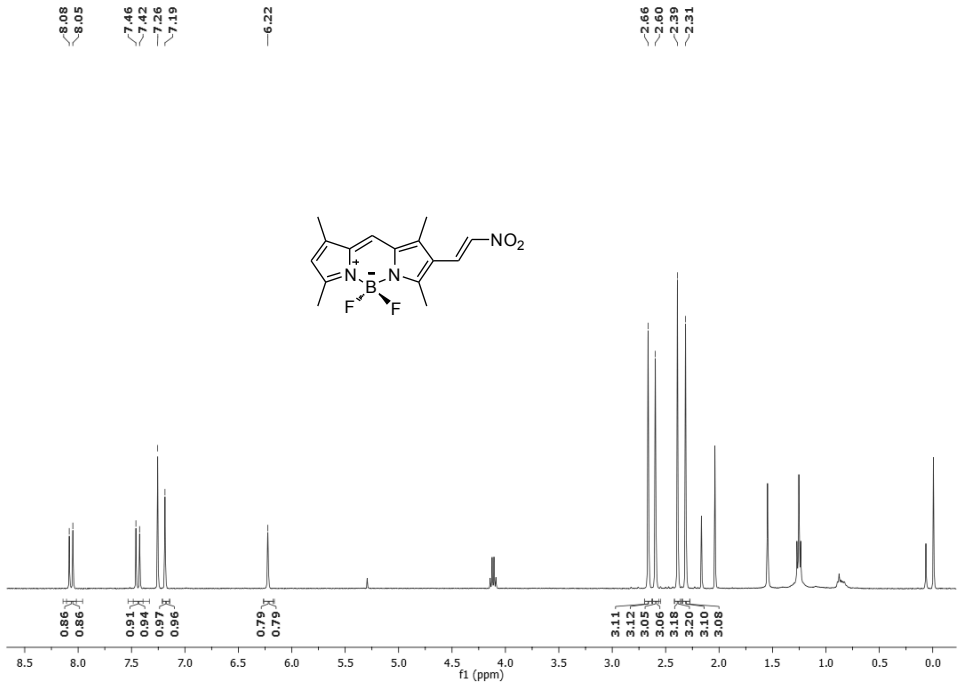

7.0
6.0
5.0
4.0
3.0
2.0
1.0
ppm (t1)

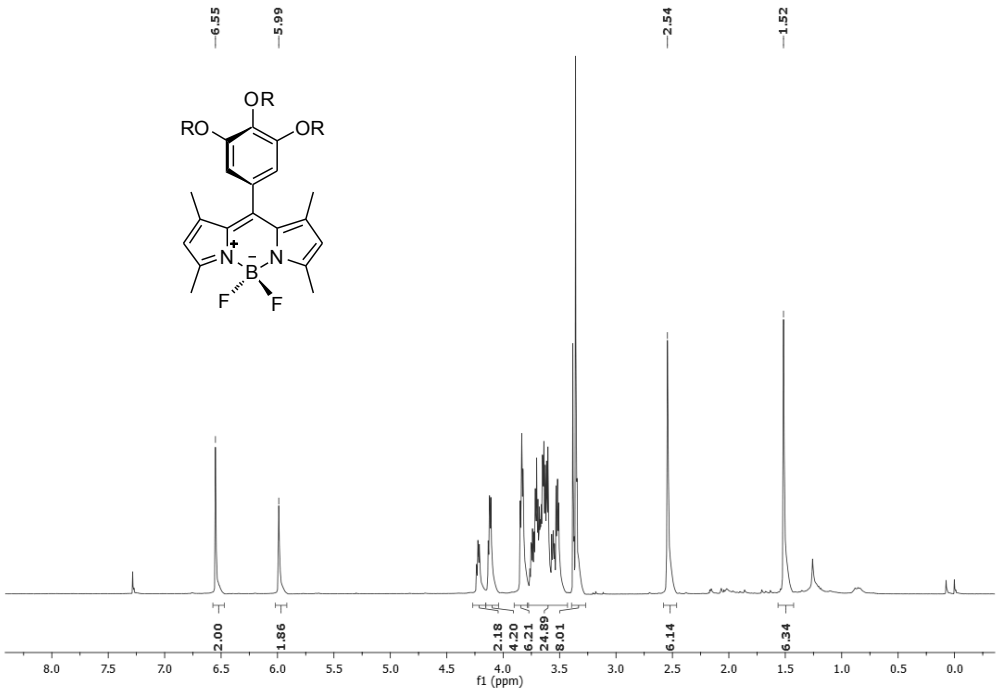

150
100
50
0
ppm (t1)

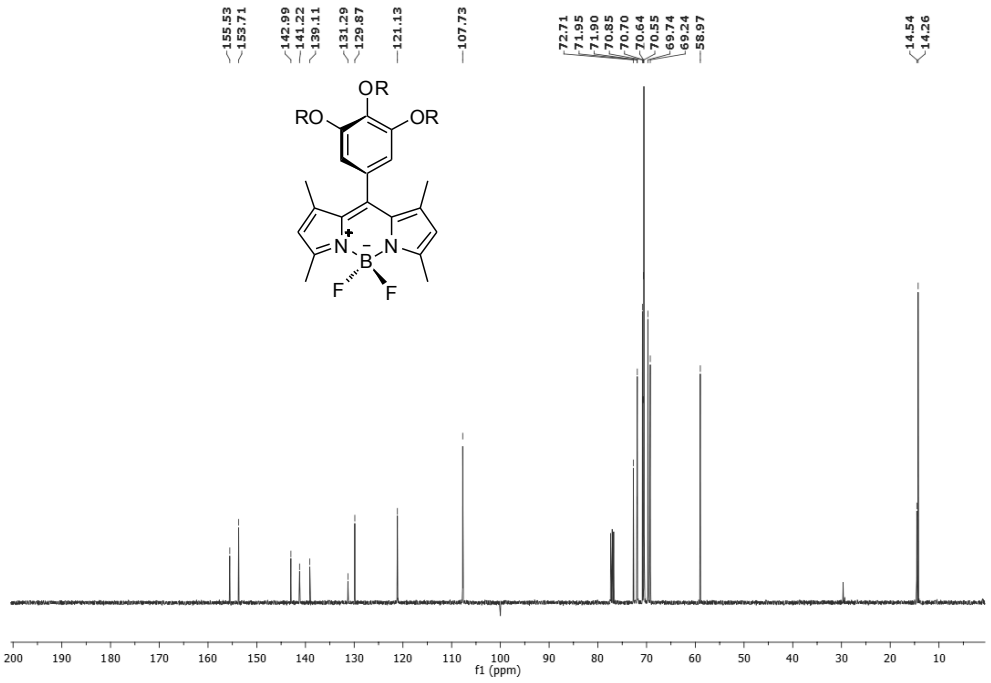

x10 5
+ESI Scan (0.196-0.550 min, 31 scans) Frag=175.0V 10.d
2.4
2.2
2
1.8
1.6
1.4
1.2
1
0.8
0.6
0.4
0.2
0
1374 1375 1376 1377 1378 1379 1380 1381 1382 1383 1384 1385 1386 1387 1388 1389 1390 1391 1392
Counts vs. Mass-to-Charge (m/z)

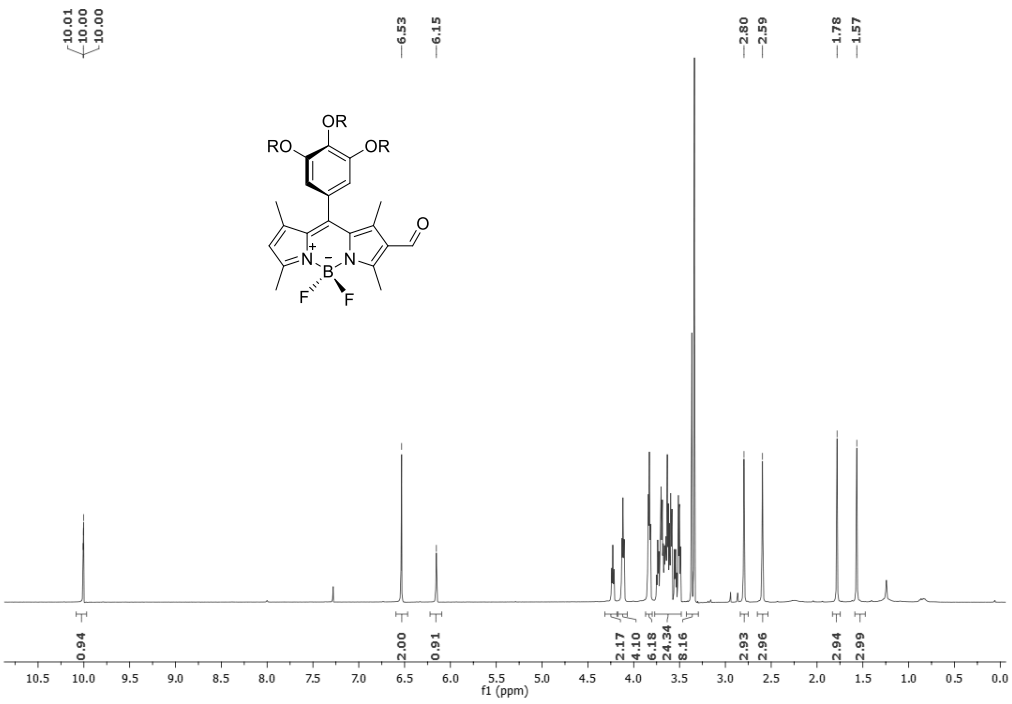
A4. Chromogenic and FluorogenicSensing of Biological Thiols in Aqueous Solutions Using BODIPY Based Reagents

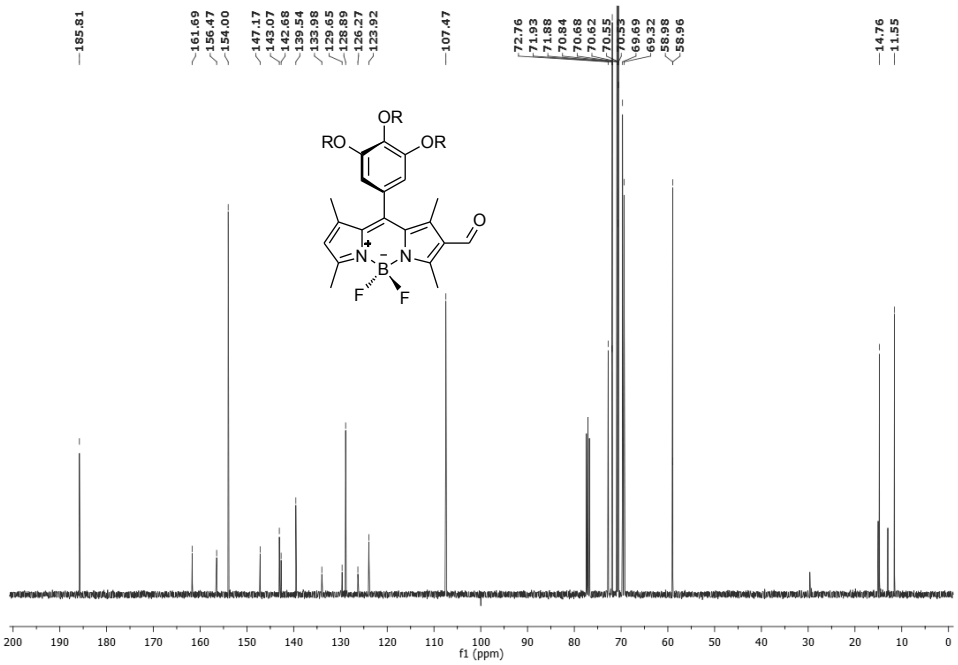
A4.1. ^{1}H, ^{13}C and Mass Spectra

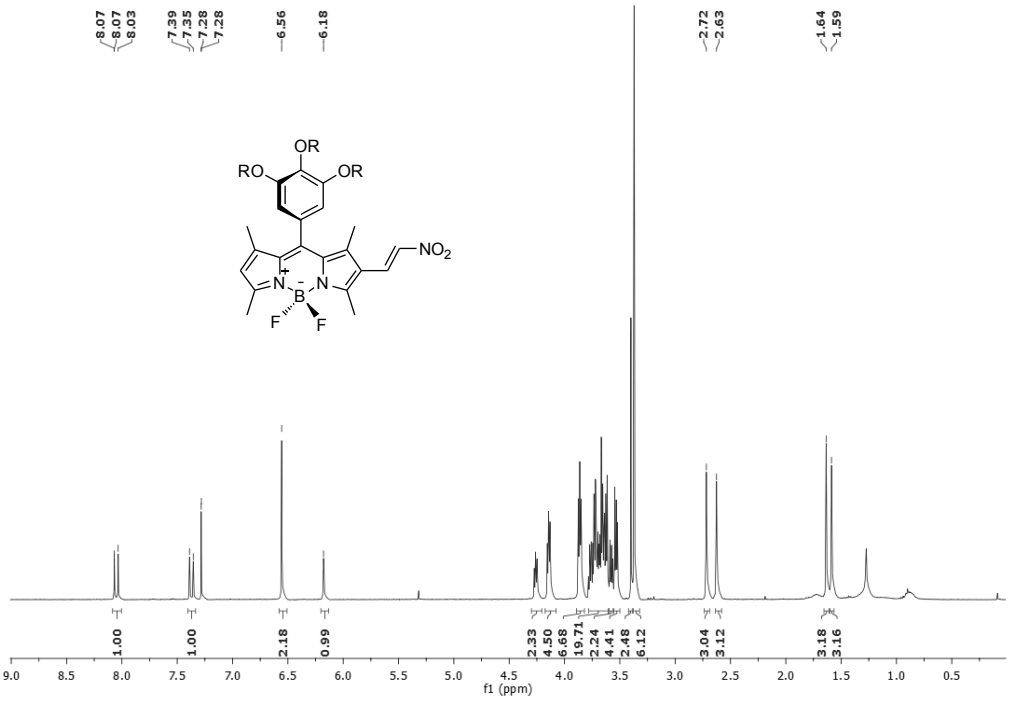


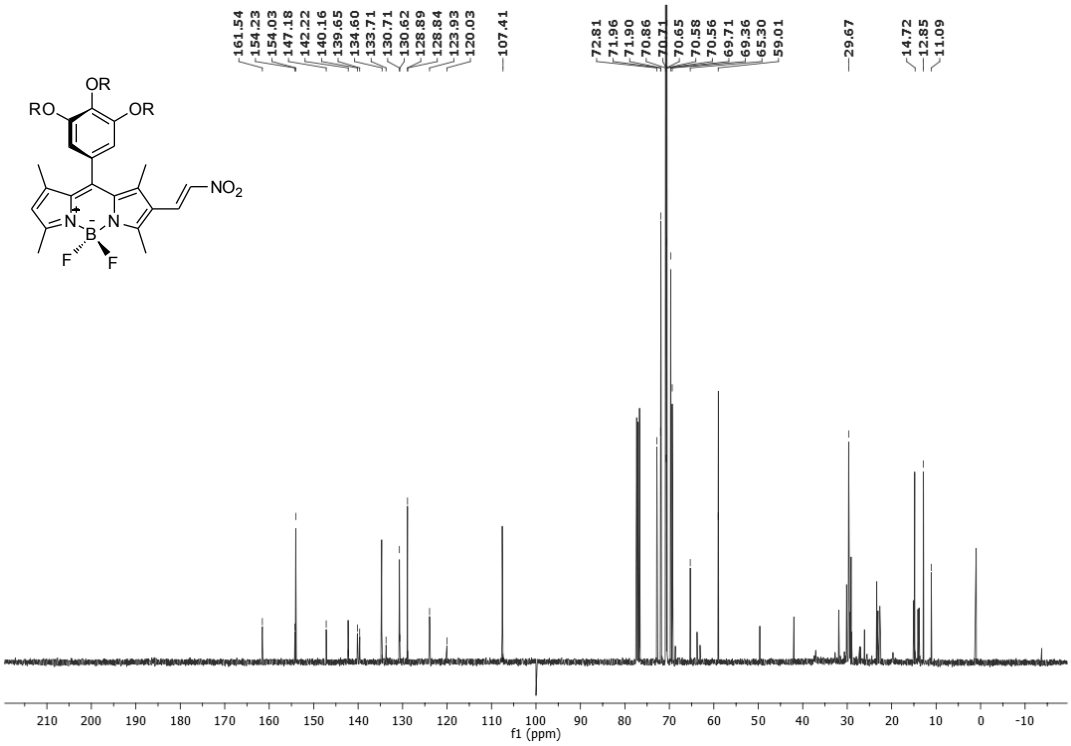


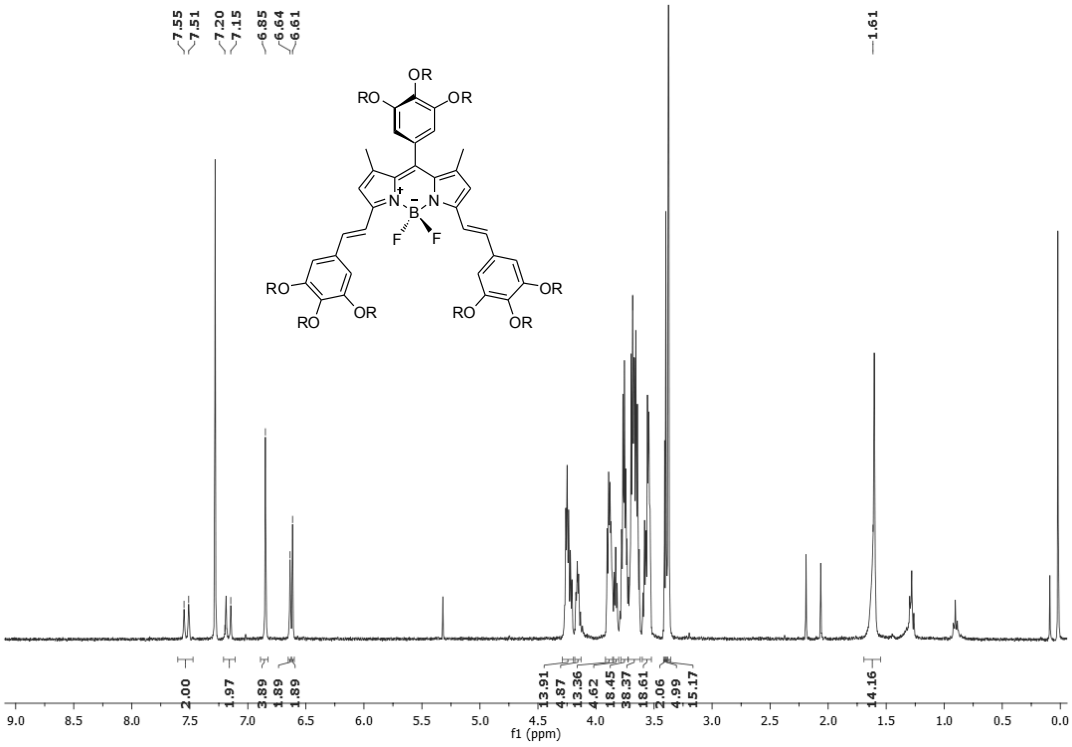

155.53
153.71
142.99
141.22
139.11
131.29
129.87
121.13
107.73
72.71
71.95
71.90
70.85
70.70
70.64
70.55
69.74
69.24
58.97
14.54
14.26
OR
RO
OR
N
B
N
F
F
f1 (ppm)

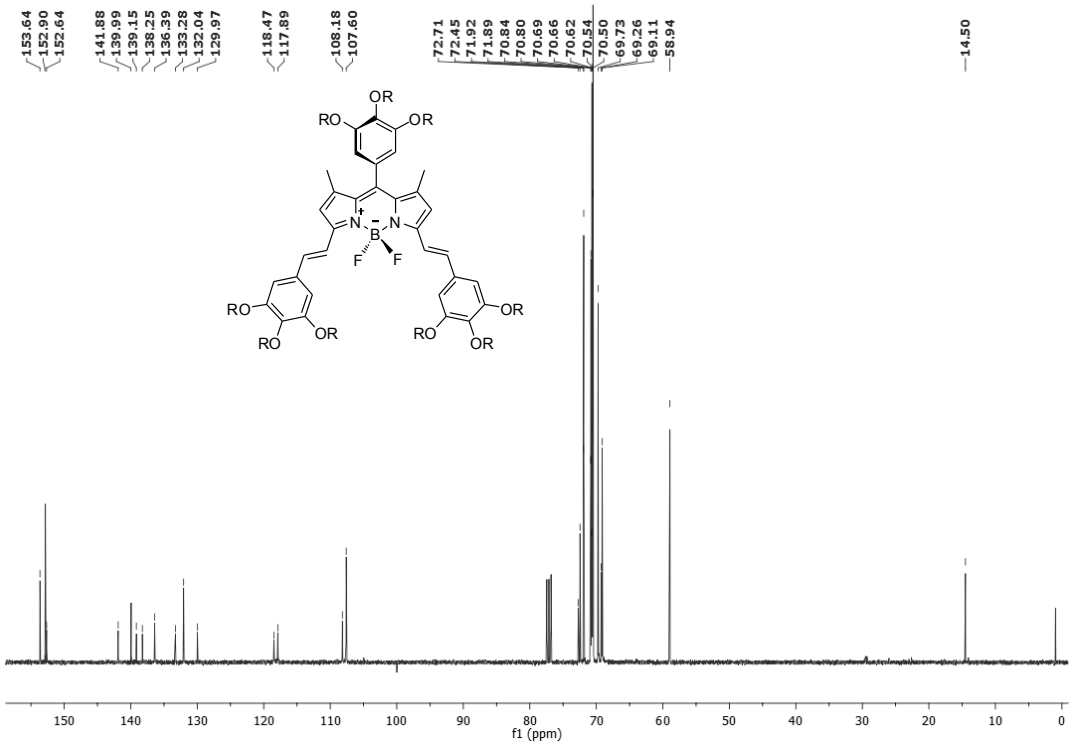

10.01
10.00
10.00
6.53
6.15
2.80
2.59
1.78
1.57
OR
RO
OR
O
N
B
N
F
F
0.94
2.00
0.91
2.17
4.10
6.18
24.34
8.16
2.93
2.96
2.94
2.99
f1 (ppm)

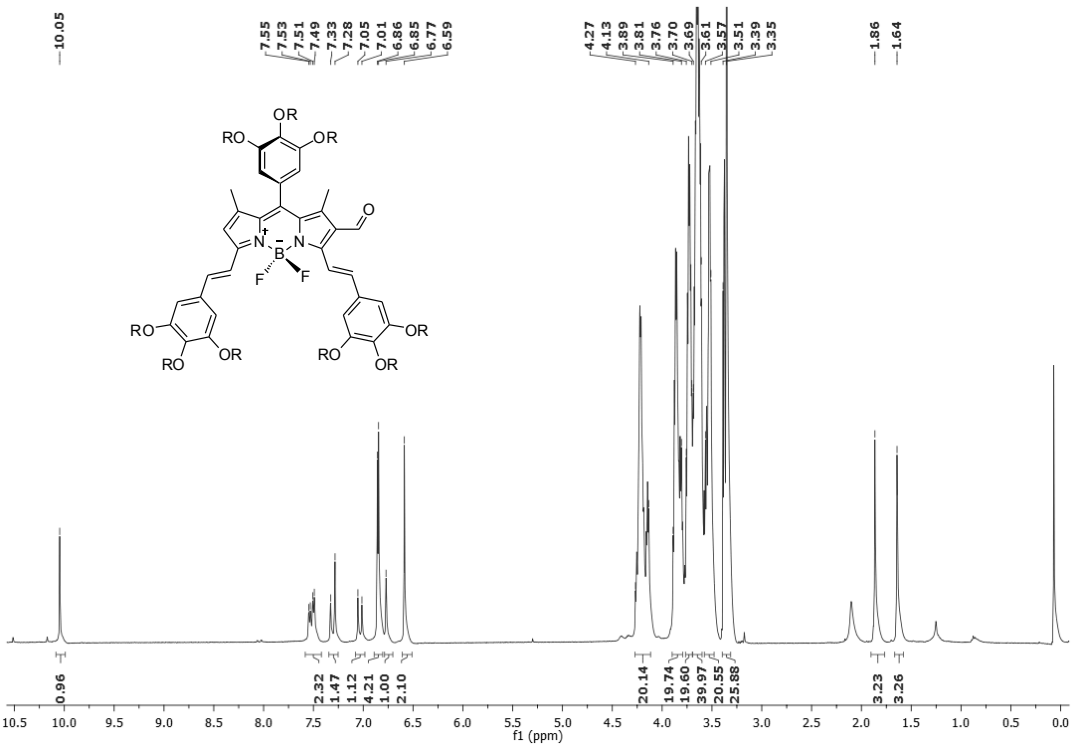

185.81
161.69
156.47
154.00
147.17
143.07
142.68
139.54
133.98
129.65
128.89
126.27
123.92
107.47
72.76
71.93
71.88
70.84
70.68
70.62
70.55
70.53
69.69
69.32
58.98
58.96
14.76
11.55
OR
RO
OR
O
N
B
N
F
F
f1 (ppm)

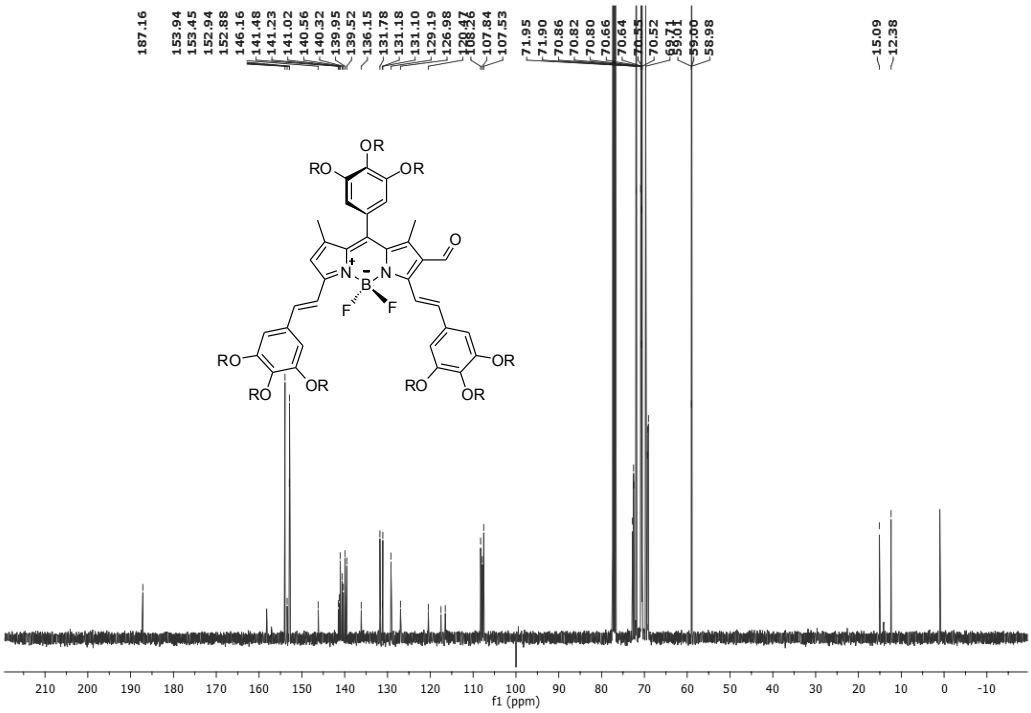

8.07
8.07
8.03
7.39
7.35
7.28
7.28
6.56
6.18
2.72
2.63
1.64
1.59
OR
RO
OR
NO2
N
B
N
F
F
1.00
1.00
2.18
0.99
2.33
4.50
6.68
19.71
2.24
4.41
2.48
6.12
3.04
3.12
3.18
3.16
f1 (ppm)

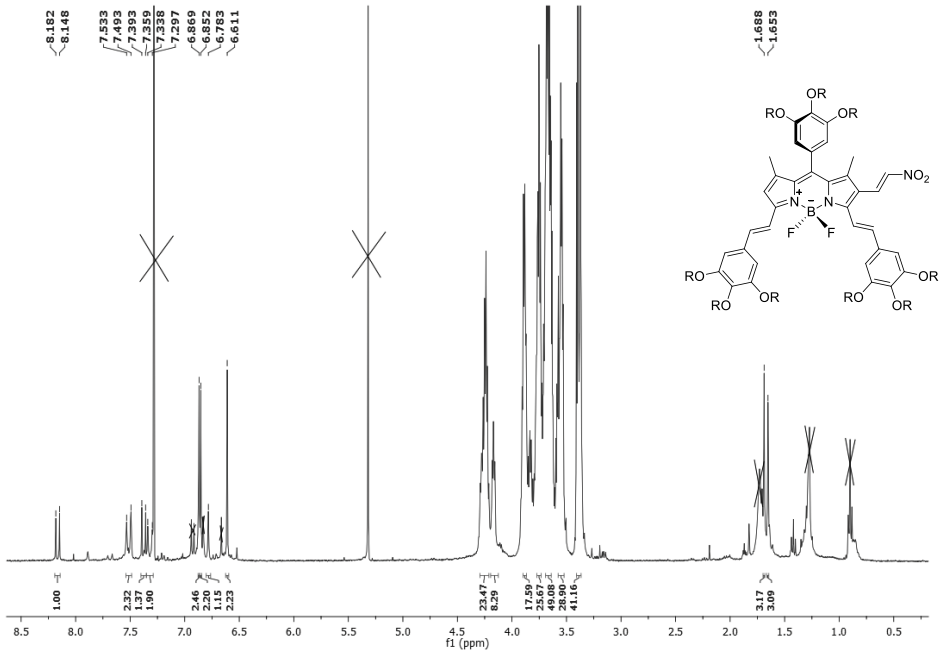

161.54
154.23
154.03
147.18
142.22
140.16
139.65
134.60
133.71
130.71
130.62
128.89
128.84
123.93
120.03
107.41
72.81
71.96
71.90
70.86
70.71
70.65
70.58
70.56
69.71
69.36
65.30
59.01
29.67
14.72
12.85
11.09
OR
RO
OR
NO2
N
B
N
F
F
f1 (ppm)

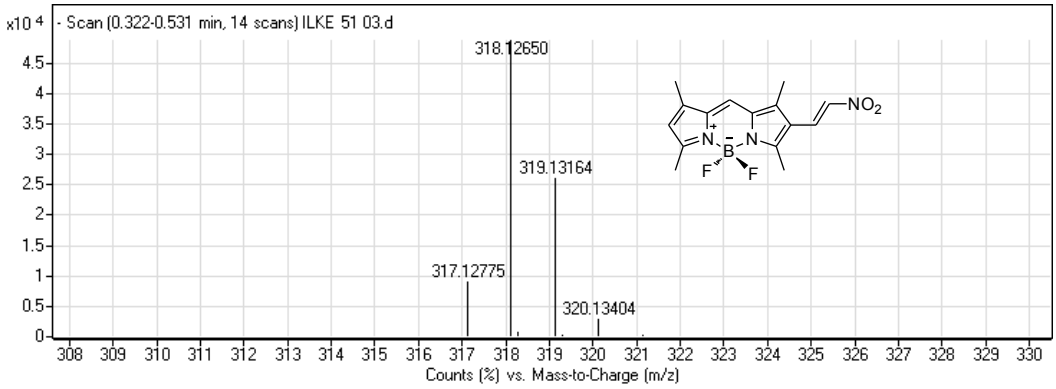

7.55
7.51
7.20
7.15
6.85
6.64
6.61
1.61
OR
RO
OR
RO
OR
RO
OR
RO
OR
2.00
1.97
3.89
1.89
1.89
13.91
4.87
13.36
4.62
18.45
38.37
18.61
2.06
4.99
15.17
14.16
f1 (ppm)

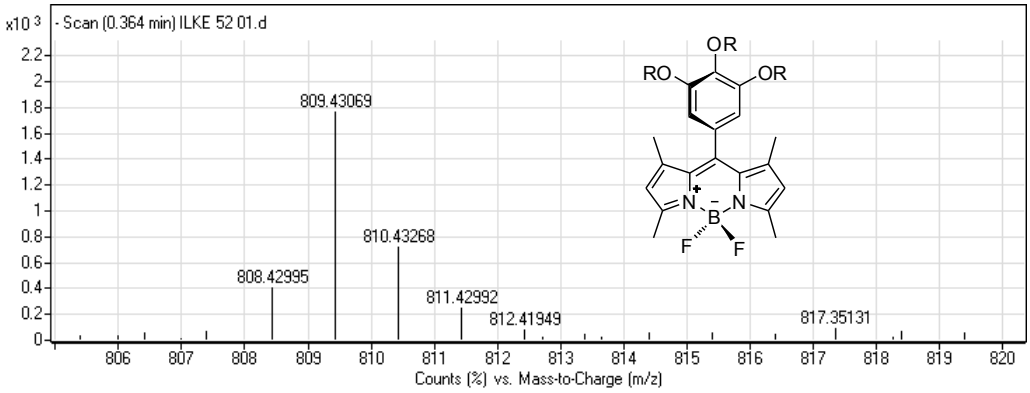

153.64
152.90
152.64
141.88
139.99
139.15
138.25
136.39
133.28
132.04
129.97
118.47
117.89
108.18
107.60
72.71
72.45
71.92
71.89
70.84
70.80
70.69
70.66
70.62
70.54
70.50
69.73
69.26
69.11
58.94
14.50
OR
RO
OR
N
B
N
F
F
RO
OR
RO
OR
RO
OR
RO
OR
150
140
130
120
110
100
90
80
70
60
50
40
30
20
10
0
f1 (ppm)

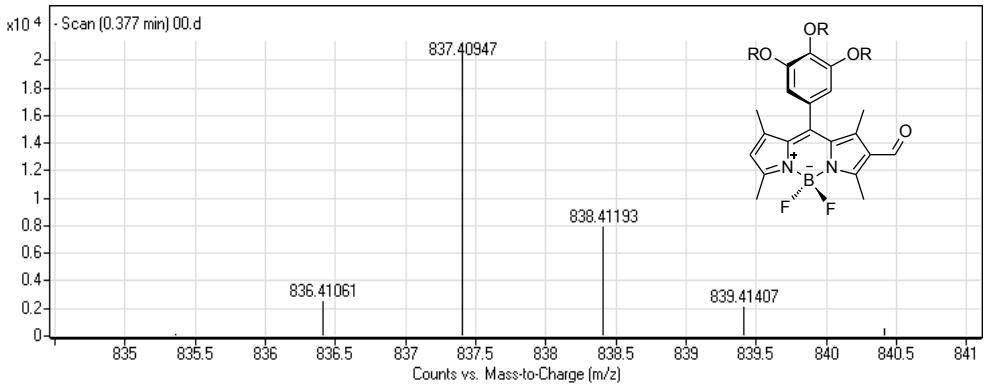

10.05
7.55
7.53
7.51
7.49
7.33
7.28
7.05
7.01
6.86
6.85
6.77
6.59
4.27
4.13
3.89
3.81
3.76
3.70
3.69
3.61
3.57
3.51
3.39
3.35
1.86
1.64
OR
RO
OR
O
N
B
N
F
F
RO
OR
RO
OR
RO
OR
RO
OR
0.96
2.32
1.47
1.12
4.21
1.00
2.10
20.14
19.74
19.60
39.97
20.55
25.88
3.23
3.26
10.5
10.0
9.5
9.0
8.5
8.0
7.5
7.0
6.5
6.0
5.5
5.0
4.5
4.0
3.5
3.0
2.5
2.0
1.5
1.0
0.5
0.0
f1 (ppm)

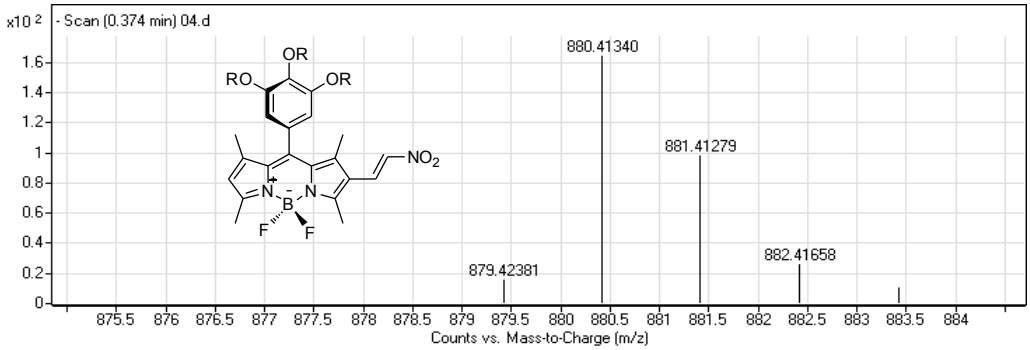

187.16
153.94
153.45
152.94
152.88
146.16
141.48
141.23
141.02
140.56
140.32
139.95
139.52
136.15
131.78
131.18
131.10
129.19
126.98
120.47
108.26
107.84
107.53
71.95
71.90
70.86
70.82
70.80
70.66
70.64
70.52
69.01
59.00
58.98
15.09
12.38
OR
RO
O
N
B
F
210 200 190 180 170 160 150 140 130 120 110 100 90 80 70 60 50 40 30 20 10 0 -10
f1 (ppm)

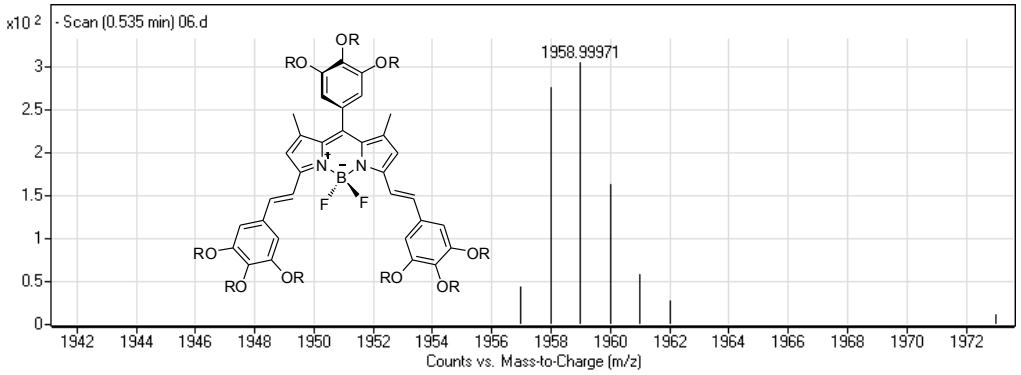

8.182
8.148
7.533
7.493
7.393
7.359
7.338
7.297
6.869
6.852
6.783
6.611
1.688
1.653
NO2
1.00
2.32
1.37
1.90
2.46
2.20
1.15
2.23
23.47
8.29
17.59
25.67
49.08
28.90
41.16
3.17
3.09
8.5 8.0 7.5 7.0 6.5 6.0 5.5 5.0 4.5 4.0 3.5 3.0 2.5 2.0 1.5 1.0 0.5
f1 (ppm)

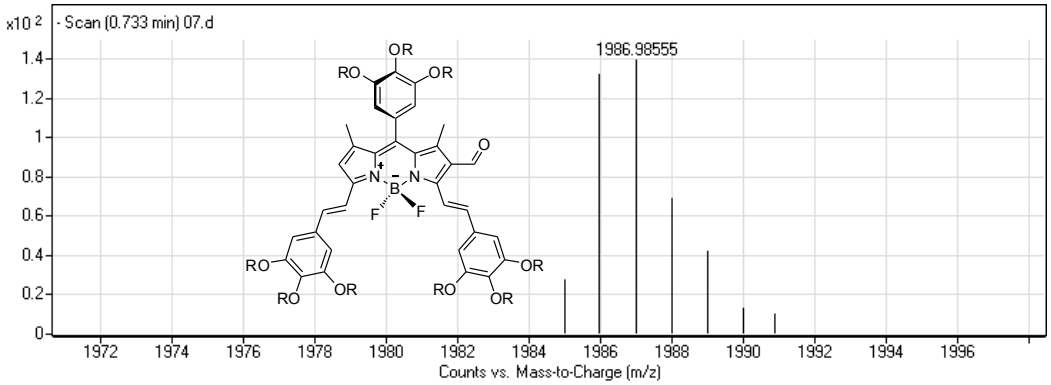

x10 4 - Scan (0.322-0.531 min, 14 scans) ILKE 51 03.d
318.12650
319.13164
317.12775
320.13404
NO2
Counts (%) vs. Mass-to-Charge (m/z)

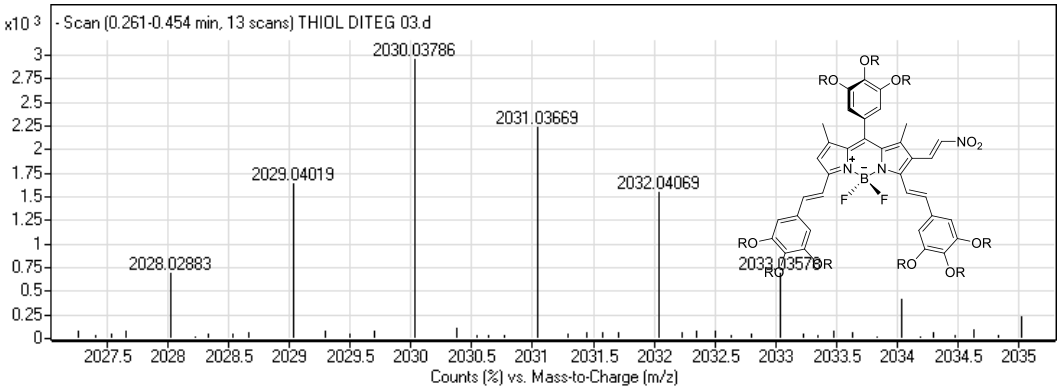

x10 3 - Scan (0.364 min) ILKE 52 01.d
809.43069
810.43268
808.42995
811.42992
812.41949
817.35131
OR
RO
OR
Counts (%) vs. Mass-to-Charge (m/z)


x10 4 - Scan (0.377 min) 00.d
837.40947
838.41193
836.41061
839.41407
OR
RO
OR
O
Counts vs. Mass-to-Charge (m/z)


x10 2 - Scan (0.374 min) 04.d
880.41340
881.41279
879.42381
882.41658
OR
RO
OR
NO2
Counts vs. Mass-to-Charge (m/z)

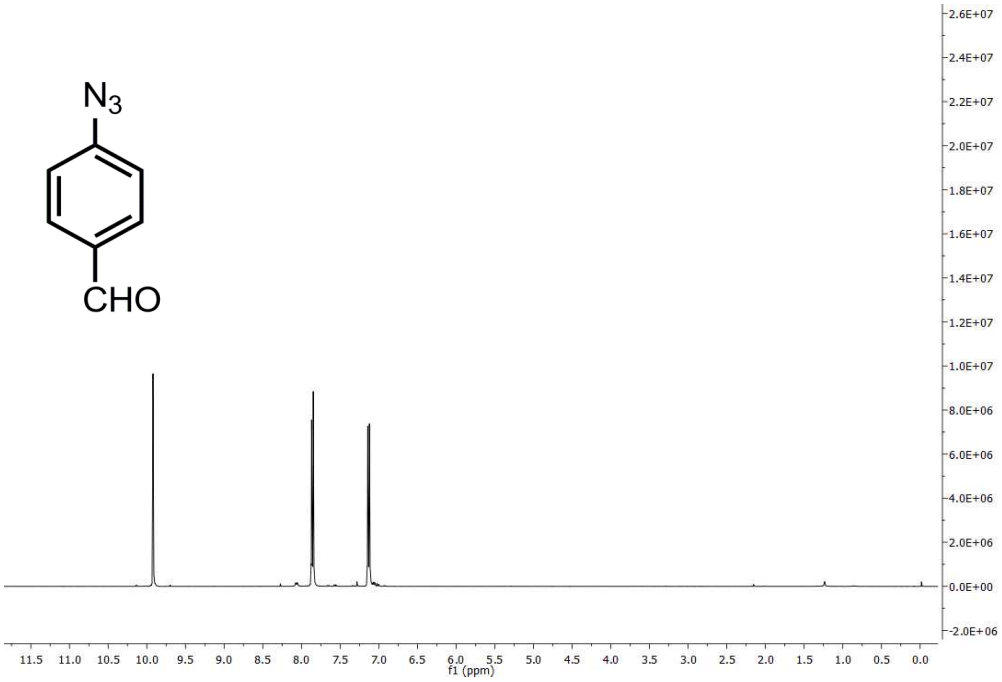

x10 2
- Scan (0.535 min) 06.d
1958.99971
Counts vs. Mass-to-Charge (m/z)

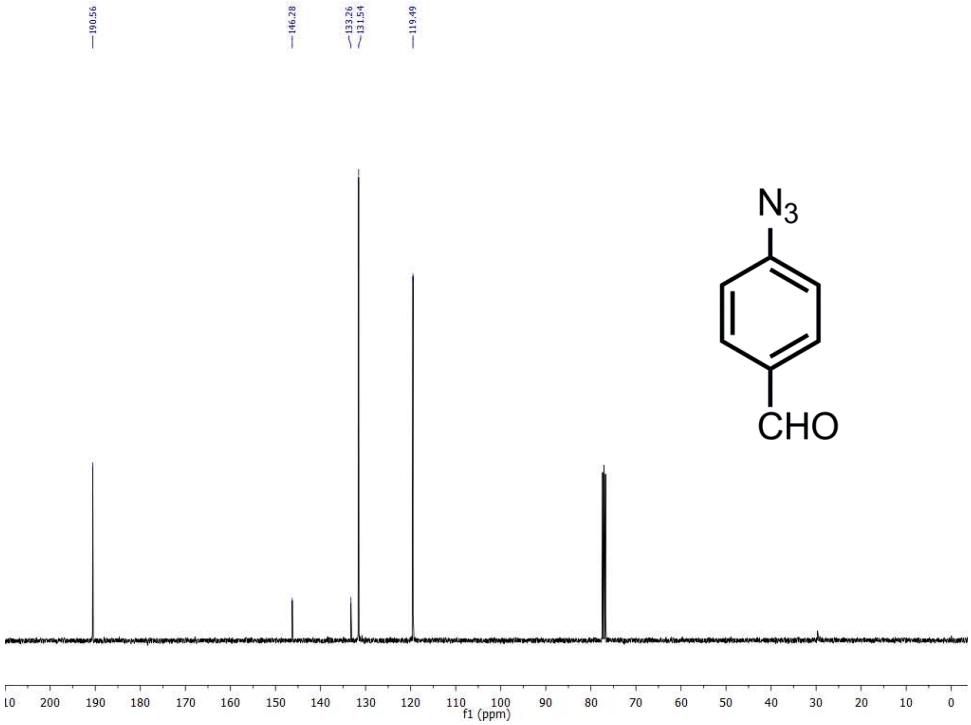

x10 2
- Scan (0.733 min) 07.d
1986.98555
Counts vs. Mass-to-Charge (m/z)

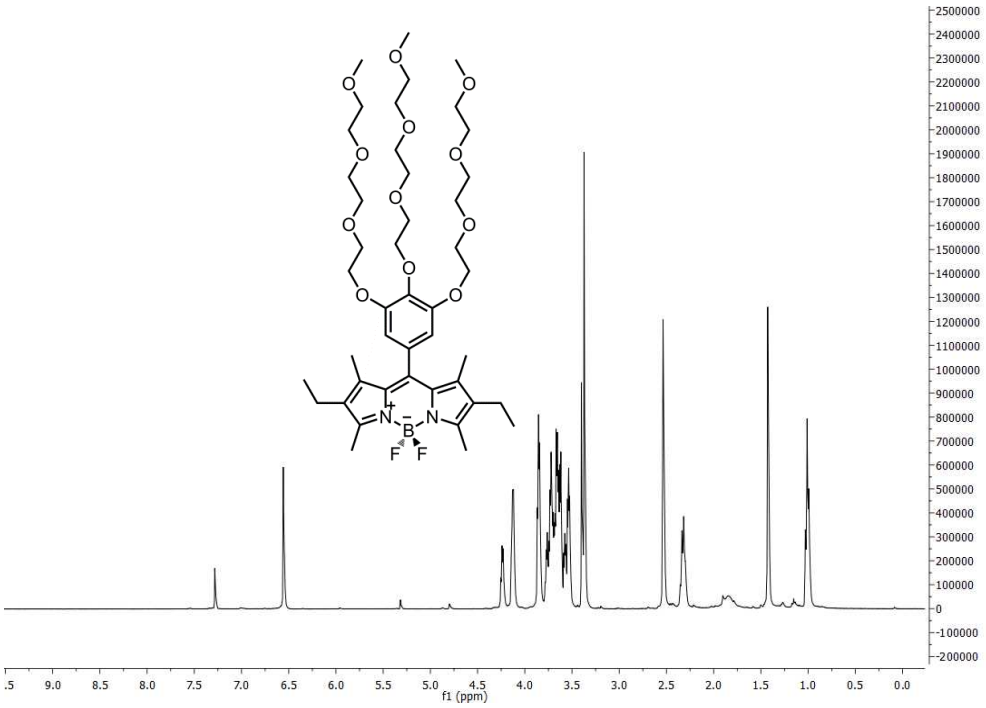

x10 3
- Scan (0.261-0.454 min, 13 scans) THIOL DITEG 03.d
2030.03786
2031.03669
2029.04019
2032.04069
2028.02883
2033.03578
Counts (%) vs. Mass-to-Charge (m/z)

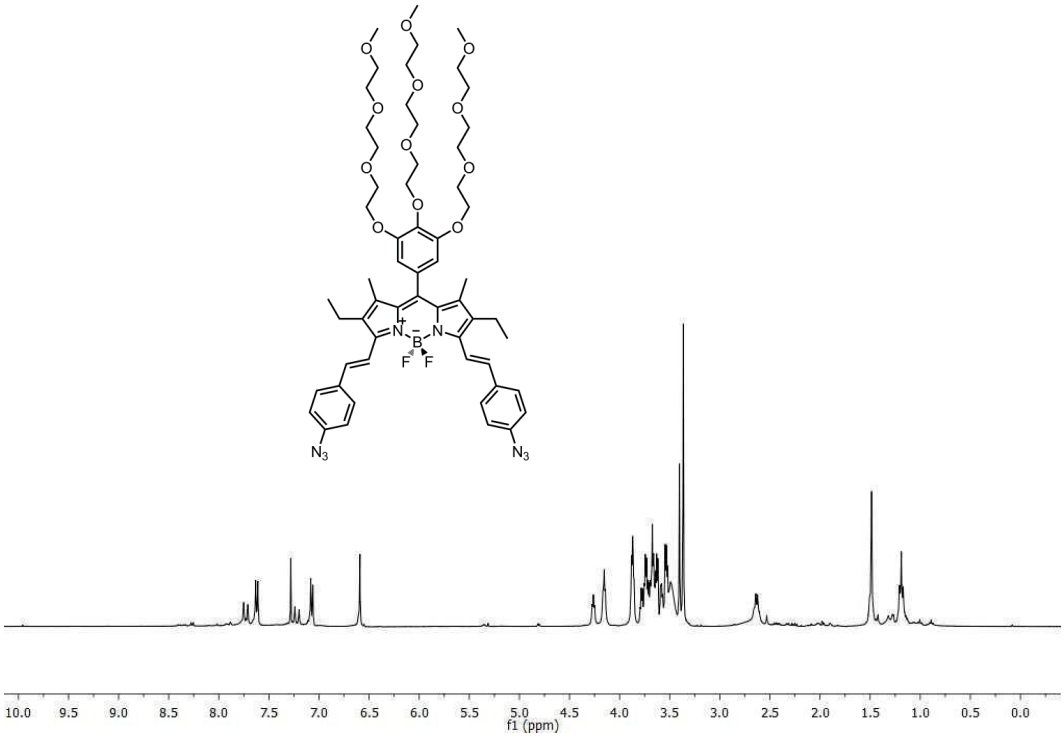
A5. Fast Responding and Selective Near-IR BODIPY Dye for Hydrogen Sulfide Sensing

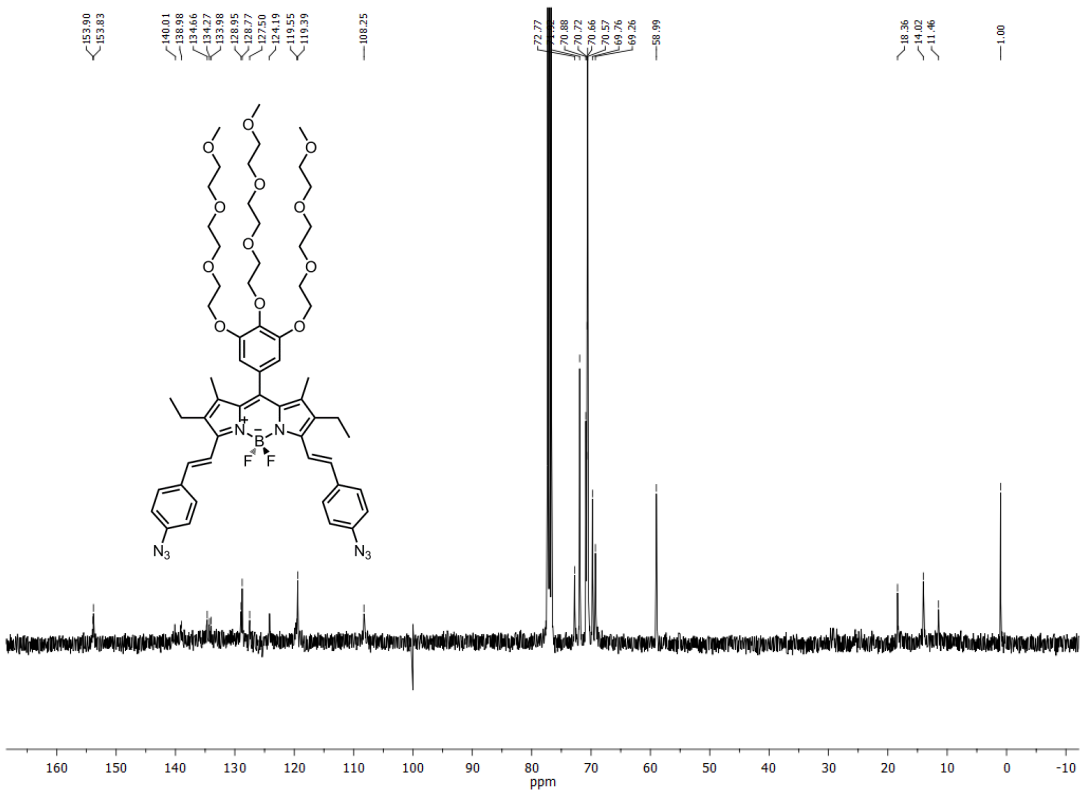
A5.1. ^{1}H, ^{13}C and Mass Spectra

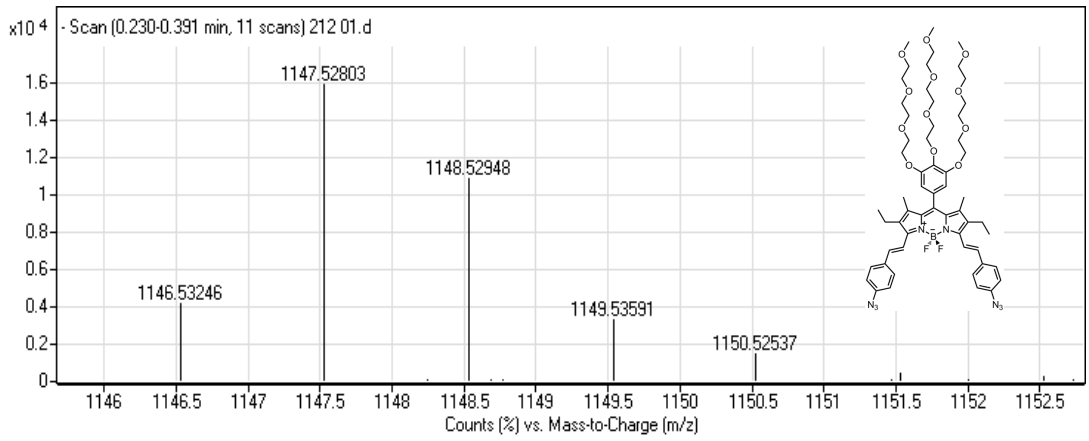


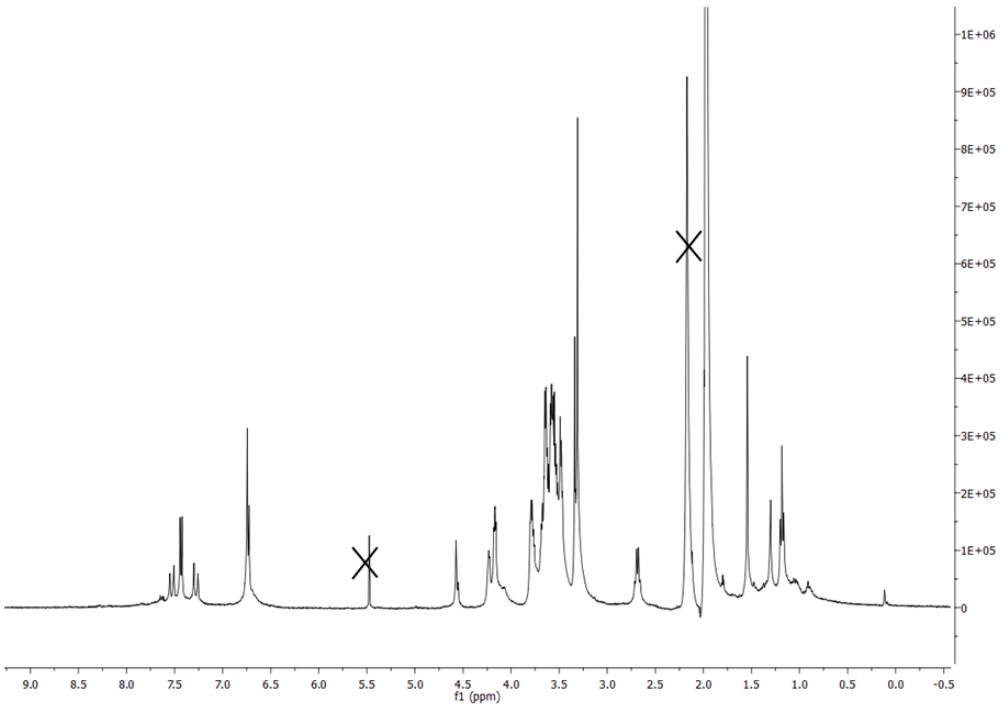



f1 (ppm)


f1 (ppm)


153.90
153.83
140.01
138.98
134.66
134.27
133.98
128.95
128.77
127.50
124.19
119.55
119.39
108.25
72.77
70.88
70.72
70.66
70.57
69.76
69.26
58.99
18.36
14.02
11.46
1.00
160
150
140
130
120
110
100
90
80
70
60
50
40
30
20
10
0
-10
ppm

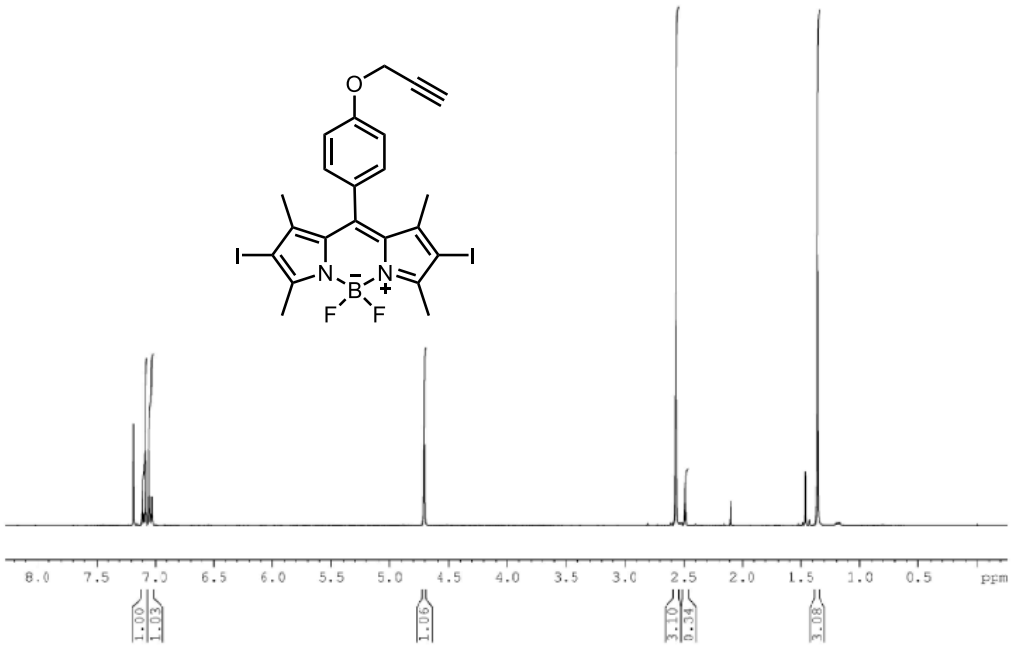

x10 4
- Scan (0.230-0.391 min, 11 scans) 212 01.d
1147.52803
1148.52948
1146.53246
1149.53591
1150.52537
1.6
1.4
1.2
1
0.8
0.6
0.4
0.2
0
1146
1146.5
1147
1147.5
1148
1148.5
1149
1149.5
1150
1150.5
1151
1151.5
1152
1152.5
Counts (%) vs. Mass-to-Charge (m/z)

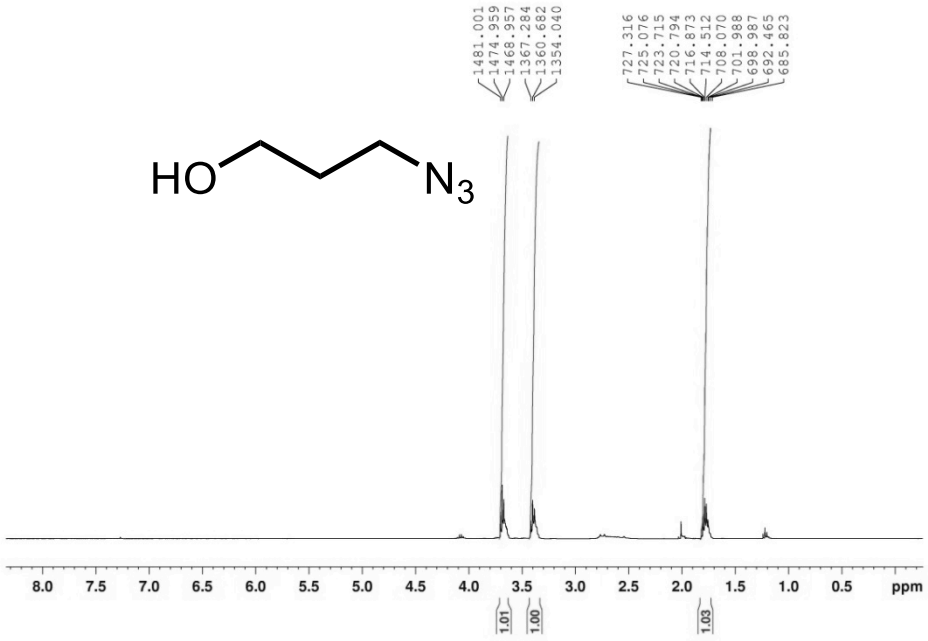


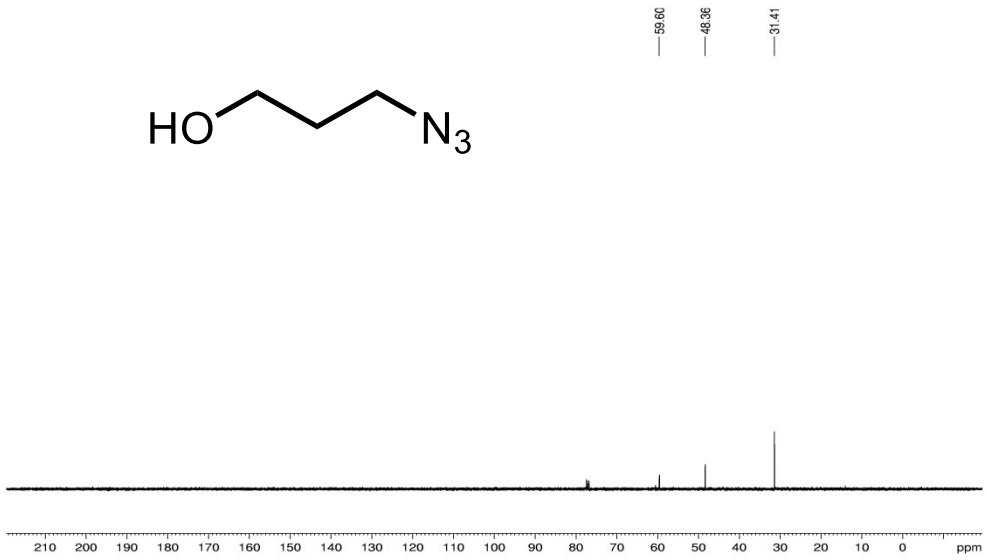
^{1}H NMR spectrum of Compound **1** after addition the addition of Na_2S.

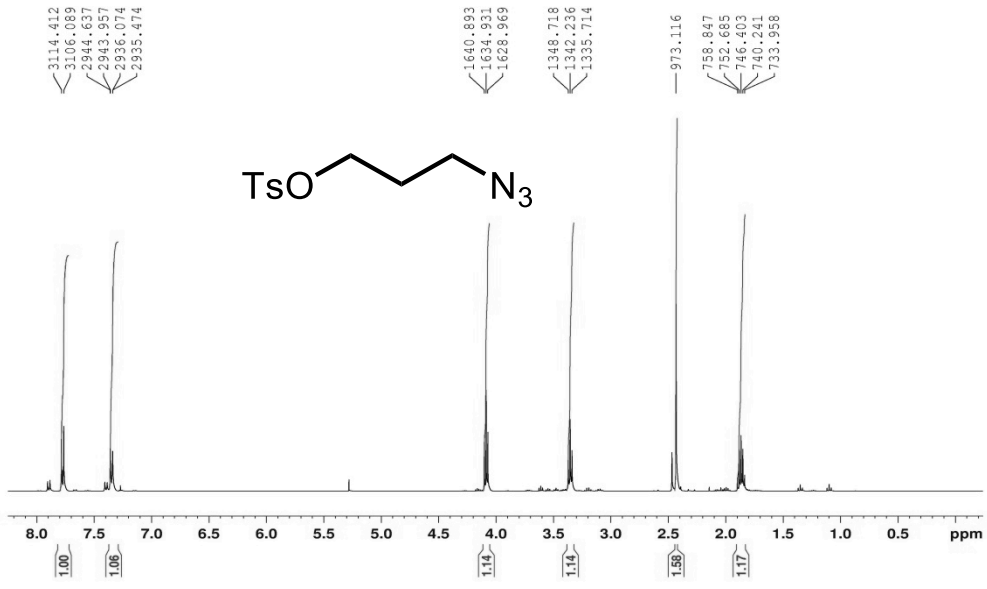
A6. Persistent Luminescent Nanoparticles (PLNP) Mediated Activation of Photosensitizers for Photodynamic Therapy

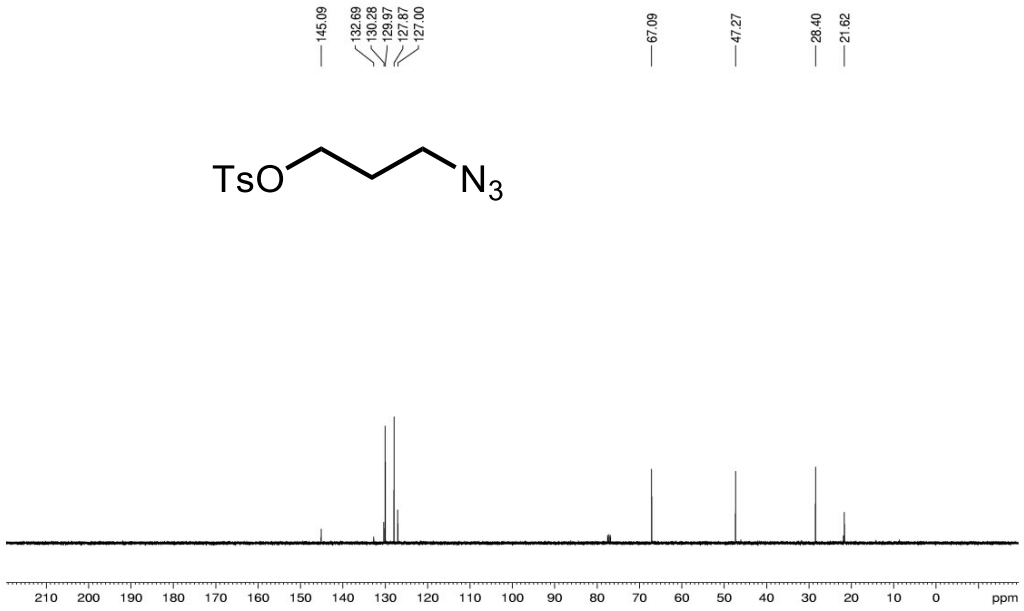
A6.1. ^{1}H, ^{13}C and Mass Spectra

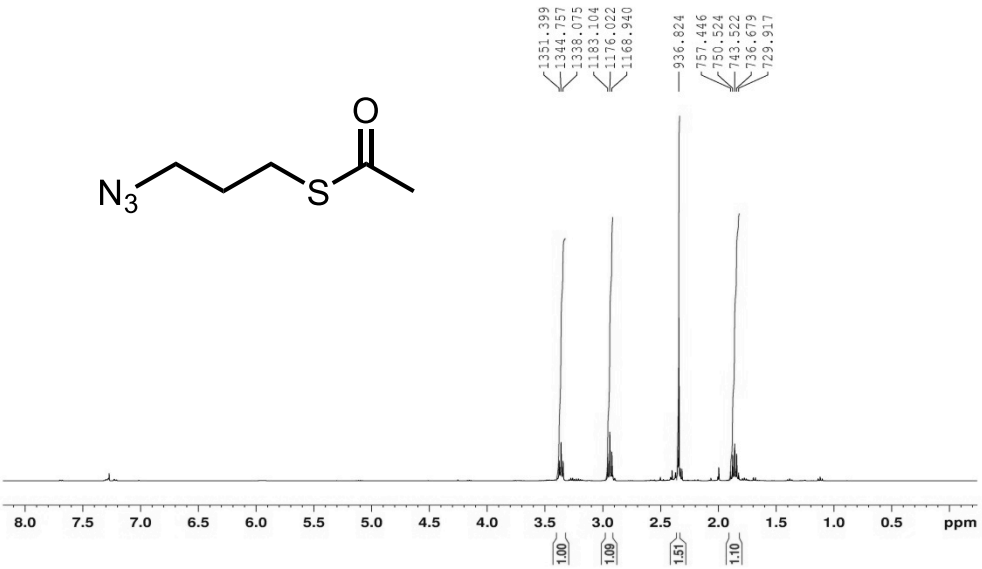




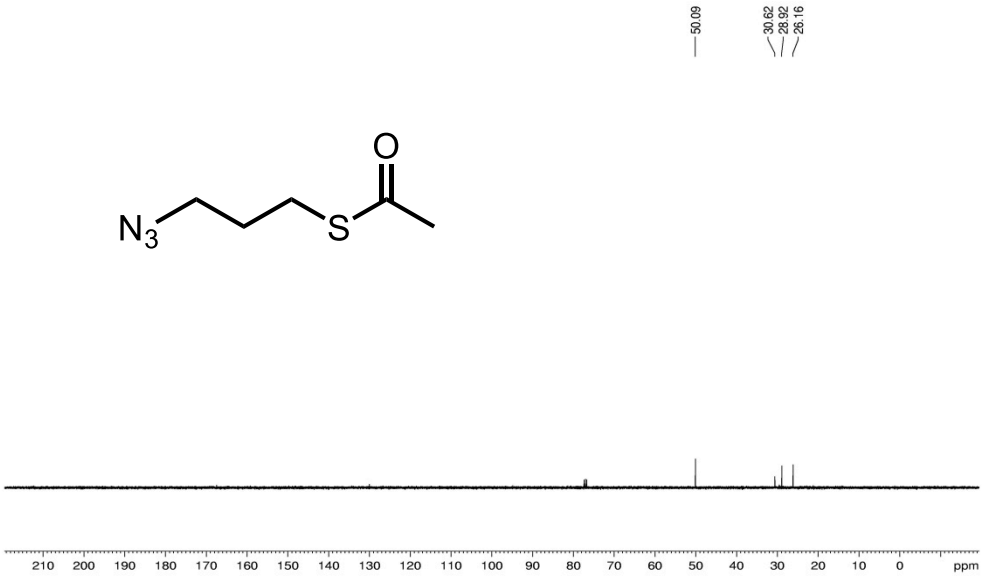

59.60
48.36
31.41
HO
N3
210 200 190 180 170 160 150 140 130 120 110 100 90 80 70 60 50 40 30 20 10 0 ppm

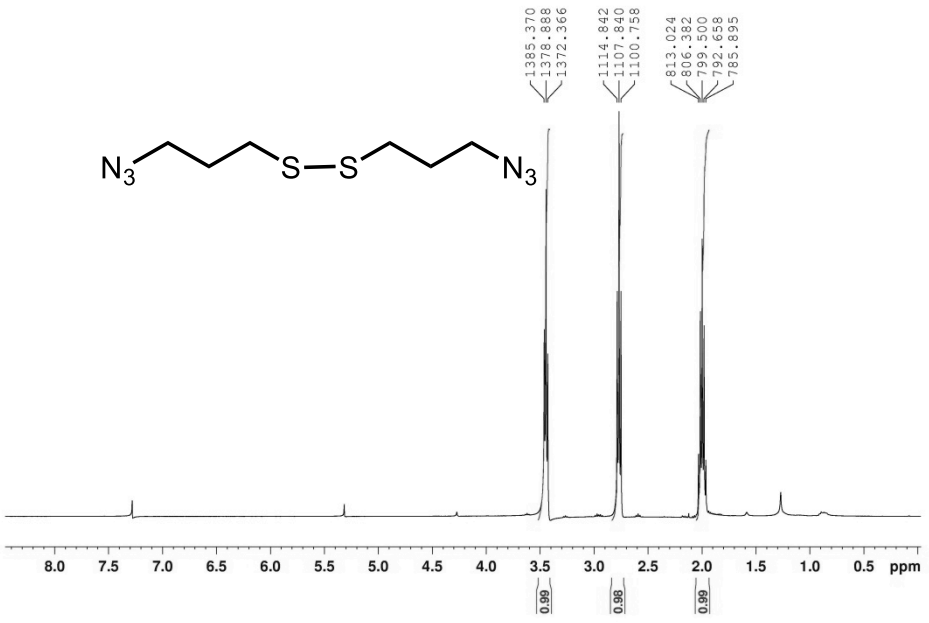

3114.412
3106.089
2944.637
2943.957
2936.074
2935.474
1640.893
1634.931
1628.969
1348.718
1342.236
1335.714
973.116
758.847
752.685
746.403
740.241
733.958
TsO
N3
8.0 7.5 7.0 6.5 6.0 5.5 5.0 4.5 4.0 3.5 3.0 2.5 2.0 1.5 1.0 0.5 ppm
1.00
1.06
1.14
1.14
1.58
1.17

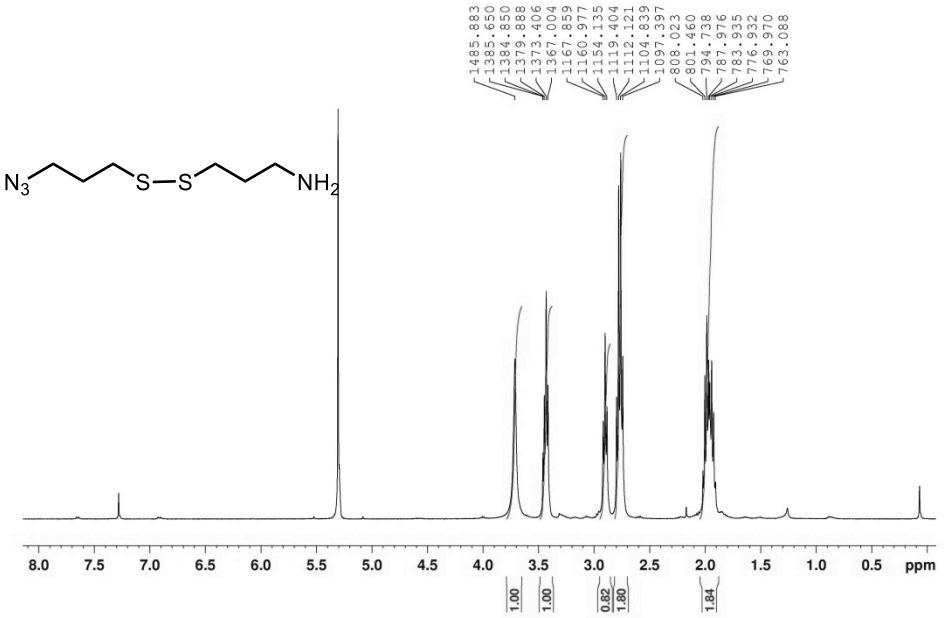

145.09
132.69
130.28
129.97
127.87
127.00
67.09
47.27
28.40
21.62
TsO
N3
210 200 190 180 170 160 150 140 130 120 110 100 90 80 70 60 50 40 30 20 10 0 ppm

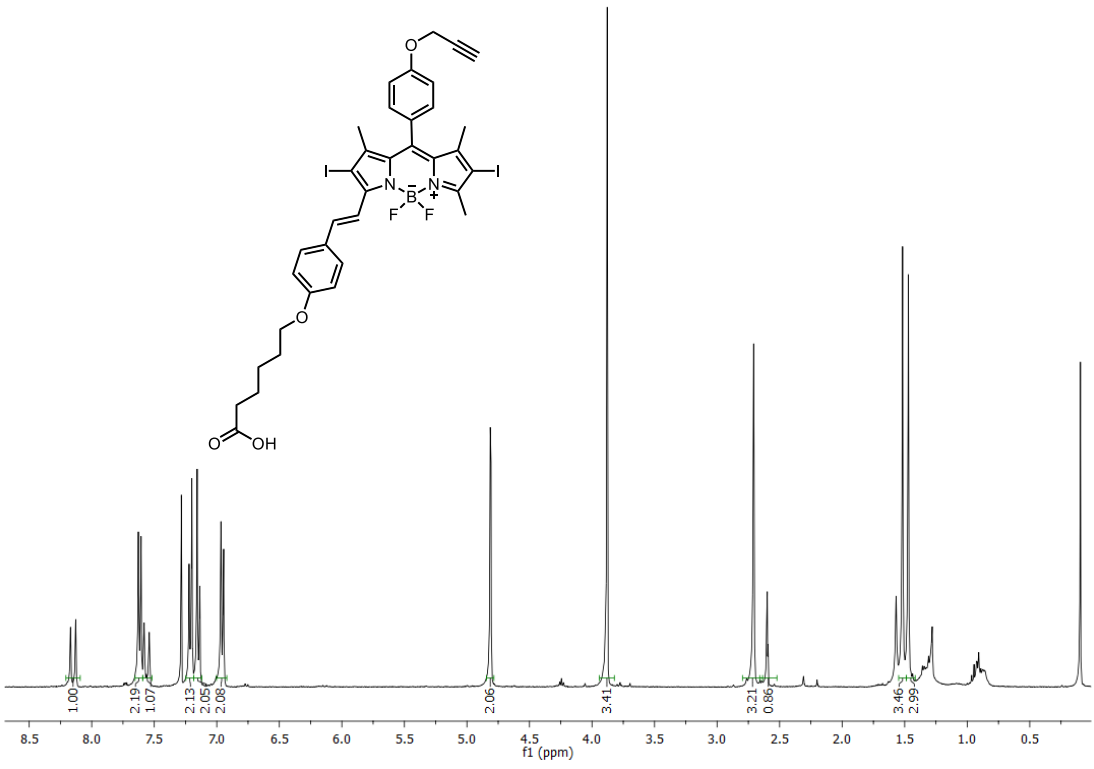

1351.399
1344.757
1338.075
1183.104
1176.022
1168.940
936.824
757.446
750.524
743.522
736.679
729.917
O
N3
S
8.0 7.5 7.0 6.5 6.0 5.5 5.0 4.5 4.0 3.5 3.0 2.5 2.0 1.5 1.0 0.5 ppm
1.00
1.09
1.51
1.10

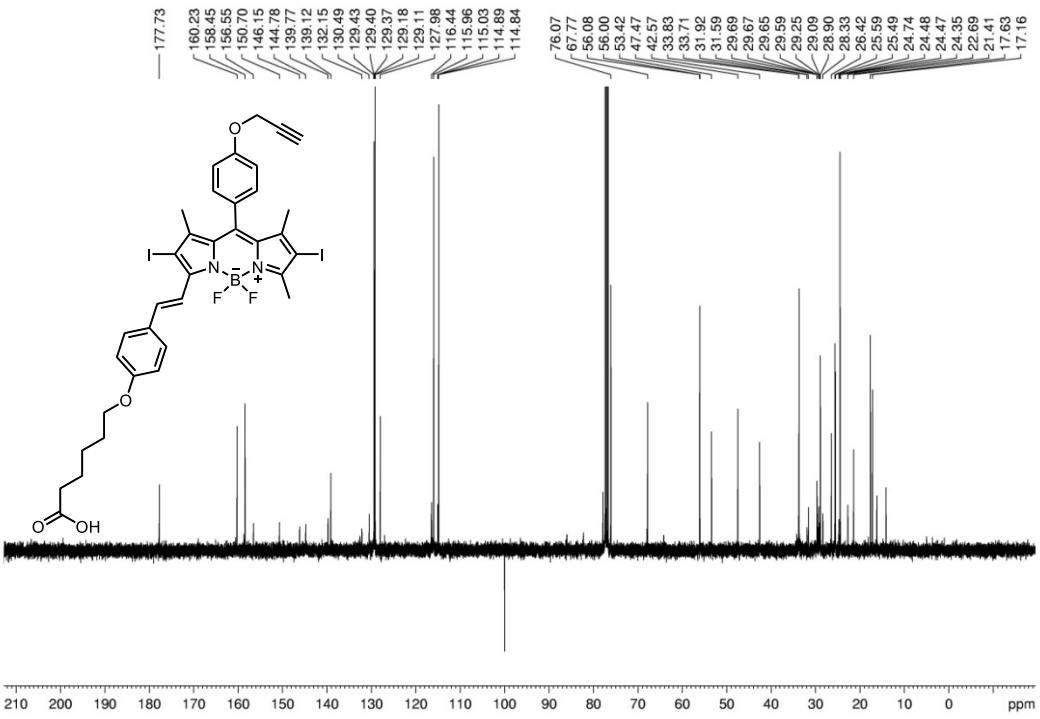
O
N3
S

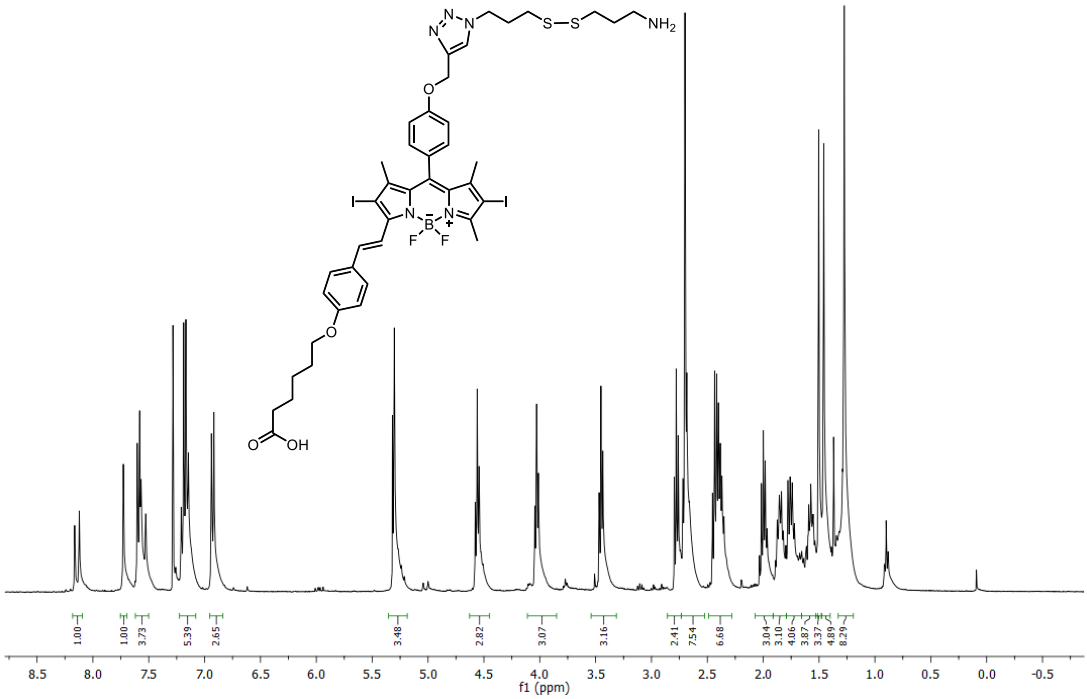

50.09
30.62
28.92
26.16
210 200 190 180 170 160 150 140 130 120 110 100 90 80 70 60 50 40 30 20 10 0 ppm

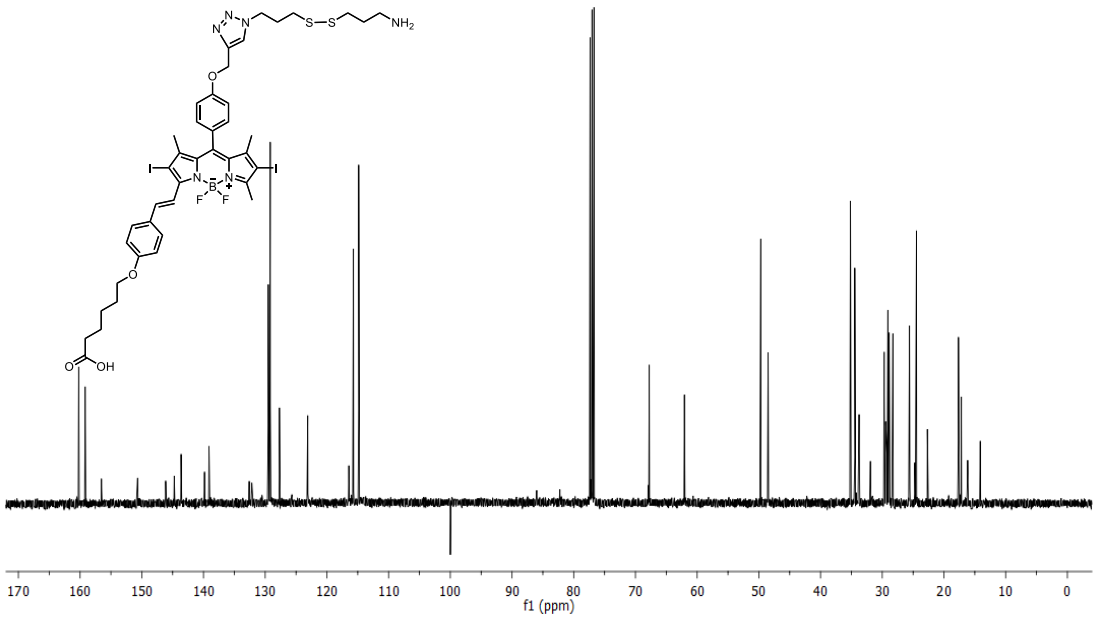

1385.370
1378.888
1372.366
1114.842
1107.840
1100.758
813.024
806.382
799.500
792.658
785.895
N3
S
S
N3
8.0 7.5 7.0 6.5 6.0 5.5 5.0 4.5 4.0 3.5 3.0 2.5 2.0 1.5 1.0 0.5 ppm
0.99
0.98
0.99

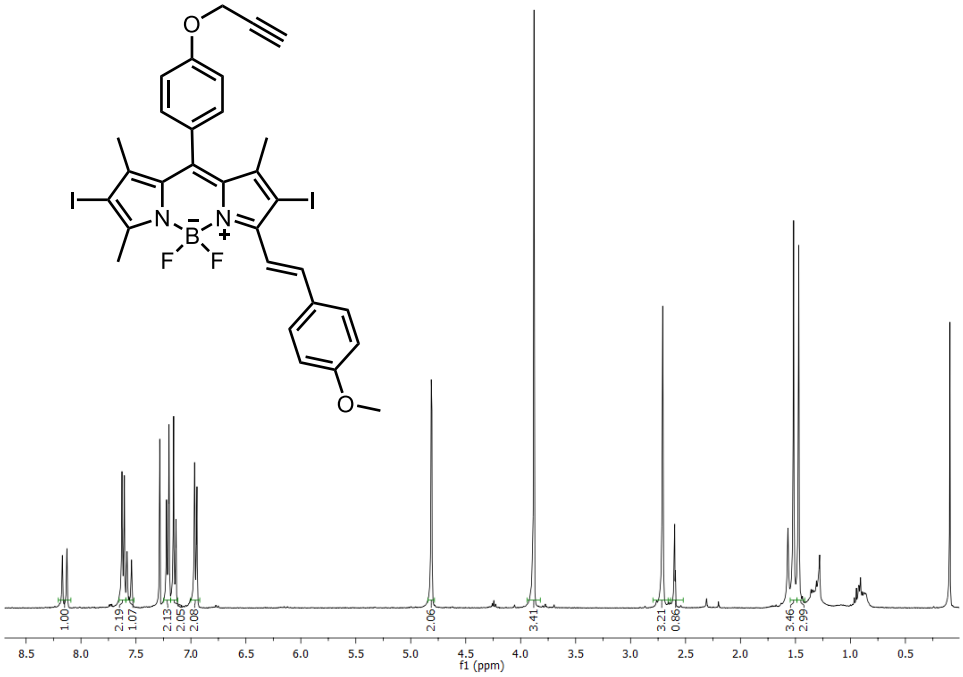

1485.883
1385.650
1384.850
1379.888
1373.406
1367.004
1167.859
1160.977
1154.135
1119.404
1112.121
1104.839
1097.397
808.023
801.460
794.738
787.976
783.935
776.932
769.970
763.088
N3
S
S
NH2
8.0
7.5
7.0
6.5
6.0
5.5
5.0
4.5
4.0
3.5
3.0
2.5
2.0
1.5
1.0
0.5
ppm
1.00
1.00
0.82
1.80
1.84

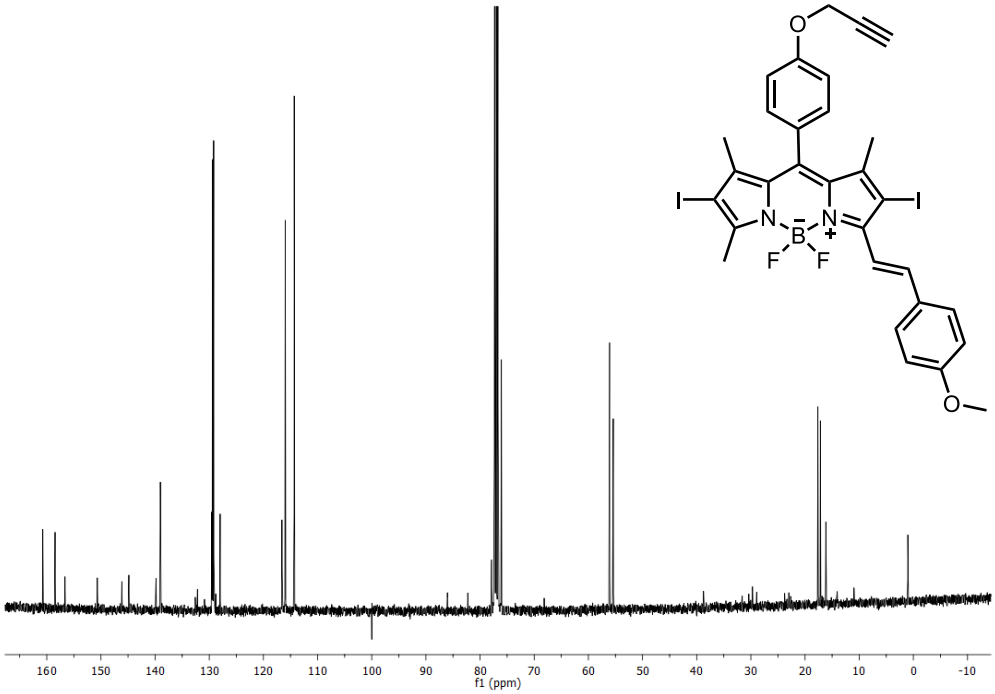

O
I
I
N
B
N
F
F
O
O
OH
1.00
2.19
1.07
2.13
2.05
2.08
2.06
3.41
3.21
0.86
3.46
2.99
8.5
8.0
7.5
7.0
6.5
6.0
5.5
5.0
4.5
4.0
3.5
3.0
2.5
2.0
1.5
1.0
0.5
f1 (ppm)

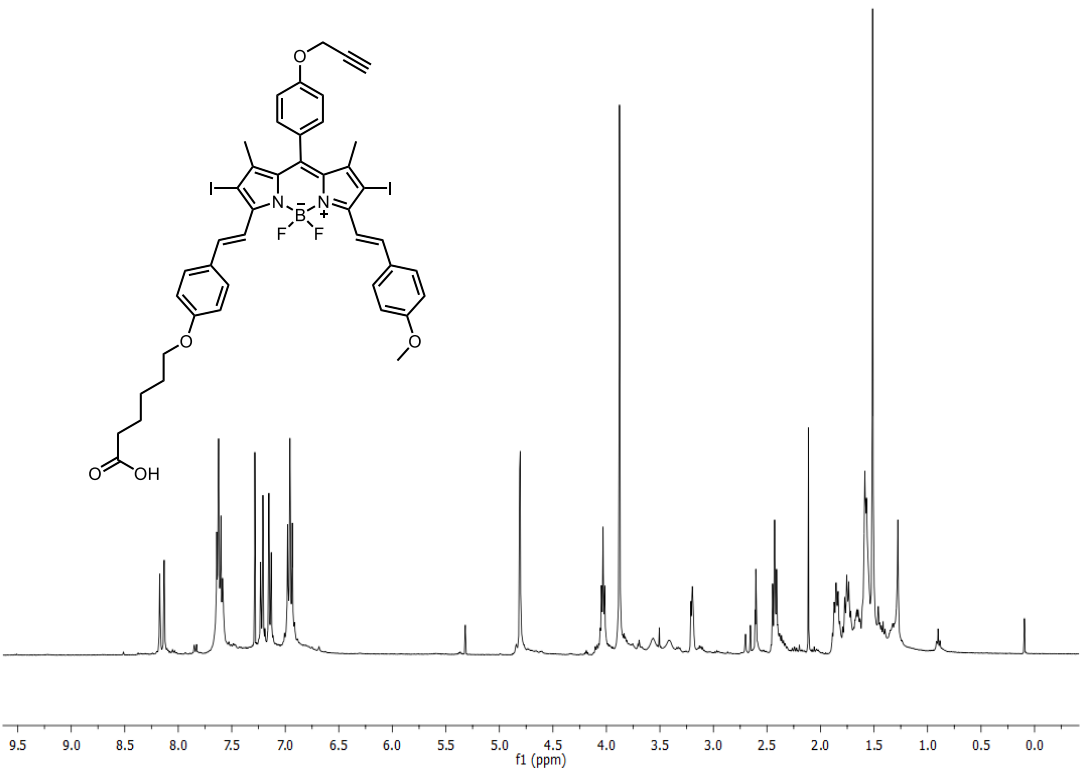

177.73
160.23
158.45
156.55
150.70
146.15
144.78
139.77
139.12
132.15
130.49
129.43
129.40
129.37
129.18
129.11
127.98
116.44
115.96
115.03
114.89
114.84
76.07
67.77
56.08
56.00
53.42
47.47
42.57
33.83
33.71
31.92
31.59
29.69
29.67
29.65
29.59
29.25
29.09
28.90
28.33
26.42
25.59
25.49
24.74
24.48
24.47
24.35
22.69
21.41
17.63
17.16
O
I
I
N
B
F
F
O
O
OH
210
200
190
180
170
160
150
140
130
120
110
100
90
80
70
60
50
40
30
20
10
0
ppm

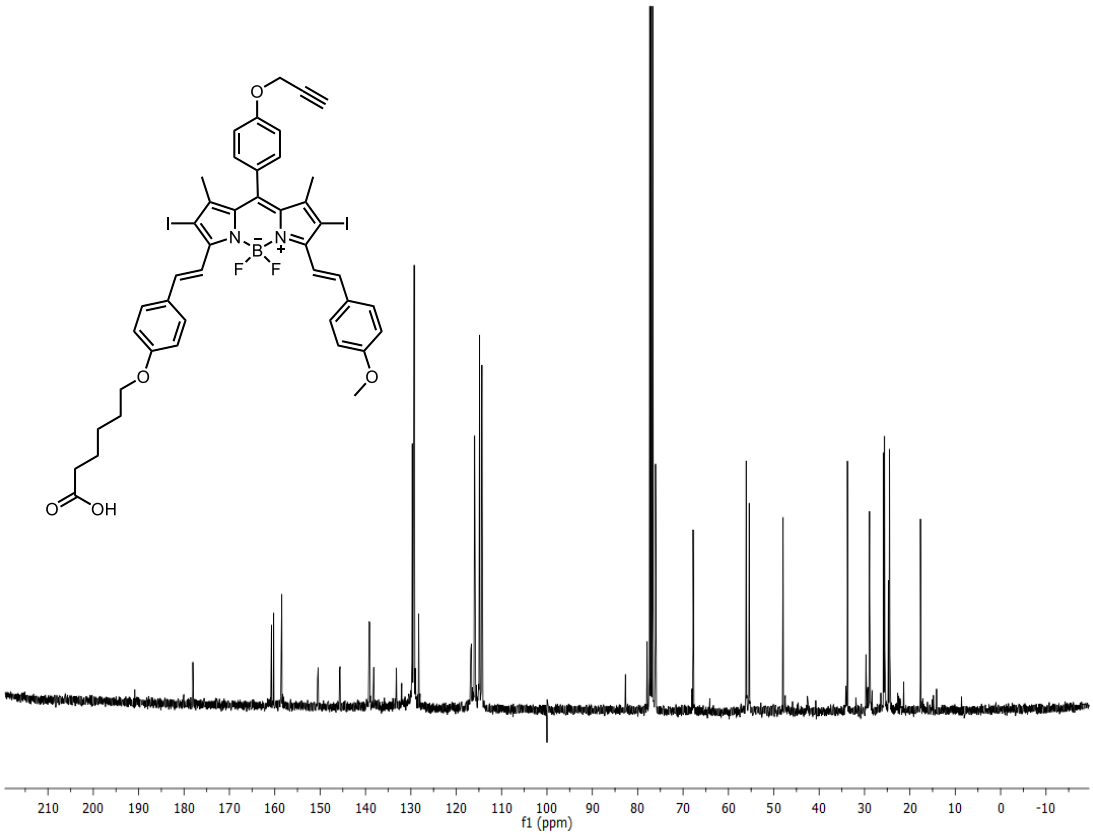

N
N
N
S
S
NH2
O
I
I
N
B
F
F
O
O
OH
1.00
1.00
3.73
5.39
2.65
3.48
2.82
3.07
3.16
2.41
7.54
6.68
3.04
3.10
4.06
3.87
3.37
4.89
8.29
8.5
8.0
7.5
7.0
6.5
6.0
5.5
5.0
4.5
4.0
3.5
3.0
2.5
2.0
1.5
1.0
0.5
0.0
-0.5
f1 (ppm)

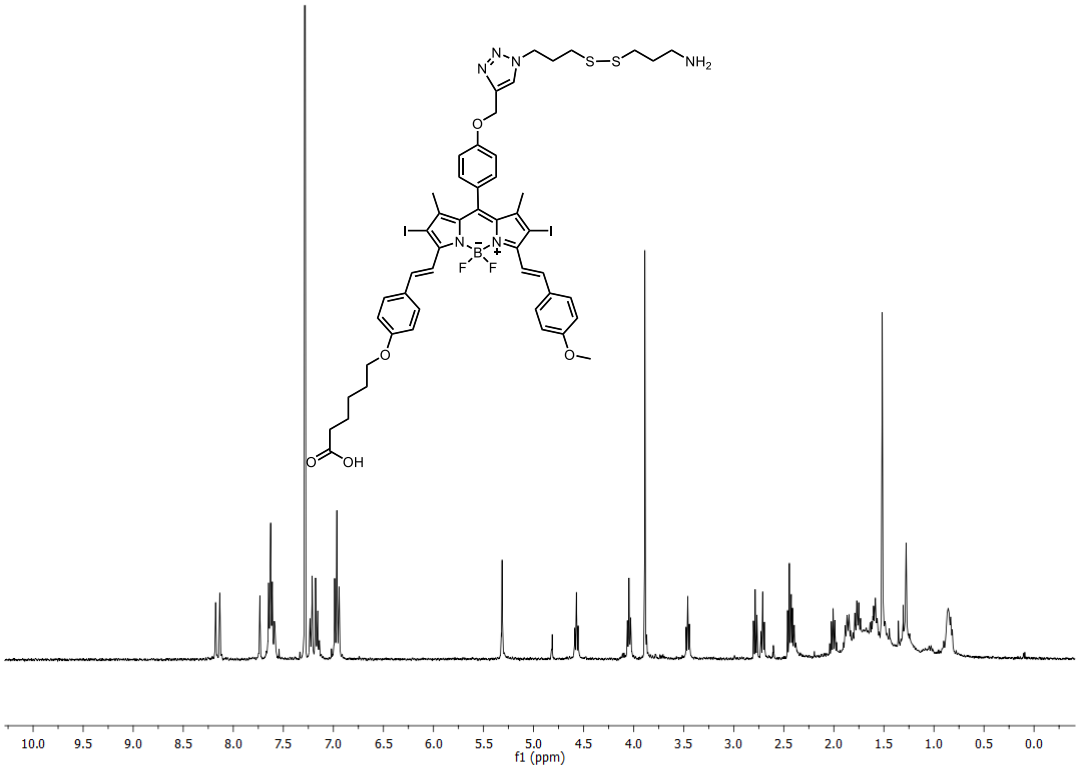

NH2
OH
170 160 150 140 130 120 110 100 90 80 70 60 50 40 30 20 10 0
f1 (ppm)

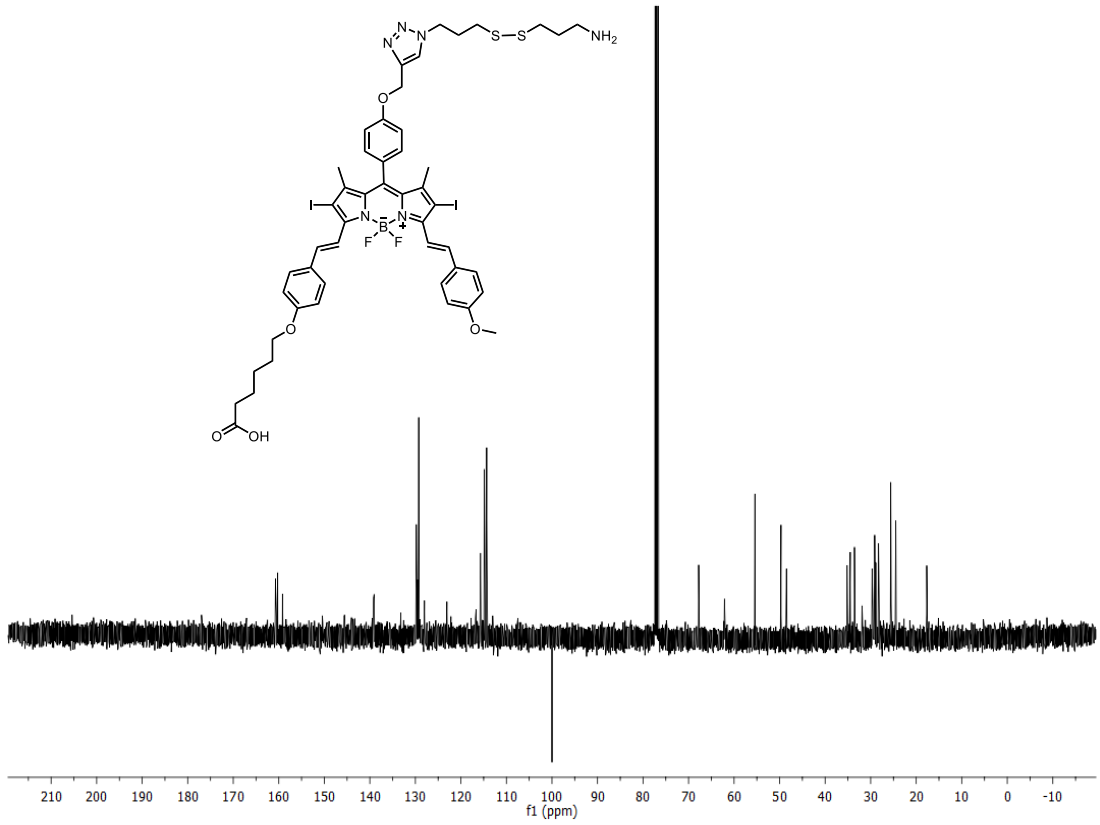

1.00
2.19
1.07
2.13
2.05
2.08
2.06
3.41
3.21
0.86
3.46
2.99
8.5 8.0 7.5 7.0 6.5 6.0 5.5 5.0 4.5 4.0 3.5 3.0 2.5 2.0 1.5 1.0 0.5
f1 (ppm)

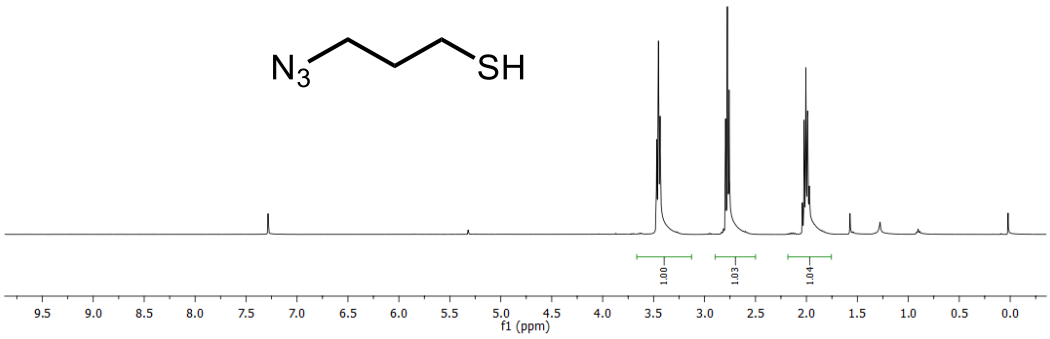

O
I
N
B
F
F
I
O
160 150 140 130 120 110 100 90 80 70 60 50 40 30 20 10 0 -10
f1 (ppm)

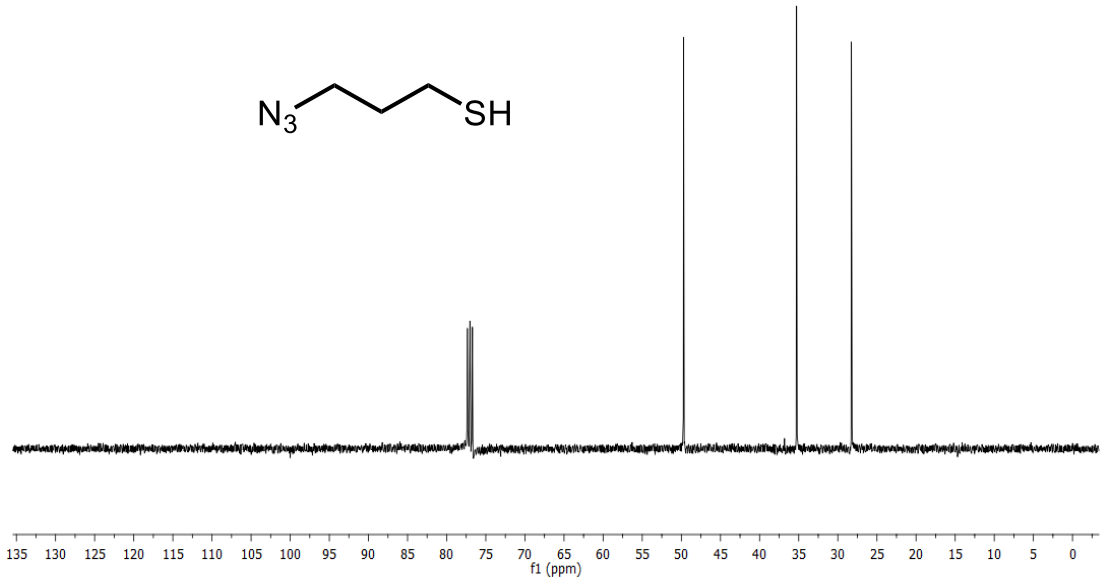

O
I
N
B
F
F
I
O
O
O
OH
9.5 9.0 8.5 8.0 7.5 7.0 6.5 6.0 5.5 5.0 4.5 4.0 3.5 3.0 2.5 2.0 1.5 1.0 0.5 0.0
f1 (ppm)

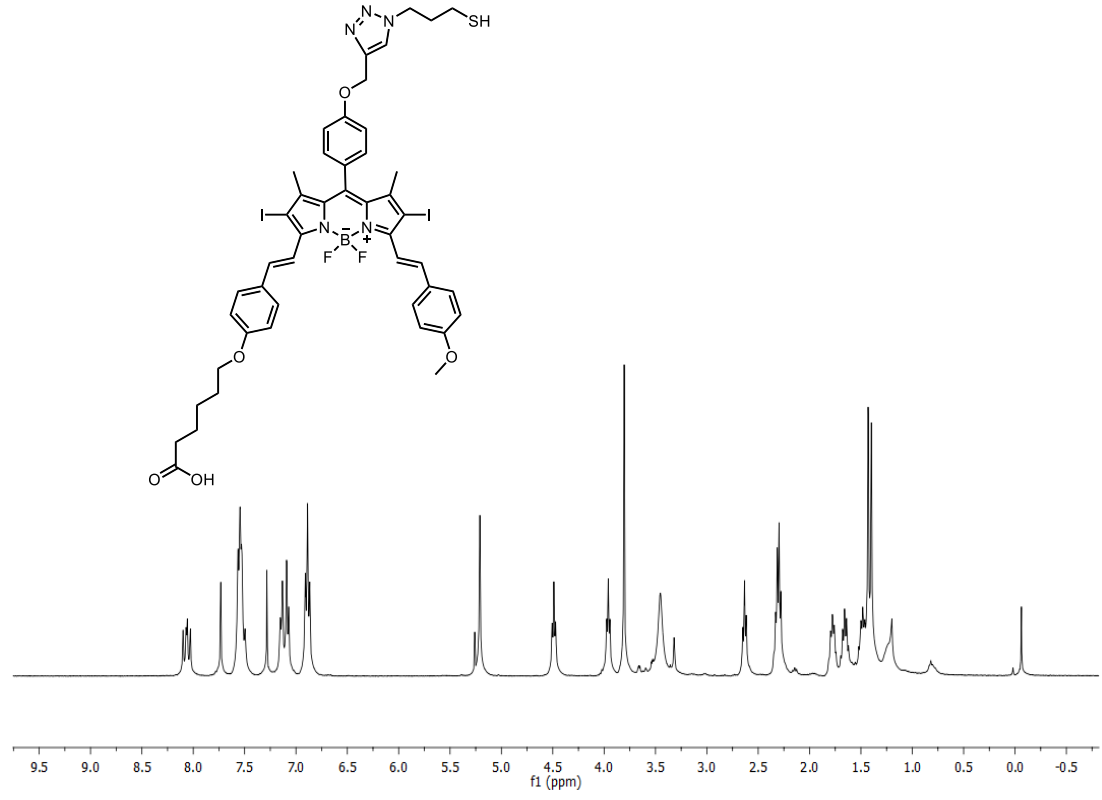

O
I
N
B
F
F
I
O
O
O
OH
210 200 190 180 170 160 150 140 130 120 110 100 90 80 70 60 50 40 30 20 10 0 -10
f1 (ppm)

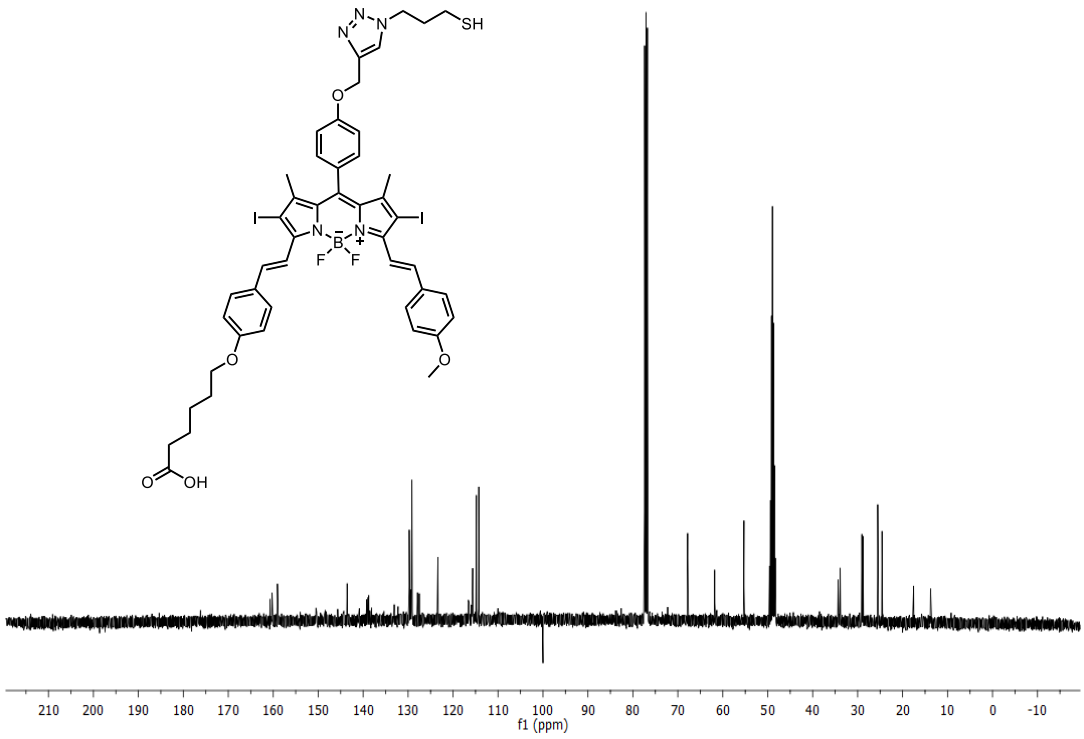

N
N
N
S
S
NH2
O
I
N
B
F
F
I
O
O
O
OH
10.0 9.5 9.0 8.5 8.0 7.5 7.0 6.5 6.0 5.5 5.0 4.5 4.0 3.5 3.0 2.5 2.0 1.5 1.0 0.5 0.0
f1 (ppm)

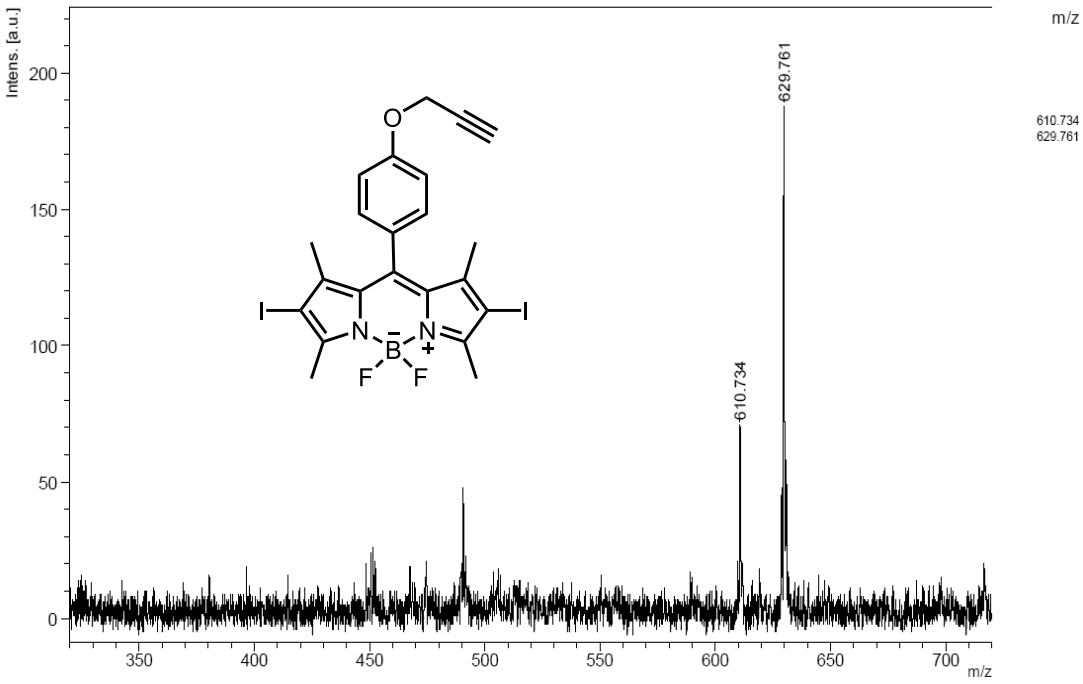

NH2
OH
F
F
210 200 190 180 170 160 150 140 130 120 110 100 90 80 70 60 50 40 30 20 10 0 -10
f1 (ppm)

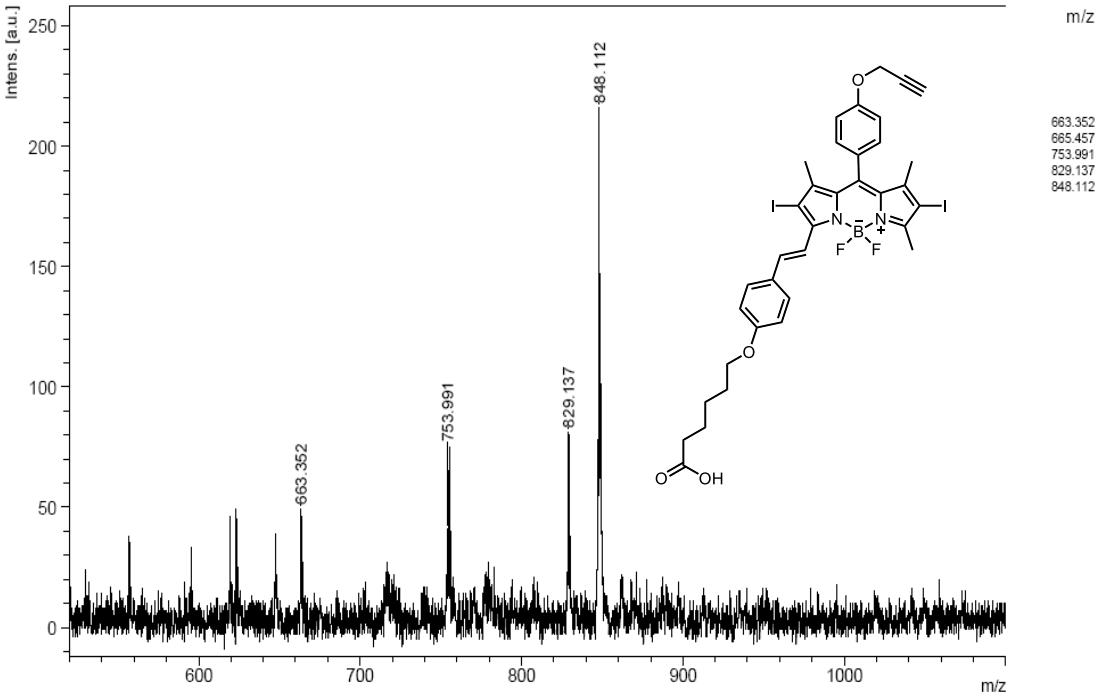

N3
SH
1.00
1.03
1.04
9.5 9.0 8.5 8.0 7.5 7.0 6.5 6.0 5.5 5.0 4.5 4.0 3.5 3.0 2.5 2.0 1.5 1.0 0.5 0.0
f1 (ppm)

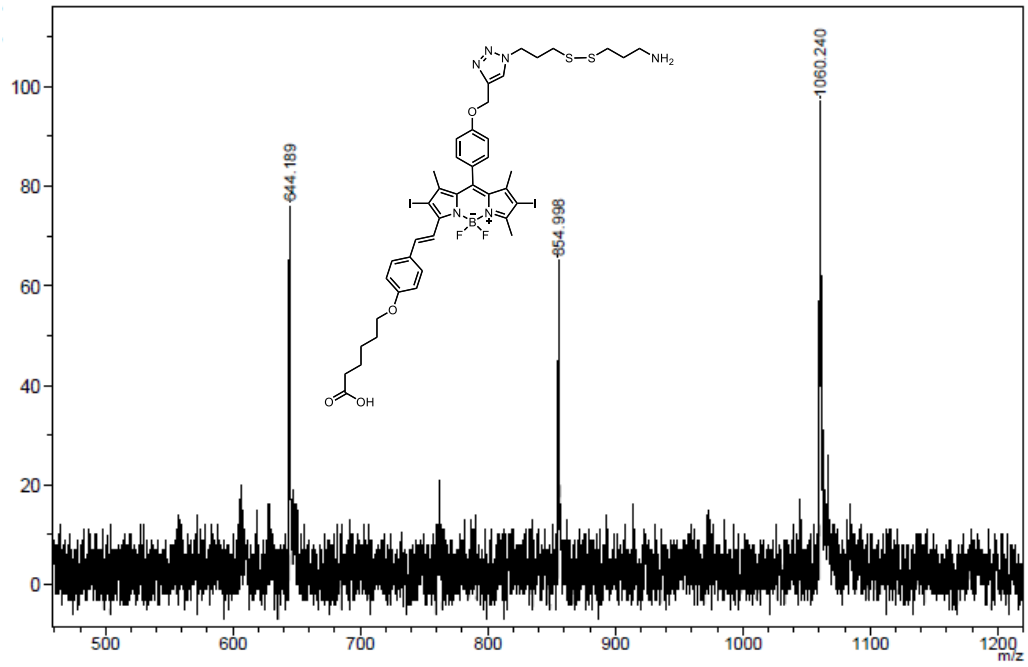

N3
SH
135 130 125 120 115 110 105 100 95 90 85 80 75 70 65 60 55 50 45 40 35 30 25 20 15 10 5 0
f1 (ppm)

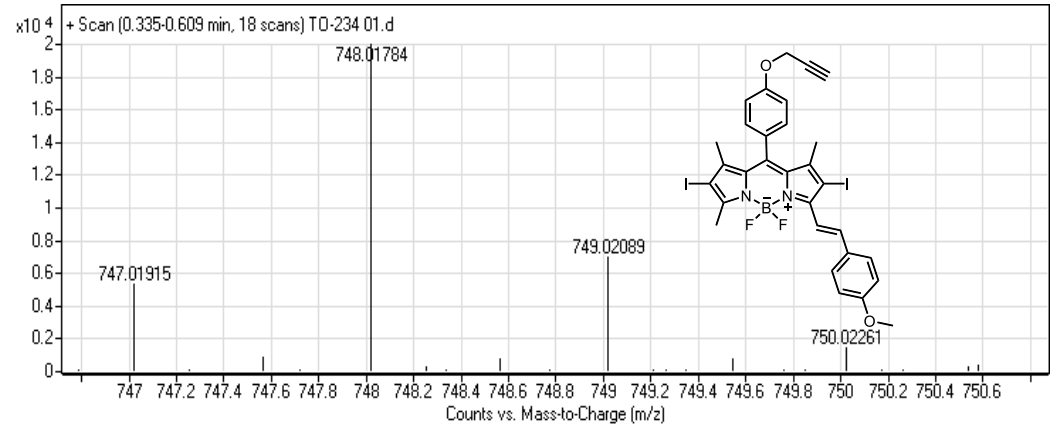

SH
I
I
F
F
O
OH
9.5 9.0 8.5 8.0 7.5 7.0 6.5 6.0 5.5 5.0 4.5 4.0 3.5 3.0 2.5 2.0 1.5 1.0 0.5 0.0 -0.5
f1 (ppm)

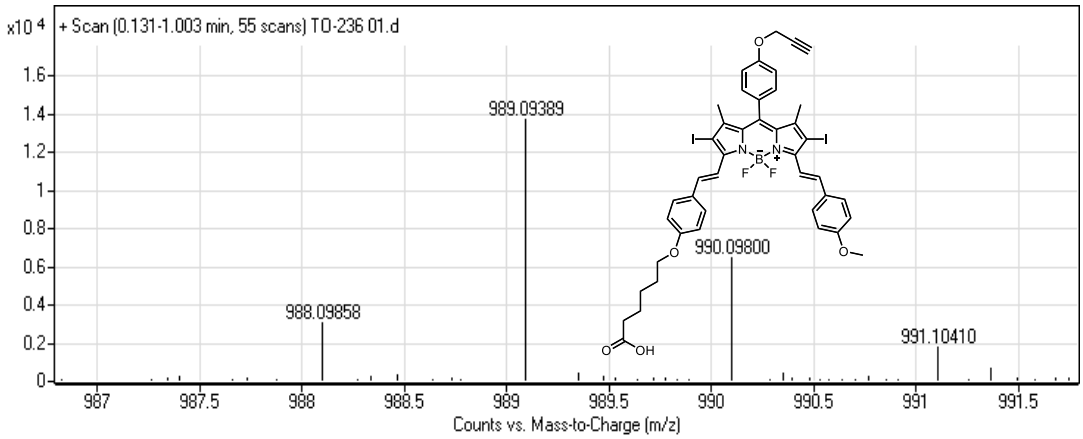

SH
OH
f1 (ppm)

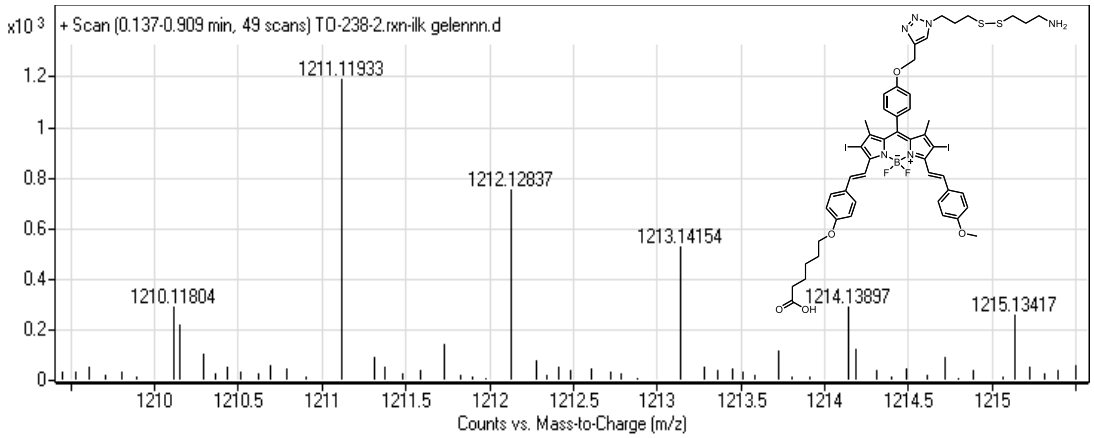

Intens. [a.u.]
m/z
629.761
610.734
610.734
629.761

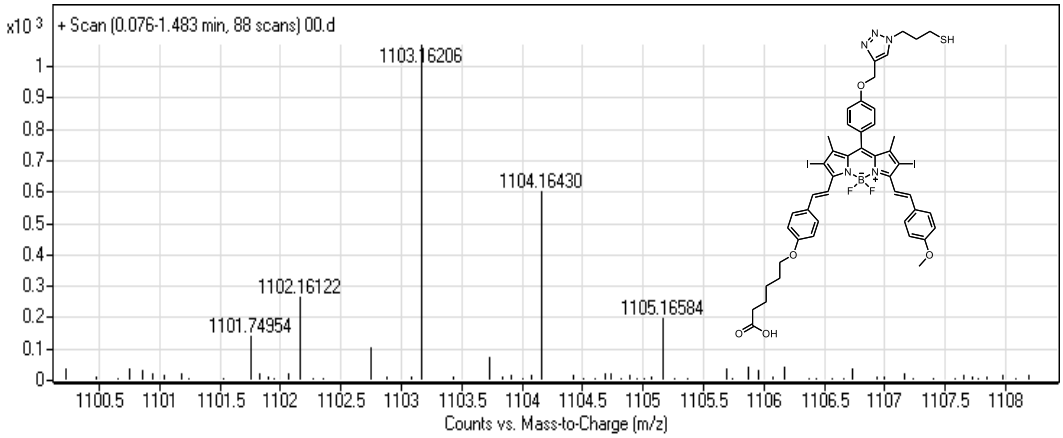

Intens. [a.u.]
m/z
663.352
753.991
829.137
848.112
663.352
665.457
753.991
829.137
848.112


644.189
854.998
1060.240
m/z


x10 4
+ Scan (0.335-0.609 min, 18 scans) TO-234 01.d
748.01784
749.02089
747.01915
750.02261
Counts vs. Mass-to-Charge (m/z)


x10 4
+ Scan (0.131-1.003 min, 55 scans) TO-236 01.d
989.09389
990.09800
988.09858
991.10410
OH
Counts vs. Mass-to-Charge (m/z)


x10 3
+ Scan (0.137-0.909 min, 49 scans) TO-238-2.rxn-ilk gelennn.d
1211.11933
1212.12837
1213.14154
1210.11804
1214.13897
1215.13417
NH2
OH
Counts vs. Mass-to-Charge (m/z)


x10 3
+ Scan (0.076-1.483 min, 88 scans) 00.d
1103.16206
1104.16430
1102.16122
1101.74954
1105.16584
1
0.9
0.8
0.7
0.6
0.5
0.4
0.3
0.2
0.1
0
1100.5
1101
1101.5
1102
1102.5
1103
1103.5
1104
1104.5
1105
1105.5
1106
1106.5
1107
1107.5
1108
Counts vs. Mass-to-Charge (m/z)